

Role of platelets in liver damage and regeneration

Inaugural-Dissertation

zur Erlangung des Doktorgrades
der Mathematisch-Naturwissenschaftlichen Fakultät
der Heinrich-Heine-Universität Düsseldorf

vorgelegt von

Friedrich Wilhelm Bernd Reuswig
aus Gelnhausen

Düsseldorf, Dezember 2020

Aus der Arbeitsgruppe Experimentelle Vaskuläre Medizin
der Klinik für Gefäß- und Endovaskularchirurgie
des Universitätsklinikums der Heinrich-Heine-Universität Düsseldorf

Gedruckt mit der Genehmigung der
Mathematisch-Naturwissenschaftlichen Fakultät der
Heinrich-Heine-Universität Düsseldorf

Berichtersteller:

1. Prof. Dr. Margitta Elvers
2. Prof. Dr. Jürgen Scheller
3. Prof. Dr. Beate E. Kehrel

Tag der mündlichen Prüfung: 01.06.2021

Table of content

List of Tables.....	I
List of Figures	II
List of Abbreviations.....	III
Zusammenfassung.....	V
Abstract	VI
1. Introduction	1
1.1 Platelets in hemostasis and thrombosis.....	1
1.2 Megakaryocyte and platelet maturation.....	6
1.3. The liver between structure and function.....	9
1.4 The basics of liver injury and regeneration.....	13
1.5 Bleeding risk, thrombosis, and thrombocytopenia after liver injury	15
1.6. Scope of the study	17
2. Material	18
2.1 General devices and equipment.....	18
2.2. Chemicals and buffer	21
2.3 Antibodies	25
2.4 Oligonucleotides.....	27
2.5 Kits	27
2.6 Software	28
2.7 Animals	28
2.8 Human blood samples	29
3. Methods.....	30
3.1 Liver injury models	30
3.2 <i>In vivo</i> hemostasis and thrombosis models	32
3.3 Preparation of murine tissue.....	33
3.4 Cell biological methods.....	34
3.5 Protein biochemical methods	39
3.6 Histological analysis and Immunohistochemistry.....	42
3.7 Molecular biological methods	44
3.8 Statistical analysis	47
4. Results	48
4.1 Bile duct ligation leads to platelet activation defects in mice	48
4.2 High levels of bile acids account for platelet activation defects	56
4.3 Partial hepatectomy impairs hemostasis and modulates platelet biogenesis.....	64
4.4 IL-6R supports TPO expression and release to enhance megakaryopoiesis after liver injury and modulates platelet activation.....	87
4.5 IL-6 trans-signaling induces thrombopoiesis after PHx.....	101

4.6 Thrombocytopenia leads to delayed liver regeneration	105
5. Discussion	109
5.1 Bile duct ligation impairs platelet function and propagates bleeding risk <i>in vivo</i> ...	109
5.2 Bile acids as a modulator of platelet activity	113
5.3 Diminished platelet activation and bleeding risk in mice with partial hepatectomy	115
5.4 The crucial role of IL-6R and AMR in TPO regulation and platelet biogenesis	120
5.5 IL-6R deficiency induces enhanced platelet turn over and platelet hyper reactivity	125
5.6 Thrombocytopenic mice display reduced liver regeneration	129
5.7 Conclusion.....	131
6. References	132
7. Appendix	147
7.1 Unshown data	147
7.2 Acknowledgements	150
7.3 List of publications.....	151
7.4 International Conferences	152
7.5 Affidavit	153
7.6 Eidesstattliche Erklärung.....	153

List of Tables

Table 1. Summary of experimental mice strains used throughout this thesis including the scientific focus and the experimental approaches for which they were sacrificed	29
Table 2. Steps to exchange hydrophilic and hydrophobic state of the paraffin embedded tissue before and after histological procedure.	42
Table 3. Composition of the PCR reaction mixture using the KAPA – Mouse - Genotyping Hot Start Kit.	44
Table 4. Reaction steps of the PCR for murine genotyping.....	44
Table 5. Composition of the reverse transcription reaction of isolated RNA.....	46
Table 6. Reaction steps used to synthesize cDNA.....	46
Table 7. Composition of the qRT-PCR reaction used in this study.....	46
Table 8. qRT-PCR program used to analyze RNA expression of target genes.....	47
Table 9. Serum analysis and organ weight of mice 7 days after BDL	48

List of Figures

Figure 1. Primary hemostasis after vessel wall injury.	3
Figure 2. Scanning electron microscopy images of the shape change of murine platelets after activation	5
Figure 3. Thrombopoietin is synthesized in hepatocytes and induces platelet biogenesis	8
Figure 4. Functional anatomy of the liver	11
Figure 5. Images of the partial hepatectomy performed in mice (PHx)	30
Figure 6. BDL causes liver damage and enhanced megakaryopoiesis	49
Figure 7. Dysregulated total blood cell count of mice undergoing bile duct ligation .	50
Figure 8. Enhanced levels of platelet inhibiting plasma factors after bile duct ligation	51
Figure 9. Reduced platelet activation following bile duct ligation in mice	53
Figure 10. Bile duct ligation causes defective thrombus formation ex vivo and altered hemostasis in vivo	54
Figure 11. Platelet invasion into cholestatic liver tissue	55
Figure 12. Bile acid pool analysis of serum samples from C57Bl6/J mice	57
Figure 13. Bile acids have minor impact on murine platelet activation.....	58
Figure 14. Bile acids influence static adhesion of platelets	59
Figure 15. Bile acids have minor impact on short-term human platelet activation ...	61
Figure 16. Effects of bile acids on long-term human platelet activation	62
Figure 17. Bile acids influence static adhesion of human platelets to fibrinogen	63
Figure 18. Mild thrombocytopenia and anemia early after partial hepatectomy	65
Figure 19. Platelet activation defects 1 day after PHx	66
Figure 20. Partial hepatectomy causes defective thrombus formation and hemostasis 1 day after PHx.....	67
Figure 21. 3 days after PHx mild platelet activation defects were detected	68
Figure 22. Partial hepatectomy causes defective thrombus formation and hemostasis 3 days after PHx	69
Figure 23. Unaltered platelet activation and thrombus formation 7 days after PHx .	70
Figure 24. Unaltered platelet activation and thrombus formation 14 days after PHx	71
Figure 25. Enhanced levels of hemostatic inhibiting factors after partial hepatectomy	72
Figure 26. Phosphorylation of VASP at Ser157 in platelets one day after PHx	73
Figure 27. Phosphorylation of VASP at Ser236 in platelets one day after PHx	74
Figure 28. Enhanced taurine conjugation in mice undergoing PHx	75
Figure 29. Analysis of platelet populations after PHx indicates tight platelet count regulation.....	77
Figure 30 PHx results in enhanced plasma von Willebrand Factor (vWF) levels accompanied by enhanced vWF-platelet binding and neuraminidase-1 (Neu-1) expression on platelets 1d after PHx	78
Figure 31. Platelet accumulation in the regenerative liver tissue after PHx.	80
Figure 32. Enhanced TPO synthesis after PHx is associated with upregulated Il-6R and AMR.....	82
Figure 33. PHx induces JAK2/STAT3 signaling in WT mice early after PHx	83
Figure 34. Mild splenomegaly and enhanced megakaryopoiesis in spleen following PHx.....	85
Figure 35. Enhanced megakaryopoiesis in the bone marrow after liver injury.	86
Figure 36. Enhanced platelet sequestration into the spleen following liver injury. ...	87

Figure 37. IL-6 receptor deficiency is accompanied by dysregulated platelet counts and impaired liver regeneration.	89
Figure 38. Platelets from IL-6R ^{-/-} exhibit enhanced platelet activation under resting and stimulated conditions.	90
Figure 39. Loss of IL-6R leads to altered platelet activation after PHx.	91
Figure 40. After PHx only GPVI mediated signaling is reduced in IL-6R ^{-/-} derived platelets.	93
Figure 41. Enhanced TPO synthesis after PHx is associated with upregulated AMR in IL-6R deficient mice.	94
Figure 42. Dysregulated TPO protein expression and serum concentrations in native IL-6 deficient mice and after PHx.	96
Figure 43. Enhanced platelet sequestration in the spleen of IL-6R ^{-/-} mice.	98
Figure 44. Enhanced megakaryopoiesis in the spleen of IL-6R ^{-/-} mice before and 1 day after PHx.	99
Figure 45. Asgr2 ^{-/-} mice display higher TPO synthesis	100
Figure 46. Pre-operative administration of hyper-IL-6 (hIL-6) leads to enhanced TPO plasma concentrations.	101
Figure 47. Administration of hIL-6 results in decreased GPIIb α expression and reduced platelet activation 1d after PHx.	103
Figure 48. Pre-operativ administration of hyper-IL-6 results in enhanced splenic megakaryopoiesis 1d after PHx.	104
Figure 49. Mpl ^{-/-} mice display thrombocytopenia, leukocytopenia and anemia after PHx.	106
Figure 50. Mpl ^{-/-} mice develop splenomegaly and show reduced liver regeneration and IL-6 plasma levels.	107
Figure 51. Mpl ^{-/-} mice display reduced SDF-1 plasma levels early after PHx.	108
Figure 52. Thrombopoietin biogenesis and platelet formation after PHx.	124

List of Abbreviations

A	ADP	Adenosine diphosphate
	ALP	Alkaline phosphatase
	ALT	Alanine aminotransferase
	AMR	Ashwell morell receptor
	APS	Ammoniumperoxodisulfate
	Asgr1	Asiglycoprotein receptor1
	Asgr2	Asioglycoprotein receptor 2
AST		Aspartate aminotransferase
B	BA	Bile acid
	BDL	Bile duct ligation
	BM	Bone marrow
	Botro	Botrocetin
	BSA	Bovine serum albumin
C	CD	Cluster of Differentiation
	CH ₃ OH	Methanol
	CLEC-2	C-type lectin-like type II
	CRP	Collagen related peptide
D	Cy5	Cyanine5
	dH ₂ O	Distilled water
	DTT	Dithiothreitol
E	ECA	<i>Erythrina cristagalli</i> lectin
	ECL	Electrochemiluminescence
	ECM	Extracellular matrix
	EDTA	Ethylenediaminetetraacetic acid
	ELISA	Enzyme linked immunosorbent assay
	eNOS	Endothelial NO-Synthethase
F	FACS	Fluorescence-activated cell sorting
	FcR	Fc receptor
	FITC	Fluorescein-Isothiocyanat
	FSC	Forward scatter
	FXR	Farnesoid-X receptor
G	g	Gramm
	GAPDH	Glyceraldehyde 3-phosphate dehydrogenase
	GCDC	Glycodeoxycholate
	GP	Glycoprotein
H	GPCR	G-coupled protein receptor
	h	Hours
	HCl	Hydrochloric acid
	HE-staining	Hemalun-eosin staining
	HRP	Horse Radish Peroxidase
	hIL-6	hyper Interleukin-6
	HSC	Hematopoeitic stemm cell
I	IL-6	Interleukin-6
	IL-6R	Interleukin-6 receptor
J	JAK	Janus kinase
K	KC	Kupffer cell
	KCl	Potassium chloride
	kDa	Kilo Dalton
L	L	Liter
	LSEC	Liver sinusoidal endothelial cell
M	mAb	Monoclonal antibody
	MgCl ₂	Magnesium chloride

	MGL	Macrophage galactose-type lectin receptor
	MK	Megakaryocyte
	MM	Master mix
	Mol	molarity
	MP	Milk powder
	Mpl	Myeloproliferative leukemia virus oncogene
N	Na ₃ OV ₄	Sodium orthovanadate
	NaCl	Sodium chloride
	NaH ₂ PO ₄	Monosodium phosphate
	NaHCO ₃	Sodium bicarbonate
	NaOH	Sodium hydrate
	Neu-1	Neuraminidase 1
	NO	Nitric Oxid
P	PAP-complex	Plasmin-antiplasmin complex
	PAR-4	Protease activated receptor 4
	PBC	Primary biliary cholangitis
	PBS	Phosphate buffered saline
	PCR	Polymerase chain reaction
	PE	Phycoerythrin
	PGE ₁	Prostaglandin E1
	PGI ₂	Prostacyclin I2
	PHx	Partial Hepatectomy
	Plt	Platelet
	PRP	Platelet rich plasma
Q	qRT-PCR	quantitative Real-Time-PCR
R	RBC	Red blood cell
	RCA-1	<i>Ricinus communis</i> agglutinin 1
	RT	Room temperature
S	SDF-1a	Stem cell derived factor alpha
	SDS	Sodium dodecyl sulfate
	sIL-6R	Soluble Interleukin-6 receptor
	SSC	Sideward scatter
	STAT	Signal transducer and activator of transcription
T	TC	Taurocholate
	TCDC	Taurochenodeoxycholate
	TDC	Taurodeoxycholate
	TEMED	N, N, N', N'-Tetramethylethylenediamin
	TGR5	Gpbar1(g-protein coupled bile acid receptor)
	TLC	Taurolithocholate
	TO	Thiazole Orange
	t-PA	Tissue plasminogen activator
	TPO	Thrombopoietin
	TxA2	Thromboxane A2
U	U46	U46619 (Thromboxane A2 Analogue)
V	VASP	Vasodilator stimulated phosphoprotein
	vWF	von Willebrand Factor
W	WB	Whole blood
	WBC	White blood cell
	WGA	Wheat germ lectin
	WT	Wildtype mice

Zusammenfassung

Die Rolle von Thrombozyten nach Leberschädigung wird in der Literatur kontrovers diskutiert. Die Folgen einer fehlerhaften Thrombozytenaktivierung und Thrombozytopenie sind jedoch in diesem Bereich bis heute nicht vollständig verstanden. Bisher ist beschrieben, dass die Effekte nach Leberschädigung durch Thrombozyten sowohl verstärkt als auch verringert werden können. Bisher gibt es nur wenige Hinweise auf zeitabhängige Veränderungen der Thrombozyten-aktivierung und deren Fortschreiten bei Lebererkrankungen. Dementsprechend wurde in dieser Arbeit die Rolle der Thrombozyten bei der Leberschädigung und Leberregeneration anhand von zwei Operationsmodellen für akute und chronische Leberschädigung, der Gallengangligatur und der partiellen Hepatektomie, untersucht. Der Schwerpunkt lag auf der Thrombozytenaktivierung, der Wiederherstellung der Thrombozytenzahl und den mit diesen Phänomenen verbundenen Primäreffekten.

Die Ergebnisse dieser Studie zeigen, dass beide Leberschädigungsmodelle die primäre Hämostase negativ modulieren, was zu einer leichten Thrombozytopenie, Defekten in der Thrombozytenaktivierung und einem erhöhten Blutungsrisiko *in vivo* führt. Nach den vorliegenden Beobachtungen beeinflussen multiple Effekte die Thrombozytenaktivierung. Einerseits kommt es vermehrt zur Bildung von inhibitorischen Plasmafaktoren, wie z. B. NO und PGI₂, welche eine Phosphorylierung des thrombozytären Proteins VASP induzieren, welches als Negativregulator der Thrombozytenaktivierung bekannt ist. Andererseits wurde gezeigt, dass die Aktivierung von murinen und humanen Thrombozyten durch erhöhte Gallensalzspiegel vermindert wird, wodurch es zu einer weiteren Hemmung der primären Hämostase kommt. Zusätzlich kommt es zu einem erhöhten Verbrauch von Thrombozyten durch eindringende Thrombozyten in geschädigtes Lebergewebe. Dem wird durch eine verstärkte Megakaryopoese in Milz und Knochenmark der Mäuse entgegengewirkt.

Außerdem wird in dieser Arbeit erstmals beschrieben, dass es zu einer komplementären Regulation der TPO-Biogenese nach Leberresektion kommt. Die TPO-Synthese wird durch desialylierte Thrombozyten und/oder IL-6 über den AMR/IL-6R-JAK2-STAT3-Signalweg vermittelt, um den erhöhten Thrombozytenumsatz nach Leberschädigung zu kompensieren. Die genetische Deletion von IL-6 oder c-Mpl (TPO-Rezeptor) unterstreicht die Rolle der Thrombozyten, da Mäuse, denen diese Rezeptoren fehlen, nach einer partiellen Hepatektomie eine verminderte oder gar keine Leberregeneration zeigen.

Die hier vorgestellten Ergebnisse unterstreichen die entscheidende Rolle einer veränderten Thrombozytenaktivierung nach Leberschädigung und zeigen erstmalig, wie die Zahl der Thrombozyten nach Leberschädigung reguliert wird und somit die Leberregeneration durch direkte und indirekte Effekte unterstützt.

Abstract

Platelet mediated mechanisms after liver injury are controversially discussed in literature. However, the consequences of defective platelet activation and thrombocytopenia are not fully understood to date. Different reports provide evidence that platelets play a bivalent role, either preventing or even further accelerating liver injury. To date, little evidence is given about time-dependent alterations in platelet activation and their progression in liver disease.

In this thesis, the role of platelets during liver damage and liver regeneration were examined using two operation models for acute and chronic liver injury, namely bile duct ligation and partial hepatectomy. The focus was set on platelet activation, platelet count restoration and primary effects related to these phenomena.

Using different liver injury models the recent study reveals that primary hemostasis is negatively modulated resulting in mild thrombocytopenia and enhanced bleeding risk *in vivo*. According to the present observations, multiple effects influence platelet activation through increased production of inhibitory plasma factors. These factors include NO and PGI₂, which induce a strong phosphorylation of platelet VASP, a well-known inhibitor of platelet activation. Additionally, high plasma levels of bile acids affect platelet activation of murine and human platelets, propagating further inhibition of primary hemostasis. The enhanced platelet consumption due to invading platelets in the inflammatory liver tissue is thereby encountered by enhanced megakaryopoiesis in the spleen and bone marrow of mice in both models.

Additionally, this work describes for the first time the complementary regulation of TPO biogenesis after liver resection. TPO synthesis is mediated by desialylated platelets and/or IL-6 via the AMR/IL-6R-JAK2-STAT3 signaling pathway to compensate the enhanced platelet turnover after liver injury. The genetic deletion of either IL-6 or c-Mpl (TPO receptor) highlights the prominent role of platelets as mice lacking these receptors show diminished or even no liver regeneration after partial hepatectomy.

These results presented here emphasize the crucial role of altered platelet activation after liver injury and report for the first time how platelet counts are regulated after liver injury and support liver regeneration through direct and indirect effects.

1. Introduction

1.1 Platelets in hemostasis and thrombosis

The human body relies on the vascular system and the blood to ensure the distribution of oxygen and nutrition in all tissue types. The cellular part of the blood stream consists of different cell types, which have different functions e.g., oxygen supply (erythrocytes), the immune system (leucocytes), and to prevent bleeding after vascular injury (platelets). The most important cell type of the blood system after vascular injury are platelets, which are essential for blood clotting. Beside the unique role in primary hemostasis, platelets are also important in other physiological processes like angiogenesis, tumor growth, inflammation, and tissue regeneration [1].

1.1.1 Platelet physiology

Platelets are one of the smallest cells in the human body and have a diameter of approximately 4 μm [2]. Platelets have a lifespan of 8-10 days in the human system and do not have a cell nucleus but synthesize proteins due to the storage of mRNA in their cytoplasm [3]. In contrast to that, in the murine system platelets are smaller in size (2 μm) and have a shorter lifespan of 3-4 days [4]. In the bone marrow (BM) platelets are formed by cytoplasmic constrictions (proplatelets) of megakaryocytes (MKs); in rodents, they are additionally formed in the spleen [4]. Latest studies by Lefrançois *et al.* were also able to detect the lungs as new hematopoietic tissue [5]. After proplatelet elongation into the blood vessel, the proplatelets are shed into platelets by the blood stream and typical characteristics establish, such as high content of α and δ (dense)-granules, lysosomes, and the open intracanalicular system [6]. In line with their maturation, platelets lose their RNA content and are only moderately active regarding biosynthesis [6, 7]. Senescent, aged platelets need to be cleared out of the vascular system. This process of platelet clearance is mediated by macrophages in the liver and spleen through scavenger receptors located on their cell membrane [8]. On average, humans have 1.5 – 3.5 $\times 10^6$ platelets per μl blood. In mice, 1.1 $\times 10^6$ platelets per μl blood are present [3, 4].

1.1.2 Platelet function and signaling in primary hemostasis

1.1.2.1 Regulation of platelets and vascular integrity

In a steady state system, platelets exist in a so-called resting state, without adhering to the vessel wall or other cells. This inactive state is maintained through different control mechanisms mainly driven by the endothelium of the vessel. Membrane bound ectonucleotidases like the human CD39 (e.g. apyrase) are commonly expressed among various tissues in the human and murine system, regulating platelet activation in the vascular system via ATP and ADP degradation [9, 10].

Thrombomodulin is an enzyme also expressed by the endothelial cells of mammals. It contributes to the regulation of thrombin by binding and deactivating of its thrombotic activity [11]. Besides, platelets are also directly inhibited via intracellular signaling cascades. Prostaglandin H₂ is converted into prostaglandin I₂ [or prostacyclin (PGI₂)] inside the endoplasmic reticulum (ER) in endothelial cells through the prostacyclin synthetase [12]. Secreted PGI₂ binds the IP receptor at the platelet surface, a G-protein coupled receptor (GPCR), initiating G α_s signaling, leading to the activation of adenylyl cyclases, which subsequently lead to increased intracellular cAMP levels [13]. Similarly, nitric oxide (NO), which is produced by the endothelium or even in platelets itself via eNOS (endothelial NO-synthetase), directly interacts in platelets with guanylyl cyclase (GC) leading to increased levels of cGMP [14, 15]. Enhanced intracellular levels of cGMP and cAMP in platelets lead to the activation of the protein kinase A/G resulting in phosphorylation of the vasodilator stimulated phosphoprotein (VASP) at serine 157 or 239. Following VASP phosphorylation, platelet function is inhibited through the down regulation of intracellular Ca²⁺ concentration and cytoskeletal reorganization [16].

1.1.2.2 Platelet activation in primary hemostasis

In primary hemostasis, platelets become activated and form a thrombus that is unstable in flowing blood. Under physiological conditions, platelets do not adhere to the surface of the blood vessels as described under 1.1.2.1. In case of a vascular wall injury, parts of the subendothelial extracellular matrix (ECM) become exposed to the blood stream such as collagen, laminin or vitronectin. This results in the accumulation of the plasmatic von Willebrand factor (vWF) on the collagen of the ECM, which allows vWF to bind to the glycoprotein-Ib-V-IX (GPIb-V-IX) complex at the platelet surface [17]. This binding leads to weak platelet activation and allows unstable transient adhesion (tethering) of platelets at the vessel wall, where they „roll” the injured tissue. This enables the binding of the GPVI receptor

Introduction

to the exposed collagen of the vessel wall. The collagen receptor itself is coupled to an Fc receptor (FcR) γ -chain that initiates a signaling cascade through the immunoreceptor, tyrosine-based activation motif (ITAM). GPVI crosslinking facilitates ITAM autophosphorylation and thus the activation of platelets is initiated [18]. GPIb-induced trapping of platelets followed by GPVI-mediated activation triggers various signaling pathways within platelets, which include integrin activation, the release of granules, cytoskeletal reorganization (platelet shape change), and the recruitment of new platelets from the bloodstream to the growing thrombus [19-22]. This process is summarized in Figure 1.

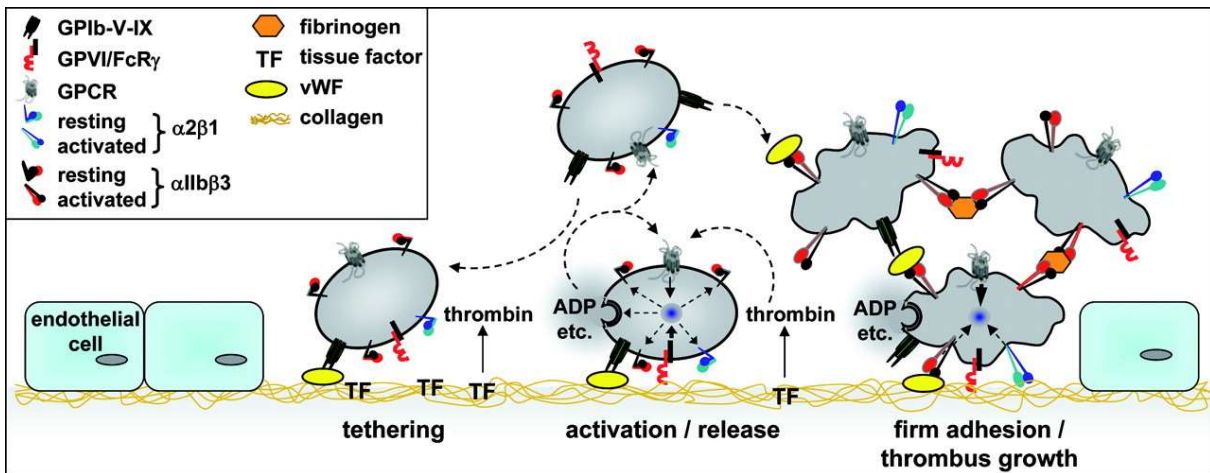


Figure 1. Primary hemostasis after vessel wall injury. After vessel wall injury the subendothelial extracellular matrix (ECM) is exposed. Plasmatic von Willebrand Factor (vWF) binds to the exposed collagen, allowing a loose binding of the GPIb-V-IX complex on the platelet membrane to the ECM. This tethering of platelets at the ECM allows GPVI binding to collagen leading to platelet activation and granule release. Simultaneously, tissue factor (TF) synthesized by subendothelial cells and exposed after vessel wall injury constantly generates thrombin from plasmatic prothrombin. The local generated thrombin in combination with ADP released by platelets leads to a recruitment of additional platelets from the blood stream to the site of injury due to the activation of G-protein coupled receptors (GPCR) on the platelet membrane. The synergistically activation of platelets through GPVI, the GPIb-V-IX-complex and the GPCR induces inside-out signaling which results in conformational changes and activation of integrin $\alpha_2\beta_1$ and $\alpha_{IIb}\beta_3$. Activated integrin $\alpha_2\beta_1$ supports firm adhesion at the site of vessel injury, while integrin $\alpha_{IIb}\beta_3$ initiates crosslinking of platelets through fibrinogen and stable adhesion by binding to vWF leading to thrombus formation and growth. License Number – 4947120827980 [23].

1.1.2.3 Integrin inside out and outside in signaling

The fibrinogen receptor integrin $\alpha_{IIb}\beta_3$ plays a central role in the activation of platelets. In the resting state of platelets, integrin $\alpha_{IIb}\beta_3$ appears in a conformation with low affinity to its ligand fibrinogen [23]. Binding of the GPIb complex and the GPVI receptors to the ECM triggers signaling pathways within platelets that lead to the activation of integrin $\alpha_{IIb}\beta_3$ [23]. The affinity modulation is provoked by a change in the extracellular conformation of the integrin into an active state. Afterwards, the affinity for its specific ligand fibrinogen or collagen-bound vWF increases [23, 24]. With appropriate stimulus, the integrin clusters on the cell membrane of platelets, which is known as avidity modulation and leads to stabilized and enhanced ligand interaction of the integrin [25, 26]. These processes, the avidity and affinity modulation of the integrin $\alpha_{IIb}\beta_3$, are known as inside-out signaling [23, 25, 27].

Introduction

The active binding of ligands to the extracellular part of the integrin leads to a further change in the intracellular conformation of the integrin. This in turn leads to transphosphorylation of the cytoplasmic tail of the receptor and to a downstream signaling cascade (“outside-in signaling”) [28, 29]. The outside-in signaling of integrin $\alpha_{IIb}\beta_3$ results in strong platelet activation, accompanied by an increase in platelet surface area (shape change) and platelet aggregation via fibrinogen binding [30, 31].

In addition to the integrin signaling pathway described above the binding of GPVI to collagen leads to the release of intracellular granules. These granules contain for example fibrinogen, thromboxane (TxA₂) and adenosine diphosphate (ADP) [23]. As the granules are released, integrin $\alpha_{IIb}\beta_3$ receptors are increasingly externalized on the platelet surface, resulting in increased inside-out signaling promoting platelet activation and recruitment in an autocrine manner [29].

1.1.2.4 Platelet activation and shape change via second wave mediators

TxA₂ and ADP contribute to platelet activation by stimulating various receptors [20, 23]. The release of these second wave mediators likewise stimulates resting platelets in the blood stream that do not come into contact with the subendothelial ECM (fig. 1). This is mediated by receptor binding of ADP to the platelet receptors P₂Y₁ or P₂Y₁₂ [32]. In addition, binding of ADP to platelets also leads to platelet shape change, mobilization of calcium and aggregation of platelets [33]. While the ADP receptor P₂Y₁ is responsible for shape change and calcium mobilization [34], the receptor P₂Y₁₂ inhibits the adenylyl cyclase, stabilizes platelet aggregation, and leads to $\alpha_{IIb}\beta_3$ integrin activation [35].

Arachidonic acids are converted from cyclooxygenase 1/2 (COX 1/2) into prostaglandin H₂ (PGH₂), which is the substrate for the TxA₂ synthetase. Synthesized TxA₂ is then stored in platelet granules and released after activation. TxA₂ signaling is mediated through binding of the G-protein coupled thromboxane A₂ receptors, TP α and TP β (T-prostanoid receptor; TP-Receptor) [36, 37], which induce calcium mobilization and subsequently $\alpha_{IIb}\beta_3$ integrin activation and platelet shape change [38, 39].

In addition to ADP and TxA₂, platelet degranulation also releases adhesion proteins such as fibronectin, P-selectin, and vWF. Thus, degranulation changes the local plasma composition, hereby increasing the recruitment of further platelets to the thrombus [17].

As already mentioned, various platelet activation pathways lead to a change in shape and surface area of platelets, as shown by scanning electron microscopy in fig. 2 (Elvers; unpublished data). In a resting state, platelets circulate through the blood in a discoid (disc-shaped) form [40] (fig. 2A). After platelet activation, platelets lose their discoid shape and become smaller and spherical [41] (fig. 2B). They develop filopodia and lamellipodia to enlarge

Introduction

their surface area (fig. 2B-C). This increase in surface area and shape change of platelets, triggered by the polymerization of actin and the cytoskeletal reorganization, enables platelets to firmly adhere to the subendothelial ECM and to crosslink with other platelets [17, 41-43].

The combination of the simultaneously occurring signaling pathways described above results in stable adhesion and local recruitment of platelets. This creates a cellular thrombus at the injured vascular wall, which is stabilized by processes of the following secondary hemostasis.

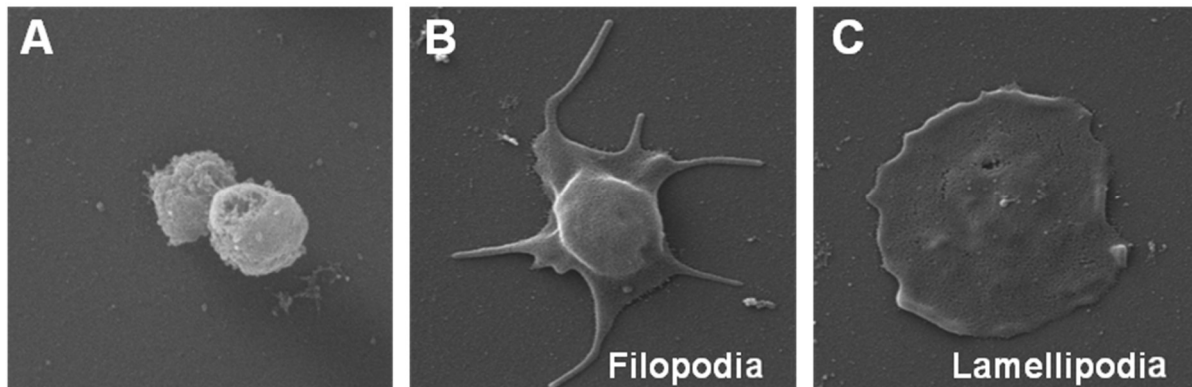


Figure 2. Scanning electron microscopy images of the shape change of murine platelets after activation. In a resting state (A) the platelets have a discoid shape and after activation platelet form (B) filopodia and (C) lamellipodia. [unpublished data; Research group: Exp. Vascular Medicine; Prof. Dr. Margitta Elvers]

1.1.3 Enhanced platelet activation due to secondary hemostasis

The unstable thrombus can dissolve due to the prevailing blood flow; therefore, the thrombus is stabilized by a secondary hemostasis. This process is dependent on the cleavage of prothrombin to thrombin by coagulation factors [44]. Thrombin in turn is involved in the cleavage of fibrinogen to fibrin. Moreover, fibrin is then integrated into the thrombus, which leads to stabilization of the thrombus. In addition, thrombin, as one of the strongest physiological agonists of platelets, can proteolytically cleave and activate the protease-activated receptors (PAR) on the platelet surface leading to strong platelet activation [45, 46]. Thrombin triggers a PAR1 and PAR4 signaling cascade in human platelets [47], whereas it induces signaling of PAR3 and PAR4 in murine platelets [45]. The simultaneous processes of thrombin activation and fibrin cross-linking lead to stabilization of the thrombus and accumulation of other cells like erythrocytes [48].

The generation of a procoagulant surface is important for thrombin generation and mediated through exposure of phosphatidyl serine (PS) at the platelet surface [49]. This facilitates the generation of a platelet intrinsic prothrombinase complex resulting in local thrombin generation at the site of vessel wall injury. Besides, PS exposure at the membrane of platelets generates the coating of platelets with different proteins released after degranulation like fibrinogen,

Introduction

fibronectin, thrombospondin, and vWF to stabilize the growing thrombus through binding of coagulation factors and crosslinking of platelets [50, 51].

1.1.4 Plasmin activity and thrombus lysis.

After primary and secondary hemostasis, a stable clot has formed at the site of vessel injury to prevent blood loss. In the course of the removal of the thrombus, the fibrin clot must be removed. For this purpose, plasmin is formed from plasminogen by proteolytic cleavage, mediated by the enzyme tissue plasminogen activator (t-PA). tPA itself is generated and released from the endothelium [52]. Activated plasmin cleaves the crosslinked fibrin network allowing a lysis of the stable thrombus. A direct regulator of active plasmin is the inhibitor anti-plasmin. Plasmin and anti-plasmin rapidly form a 1:1 stoichiometric complex leading to an enzymatic inhibition of plasmin [53]. This stable plasmin-anti-plasmin (PAP)-complex is a useful indicator of an intact fibrinolysis.

1.2 Megakaryocyte and platelet maturation

Megakaryocytes are the largest cells within in the BM of humans with an approximately diameter of 50-100 μm [54, 55]. Rodents like mice also develop some megakaryocytes in splenic tissue besides the BM[56]. The main function of MKs is to produce platelets, thereby indirectly affecting the vascular integrity. A single MK produces around 2000-5000 platelets to provide a physiological platelet count within the blood stream [57].

1.2.1 Megakaryopoiesis

MKs are derived from the hematopoietic stem cells (HSCs) in the BM. Quiescent HSC stay in their osteoblastic niche within the BM. A major factor in the osteoblastic niche is the cytokine thrombopoietin (TPO) and its receptor c-Mpl (myeloproliferative leukemia virus oncogene). TPO binds to the Mpl receptor on HSCs to stimulate maturation into MKs. In this context, TPO is not regulating the maturation of MKs, but stimulates their generation from HSCs [58]. Furthermore, mature MKs are also able to regulate the osteoblastic niche via secretion of platelet factor 4 (Pf4) as well as transforming growth factor- β 1 (TGF- β 1). HSCs therefore stay in their quiescent state because their cell cycle is negatively regulated by both factors [59]. Within this differentiation from HSCs to MKs, they migrate to the vascular niche to get in direct contact with the BM sinusoids [60]. This migration is mediated through different chemokines such as stromal cell-derived factor-1 α (SDF-1 α), angiopoietin-1 (Ang-1) and TPO [59, 61, 62]. Within the maturation process, MKs become polyploid by undergoing several replication cycles

Introduction

and contain a cell nucleus, typically multilobed with up to 128 sets of chromosomes (128N) [63]. This process is called endomitosis [64]. Endomitosis serves as preparation for high protein biosynthetic effort that is accompanied by platelet formation.

Platelets are released from the MKs into the vascular system due to proplatelet protrusions. Mature MK form a pseudopod with a proplatelet shaft of about 2-4 μm of diameter. This pseudopod is extended until it reaches into the BM sinusoids. In the sinusoids, due to cytoskeletal reorganization and shear stress, proplatelet tips form and are shed into the circulating blood. These proplatelets are larger in size than circulating platelets, have a different cell shape [65] and differentiate into mature platelets within the circulation [66].

As previously described, platelets lose their mRNA content upon aging. Directly after platelet formation, platelets inherit the highest amount of mRNA. Therefore, mRNA loss correlates with platelet maturation [67, 68]. However, the overall RNA content also changes within the platelet life span, since platelets can partly regulate and change their protein biosynthesis through their micro RNA cargo [69]. Due to maturation, platelets age and need to be cleared out of the vascular system. As already described above, platelet clearance takes place in the liver and in the spleen mediated by phagocytic active cells.

1.2.2 The megakaryocyte growth cytokine - TPO

TPO is the key cytokine involved in MK maturation leading to platelet production. TPO was firstly cloned in 1994 and identified as a megakaryocytes growth and developmental factor [70]. The human gene encoding thrombopoietin is located on the chromosome 3q27 and encodes for a protein consisting of 353 amino acids with a calculated molecular weight of 38 kDa [71]. TPO is mainly generated in the liver by hepatocytes [72], but is also generated in the kidney and in the BM by stromal cells [73]. While TPO is synthesized in different tissues, it is always secreted into the vascular system as its biological function is related to megakaryopoiesis in the BM. The natural receptor for TPO is c-Mpl, which is abundant on platelets and in the BM on HSCs and MKs [74]. Newly formed platelets show a high frequency of c-Mpl on their cell membrane, which actively removes TPO from the plasma (fig. 3). Platelets are in a negative reciprocal correlation to the TPO concentration in the plasma to control TPO plasma levels and subsequently regulate megakaryopoiesis and platelet formation [74-76].

In contrast to common knowledge, it was firstly described in 2015 that TPO is regulated and not commonly expressed as assumed in the past [77]. This process is mediated by desialylated, aged platelets that bind to the Ashwell Morell receptor (AMR). The AMR typically consists of two subunits, namely ASGPR1 (Asioglycoprotein receptor 1) and ASGPR2 (Asioglycoprotein receptor 2). It is a transmembrane hetero-oligomeric GP complex that is highly conserved among mammalian species [78]. The AMR itself is the first mammalian lectin

Introduction

receptor described in literature. It binds asialoglycoproteins and is involved in their hepatic clearance [77, 78]. These clearance mechanisms are enhanced by exposure of terminal galactose on glycan chains of GPs. Upon ageing, platelets lose the sialic acid moiety on their GPs, leading to exposure of terminal β -N-acetyl-D glucosamine (β -GlcNAc) [79]. Consequently, platelets bind to the AMR (fig. 3).

The binding of desialylated platelets to the AMR leads to a signaling cascade downstream of the AMR in hepatocytes *in vivo* and *in vitro* as recently shown by Grozovsky *et al.* Janus kinase 2 (JAK2) is phosphorylated, leading to the activation of the signal transducer and activator of transcription 3 (STAT3) [77]. This transcription factor induces hepatic TPO mRNA expression to facilitate platelet biogenesis in mice (fig. 3) [77].

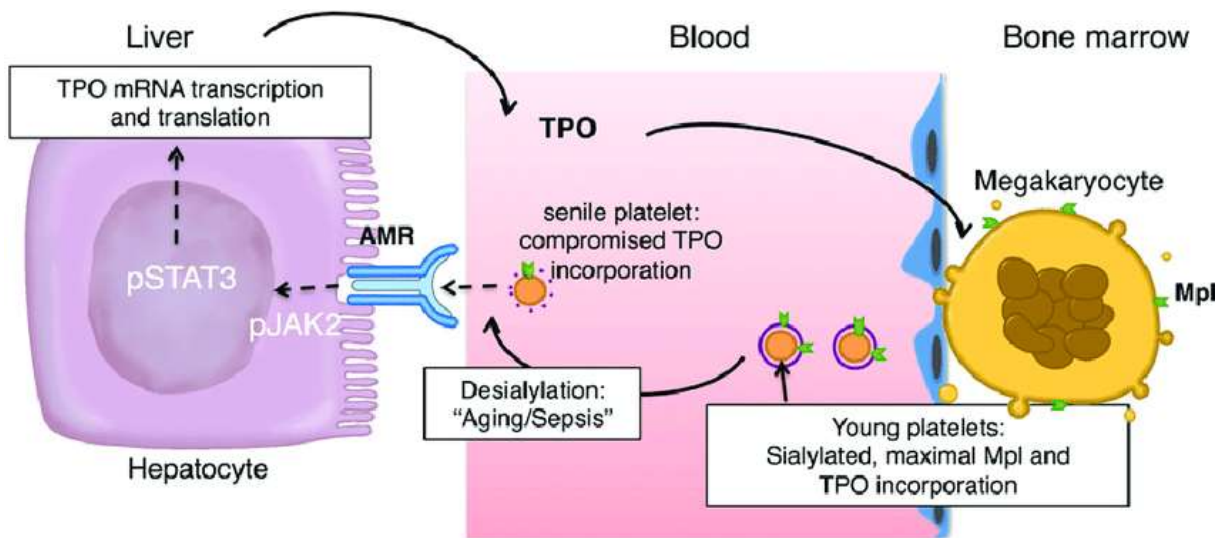


Figure 3. Thrombopoietin is synthesized in hepatocytes and induces platelet biogenesis. Senile, aged platelets bind to the Ashwell-Morell receptor (AMR), which is located on the membrane of hepatocytes, through the loss of their sialic acid moiety (desialylation). AMR induces phosphorylation of Janus kinase 2 (JAK2) resulting in phosphorylated signal transducer and activator of transcription 3 (STAT3). Subsequent TPO mRNA transcription and translation leads to the secretion of TPO into the blood. TPO binds to its receptor, myeloproliferative leukemia virus oncogene (Mpl), at the surface of megakaryocytes and induces the production of new platelets. New platelets are characterized by an enhanced abundance of Mpl at their surface leading to TPO extraction out of the blood. Thus, platelets and plasma TPO levels stay in a negative reciprocal correlation to each other important to control platelet counts. License Number 1077649-1 [80].

1.2.3 Role of IL-6 signaling in TPO generation

Different *in vitro* studies have shown that IL-6 is important for TPO generation beside the already described effects of desialylated platelets [81]. IL-6, secreted by monocytes, macrophages, and endothelial cells, is an acute phase cytokine and promotes the acute phase response in the liver [82, 83]. IL-6 binds to a receptor complex consisting out of the IL-6 receptor (IL-6R) and GP130. Once IL-6 is bound, IL-6 mediated “classic” signaling is induced through the GP130 receptor subunit. Hepatocytes, Stellate and Kupffer cells (KC) express IL-6R and thus are able to mediate IL-6 signaling in the liver[84]. Another way to induce IL-6 signaling is the IL-6 trans-signaling pathway. Cells that do not express IL-6R are able to induce

Introduction

IL-6 signaling by the soluble IL-6R. IL-6 and soluble IL-6R, e.g. released by platelets [85], form a complex and bind to cells which express GP130 [86].

In a clinical study from 2001, Kaser and colleagues provided evidence for the up-regulation of TPO plasma levels by IL-6 treatment of cancer patients [87]. Moreover, various clinical studies provided evidence for enhanced platelet counts after IL-6 treatment in humans [88-91]. However, the exact mechanism how TPO and platelet counts are regulated by IL-6 treatment remains unknown. As described above, TPO is synthesized through a JAK2/STAT3 signaling pathway. IL-6 induced signaling via IL-6R and GP130 activates different signaling cascades including the JAK2/STAT3 signaling [92]. Thus, the hepatic AMR and IL-6R/GP130 share the same signaling pathway.

1.3. The liver between structure and function

As the central metabolic organ, the liver regulates many metabolic processes. In the carbohydrate metabolism it ensures glycogen synthesis and the regulation of the blood sugar level. In lipid metabolism, the liver is responsible for the synthesis and breakdown of fatty acids as well as the synthesis of bile acids (BA) from cholesterol. The synthesis and degradation of blood plasma proteins (e.g., acute phase proteins or components of the complement system) and coagulation factors also take place in the liver. Moreover, the liver is the most important detoxification and excretion organ as it filters e.g., toxins associated with food or toxic metabolites from the blood (detoxification); also, it converts them into non-toxic substances, which are then excreted by the urine or are eliminated with the bile. Additionally, under certain conditions, the liver is capable to completely regenerate its volume and function after liver damage [93].

1.3.1 The micro- and macroanatomy of the liver

The liver is an accessory gland of the middle intestine and is the largest metabolic organ of the vertebrate organism. In humans it is positioned in the right upper abdomen under the diaphragm [94]. Mice are used in research as experimental animals due to the similarities in their anatomical and physiological organization of the liver. While the human liver is clearly divided into two large liver lobes [95], the murine liver consists of four liver lobes (the left lateral lobe, the right lateral lobe, the caudate lobe and the median lobe) [96]. The left and right lateral lobe are additionally separated by *incisurae* that are slightly movable against each other (the left lateral lobe (*lobus hepatis sinister lateralis* and *medialis*); the right lateral lobe (*lobus hepatis dexter lateralis dorsalis* and *medialis*)). The *hepatis dexter lateralis ventralis* (median

Introduction

lobe) and the *lobus caudatus* (caudate lobe) are found in the hilum area. The liver gate (*porta hepatis*), which is the entry and exit point for nerve fibers, blood vessels, bile, and lymphatic vessels, is located between these lobes [96]. The hepatic artery (*A. hepatica*) branches off directly from the aorta and supplies oxygen-rich blood into the liver [97]. The portal vein (*V. portae*) also enters at the liver gate, loaded with venous, nutrient-rich blood. Since the venous blood comes from the unpaired abdominal organs, it is also enriched with metabolic breakdown products. In brief, the liver gate system represents a supply and disposal system for the digestive organs of the body. Additionally, the bile ducts emerging from the liver, unite at the hepatic portal to form the common hepatic duct. The bile is either released directly into the intestine (liver bile) or is stored in the gallbladder (fig. 4a) [98].

The microarchitecture of the human and murine liver consists of hexagonal 1 x 2 mm large central vein lobes (*Lobuli hepatici*; fig. 4b). The periportal field is always formed at the corner point of three aligned liver lobes. In this field, the terminal branches of the *V. portae* and *A. hepatica* as well as the derivative branches of the bile ducts form the so-called Glisson's triangle (Glisson's triad). The hepatocytes, which represent 80% of all cells in the liver, are arranged in a ray around the central vein. They are the most diverse cell type in the whole body as they inherit all main functions of the liver [99]. Hepatocytes are polarized, as they form an apical membrane and a basolateral membrane, which are separated from each other by tight junctions formed with other hepatocytes. The basal side of the hepatocytes is separated from the liver sinusoidal endothelial cells (LSECs) by the space of Disse. In this space, the exchange of substances between blood and hepatocytes is mediated [100]. At the apical side of the hepatocytes the bile duct canaliculi are formed in order to collect the secreted bile and discharge it into the bile ducts [101]. In addition to the endothelial cells, there are other non-parenchymal cells in the liver: Kupffer's stellate cells are the irregularly shaped macrophages of the liver and are found luminally on the wall of the sinusoid. On the one hand, they phagocytize substances and pathogens from the blood (e.g., endotoxins, bacteria, and viruses) and therefore fulfill an important function in the immune defense. On the other hand, they secrete mediators that regulate the immune response and are important for tissue integrity (cytokines, NO, and ROS (reactive oxygen species)) [102, 103]. Para sinusoidal Ito cells (hepatic stellate cells) are fat-storing, interstitial cells. They synthesize the hepatocyte growth factor (HGF) and store vitamin A. Furthermore, they are important for the production of the extracellular matrix [104]. A summary of the cellular architecture of the liver is shown in fig. 4.

Introduction

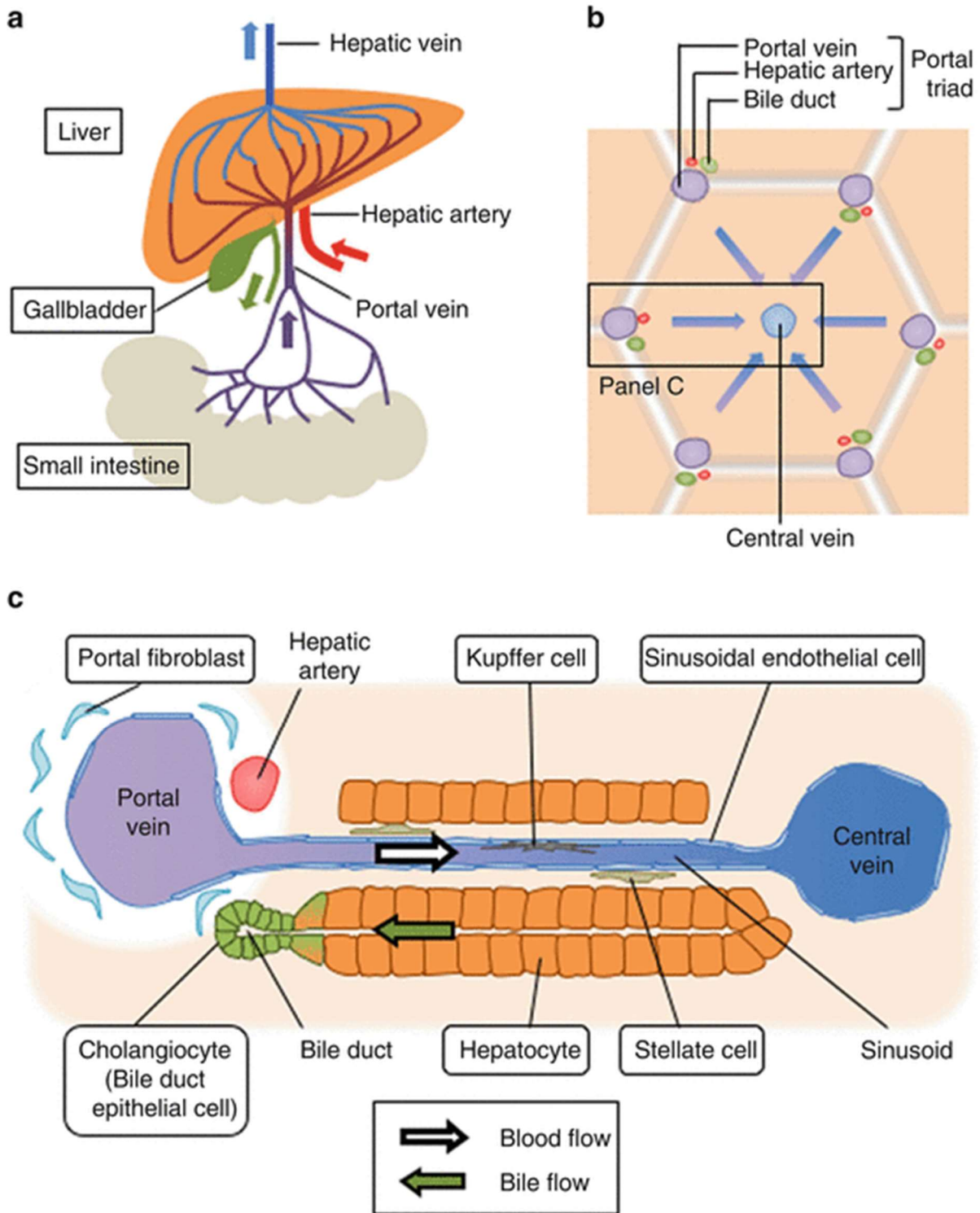


Figure 4. Functional anatomy of the liver. (a) The liver is directly connected to the blood flow of the small intestine via the portal vein while bile is secreted from the gallbladder into the small intestine. (b) Hexagonal structure of the liver lobules with the central vein and the portal triad (Glisson's triad). (c) Functional anatomy of the liver lobules with typical cells appearing in the liver. Nutrient rich blood from the small intestine enters the liver through the portal vein and flows through the liver lobule into the central vein. Blood flow from the hepatic artery provides oxygen supply of hepatic cells. The bile secreted by hepatocytes is assembled through the bile canaliculi which are located between the hepatocytes. It enters the bile duct and is stored in the gallbladder. License Number 4950671052767 [105]

1.3.2 Bile acids and the enterohepatic cycle

Bile formation is an osmotic process that is caused by active secretion of the bile components from liver parenchymal cells into the bile duct. The hepatic bile consists of water, bile salts (BS), bilirubin, fat (cholesterol, fatty acids, and lecithin) and inorganic salts [106]; whereas BS represent the largest proportion of dissolved substances in the bile. Bile is secreted from the gallbladder into the small intestine and is physiologically needed for the efficient lipid absorption from food. It also regulates cholesterol homeostasis and the metabolism or excretion of endogenous (e.g., bilirubin) and exogenous (e.g., heavy metals, medication) substances. To prevent the loss of bile salts through excretion, two different mechanisms work synergistically. BS are steadily synthesized in liver parenchymal cells and then reabsorbed from the intestine [107].

In hepatocytes, 7-hydroxycholesterol is synthesized from cholesterol through several enzymatic steps. Primary BA such as cholic acid (CA) and chenodeoxycholic acid (CDCA), – are synthesized from 7-hydroxycholesterol. These primary BA are conjugated either with taurine or glycine to form the primary bile salt conjugates: Glycocholic acid (GCA), Taurocholic acid (TCA), Glycochenodeoxycholic acid (GCDCA) and taurochenodeoxycholic acid (TCDCA). At the apical membrane of hepatocytes, these primary BA conjugates are secreted into the bile duct and enter the gallbladder. The active canalicular secretion of the conjugated BS occurs either via the transporter BSEP (Bile Salt Export Pump, Abcb11) [108, 109], or is passively mediated through the MRP2 transporter (multidrug resistance protein 2, Abcc2) and sub-canalicular vesicles [110, 111]. Once in the intestine, bile salts are either deconjugated by intestinal bacterial or they are converted into the secondary BA deoxycholic acid (DCA) and the toxic lithocholic acid (LCA). Over 95% of the bile salt metabolites in the intestine are re-absorbed through passive diffusion from the gastrointestinal wall membrane into the portal vein blood. The absorption into hepatocytes is mediated via the sinusoidal sodium-dependent bile salt transporter NTCP (Na^+ -taurocholate cotransporting polypeptide; Slc10a1) and members of the sodium-independent organic anion transporting polypeptide (SLCO/OATP) transport family [109, 112, 113]. They are located on the basolateral membrane of hepatocytes and distributed over the liver lobule. Up to 80% of the conjugated (e.g. TCA) and 50% of the unconjugated BS are transported through this transporter [109, 114-116].

Furthermore, the transporter MRP3 (Multidrug Resistance Protein 3, Abcc3) is located on the basolateral membrane of hepatocytes. MRP3 mediates ATP-dependent transport of conjugated primary BA from hepatocytes into the sinusoidal blood to prevent an intrahepatic enrichment of toxic BA [117]. This process of secretion from hepatocytes through the gallbladder into the intestine and reabsorption from the intestine into the hepatocytes is called the enterohepatic circulation of BA. Thereby, only a small part of the water-soluble BAs are excreted via feces and urine and needs to be newly synthesized.

1.4 The basics of liver injury and regeneration

In humans and rodents, there is a close correlation between body size and liver mass that is accompanied by a pronounced ability of the liver to regenerate after damage or tissue injury [118]. In principle, two mechanisms of liver regeneration can be distinguished:

If there is a functional impairment due to a chronic liver injury (e.g. chronic poisoning, alcohol abuse, or chronic hepatitis), which leads to a limited replication potential of hepatocytes, an optional cellular compartment in the liver is activated [119, 120]. These cells exhibit properties of stem cells and are inactive in the normal state [121, 122]. Proliferating cells quickly emerge from this cell compartment and differentiate into hepatocytes or cholangiocytes [123, 124]. In rodents this bi-potent cell type is called oval cell, the human equivalent is the hepatic progenitor cell (HPC) [125].

In case the acute liver injury (e.g. trauma, acute poisoning, liver resections or infections) is accompanied with a loss of liver mass without losing the functional integrity of the remaining liver tissue, the regeneration is mainly guaranteed through differentiated hepatic cells like the hepatocytes and cholangiocytes [93, 126]. Therefore, a compensatory hyperplasia of the remaining liver tissue is developed.

1.4.1 Cholestasis as example for chronic liver injury

One type of chronic liver damage is cholestasis. Cholestasis is induced by restricted or interrupted bile secretion and flow, resulting in an enrichment of bile substances in the blood and the liver parenchyma. Functional impairment of hepatocytes or the mechanical obstruction of the excretory pathway of the draining bile ducts lead to interrupted bile secretion. A distinction is made between intrahepatic and extrahepatic cholestasis [127].

In intrahepatic cholestasis, bile excretion from the hepatocytes is disrupted and the bile is retained in the liver. Intrahepatic cholestasis can be caused by a hepatocellular carcinoma, liver cirrhosis or primary biliary cholangitis (PBC). In addition, it has been shown that rats treated with endotoxin (LPS) develop a sepsis induced cholestasis [128].

An obstructive, extrahepatic cholestasis is caused by mechanical disruption of the biliary tract, e.g., by carcinomas or gallstones [127]. In the experimental animal model, obstructive cholestasis is caused by bile duct ligation (BDL) [127, 129]. Laboratory parameters characterizing a cholestasis in humans are an increase in conjugated bilirubin, enhanced levels of alkaline phosphatase (ALP) and γ -glutamyl transferase (γ -GT) in the serum as well as different expression profiles of hepatobiliary transport proteins [130, 131].

1.4.2 Partial hepatectomy as example for an acute liver injury and regeneration

Liver resection is one of the most important therapeutic approaches for liver cancer treatment (hepatocellular carcinoma, HCC; cholangiocellular carcinoma, CCC) [132, 133]. However, liver resection is limited by the required residual volume and the ability of the liver to regenerate. A resected and transplanted liver which is too small increases the risk of post-hepatectomy liver failure [134]. The transplanted liver is either too small in size for the body mass of the recipient (<0.8 - 1%); or the residual liver is too small for the donor. This can lead to life-threatening organ failure (small for size syndrome) [135]. A better understanding of the processes involved during liver regeneration could lead to the development of therapies that would improve survival of patients and organ donors after liver resection or liver transplantation.

To study the regenerative capability of the liver, different *in vivo* models are used. A distinction is drawn between surgical [partial hepatectomy (PHx) and BDL] or chemical/toxical (e.g., carbon tetrachloride (CCl₄), D-Galactosamine or acetaminophen) models. Using the model of PHx, 70% of the physiological liver mass is removed. The ligation of the bile duct leads to biliary congestion by ligating the common hepatic duct in the liver, which results in fibrosis after a short time period. Through an application of CCl₄, hepatotoxic liver injury (hepatitis) is chemically induced that leads to apoptosis of the liver parenchyma [136]. The advantage of this application is, in contrast to PHx or BDL, the easy performance. Disadvantages of this model are the low reproducibility and a higher variation of the resulting liver damage and regeneration [137]. With a dissection of more than 70% of the total liver volume, the regenerative capacity is reduced and the mortality is increased in the mouse model of PHx [138].

1.4.2.1 Liver regeneration in mice

The ability of the liver to regenerate was made public by the pioneering 2/3 PHx model shown on rodents by Higgins and Anderson in 1931 [139]. After the surgical removal of two thirds of the liver (70%), the remaining liver tissue increases until the original liver mass is restored. Under physiological conditions the cell cycle of mature hepatocytes is usually at rest (G₀ stage). In rodents, 44-48 hours after a PHx an orchestrated division of almost all mature hepatocytes (95%) takes place [140]. If only 30% of the liver is dissected, the residual liver tissue will regenerate slowly, and the division of the hepatocytes is not synchronized [135]. In the liver lobule, DNA synthesis starts in hepatocytes that surround the portal vein and it proceeds in hepatocytes towards the central vein [141]. After 24 hours, about 1/3 of the hepatocytes divide again. The division of the non-parenchyma cells takes place approx. 12-24 hours after the first hepatocyte mitosis. Every hepatocyte passes the cell cycle 1.4 times on average before it returns to the G₀-phase [142]. The liver tissue increases until an optimal ratio

Introduction

between liver and body mass is reached, ensuring perfect metabolic function [143]. Strikingly, serial transplantations performed in mice showed that adult murine hepatocytes are comparable to hematopoietic stem cells and can undergo up to 80 cell divisions [144], although mammalian cells usually age after 20-30 cell divisions [135]. Thus, the healthy liver can maintain its organ-specific function after injury until it is fully regenerated. In rodents and humans, liver regeneration is completed within approximately 7 - 14 days [145, 146].

1.4.2.2 IL-6 signaling and liver regeneration

As acute phase cytokine, IL-6 is important for liver regeneration after PHx or liver injury in general since IL-6 knock out mice display an impaired acute phase response [147]. An inflammatory stimulus of KCs leads to expression and secretion of TNF α . This stimulus promotes the expression of IL-6 [142]. IL-6 signaling thereby facilitates the expression of hepatocyte growth factor [148]. Genetic deletion of IL-6 leads to impaired liver regeneration, while treatment with recombinant IL-6 reverts impaired liver regeneration [149]. Additionally, recent studies from Modares *et al* revealed that blockade of overall IL-6 signaling or selective inhibition of IL-6 trans-signaling leads to impaired liver regeneration and survival in the murine model of PHx [148]. Similar results were already shown in the model of CCl₄ induced liver damage by blocking the IL-6 trans-signaling [150].

1.5 Bleeding risk, thrombosis, and thrombocytopenia after liver injury

Platelets are major players in hemostasis and thrombosis but also modulate inflammation, angiogenesis, apoptosis, and stem cell recruitment after organ damage [151]. The hemostatic system is constantly in a balance between pro- and anti-hemostatic processes to avoid bleeding complications on the one hand and thrombotic events on the other hand.

Far-reaching hemostatic changes in patients with liver disease are known. Many proteins of the hemostatic system are synthesized in the liver such as fibrinogen and the coagulations factors II, V, VII, IX, X, XI and XII [152-155]. Only two hemostatic proteins, namely vWF and Factor VIII, are not mainly synthesized in the liver, [156-158]. Furthermore, a diseased liver shows diminished hepatic clearance due to a reduced ability to metabolize activated proteins of the hemostatic system [159]. Therefore, liver diseases are usually characterized by decreased coagulation but also hypercoagulability is examined, e.g. in patients with liver cirrhosis [159, 160]. Beside alterations in coagulation, thrombocytopenia and platelet defects are described in patients with liver disease often leading to bleeding complications. This

Introduction

suggests a bivalent role of platelets in liver disease [161-164]. Additionally, platelet invasion into the sinusoidal space of the diseased liver tissue was already shown in mice after BDL [165].

The recruitment of platelets into the liver is supported by systemic inflammatory stimuli. The current consensus is that the close connection between blood and liver cells in the sinusoids of the liver enables platelets to participate in inflammatory processes upon liver injury. This hypothesis is supported by new studies from Sitia *et al*, who were able to demonstrate a reduced virus-specific T-cell-mediated inflammation after antithrombotic therapy in chronic hepatitis B infection [166]. Additionally, various studies in recent years indicated that platelets could modulate liver regeneration after liver damage and exert protective effects by inhibiting fibrotic events. According to literature, there is evidence for platelets supporting liver regeneration via serotonin, insulin-like growth factor 1 (IGF-1) and hepatocyte growth factor (HGF) [161, 167-169]. An increase in platelet counts showed an improvement in acute hepatitis, whereas cholestasis-induced liver fibrosis in mice worsened upon thrombocytopenia [169, 170]. In contrast, platelet recruitment leads to reduced microcirculation through the release of serotonin after virus-induced hepatitis [171]. Therefore, it is currently assumed that platelets play a bivalent role in liver diseases, which are often associated with thrombocytopenia, but also lead to platelet recruitment and thus to ischemic and inflammatory events. However, the molecular mechanisms underlying platelet-mediated effects after liver damage are largely unknown.

1.6. Scope of the study

In literature, platelet mediated mechanisms after liver injury are controversially discussed. To date, it is only incompletely understood whether platelets act hepatoprotective or not. Nevertheless, various reports provided evidence that primary hemostasis is differently affected in various liver diseases, thereby either preventing or even further accelerating liver injury.

In this thesis, the role of platelets in liver damage and liver regeneration was investigated using two operation models for acute and chronic liver injury, namely PHx and BDL. At first, the aim of the study was to analyze platelet function, thrombus formation and bleeding risk in mice undergoing the two different liver injury models. Notably, among common agents inhibiting platelet function like NO and PGI₂, an analysis of BA mediated effects on platelet function was considered. To study hemostatic dysfunction, all experiments were initially performed using wildtype mice (C57Bl6/J mice), to get a precise overview of the influence of BDL and PHx on primary hemostasis alone.

Additionally, a detailed analysis of the regulation of platelet counts after PHx was performed, as liver injury is often accompanied by thrombocytopenia. Therefore, different knock out mouse models were used which are known or assumed to be involved in the regulation of hepatic TPO. It is already known that hepatic TPO production is regulated through the hepatic AMR in steady state conditions. However, nothing is known about TPO regulation via the AMR signaling cascade upon acute inflammation and after liver resection. Likewise, nothing is known about the impact of IL-6R signaling in TPO biosynthesis and regulation of platelet counts. Therefore, TPO signaling pathways in the liver tissue of wildtype and IL-6R deficient mice before and after liver resection were examined. In comparison, IL-6R mediated signaling was investigated in *Asgr2*^{-/-} mice. As TPO is the ligand for the c-Mpl receptor that subsequently induces megakaryopoiesis, c-Mpl deficient mice were used as a tool to study liver regeneration under thrombocytopenic conditions.

Overall, the aim of this thesis was to gain a deeper understanding how platelet defects and defective hemostasis develop upon acute and chronic liver injury and how platelet counts are regulated in mice especially with reduced liver tissue. Thus, the results of this study might help to develop new therapeutic approaches to improve the outcome of patients with liver disease.

2. Material

2.1 General devices and equipment

If not other stated general material like tubes, falcons, pipette tips, syringes, etc. were purchased from ErgoOne, Starlab, Sarstedt and Braun.

2.1.1 General Devices

Equipment	Model	Company
Micropipettes	Research plus	Starlab & Eppendorf
Multichannel pipette	Peqette	Peqlab
Multipipette	Multipette® plus	Eppendorf
Pipettor	Pipetboy acu	Integra Biosciences
Magnetic stirrer	RET basic	IKA Labortechnik
Benchtop, pH-Meter	WTW pH526	Xylem Inc.
Roll mixer	RM5	CAR
Thermo shaker	TS-100C	bioSan
Glass capillaries	minicaps®, Na-hep	Hirschmann
Citrate tube	BD Vacutainer; BD	BD BioSciences
Cover slip	24x60 mm	Kindler
FACS tubes	5 ml tube, 75 x 12 mm, PS	Sarstedt
96-Well microtiter plate	Luminunc™ F96 Microwell™	VWR
Filter paper		Whatman
Bench scale	AE166	Mettler -Toledo
Bench scale	Secura®	Sartorius
Bench scale	Practum®	Sartorius
Microwave	NN-E201WM	Panasonic
Centrifuge, Mini	D-6020	neoLab
Centrifuge, tabletop	5415-C	Eppendorf
Centrifuge, cooling	5424-R	Eppendorf
Centrifuge, cooling	5804-R	Eppendorf
Centrifuge, tabletop	2-16	Sigma-Aldrich
Photometer	BioPhotometer® D30	Eppendorf
Cuvette	µCuvette® G1.0.	Eppendorf
Syringe pump	KDS100	KD Scientific Inc.

2.1.2 Equipment for tissue preparation and histology

Equipment	Model	Company
Automatic microtome	Microm HM355	Thermo Fisher Scientific
Paraffin Dispenser	round model	Medax
Humidity Chamber		Simpore Inc.
Paraffin section flotation bath	MH8517	Electrothermal
Precellys® 24 homogeniser	432-3750	Bertin Technologies

2.1.3 Equipment for electrophoresis, western blot and imaging

Equipment	Model	Company
Nitrocellulose membrane		GE Healthcare
Universal power supply	PowerPac™	BioRad Laboratories
Semi-Dry blot system	PerfectBlue™	Peqlab
Double gel system	PerfectBlue™	Peqlab
Horizontal agarose gel	PerfectBlue™ Wide Format Gel System	Peqlab
Chemiluminescence Imager	Vilber Fusion-FX6	Vilber Lourmat
Microscope, inverse	Axio Observer D1	Zeiss
Microscope- color camera	Axiocam 503 color	Zeiss
Microscope	Axioskop	Zeiss
Microscope- color camera	Axiocam 105 color	Zeiss
Microscope- lamp module	HXP 120C	Zeiss

2.1.4 Special equipment for sample analysis

Equipment	Model	Company
Mikrotiter plate reader	GloMax® Multi+	Promega
Spotchem-biochemical analyzer	EZ SP-4430	AxionLaB
Reflotron®	Plus	Roche
ViiA™ 7 Real-Time PCR System	7 Flex System	Thermo Fisher Scientific
PCR Cycler	Mastercycler nexus gradient	Eppendorf
Flow chamber system		Maastrich Instruments
Flow cytometer	FACS Calibur	BD BioSciences
Hematology analyzer	KX-21N	Sysmex

2.1.5 Special Equipment for surgical procedures

Equipment	Model	Company
Clamps	13 cm	S&S Medizintechnik
Needle holder	15 cm, # 03E-022	S&S Medizintechnik
Scissors, cutticle	11,5 cm, # BC106R	S&S Medizintechnik
Scissors	14 cm, #BC242R	S&S Medizintechnik
Forceps, surgical	11,5 cm, # BD555R	S&S Medizintechnik
Forceps, anatomical	11,5 cm, # BD043A	S&S Medizintechnik
Forceps, micro	07.61.82	Medicon eG
Forceps, tying	FD-281 R	Aesculap AG
Suture tie, vicryl 5-0	#V396H	Ethicon
Suture tie, mersilene 4-0	# EH7632H	Ethicon
Clipper	Isis Aescular GT420	Braun
Transparent polyurethane film	Opsite	Smith & Netphen
Heating mat	ThermoLux®	Wiite + Sutor GmbH
Binokular	Mod.A1; s/n 250023	Optech Labcenter SpA
Flowprobe	Transonic® Flowprobe	Transonic Systems Inc.

2.2. Chemicals and buffer

2.2.1 Chemicals

Chemical	Company
0.9% NaCl solution	Fresenius Kabi
4-2-Hydroxyethyl-piperazinyl-ethanesulfonic acid (HEPES)	Carl ROTH GmbH
4',6-diamidino-2-phenylindole (DAPI)	Roche
Acetic acid (CH ₃ COOH)	Sigma-Aldrich
Acrylamide	Carl ROTH GmbH
Adenosine diphosphate (ADP)	Sigma-Aldrich
Agarose	Sigma-Aldrich
Ammonium persulfate (APS 10%)	Sigma-Aldrich
Apyrase	Sigma-Aldrich
Bovine serum albumin	Sigma-Aldrich
Buprenorphine	Sigma-Aldrich
Calcium chloride (CaCl)	Sigma-Aldrich
Chloroform	Sigma-Aldrich
Citric acid (C ₆ H ₈ O ₇)	Sigma-Aldrich
Collagen (Horm)	Takeda
Collagen related peptide (CRP)	University of Cambridge, UK
Dithiothreitol (DTT)	Sigma-Aldrich
DMSO (Dimethylsulfatoxid)	Sigma-Aldrich
DNaseI recombinant RNase - free	Roche
EDTA (ethylenediaminetetraacetate)	Sigma-Aldrich
Eosin	Carl ROTH GmbH
Ethanol 100% (EtOH)	Merck Millipore
Ferric (III) chloride (Fe ₃ Cl)	Sigma-Aldrich
Fibrinogen	Sigma-Aldrich
GCDC	Carl ROTH GmbH
Glucose	Carl ROTH GmbH
Glycine	Carl ROTH GmbH
Goat serum	Bio & Sell
Hemalun	Carl ROTH GmbH
Heparin-Natrium-25000	Braun
IGEPAL® CA-630	Sigma-Aldrich
Isoflurane	Piramal critical care
Ketamin (Ketaset)	Zoetis
Magnesium chloride (MgCl)	Carl ROTH GmbH
Methanol 100% (MeOH)	Merck Millipore
Mounting medium Aquatex	Merck Millipore
Neuraminidase (<i>Vibrio Cholerae</i>)	Roche
PAR4-peptide	Tocris Bioscience

Material

Paraffine	Carl ROTH GmbH
Paraformaldehyde 4%	Carl ROTH GmbH
Phosphate buffered saline (PBS)	Sigma-Aldrich
Ponceau-solution	Sigma-Aldrich
Potassium permanganate (KMnO ₄)	Merck Millipore
Powdered skim milk	Frema Reform
Precision Plus Protein Dual Color Standards	BioRad Laboratories
Prostaglandin	Merck Millipore
Proteinase-inhibitor (cOmplete Tablets Mini Easypack)	Roche
RNase-1	Thermo Fisher Scientific
Roti Histokitt	Carl ROTH GmbH
Roti Histol	Carl ROTH GmbH
Roti Quant 40%	Carl ROTH GmbH
Roti [®] Histol	Carl ROTH GmbH
Sodium chloride (NaCl)	Sigma-Aldrich
Sodium orthovanadate (Na ₃ VO ₄)	Sigma-Aldrich
Sodium nitroprussid (SNP)	Merck Millipore
Sodium phosphate dibasic (Na ₂ HPO ₄)	Carl ROTH GmbH
Sodium dihydrogenphosphate(NaH ₂ PO ₄)	Carl ROTH GmbH
Sodium acid (NaN ₃)	Carl ROTH GmbH
Sodium hydrogencarbonate (NaHCO ₃)	Merck Millipore
TC	Carl ROTH GmbH
TCDC	Carl ROTH GmbH
TDC	Carl ROTH GmbH
Tetramethylethylenediamine (TEMED)	Carl ROTH GmbH
Thrombin 20U	Roche
TLC	Carl ROTH GmbH
Trisodium citrate	Carl ROTH GmbH
Triton [™] X-100	Sigma-Aldrich
Trizma [®] -base	Sigma-Aldrich
Trizma [®] -HCl	Sigma-Aldrich
TRIZol [®]	Sigma-Aldrich
Tween20	Merck Millipore
U46619 (U46)	Tocris Bioscience
Xylazine (Xylazinhydrochlorid)	Serumwerk Bernburg
β-mercaptoethanole	Carl ROTH GmbH
ε-aminocaproic acid (C ₆ H ₁₃ NO ₂)	Sigma-Aldrich

2.2.2 Buffers & Solutions

Buffer/Solution	Recipe
IP-Buffer (stock solution 5x)	15 mM Tris-HCl 155 mM NaCl 1 mM EDTA 0,005% NaN ₃ 1 L dH ₂ O
Annexin V binding buffer	10mM Hepes (pH: 7.4) 140 mM NaCl 2.5 mM CaCl ₂
blot buffer A	36,3 g Trizma-Base 200 mL MeOH 800 mL dH ₂ O pH 10,4
blot buffer B	3,03 g Trizma-Base 200 mL MeOH 800 mL dH ₂ O pH 10,4
blot buffer C	5,2 g ε-aminocaproic acid 200 mL MeOH 800 mL dH ₂ O
citrate buffer	41 mL 0.1 M trisodium citrate 9 mL 0.1 M citrate acid 450 mL dH ₂ O pH 6.0
decalcification buffer	10% EDTA PBS pH 8.0
heparin-solution (20 U/ml)	40 µl heparin natrium 5000 I.E 10 ml PBS
human Tyrode's buffer	137 mM NaCl 12 mM NaHCO ₃ 2.8 mM KCl 0.4 mM NaH ₂ PO ₄ 5.5 mM glucose pH 7.4
Laemmli (6x)	0,93 g DTT 1 g SDS 7 mL 4x stacking gel buffer 3 mL glycerine 0.02% bromphenol blue
Lysis buffer (5x stock solution)	5 x IP-Puffer (2mL) 5% IGPAL

Material

murine Tyrode's buffer	5 mM NaVO ₄ 1x Proteaseinhibitor cOmplete plus Roche 134 mM NaCl 12 mM NaHCO ₃ 2.9 mM KCl 0.34 mM Na ₂ HPO ₄ 20 mM HEPES 10 mM MgCl ₂ 5 mM glucose 0.2 mM CaCl ₂ pH 7,35
RIPA-Puffer	150 mM NaCl 50 mM Tris 0.1% SDS 0.5% sodium deoxycholate 1% TritonX-100
SDS-PAGE-running buffer (5x stock solution)	15.1 g Trizma-Base 72 g glycine 5 g SDS <i>ad</i> 1 L dH ₂ O pH 8.3
SDS-PAGE stacking gel buffer (4x stock solution)	6.05 g Trizma-Base 80 mL dH ₂ O pH 6.8 <i>ad</i> 100 mL dH ₂ O 0.4 g SDS
SDS-PAGE running gel buffer (4x stock solution)	91 g Trizma-Base 400 mL dH ₂ O pH 8,8 <i>ad</i> 500 mL dH ₂ O
Tris buffered saline (TBS, 5x stock solution))	15,8 g Trizma-HCl 45 g NaCl <i>ad</i> 1 L dH ₂ O pH 7,6
TBS-T	100 mL 5x TBS-Puffer 500 µL Tween 400 mL dH ₂ O
Tris acetate EDTA (TAE)-buffer	242 g Trisma-base 57.1 ml acetic acid 100 ml 0.5% EDTA pH = 8

2.3 Antibodies

2.3.1 Primary antibodies

Antigen	Host species	Clonality	Use	Company
TPO sc-398525	mouse	polyclonal	WB	Santa Cruz
STAT3 #12604	rabbit	monoclonal	WB	Santa Cruz
Phospho-STAT3 Tyr705, #9145	rabbit	monoclonal	WB	Cell Signaling
STAT5 #9363	rabbit	monoclonal	WB	Cell Signaling
Phospho-STAT5 Tyr694, #9351	rabbit	monoclonal	WB	Cell Signaling
JAK2 #3230	rabbit	monoclonal	WB	Cell Signaling
Phospho-JAK2 Tyr1007/1008, #3771	rabbit	monoclonal	WB	Cell Signaling
VASP #3112	rabbit	monoclonal	WB	Cell Signaling
Phospho-VASP Ser157 #3111	rabbit	monoclonal	WB	Cell Signaling
Phospho-VASP Ser239 #3114	rabbit	monoclonal	WB	Cell Signaling
Actin #4979	rabbit	monoclonal	WB	Cell Signaling
GAPDH 14C10, # 2118	rabbit	monoclonal	WB	Cell Signaling
GPIb α	rat	monoclonal	IF	Emfret analytics
GPIX	rat	monoclonal	IF	Emfret analytics
GPIb β (DyLight488)	rat	monoclonal	flow chamber	Emfret analytics

2.3.2 Secondary antibodies

Antigen	Species	Clonality	Conjugate	Dilution	Company
Anti-rabbit	goat	polyclonal	horseradish-peroxidase	1:10000	Invitrogen
Anti-mouse	goat	polyclonal	horseradish-peroxidase	1:10000	Invitrogen
Anti-rat	goat	polyclonal	Alexa-Fluor555	1:200	Invitrogen
Anti-rat	goat	polyclonal	Alexa-Fluor594	1:250	Invitrogen

2.3.3 Antibodies for Flow Cytometry

All Antibodies used for flow cytometric analysis were monoclonal except for vWF and Neu-1 (both polyclonal) and used in a 1:10 dilution in respective Tyrode's buffer.

Antigen	Term/Clone	Species	Company
Mouse CD62P	P-selectin/Wug.E9	rat	Emfret analytics
Mouse CD41/CD61	JON/A	rat	Emfret analytics
Mouse CD61	Luc.H11	rat	Emfret analytics
Mouse GPVI	JAQ1	rat	Emfret analytics
Mouse CD49e	Tap.A12	rat	Emfret analytics
Mouse CD42b	Xia.G5	rat	Emfret analytics
Mouse vWF	polyclonal	rat	Emfret analytics
Human CD41/CD61	PAC-1	mouse	BD BioSciences
Human CD62P	P-Selectin	mouse	BD BioSciences
Human Neu-1	polyclonal	mouse	Santa Cruz Biotech.

2.3.4 Peptides and dyes for flow cytometric analysis

Peptide/Dye	Conjugate	Dilution	Company
Thiazole Orange (ReticCount)	-	1:1000	BD BioSciences
RCA-1	FITC	1:100	Vectorlabs
WGA	FITC	1:100	Vectorlabs
EGA	FITC	1:100	Vectorlabs
Annexin V	Cy5	1:10	BD BioSciences

2.4 Oligonucleotides

All used Oligonucleotides in this study were synthesized and purchased from Eurofins Scientific.

Target gene	Direction	Primer sequence
<i>Il-6r</i>	forward	5'-CTGCCAACCTTGTGGTATCAG-3'
	reverse	5'-GCAGCAAGTAGTAACTCGGGT-3'
<i>Asgr1</i>	forward	5'-ACGTGAAGCAGTTAGTGTCTG-3'
	reverse	5'-CCTTCATACTCCACCCAGTTG-3'
<i>Asgr2</i>	forward	5'-GCTCAGTGGCGATGATGAAC-3'
	reverse	5'-AGAGGCGCTGAGGAAAGG-3'
<i>Tpo</i>	forward	5'-CACAGCTGTCCCAAGCAGTA-3'
	reverse	5'-CATTACAGGTCCGTGTGTC-3'
<i>Gapdh</i>	forward	5'-GGTGAAGGCGGTGTGAACG-3'
	reverse	5'-CTCGCTCCTGGAAGATGGTG-3'
<i>Mpl</i>	forward WT	5'-GTCTCCATGGAGGCTTAGGTGGGA-3'
	forward KO	5'-GAAGAGCTTGGCGGCGAATGGGCT-3'
	reverse KO	5'-TCCAAGGTAAGCACTGAAGTCCA-3'

2.5 Kits

Kit	Catalog No.	Company
PGI2 Kit	CSBE13698m	CUSABIO BIOTECH
NO Assay	KGE001	R&D Systems
ELISA Kit for Tissue Plasminogen Activator (tPA)	SEA525Mu	Usn Life Science Inc
Mouse plasmin-antiplasmin complex ELISA	CSB-E08436m	CUSABIO BIOTECH
Mouse IL - 6 DuoSet ELISA	DY406	R&D Systems
Mouse CXCL12/SDF-1 DuoSet ELISA	DY460	R&D Systems
Mouse Thrombopoietin DuoSet ELISA	DY488	R&D Systems
Serotonin ELISA Kit	ADI-900-175	Enzo Life Sciences
Precellys Lysing Kit	P000918-LYSK0-A	Bertin Technologies
RNeasy Mini Kit	74104	Qiagen
InPromII Reverse transcription System	A3800	Promega
Fast Sybr Green Master Mix	4385610	Life Technologies
KAPA-Mouse-Genotyping Hot Start Kit	07-KK7352-01	Peqlab
ALT/AST/Bilirubin	77182	Arkray
ALP	77176	Arkray
Mouse Von Willebrand Factor A2 ELISA	ab208980	Abcam
Neuraminidase Assay Kit	ab138888	Abcam

2.6 Software

Software	Company
Microsoft Office 2010	Microsoft Corporation
Graph Pad Prism 7.02	GraphPad Software
Fiji Is Just ImageJ	NIH Image
FlowJo Single Cell Analysis v10	FlowJo LLC
ViiA™ 7 Software	Thermo Fisher Scientific
ZEN 2012 (blue)	Zeiss
LabChart Reader 8.1.6 Windows	ADInstruments

2.7 Animals

All mice used for animal experiments were either obtained from commercial animal suppliers or generated in the animal facility of the Heinrich Heine University of Düsseldorf (ZETT). All mice were kept under standard laboratory specific pathogen-free (SPF) conditions according to the guidelines of FELASA (Federation of European Laboratory Animal Science Association). Mice were kept in groups in plastic cages (GMOs) with a standardized 12 h day/night rhythm. They were fed with standard rodent chow and water *ad libitum*.

For the analysis of wild type mice, C57BL/6J mice were obtained from Janvier Labs. *IL-6R^{-/-}* (Stock No: 012944) mice were obtained from Jackson Laboratory. *Mpl^{-/-}* mice (B6;129S1-Mpl^{tm1Wsa}/Mpl^{tm1Wsa}) were kindly provided by Prof. Ute Modlich (Paul Ehrlich Institute, Langen). *IL-6R^{-/-}* and *Mpl^{-/-}* mice were raised in inbreeding strains in the animal facility of the Heinrich Heine University of Düsseldorf (ZETT). Samples from *Asgr2^{-/-}* mice (Stock No: 002361, Jackson Laboratory) were kindly provided by Prof. Karin Hoffmeister (Versiti Blood Research Institute, WI). All experiments carried out in this work were performed with male mice at the age of 8-16 weeks. All animal experiments were conducted according to the Declaration of Helsinki and the guidelines from the Directive 2010/63/EU of the European Parliament on the protection of animals. The protocols were approved by the Heinrich-Heine-University Animal Care Committee and by the State Agency for Nature, Environment and Consumer Protection of North Rhine-Westphalia (LANUV, NRW; Permit Number 84-02.04.2015.A462; 84-02.04.2016.A196; O 86/12 and 84-02.04.2016.A493).

Material

Table 1. Summary of experimental mice strains used throughout this thesis including the scientific focus and the experimental approaches for which they were sacrificed.

Mice strains	Term	Objective	Experimental model
C57Bl6/J	WT	Hemostasis and Thrombosis after liver injury & TPO regulation	Sham PHx + BDL
<i>IL-6R</i> ^{-/-}	<i>IL-6R</i> ^{+/+} <i>IL-6R</i> ^{-/-}	TPO regulation & Hemostasis	PHx
<i>Mpl</i> ^{-/-}	<i>Mpl</i> ^{+/+} <i>Mpl</i> ^{-/-}	Liver regeneration	Sham PHx
<i>Asgr2</i> ^{-/-}	<i>Asgr2</i> ^{+/+} <i>Asgr2</i> ^{-/-}	TPO regulation	Native

The mice were either sacrificed by cervical dislocation or after successful anesthesia with ketamine [100 mg/kg] and xylazine [10 mg/kg]. After anesthesia the thorax was opened and an incision was made in the right atrium followed by directly purging of cold heparin solution through the left ventricle of the heart.

There is an exceptional permission according to § 16 Abs. 1 Satz 5 TierSchVersV, which allows Mr. Friedrich Reusswig to carry out the surgical animal experiments described in the above mentioned permission (file number 84-02.04.2016.A493; file number 39/11-1-102_7 HHU). Mr. Friedrich Reusswig has completed a laboratory animal science course according to FELASA guidelines (category B).

2.8 Human blood samples

Ethics vote

Experiments with human blood were reviewed and approved by the Ethics Committee of the Heinrich-Heine University, who approved the collection and analysis of the blood. Subjects provided informed consent prior to their participation in the study (patients' consent): Permit/Study Number 2018-140-KFogU.

3. Methods

3.1 Liver injury models

3.1.1 Partial hepatectomy

The PHx serves as a model to study the regenerative capacity of the liver. In this study a 2/3 PHx was performed, meaning that two third of the liver mass were dissected (fig. 5).



Figure 5. Images of the partial hepatectomy performed in mice (PHx). (A) Mice were kept under anesthesia with an inflow of 2% isoflurane and an oxygen flow rate of 1 L/min. (B) The abdominal cavity was opened by a 3 cm long, median laparotomy. (C) First, the left lateral lobe was ligated and dissected. (D) Second, the left and right segments of the median lateral lobe were likewise removed. After dissection, the abdominal cavity was rinsed with preheated sterile saline buffer and closed using interlocking running stitches.

PHx of mice was performed by using a modification of the method described by Greene and Puder [172] with two separate ligatures and removal of the gallbladder. The operation was always performed between 8 - 12 am. In order to reduce post-operative pain, mice were treated with Buprenorphin [0.1mg/kg] *i.p.* before surgery. Mice were placed into an acrylic glass chamber for induction of the anesthesia with an inflow of 3% isoflurane and an oxygen flow rate of 1 L/min. After induction of a sufficient depth of anesthesia, which was characterized by a lack of reflexes in response to pinching the mice foot, the mice were fixed in a supine position on a heated surgical pad. The mice head was placed in a mask connected to an evaporator with a constant inflow of 2% isoflurane and an oxygen flow rate of 1 L/min. The abdomen of the mouse was shaved and subsequently disinfected. PHx was initiated by an approximately 3 cm long, median laparotomy starting distal and ending proximal to the *processus xiphoideus*, thus severing the skin and muscle layers of the abdomen in two separate incisions. During surgery, the liver was manipulated and moved using saline wetted Q-tips to avoid injury. At first, the *ligamentum falciforme* was cut using microdissection scissors. Next, the left lateral lobe as well as the left and right segments of the median lobe containing the gallbladder were ligated using 4-0 polyester suture tie resulting in a 2/3 PHx. After ligation, the individual lobes

Methods

were resected, and the abdomen was flushed with 5 mL of a preheated sterile saline solution to ensure the removal of blood as well as to decrease contamination of the abdominal cavity. Sham operated control mice underwent the same surgical procedure, without ligating and removing of liver tissue. After the removal of 2/3 of the liver, the abdominal cavity was closed using an interlocking running stitch with 5-0 polyester suture tie. Hypoderm and skin were likewise closed. Subsequently, the mice were weighed in order to enable the determination of weight losses or gains on following days. The mice received either 0,1 mg /kg Buprenorphine via *i.p.* injection 6 h post operation or continuously through the drinking water (conc. 0.009 mg /mL Buprenorphine in H₂O).

For a better differentiation between classic and trans-signaling of IL-6, a method was used to increase IL-6 trans-signaling. To induce IL-6 trans-signaling, C57Bl6 mice were injected once with 20 µg of the fusion IL-6/sIL-6R protein (hyper-IL-6) 1d before PHx as described by Behnke *et al.* [173]. As vehicle control group, C57Bl6 mice were injected with the same amount of PBS.

3.1.2 Bile duct ligation

The BDL serves as a model for obstructive cholestasis, which is an inflammatory disease. Obstructive cholestasis is induced by ligation of the common biliary duct. The mice were first anesthetized by inhalation with isoflurane and prepared for the median laparotomy as described in 3.1.1. To alleviate the post-operative pain, the mice were treated with analgesics (carprofen 5 mg/kg body weight diluted with physiological saline solution) administered subcutaneously. The mice were fixed to a heatable surface with sterile transparent polyurethane film. The anesthesia was carried out by a respirator with adjustable supply of a mixture of isoflurane (2%) and oxygen (1 L /min). The laparotomy of the abdomen was performed using a 2 cm incision through the skin and a slightly shorter incision along the *linea alba* through the layers of the abdominal muscles and the peritoneum. The liver gate and the bile duct were exposed. After double ligation, the bile duct was severed, and the gallbladder was removed. The abdomen was rinsed several times with 3 mL of sterile saline solution [0.9% NaCl], whereas approximately 1 mL remained in the body to compensate for the loss of fluid during the procedure. The muscle layers were closed by a continuous seam, while the skin was closed by a continuous seam and an additional single button seam. As control group (sham) mice were operated as described above without ligation of the bile duct. After exposure of the liver portal and the bile duct, the abdomen was directly closed again. After termination of the inhalation anesthesia, the mice recovered from anesthesia within a few minutes. The operated mice were first kept under observation in a heated cage and then brought into the keeping. All BDL operations were carried out by Dr. rer. nat. Maria Reich (Department of Experimental Hepatology, Heinrich Heine University, Düsseldorf).

3.2 *In vivo* hemostasis and thrombosis models

3.2.1 Bleeding time

Mice were anesthetized by intraperitoneal administration of ketamine [100 mg/kg]/xylazine [10 mg/kg] and the tail was transacted 3 mm from the tip using a scalpel. The tail was immersed in normal saline solution (37 °C). The time period between the incision to the termination of bleeding, which was defined as lack of blood flow for at least 1 min, was recorded as described previously [174].

3.2.2 Iron (III) chloride (FeCl₃) injured carotid artery

The right *A. carotis communis* was prepared and placed into a flow probe (Transonic Systems, 0.5 PSB, AD Instruments). Before starting the measurement, the artery and the surrounding area were moisturized with 0.9% NaCl solution and the blood flow was measured in mL/min. Then, a small pad was placed under the artery below the measuring head and the environment of the artery was dried with a sterile tissue. A 0.5 x 1 mm filter paper (Whatmann No. 1) saturated with 10% FeCl₃ solution (Sigma-Aldrich) was placed at the area of the carotid artery below the measuring head for 3 min. After removing the filter paper, the environment of the artery was again moisturized with 0.9% NaCl solution. The formation of occlusions or thrombi in the artery was recorded by the software for up to 5 min after a firm occlusion (stopped blood flow) was observed or - if there was no occlusion - until the measurement reached a maximal duration of 30 min. This *in vivo* thrombosis model was carried out by the veterinarian Irena Krüger (Clinic for Vascular and Endovascular Surgery, University Clinic of the Heinrich Heine University).

3.3 Preparation of murine tissue

3.3.1 Mouse serum and plasma preparation

Mice were anesthetized in a polystyrene box by a respirator with adjustable supply of a mixture of isoflurane (2%) and oxygen (1 L/min). As soon as the mouse had reached an adequate anesthesia depth, which was checked by an absence of the toe pain reflex, blood was collected by puncturing the retrobulbar venous plexus with a microcapillary. The blood was collected in a 1.5 mL reaction tube containing 300 μ L of anti-coagulant heparin buffer. After blood collection, the sample was centrifuged for 10 min at 8,000 g at RT to sediment all cellular blood components. The upper aqueous phase, the blood plasma, was transferred into clean reaction tubes and stored at -80 °C for further analysis. For serum analysis, mice were bled directly into a 1.5 mL reaction tube. The samples were allowed to clot for 10 min at RT. Next, a centrifugation step at 8,000 g at 4 °C for 10 min was performed to sediment all cellular blood components and fibrinogen.

3.3.2 Mouse tissue preparation

For histological analysis, different murine tissues were embedded in paraffin. For this purpose, the mice were sacrificed after a successful anesthesia with ketamine [100 mg/kg] and xylazine [10 mg/kg] via opening the thorax and flushing the heart with approximately 20 mL cooled heparin solution to prevent blood clotting in the tissues. The heparin solution was placed into the *apex cordis* of the left ventricle of the beating heart, while the right atrium was incised to ensure a systemic flush. For tissue analysis, spleen, liver, and the femur were dissected and weighed. Liver and spleen were divided to store one part of the tissue for protein and RNA analysis at -80 °C, whereas another part was directly fixed in 4% paraformaldehyde (PFA) for immunohistochemistry and histological analysis. The femur was directly dissected out of the basin pan, including the knee joint to protect the BM tissue from destruction. Next, the femur was put into 4% PFA for tissue fixation and afterwards transferred into decalcification buffer containing 10% (w/v) EDTA for at least 7 days. All tissues were fixed for at least 24 h and stored at 4 °C protected from light until use.

3.3.3 Paraffin fixation

After fixation in 4% PFA all organs were transferred into organ cartridges and washed in running tap water, dehydrated using an ascending ethanol row (stepwise from 100% to 70%) and incubated in Roti®Histol (Carl Roth) for 12 h. Afterwards, the tissue was equilibrated in

Methods

liquid paraffin for 4-6 h (Roth) and finally embedded. The embedded and cooled organs were stored at RT until tissue sections were prepared for immunohistochemistry.

3.4 Cell biological methods

3.4.1 Human platelet preparation

Fresh acid citrate dextrose anticoagulated blood was obtained from healthy volunteers between the ages of 18 and 50 years. The blood was centrifuged at 200 *g* for 10 min without brake. As a result, a biphasic solution was formed, whereas the upper phase contained platelet rich plasma (PRP), while the lower phase consisted of granulocytes and red blood cells. In the white interphase, lymphocytes and monocytes were located. Next, the PRP was separated and the interphase as well as the lower phase was discarded. The PRP was added to phosphate-buffered saline (PBS) [pH 6.5, apyrase (2.5 U/mL: Sigma), 1 μ M Prostaglandin E₂ (PGE)] in a 1:1 volumetric ratio and centrifuged at 1000 *g* for 6 min without brake. The platelet pellet was resuspended in human Tyrode's buffer and the platelet count was determined in a 1:10 dilution in PBS using an automatic hematology analyzer (Sysmex - KX21N, Sysmex Corporation). The platelet count was adjusted as required for the applied functional assay. For flow cytometric analysis undiluted human PRP was used without further adjusting a dilution.

3.4.2 Murine platelet preparation

Mice were bled into a 1.5 mL reaction tube as described in 3.1.1 and platelets were isolated through centrifugation. Thereby, all centrifugation steps were performed without break to avoid platelet preactivation.

First, the heparinized whole blood was centrifuged for 5 min at 250 *g*/RT to separate the individual blood components. The upper phase and the whole interphase were transferred into a new reaction tube, and again centrifuged for 5 min at 50 *g*/RT. The resulting platelet-rich plasma (upper phase) was transferred into a new reaction tube while the remaining erythrocytes were discarded. The remaining pellet was resuspended in 200 μ L murine Tyrode's buffer, centrifuged again for 5 min at 50 *g*/RT and the newly formed supernatant was combined with the previously taken PRP. To prevent the platelets from becoming preactivated during further isolation, apyrase [0.02 U/mL] and PGI₂ [0.5 μ M] were added to the cell suspension. Apyrase degrades an important platelet specific agonist - ADP, whereas PGI₂ directly induces a receptor-based signaling pathway leading to platelet inhibition. The PRP is subsequently centrifuged at 650 *g* for 5 min, washed two times with Tyrode's buffer

Methods

supplemented with PGI₂ and Apyrase and finally resuspended in 200 µL Tyrode's buffer supplemented with calcium ions [0.2 mM] to guarantee proper platelet activation.

The platelet count was determined in a 1:10 dilution in PBS using an automatic hematology analyzer (Sysmex - KX21N) and the platelet count was adjusted as required for the applied functional assay.

3.4.3 Murine platelet lysates and releasates

To analyze the protein content of platelets, a total of 40 x 10⁶ platelets/µL sample were used. To induce or inhibit platelet activation, cells were stimulated with different antagonists [SNP or PGI₂] and agonists [CRP or Thrombin] in a total reaction volume of 50 µL at 37°C with smooth agitation (300 rpm). To stop stimulation, platelets were centrifuged at 650 g at 4 °C for 5 min. The releasate (supernatant) was separately collected and stored at -80 °C to analyze platelet degranulation by using a serotonin ELISA.

The pellet was lysed in 30 µL murine platelet lysis buffer for 15 min at 4 °C. Platelet lysates were prepared with 6 µL reducing sample buffer (6x Laemmli buffer), denatured at 95 °C for 5 min and stored at -20 °C.

3.4.4 Adhesion experiments

To study cell adhesion of different extracellular matrix proteins, adhesion experiments on collagen and fibrinogen were performed using isolated platelets. Cover slips (24 x 60 mm) were either coated with fibrinogen [100 µg/mL] or type I collagen [200 µg/mL] at a defined area (10 x 10 mm) at 4 °C overnight (o/n). Afterwards, the cover slips were washed three times with PBS and blocked with 1% BSA in PBS for 60 min. A total concentration of 4 x 10⁴ isolated platelets was resuspended in 40 µL Tyrode's buffer supplemented with CaCl₂ [0.2 mM], applied on the cover slips and incubated at RT for the indicated time points.

In case of the static adhesion assays with BA, platelets were preincubated with 50 µM of the indicated BA for 60 min prior to the application on the cover slips. DMSO was added to a total volume of 0.1% as vehicle control to adjust the DMSO concentration in TLC- and TDC-treated samples. Non-adherent platelets were carefully removed by rinsing two times with PBS and adherent platelets were fixed in 4% phosphate buffered formaldehyde at 4 °C for 10 min, rinsed carefully with PBS and covered with the mounting medium Aquatex. Platelet adhesion was documented with an Axio Observer.D1 microscope. A minimum of 5 pictures (per visual field) per sample were documented. The total number of adherent platelets was counted using ImageJ-win64 software.

3.4.5 Thrombus formation assay.

Cover slips (24 x 60 mm) were coated with 200 µg/mL fibrillary type I collagen and blocked with 1% BSA (bovine serum albumin) solution as described above. Mice were anesthetized with isoflurane and blood was taken from the retroorbital plexus and collected in 1.5 mL reaction tubes containing 300 µL heparin buffer. Subsequently, the heparinized whole blood was filled in a 1 mL syringe and perfused over a collagen-coated surface at shear rates of 1000 s⁻¹ and 1700 s⁻¹ and platelet adhesion and aggregate formation was evaluated from six different microscopic areas (40x magnification, Axio observer.D1, Zeiss).

3.4.6 Flow cytometry of human samples

Flow cytometry is based on discriminating cells regarding their size (forward scatter, FSC) and their granularity (side scatter, SSC). Cells in suspension are passed through a flow cell and irradiated with a laser. Depending on the size and granularity of cells, a cell-specific scattered light is generated. Using this scattered light, a dot plot is calculated displaying the FSC and the SSC for each single cell passed through the flow cell. Beside the FSC and SSC profile of each cell, fluorescence labeled dyes or antibodies can be used to further distinguish between different cell types and subpopulations.

In this thesis, flow cytometry analysis of human platelets was performed using PRP or isolated platelets, gated towards their SSC and FSC profile. For analyzing and processing of the flow cytometry data, FlowJO Single Cell Analysis v10 Software was used.

3.4.6.1 Treatment of human PRP with bile acids

In freshly isolated human PRP, the platelet count was determined using automatic hematology analyzer. PRP was diluted with human Tyrode's buffer to a total platelet count of 100.000 platelets/µL. Samples were prepared in a total volume of 200 µL to adjust all samples to a nearly physiological cell count. To study pathophysiological effects of BAs, the samples were treated with 50 µM of the indicated BAs or with 0.1% DMSO (in Tyrode's buffer) as solvent control. The samples were incubated at 37°C for 1, 6, 12 or 24 h with BAs in a rotating mixer with 100 rpm. Afterwards, platelet activation was analyzed by measuring the mean fluorescence intensity (MFI) by using flow cytometry.

3.4.6.2 Activation of human platelets

Platelet activation was determined using two-color analysis of human platelet activation using fluorophore-labeled antibodies for P-selectin expression (P-selectin-FITC) and the active form

Methods

of $\alpha_{IIb}\beta_3$ integrin (PAC-1-PE). Either pretreated human PRP or freshly isolated human platelets were used, whereas both samples were diluted in human Tyrode's buffer to a final concentration of 5×10^4 platelets/ μL . The samples were mixed with antibodies [1:10] and stimulated with indicated agonists for 15 min at RT in the dark. The stimulation was stopped by addition of PBS and samples were analyzed using a FACSCalibur™ flow cytometer (BD Biosciences).

3.4.7 Flow cytometry of murine samples

Flow cytometry analysis of murine platelets was performed using washed whole blood of mice. Cells were gated towards their specific SSC and FSC profile and combined fluorescence upon labelling with platelet-specific antibodies. For analyzing and processing of the flow cytometry data, FlowJO Single Cell Analysis v10 Software was used.

3.4.7.1 Murine platelet activation, glycoprotein externalization and size

Briefly, two-color analysis of murine platelet activation was performed using fluorophore-labeled antibodies for P-selectin expression (Wug.E9-FITC) and the active form of $\alpha_{IIb}\beta_3$ integrin (JON/A-PE). Heparinized blood was diluted in Tyrode's buffer and washed twice. Blood samples were supplemented with 2 mM CaCl_2 , mixed with antibodies [1:10] and stimulated with indicated agonists for 15 min at RT. The stimulation was stopped by addition of PBS and samples were immediately analyzed using a FACSCalibur™ flow cytometer. For analysis of glycoprotein surface expression, blood samples were mixed with antibodies (all antibodies with a final dilution of 1:10; GPVI, JAQ1-FITC; GPIb/CD42, Xia.G5 – PE; Integrin α_5 /CD49e, Tap.A12 – FITC) and incubated for 15 min at RT. Up-regulation and activation of integrin expression was detected with antibody against integrin β_3 chain (Luc.H11-FITC). For the determination of the platelet size, the geometric mean of the CD42 positive platelets of their forward scatter (FCS) profile was analyzed.

3.4.7.2 AnnexinV binding of platelets

For detection of the PS exposure AnnexinV was used. As described in 3.4.7.1, samples were prepared and Cy™5 labeled AnnexinV (BD Biosciences) was used [1:10 final dilution] to label PS-positive platelets. While Annexin V binding buffer was used instead of PBS to stop labeling reaction. Additionally, CD42 [1:10 final dilution] was used as platelet specific marker.

3.4.7.3 Desialylation assay

In terms of aging, platelets lose their extracellular sialic acid moiety of their glycosylated membrane bound receptors. To examine the desialylation state of platelets, lectins labeled with a fluorescence dye were used in flow cytometric. For the detection of desialylated platelets, a lectin binding assay was performed. For this purpose, *Ricinus communis* agglutinin-1 (RCA-1), *Erythrina cristagalli* lectin (ECL/ECA), and *Triticum vulgare* (wheat germ) agglutinin (WGA) labeled with FITC were used. The samples were treated for 15 min at 37 °C with neuraminidase (Neuraminidase from *Vibrio Cholerae*) as positive control before the samples were incubated with RCA-1 for 15 min. The lectin binding was stopped by addition of Tyrode's buffer and samples were analyzed using a FACSCalibur™ flow cytometer.

3.4.7.4 Thiazole orange staining

For the detection of reticulated platelets, blood samples were prepared as described under 3.4.7.1. Washed blood samples were incubated with thiazole orange (ReticCount) for 30 min at RT while CD42 was used as a platelet specific marker. CD42 positive platelets were gated accordingly to their forward- and side-scatter profile and reticulated platelets were analyzed as described in Wu *et al.* [175].

3.4.7.5 von Willebrand Factor binding

For detection of vWF-binding on platelets, platelets were isolated as described under 3.4.2 and diluted to a concentration of 30.000 platelets/ μ L. Subsequent incubation with anti-vWF antibody (Emfret Analytics), anti-GPIb α antibody (Emfret Analytics) and botrocetin (Sigma) was performed for 30 min at 37°C. The reaction was stopped by addition of Tyrode's buffer and samples were analyzed using a FACSCalibur™ flow cytometer.

3.4.7.6 Expression of neuraminidase-1 at the platelet surface

For detection of Neu-1 expression on platelets, unwashed ACD anti-coagulated murine blood samples were diluted 1:2 with Tyrode's buffer after addition of 2 mM CaCl₂. Samples were stimulated with indicated agonists for 15 min at 37°C in the dark. Additionally, an anti-GPIb α antibody (GPIb/CD42, Xia.G5 – FITC) binding to the N-terminal ending of GPIb α was used to inhibit vWF-GPIb interaction. Platelets were gated according to their specific FSC and SSC and the MFI of Neu-1-PE antibody binding was analyzed.

3.5 Protein biochemical methods

3.5.1 Bradford assay

Protein concentrations from lysates were determined by the Bradford method, which is based on the binding of the Coomassie Brilliant Blue G-250 dye to proteins in acidic solution. This binding results in a shift in the absorption maximum from 465 nm to 595 nm [176].

The intensity of the color change depends on the number of cationic and non-polar side chains of amino acids and can be considered as proportional to the total protein concentration.

To measure the protein concentration of a sample, protein lysates were diluted in PBS and an aliquot of 100 μ L was transferred into a 96-well plate. To estimate the protein concentration, a BSA (bovine serum albumin) standard series (0-35 μ g/mL in PBS) was included into the measurement. The standard curve was measured in triplicates, while all samples were measured in quadruplicates throughout this work. Samples and standards were mixed with 100 μ L of Bradford dye solution, which is a mixture of Roti Quant 40% (v/v) and ddH₂O 60% (v/v) dye concentrate and incubated for 5 min at RT. Next, the absorbance was measured at 550 nm in a microplate spectrophotometer. The protein concentration of the sample was calculated based on the linear regression generated with the standard series.

3.5.2 SDS-PAGE

Sodium dodecyl sulfate polyacrylamide gel electrophoresis (SDS-PAGE) is an analytical method for the separation of proteins based on their molecular weight and charge in an electrical field. By using SDS, which binds to the hydrophobic areas of a protein, the proteins are denatured, and negative charges are introduced into the denatured polypeptide chains. As a result, the proteins migrate towards the anode in an electrical field. Additionally, β -mercaptoethanol is used to cleave disulfide bridges in order to obtain a primary, linear protein structure.

First, a separating gel was poured, which was overlaid with the stacking gel after polymerization (Table 2). The stacking gel [4% acrylamide (AA)] is used to concentrate the samples. The separating gel [10% AA] forms a small-pored structure which exhibits a sieving effect to separate the net negatively charged proteins according to their molecular weight in an electrical field. The Precision Plus Protein™ Dual Color Standards was used to estimate the size of the proteins of interest. The electrophoresis was typically carried out for 180-210 minutes in running buffer at 25 mA per gel. The gel was then directly used for a Western blot in order to transfer the size-separated proteins onto suitable membranes.

3.5.3 Western Blot

The proteins separated by gel electrophoresis were transferred onto a nitrocellulose membrane using the semi-dry Western blot method. For this purpose, buffer systems with varying ions and methanol concentrations were used to equilibrate Whatman filter paper, the nitrocellulose membrane, and the gel in a specific arrangement. The blotting chamber was assembled according to the following scheme: cathode, six Whatman filter papers moistened with buffer C, activated nitrocellulose membrane soaked in buffer B, polyacrylamide gel, six Whatman filter papers immersed in buffer A, anode plates (Table 3). The transfer was conducted for 1 h at 0.75 mA/cm² gel. After protein transfer, the membrane was first stained with a 0.1% Ponceau S solution to verify a successful protein transfer and the several times washed in TBS-T (TBS buffer supplemented with 0.1% Tween 20) to decolorize the membrane.

Subsequently, the membrane was blocked with 5% (w/v) powdered skim milk in TBS-T for 60 min and probed with appropriate antibody (see section 2.3.1). The antibody incubations were performed at 4 °C o/n. On the next day, the membrane was washed 3 times with TBS-T, and incubated with horseradish peroxidase (HRP)-conjugated secondary anti-rabbit and anti-mouse IgG antibodies in 5% powdered skim milk in TBST (GE Healthcare, Code: NA9340, 1:2500) for 1 h at RT. For visualizing protein bands, the membrane was washed 3 times with TBS-T and incubated for 1-2 min with Immobilon™ Western Chemiluminescent HRP substrate solution (BioRad) resulting in a chemiluminescence signal that was recorded with a Vilber Fusion-FX6-EDGE V.070 imaging system. Proteins were quantified based on a densitometric analysis of the chemiluminescent signals using Evolution-Capt EDGE software (Version 18.02). Relative protein amounts were normalized to GAPDH or Actin.

3.5.4 Liver specific serum parameters

Levels of liver-specific parameters were measured in the serum of mice subjected to BDL using Spotchem-biochemical analyzer EZ SP-4430 (AxionLaB/Arkray). Using different reagent strips, a 'serum liver profile' was determined and the following parameters were measured: Aspartate aminotransferase (AST), alanine aminotransferase (ALT), and total bilirubin. The reagent strips consist of a multi-layer test field in which reagents are immobilized at certain locations to specifically measure the aforementioned parameters. The test field allows for the simultaneous quantification of the molecules to be measured based on colorimetric reactions which are visualized by reflection spectroscopy. The alkaline phosphatase (ALP) was determined with the Reflotron® Plus (Roche), according to the manufacturer's instructions.

3.5.5 ELISA

A quantitative determination of the concentration of cytokines in the serum and heparinized plasma of mice were carried out using Quantikine® ELISA kits listed under 2.5: Mouse -IL-6, SDF-1 and TPO. Additionally, ELISA kits were used to detect tissue plasminogen activator (Uson Life Sciences), plasmin-antiplasmin complex (CUSABIO) and prostacyclin I₂ (CUSABIO). Serotonin was measured in the releasates of platelets (ENZO Life Sciences). The ELISAs were performed according to the manufacturer's instructions. The principle of these kits is based on the 'sandwich ELISA technique', in which a monoclonal primary antibody was pre-fixed at the bottom of a 96-well multititer plate. This immobilized antibody specifically binds to the antigen contained in the sample. A biotin-coupled secondary antibody which specifically binds to the antigen is subsequently added, so that an antibody-antigen-antibody complex (sandwich) is formed. The sandwich complex is then incubated with a streptavidin-coupled horseradish-peroxidase (HRP) which allows the quantification of an antigen by measuring an enzymatic color reaction upon adding the HRP substrate 3, 3', 5, 5'-tetramethylbenzidine (TMB). Each reaction was stopped by adding 2N sulfuric acid (H₂SO₄). The color intensity was determined photometrically at 450 nm using the GloMax microplate reader.

To detect the concentration of vWF as well as the bioactivity of neuraminidase-1 (Neu-1) in the plasma of sham and PHx treated mice, ACD buffer was used as anti-coagulant. The determination of vWF was based on "sandwich" ELISA technique describe above, while following (Mouse Von Willebrand Factor A2 ELISA-Kit, Cat. No.: ab208980 (abcam)). Neu-1 activity was determined based on substrate conversion and subsequent change of the emission spectrum. For this analysis the manufacturer's protocol was followed (Neuraminidase Assay Kit, Cat. No.: ab138888, (abcam)).

3.5.6 NO Assay

A quantitative determination of the nitrogen monoxide (NO) concentration in the serum of mice was performed by means of the total NO and Nitrate/Nitrite Assay Kit according to the manufacturer's instructions. The assay principle is based on the Griess reaction and was carried out in two steps. In the first step, the NO concentration is determined based on an enzymatic conversion of nitrate to nitrite by the nitrate reductase. In the second step, nitrite is determined using the Griess reagent. The photometric absorption measurement at a wavelength of 540 nm indicates the total nitrate-nitrite concentration (collectively referred to as NO). The concentration of nitrite and nitrate was calculated according to the instructions of the assay.

3.5.7 Determination of total bile acid concentration

BAs and their glycine- and taurine-bound derivatives were analyzed by Ultra performance liquid chromatography - tandem mass spectrometer (UPLC-MS/MS). The system consists of an Acquity UPLC-H Class (Waters, UK) coupled to a Xevo-TQS tandem mass spectrometer (Waters, UK) which is equipped with an ESI source in the negative ion mode. Data were collected in the multiple reaction monitoring (MRM) mode. Total BAs concentration analysis of serum samples was performed by Dr. Diran Herebian (Department for pediatrics, University Clinic of the Heinrich Heine University, Düsseldorf).

3.6 Histological analysis and Immunohistochemistry

All histological analysis and immunostainings throughout this work were performed on paraffin embedded tissue. For the preparation of organ sections, 5 µm sections were cut from the tissue paraffin block at a microtome, transferred in a 37°C preheated water bath and pulled up on microscope slides. Before using the sections, they were additionally heat-fixed on the slides at 37 °C o/n.

Prior staining, the tissue sections were deparaffinized in a descending ethanol concentration (Table 4), washed in PBS and used for following stainings. At the end of the HE-staining procedure, an ascending ethanol concentration was conducted to mount the slides with Roti® Histofix (Roth).

Table 2. Steps to exchange hydrophilic and hydrophobic state of the paraffin embedded tissue before and after histological procedure.

Ascending ethanol series		Descending ethanol series	
Time (min)	Reagent	Time (min)	Reagent
10	Roti Histol	2	70% EtOH
2	100% EtOH	2	80% EtOH
2	96% EtOH	2	90% EtOH
2	80% EtOH	2	100% EtOH
2	70% EtOH	10	Roti Histol

3.6.1 HE-staining

Hematoxylin - eosin (HE) staining is a standardized method to stain histological slices. This staining is based on two chemical dyes that react differently with certain tissue components. The alkaline hematoxylin reacts with acidic elements, e.g., negatively charged DNA fragments resulting in a blue staining. The eosin reacts with alkaline tissue components such as cytoplasmic proteins creating a red coloring of these components. In this study HE-staining was used to analyze the morphology of inflammatory and regenerative liver tissue and to visualize and analyze megakaryocytes located in the spleen and the femoral BM of mice subjected to PHx and BDL.

The paraffin tissue sections were deparaffinized as described in 3.6, incubated for 10 min in hemalum solution and washed once with tap water. Next, a 30-60 sec incubation step in 1% HCl/70% EtOH solution followed by a 10 min incubation step in running tap water. The slides were transferred into a 1% eosin solution for 20 seconds. Subsequently, a differentiation of the eosin staining was performed by decoloring with 70% EtOH for 20-30 sec. Afterwards the slides were directly transferred to an ascending ethanol series and mounted in Roti® Histofix.

3.6.2 Immunofluorescence staining

For visualization of platelets located in the liver of PHx and BDL mice, a fluorescence staining for the platelet specific GPIb was performed. For a further analysis of platelet sequestration in partial hepatectomized mice, a GPIX staining was performed in the spleen.

For this purpose, after deparaffinization the tissue sections were transferred into citrate buffer (pH 6.0) and boiled in the microwave with 300 W for 15 min. This step is required for a proper demasking of antigens which could be blocked due to the fixation in paraffin. The boiled sections were allowed to cool down to room temperature for approximately 30 min in the citrate buffer and washed with PBS afterwards.

All following steps were all performed in a humidity chamber to prevent dehydration of the tissue sections. The slides were positioned in the chamber and the tissue was circled with a grease pencil. Then, the tissue slides were blocked for 1 h at RT with blocking solution (5% BSA in PBS) and incubated with the primary antibody at 4 °C o/n. On the next day, unbound primary antibody was removed by washing with PBS. The tissue was incubated with fluorescence-labeled secondary antibody for 1.5 h at RT. As control staining, either specific IgG primary antibodies or no antibody (only PBS) were applied on the tissue sections. For counterstaining of cell nuclei, the sections were stained with the auto-fluorescent dye DAPI for 5 min at RT. After rinsing the slides with PBS, the tissue sections were mounted with mounting medium and let dry at 4 °C in the dark.

3.7 Molecular biological methods

3.7.1 Animal genotyping

In the present work, the genotyping of the *Mpl*^{-/-} and WT littermates was carried out following the protocol of the "KAPA - Mouse - Genotyping Hot Start Kit" obtained from PeqLab. IL-6R^{-/-} mice were genotyped by Nastaran Fazel Modares (Institute for Biochemistry II, Heinrich Heine University Düsseldorf). Genotyping of the *Asgr2*^{-/-} was performed by Melissa M. Lee-Sundlov (Versiti Blood Research Center, Wisconsin, U.S.). All mice were identified by ear punches resulting in biopsies used for genotyping. For the DNA extraction, the ear punches were lysed by heating to 75 °C in a buffer/ enzyme mixture for 10 min. Lysis was stopped by heat-inactivating the enzyme for 10 min at 95 °C. Tissue remnants were removed by centrifugation at 14,000 g for 90 seconds. The supernatants containing the extracted DNA were transferred into clean reaction tube.

Table 3. Composition of the PCR reaction mixture using the KAPA – Mouse - Genotyping Hot Start Kit.

Mastermix – Genotyping	Volume/Sample
KAPA Mix	12.5 µL
Primer forward	1.25 µL
Primer reverse	1.25 µL
HPLC-H ₂ O	9 µL
DNA	1 µL

For the following PCR, all required reagents. and their corresponding volumes for are listed in table 3.

Table 4. Reaction steps of the PCR for murine genotyping.

	Temperature (°C)	Time (s)	Cycles
Initial denaturation	95	180	1
Denaturation	95	15	40
Annealing	58	20	40
Elongation	72	15	40
Final elongation	72	180	1

The PCR products were subjected to agarose gel electrophoresis on a 1.5% agarose gel supplemented with Midori Green (Biozym)/ Tris acetate EDTA (TAE) buffer and recorded with the Vilber Fusion-FX6-EDGE V.070 system.

3.7.2 Quantitative real-time polymerase chain reaction (qRT-PCR)

The qRT-PCR enables a quantitative analysis of a PCR in presence of double stranded DNA-binding, fluorescent dyes by measuring fluorescence signals in real time. The measured fluorescence is directly proportional to the amount of amplified DNA and can therefore be used to determine the initial amount of cDNA in each sample, and therefore, to the amount of RNA. Three necessary steps are required for quantitative analysis of RNA expression: 1. Isolation of RNA, 2. Synthesis of cDNA and 3. SYBR Green based qRT-PCR.

3.7.2.1 Tissue RNA isolation

Liver tissue samples were homogenized in 500 μ L ice-cold TRIzol™ in a tissue homogenisator (Precellys® 24) and Precellys Lysing Kit (P000918-LYSK0-A). Liver samples were homogenized following the manufacturer's recommendation for soft tissue.

The lysates were spun for 5 min at 10,000 g at 4 °C to pellet unhomogenized tissue and the beads of the Precellys Lysing Kit. The supernatant was transferred to a fresh reaction tube and chloroform in [1:5] volumetric ratio was added to the lysates. The samples were resuspended and incubated for 3 min at RT. Afterwards, the lysates were centrifuged for 15 min at 14,000 g and 4 °C for phase separation. The upper aqueous phase containing the soluble RNA was collected and mixed with 1.5-fold volume of 100% ethanol for RNA precipitation. Next, the samples were loaded on RNeasy columns and the RNA was purified according to the manufacturer's protocol of the RNeasy Mini Kit (Qiagen, Hilden, Germany). Briefly, the nucleic acids were bound to a silica membrane and washed several times with different washing buffers provided with the RNeasy Mini Kit. After the last washing step, the column was air dried for 10 min at RT with open lid, to remove ethanol remnants from the washing buffers. To eluate the RNA, 50 μ L of RNase-free water was loaded on to the center of the column, incubated for 1 min and centrifuged for 30 s with 10,000 g at RT. This step was repeated with the eluate with a centrifugation time of 2 min. Total RNA in the eluate was measured with an Eppendorf BioPhotometer® D30 using 2 μ L sample in an Eppendorf μ Cuvette® G1.0.

3.7.2.2 cDNA synthesis

The ImPromII Reverse transcription System (Promega) was used for cDNA synthesis. To avoid false positive results from DNA contaminations, RNA samples were digested with recombinant DNaseI [1 U/ μ L]. The total RNA was diluted to a concentration of 0.1 μ g/mL with ddH₂O [total reaction volume 20 μ L]. The samples were heated for 30 min at 37 °C to allow DNA digestion, following a 10 min step at 75 °C for enzyme inactivation. For cDNA production, the RNA was mixed with 2 μ L Oligo (dT) Primer and 9 μ L of a master mix.

Methods

Table 5. Composition of the reverse transcription reaction of isolated RNA.

Mastermix – cDNA synthesis	Volume/Sample
ImProm 5x reaction buffer	4 µL
MgCl ₂ (7 mM).	1.5 µL
dNTP Mix (0.5 mM/ every dNTP)	1 µL
Recombinant RNasin ribonuclease inhibitor	0.5 µL
ImProm reverse transcriptase	1 µL

The cDNA synthesis was performed using the following program:

Table 6. Reaction steps used to synthesize cDNA

	Temperature (°C)	Time (min)
Annealing	25	5
Extension	42	60
Reverse transcription inactivation	72	15

3.7.2.3 SYBR green based qRT-PCR

In this study, SYBR green served as fluorescence dye that binds to double-stranded DNA. The data of the real-time PCR were measured with the ViiA™7 Real-Time PCR System (Applied Biosystems). The following real-time PCR approach (20 µL total volume) and temperature profile was always used:

Table 7. Composition of the qRT-PCR reaction used in this study.

Mastermix – qRT-PCR	Volume/Sample
Fast SYBR Green MasterMix	10 µL
Primer forward	1 µL
Primer reverse	1 µL
HPLC-H ₂ O	6 µL
cDNA	2 µL

At the end of a qRT-PCR cycles, a melting curve analysis was additionally performed. The melting curve analysis characterizes the dissociation of double-stranded DNA during constant heating and enables the specific identification of byproducts or primer dimers. PCR products are 'melted' with a slow temperature increase of 0.2 °C/s in a temperature range of typically 50-90 °C. Since the double-stranded DNA of specific PCR products has a higher melting point than non-specific primer dimers, a differentiation of PCR products and primer dimers is

Methods

possible. A double peak in the melting curve analysis also hints towards the presence of byproducts due to unspecific binding of primers to DNA sequences.

Table 8. qRT-PCR program used to analyze RNA expression of target genes

	Temperature (°C)	Time (s)	Cycles
Heat-activation	90	120	1
Denaturation	90	15	40
Annealing	60	30	40
Elongation	95	10	40
Melting curve analysis			

3.7.2.4 Calculation of the gene expression

The data were evaluated based on the $\Delta\Delta\text{Ct}$ method. The Ct (cycle of threshold) value is defined as the cycle in which an intersection of the amplification curve with a defined threshold is observed. The Ct values of all samples and all genes of interest are exported. Relative gene expression changes are calculated by normalizing the Ct-value of genes of interest to a reference gene (formerly known as housekeeping gene, e.g., GAPDH; Glyceraldehyde 3-phosphate dehydrogenase) (ΔCt value). The treated samples were related to an untreated control sample. To compare different groups of mice, the mean ΔCt value of the control group was calculated. For further analysis, the difference between the mean ΔCt value of the control group and the ΔCt values of the untreated samples and the treated samples were calculated ($\Delta\Delta\text{Ct}$ value). The value formed in this way is used in the equation: $x\text{-fold expression} = 2^{-\Delta\Delta\text{Ct}}$ to calculate the x-fold expression.

3.8 Statistical analysis

The number of analyzed individuals is indicated as n . All diagrams depict the mean value (MW) for the parameter of the ordinate (Y axis) with the standard error of the mean (SEM). Statistical analysis regarding a systemic difference in two or more matrices within different groups was calculated using the software Graph Pad Prism 7.02. Throughout this work, ANOVA or student's t-test were applied as appropriate and as stated in the respective figure legends. Significant differences were indicated with an asterisk or rhombus in all diagrams and divided into the following categories:

$p \leq 0.05 = *$ or $\#$, $p \leq 0.01 = **$ or $\#\#$, $p \leq 0.001 = ***$ or $\#\#\#$.

4. Results

4.1 Bile duct ligation leads to platelet activation defects in mice

The BDL serves as a model to study obstructive cholestasis. Therefore, the common bile duct as well as the gallbladder was dissected using only male C57Bl/6 mice. This ligation induced obstructive cholestasis results in a highly inflammatory stimulus in liver tissue due to enhanced levels of BAs, bilirubin, and other bile components, as they cannot be secreted into the duodenum. In this study, the mouse model of obstructive cholestasis was used to analyze thrombotic and hemostatic dysfunction in chronic liver disease. Accordingly, platelet count, platelet function and thrombus formation were investigated including the underlying mechanisms. Altogether, the primary hemostasis was examined 1d, 3d, 7d and 21d after BDL in this mouse model. Since the project was analyzed by several people, only data which was generated by me is shown. This mainly concerns data obtained 7 days after BDL.

4.1.1 BDL causes megakaryopoiesis and mild thrombocytopenia in mice

Typical features of BDL in the mouse model are an enlarged liver and spleen [177]. Accordingly, 7 days after BDL an increase in liver weight by 58.3% was detected in BDL operated mice compared to sham controls (table 9). At this time point mild splenomegaly could also be observed, reflected by 34,1% tissue weight increase (table 9).

Table 9. Serum analysis and organ weight of mice 7 days after BDL. BDL mice show enhanced organ weight of the liver and the spleen ($n = 3-7$ per group) and increased values for different serum parameters suggesting injured liver tissue: AST (aspartate aminotransferase); ALT (alanine aminotransferase), ALP (alkaline phosphatase) and bilirubin were measured by using the automated biochemical analyser Spotchem EZ SP-4430. * = $p < 0.05$, ** = $p < 0.01$, *** = $p < 0.001$; tested with unpaired students t-test.

factor	sham	BDL	significance
Liver weight (g)	0.96 ± 0.034	1.52 ± 0.12	**
Spleen weight (mg)	71.9 ± 5.08	96.4 ± 6.41	*
AST (IU/L)	23.0 ± 10.2	360.3 ± 52.0	**
ALT (IU/L)	20.3 ± 10.3	299.0 ± 50.9	**
Bilirubin (mg/dL)	0.2 ± 0.0	12.6 ± 1.2	***
ALP (IU/L)	80.8 ± 8.9	424.7 ± 122.9	*

Results

Besides enlargement of liver and spleen of BDL mice compared to sham operated mice, several liver specific serum enzymes were elevated as well, e.g., aspartate aminotransferase (AST), alanine aminotransferase (ALT), alkaline phosphatase (ALP) and the total bilirubin (table 9), measured via specific testing stripes described in methods part 3.5.4. All tested serum enzymes were typical markers for a diseased liver, emphasizing the high inflammatory state of the liver caused by BDL. Histological analysis of the liver tissue via HE-staining showed that a high number of cells invaded into the liver in BDL operated mice (fig. 6, left panel), accompanied by degrading liver tissue. At the same time, an enhanced number of megakaryocytes (MK) in the spleen of BDL mice could be detected via HE-staining (fig. 6, right panel) whereas no elevated MK number in the spleen of sham operated mice were detected. Thus, the enlarged spleen volume was accompanied by enhanced numbers of MK's in the spleen of BDL mice 7 days after operation.

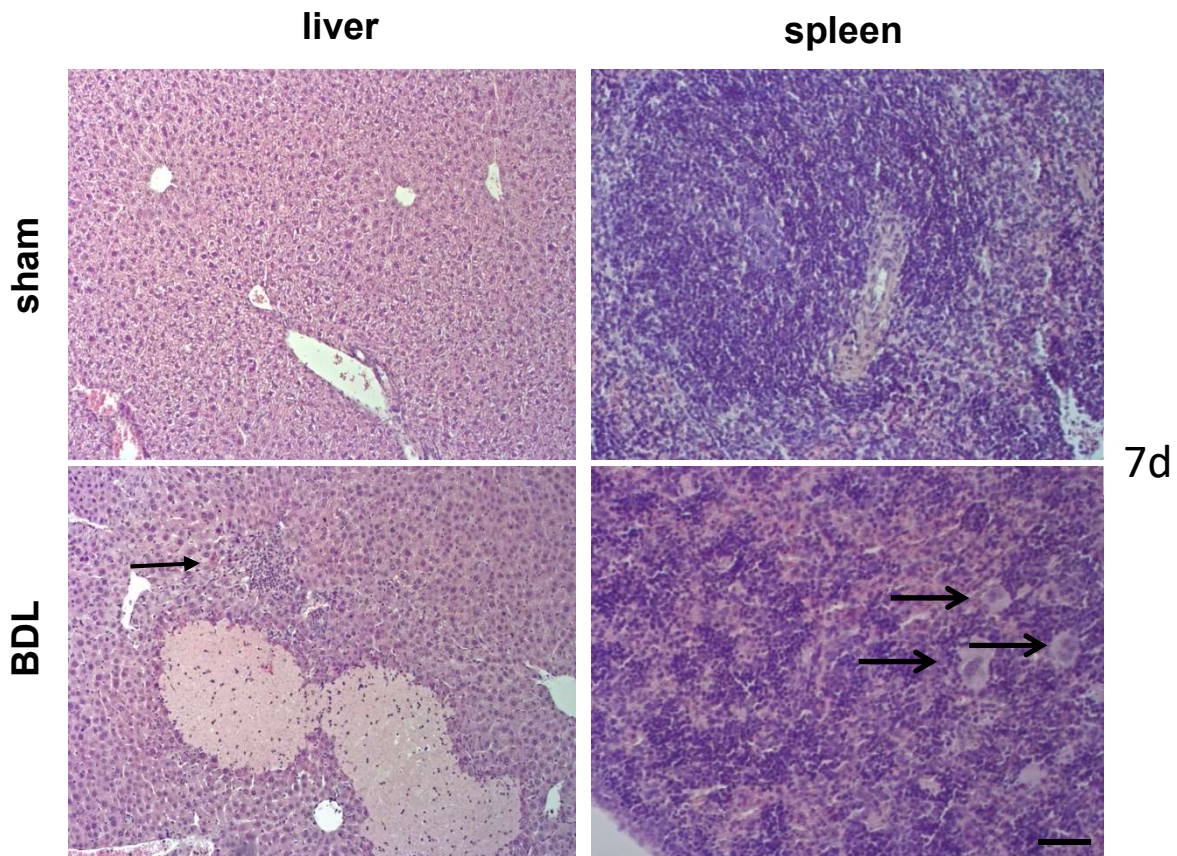


Figure 6. BDL causes liver damage and enhanced megakaryopoiesis. Liver and splenic sections of sham and BDL mice 7 days after operation were stained with HE ($n = 3-8$ per group). Liver sections of BDL mice show tissue injury, bile infarct and invading cells (marked with arrow). Spleen sections revealed an enhanced number of megakaryocytes (marked with arrows). Scale bar = 50 μm

Results

A common issue in liver disease is a low platelet count often leading to thrombocytopenia [162]. Thus, enhanced megakaryopoiesis might take place to rescue a decreasing platelet count. In the mouse model of BDL, a significantly decreased platelet count 1 day ($p = 0.0485$) and 3 days after BDL ($p = 0.0100$) compared to sham controls was measured, recovering nearly to normal platelet counts at day 7 (fig. 7A). This platelet count restoration was probably caused by enhanced megakaryopoiesis in spleen also measured at day 7 (fig. 6).

The number of red blood cells (RBC) was not altered in the first 3 days but reduced 7 days post BDL compared to the corresponding sham mice ($p = 0.042$). Within the sham mice a variable, unstable RBC count was measured at all time points with large standard deviations (fig. 7B). The analysis of white blood cells (WBCs) revealed less WBCs in whole blood in the first 3 days post BDL ($p = 0.049$). This effect was reversed and the BDL mice showed enhanced numbers of WBC in their blood on day 7 post BDL ($p = 0.0062$). Unexpectedly, in the course of sham operation the WBC number was steadily decreasing (fig. 7C).

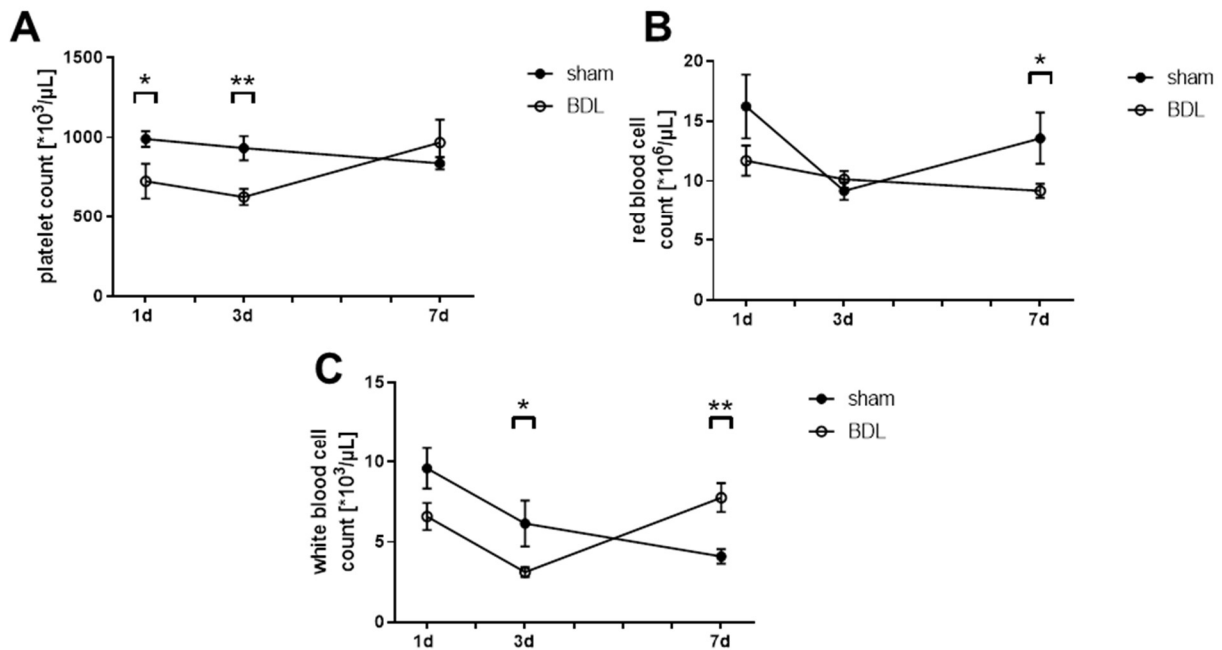


Figure 7. Dysregulated total blood cell count of mice undergoing bile duct ligation. Whole blood from sham and BDL mice was taken and analyzed with hematology analyzer (Sysmex KN-X21). (A) Platelet count analysis revealed mild thrombocytopenia within the first three days after BDL. (B) Red blood cell count analysis showed mild anemia after 7 days of BDL. (C) White blood cell count analysis suggested WBC consumption within the first 3 days after BDL ($n = 4-7$ per group). * = $p < 0.05$, ** = $p < 0.01$ tested with unpaired students t-test.

Results

4.1.2 Obstructive cholestasis leads to enhanced inhibitory plasma factors regarding platelet function.

For further investigation regarding altered enzyme levels in the serum of cholestatic mice 7 days after BDL, specific plasma factors were analyzed that are known to influence platelet activation and hemostasis. NO and PGI₂ are plasma factors leading to platelet inhibition via activation of the adenylyl cyclase (AC) or the guanylyl cyclase (GC). NO directly interacts with GC, whereas PGI₂ binds to a GPCR located on the cell surface of platelets [16]. Activation of these cyclases leads to the induction of VASP via phosphorylation causing platelet inhibition [16, 178].

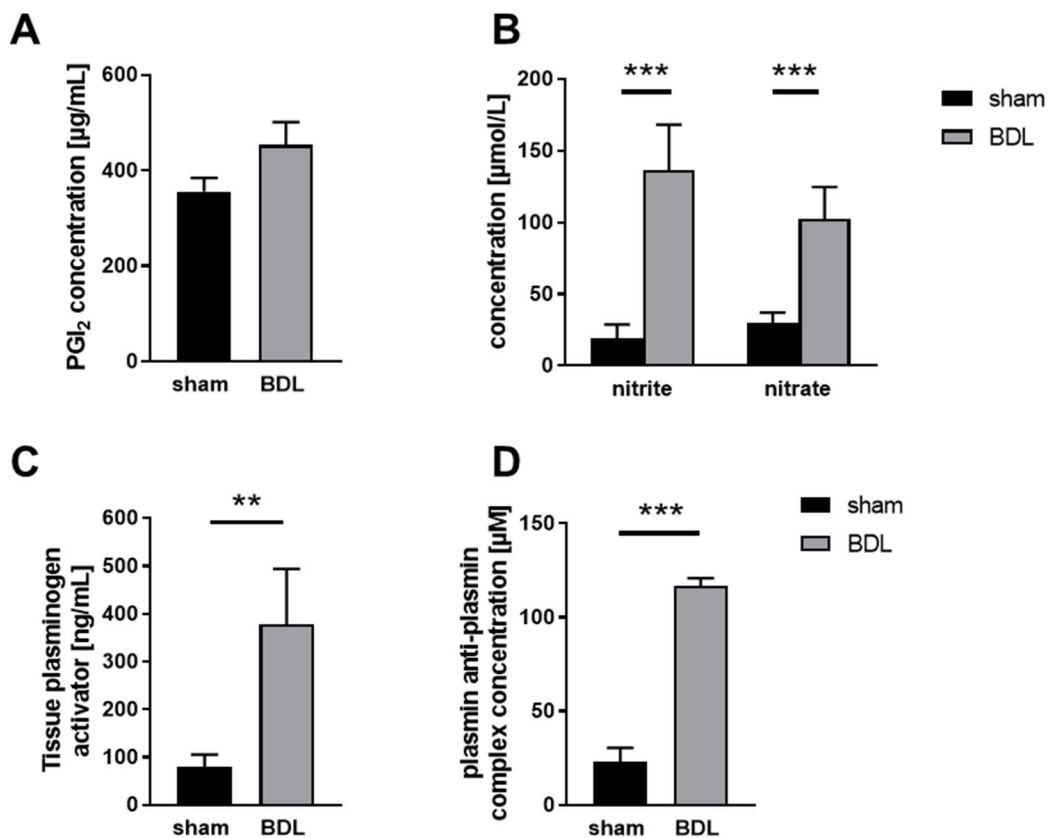


Figure 8. Enhanced levels of platelet inhibiting plasma factors after bile duct ligation. Plasma samples from BDL and sham mice 7 days after operation were taken and analyzed via antibody specific assays and the Griess reaction. (A) Prostacyclin I₂ (PGI₂) concentration in BDL mice is moderately increased. (n = 5-6) (B) Indirect measurement of NO via the metabolites nitrite and nitrate revealed enhanced NO accumulation in the blood of BDL mice (n = 6-9). (C) Tissue-plasminogen activator concentration and plasmin anti-plasmin complexes indicate enhanced proteolytic platelet receptor shedding (n = 4-5). *** = p < 0.001, ** = p < 0.01 tested with unpaired students t-test.

First, the levels of PGI₂ in the plasma of these mice were investigated. The plasma concentration of PGI₂ was only moderately increased 7 days after BDL without reaching

Results

statistical significance ($p = 0.12$; fig. 8A). Another well-known inhibitor of platelet activation is NO. Indirect measurement of the stable NO metabolites nitrate and nitrite via the Griess reaction was performed because it is known that cholestasis induces an altered NO metabolism [179]. In contrast to PGI₂, elevated levels of nitrate and nitrite were measured in plasma of BDL mice 7 days after BDL. Nitrite was enhanced up to 7-fold (sham: $19.47 \pm 9.26 \mu\text{mol/L}$; BDL: $136.26 \pm 31.76 \mu\text{mol/L}$; $p < 0.0001$, fig. 8B) compared to the respective sham controls. Similarly, nitrate was upregulated by an extend of 3.4 times (sham: $30.05 \pm 6.92 \mu\text{mol/L}$; BDL: $102.16 \pm 22.4 \mu\text{mol/L}$; $p < 0.0001$) (fig. 8B).

Beside NO and PGI₂-induced platelet inhibition, platelets are inhibited by plasma factors that degrade important glycoproteins on the surface of platelets. Plasmin is a well-known enzyme that proteolytically cleaves membrane bound platelet receptors [180]. It is activated via enzymatic cleavage of tissue plasminogen activator (t-PA) and can also be indirectly measured through plasmin-antiplasmin (PAP)-complexes in the blood of mice.

Thus, the levels of t-PA and PAP complexes were measured in plasma 7 days after BDL. Interestingly, t-PA levels were increased by 4.8 times (sham: $79.47 \pm 25.8 \text{ ng/mL}$; BDL: $378.37 \pm 115.55 \text{ ng/mL}$; $p = 0.01$) and in line with 5 times higher levels of PAP-complexes (sham: $23.17 \pm 7.31 \mu\text{M}$; BDL: $116.54 \pm 4.44 \mu\text{M}$; $p < 0.0001$) in plasma 7 days after induction of cholestasis (fig. 8 C+D). These results provided evidence that in cholestatic liver disease, different plasma factors altered platelet activation via extrinsic pathways due to plasmin induced proteolysis of platelet membrane receptors and via intrinsic platelet inhibition reflected by increasing levels of NO metabolites and PGI₂.

4.1.3 Platelet activation is strongly reduced after bile duct ligation

Activation of platelets isolated from whole blood of BDL mice was investigated due to elevated plasma factors in BDL mice that are known to inhibit platelet activation as described above.

In flow cytometric analysis, activation of integrin $\alpha_{\text{IIb}}\beta_3$ (fibrinogen receptor) and P-selectin exposure as marker for platelet degranulation was analyzed. As shown in fig. 9, the activation of integrin $\alpha_{\text{IIb}}\beta_3$ was strongly reduced with all tested agonists. The activation of the platelet specific receptor GPVI via collagen-related peptide (CRP) led to almost completely diminished activation of $\alpha_{\text{IIb}}\beta_3$ integrin independent of increasing CRP concentrations (CRP [0.1 $\mu\text{g/mL}$]: $p = 0.0007$; CRP [1 $\mu\text{g/mL}$]: $p = 0.0007$; CRP [5 $\mu\text{g/mL}$]: $p < 0.0001$).

Activation of GPCRs with thrombin or the second wave mediators ADP and the thromboxane A₂ analogue U46619 (U46) revealed decreased activation only with high concentrations of thrombin ($p = 0.005$) or a combination of the second wave mediators ADP and U46 ($p = 0.012$; fig. 9A). Accordingly, the same results were observed for the externalization of P-selectin after

Results

activation with indicated agonists. Major defects were revealed with all tested CRP concentrations. (CRP [0.1 $\mu\text{g/mL}$]: $p = 0.0228$; CRP [1 $\mu\text{g/mL}$]: $p = 0.031$; CRP [5 $\mu\text{g/mL}$]: $p = 0.0002$). Additionally, with ADP + U46 and high thrombin concentrations defects could also be detected (ADP+U46 [10 μM + 3 μM]: $p = 0.0441$; thrombin [0.1 U/mL]: $p = 0.0003$; fig. 9A). Since P-selectin is a marker for degranulation of α -granules, degranulation of dense granules was analyzed via serotonin release of activated platelets. Serotonin release was measured via ELISA in the releasate of activated platelets, revealing a strong degranulation defect upon activation of the GPVI signaling pathway which was reflected in a 59.5% reduced serotonin release (sham: 3970.09 \pm 687.11 ng/mL; BDL: 1607.66 \pm 143.56 ng/mL; $p = 0.002$). Upon platelet activation with thrombin a 32% (sham: 5210.88 \pm 125.13 ng/mL; BDL: 3544.67 \pm 370.97 ng/mL; $p = 0.019$) reduction was observed (fig. 9C).

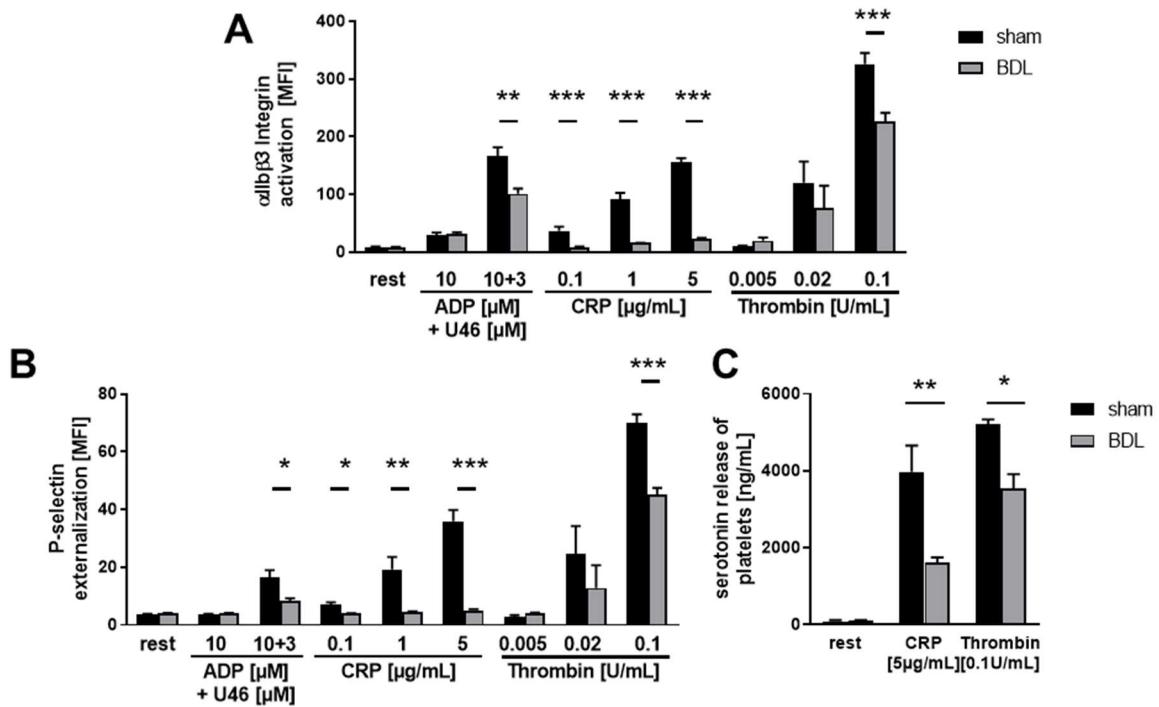


Figure 9. Reduced platelet activation following bile duct ligation in mice. Platelets drawn from sham and BDL mice 7 days after operation were analyzed due to their activation pattern via flow cytometry and ELISA of their releasates. (A) Integrin $\alpha\text{IIb}\beta\text{3}$ activation is strongly decreased with all tested agonists ($n = 5-7$) (B) Measurement of P-selectin revealed degranulation defects of BDL platelets ($n = 5-7$). (C) Isolated platelets were activated with indicated agonists and the supernatant (releasates) was analyzed for the amount of serotonin ($n = 3-6$). * = $p < 0.001$, ** = $p < 0.01$ tested with students unpaired t -test. CRP = collagen-related peptide; ADP = Adenosine-diphosphate; U46 = Thromboxane A2 analogue

Results

4.1.4 BDL induces defective thrombus formation and hemostasis *in vivo*

The obtained results show that platelet activation was strongly reduced 7 days post BDL that was possibly due to enhanced concentrations of plasma factors known to inhibit platelet activation. To investigate platelet activation and aggregate formation in a more physiological model, thrombus formation on a collagen matrix under flow conditions was analyzed in an *ex vivo* model where the surface coverage of platelet thrombi was determined. Thrombus formation upon arterial shear rates of 1000s^{-1} was reduced from $60.87 \pm 2.69\%$ surface coverage of sham mice to $28.34 \pm 6.83\%$ ($p = 0.011$) when whole blood from BDL mice was perfused through the flow chamber (fig. 10A+B).

Defective thrombus formation *ex vivo* was reflected by altered hemostasis *in vivo* as the tail bleeding time of BDL mice was prolonged (784.3 ± 29.7 s) compared to sham (313.1 ± 69.7 s; $p = 0.0048$) and native C57Bl6/J mice (175.2 ± 57.3 s; $p < 0.0001$, fig. 10C).

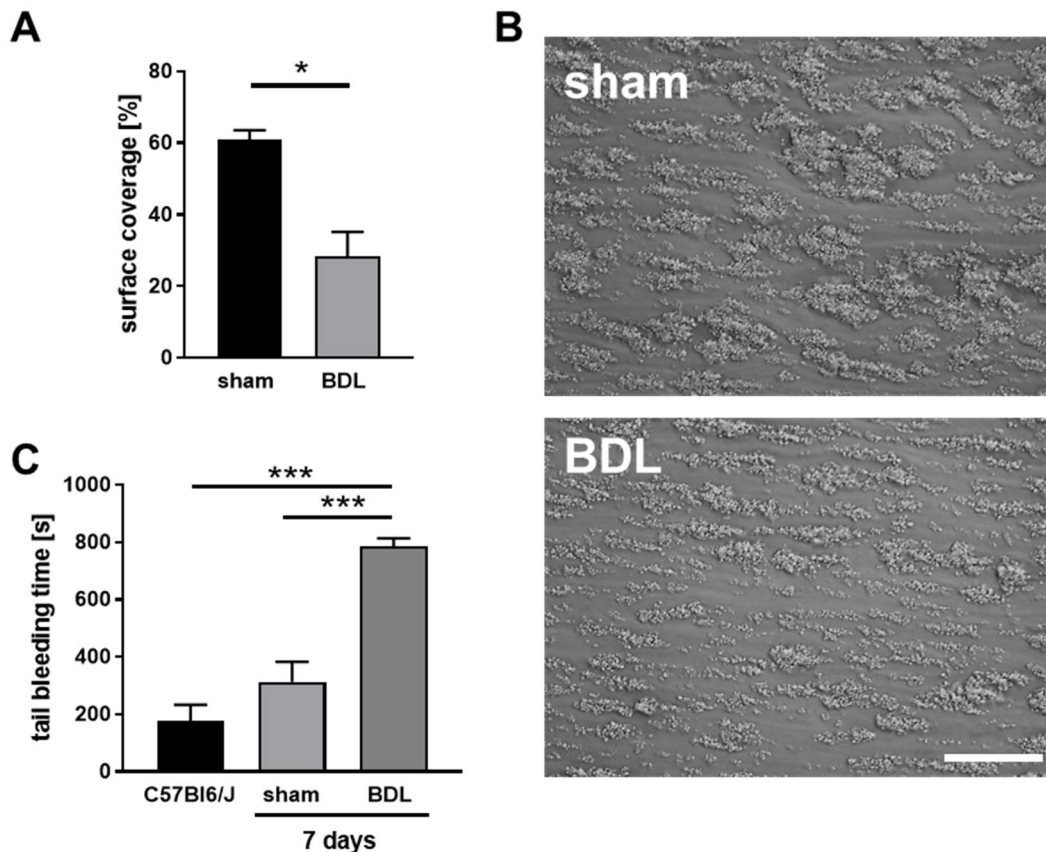


Figure 10. Bile duct ligation causes defective thrombus formation *ex vivo* and altered hemostasis *in vivo*. 7 days after operation sham and BDL mice were analyzed for thrombus formation *ex vivo* and *in vivo*. (A) Murine whole blood anticoagulated with heparin was perfused over a collagen matrix [$100 \mu\text{g/ml}$] at a shear rate of 1000s^{-1} using the flow chamber system. Reduced thrombus formation was observed with whole blood from BDL mice ($n = 3-4$) (B) Representative images of BDL mice and sham controls 7 days after BDL. Scale bar = $50 \mu\text{m}$ (C) The tail tip of mice was dissected with a diameter of 1 mm and bleeding was recorded until it stopped. BDL mice compared to steady state and sham mice showed defective hemostasis. ($n = 4-7$). *** = $p < 0.001$, ** = $p < 0.01$ tested with unpaired students *t*-test.

Results

4.1.5 Enhanced platelet invasion into cholestatic liver tissue

Besides the important role of platelets in hemostasis, platelets are known to support other cellular processes such as inflammation or thrombopoietin production via cell-cell contact with cells of the immune system or hepatocytes. For a deeper understanding of defective hemostasis and the role of platelets in cholestasis, an immunofluorescence staining of the platelet specific antigen GPIb was performed to investigate if platelets invade into the liver of cholestatic mice.

An enhanced accumulation of GPIb positive platelet aggregates in the vessels of the liver can be observed 7 days after BDL, whereas no platelets can be detected in the vessels of sham operated controls (fig. 11, upper panel). Interestingly, an invasion of platelets in the border zone of the liver endothelium can be detected accompanied by GPIb positive platelets close to nuclear cells, providing evidence for a direct cell-cell contact of platelets with immune cells and hepatocytes. Furthermore, GPIb positive staining was detectable in necrotic liver tissue indicated with a white arrow in fig. 11.

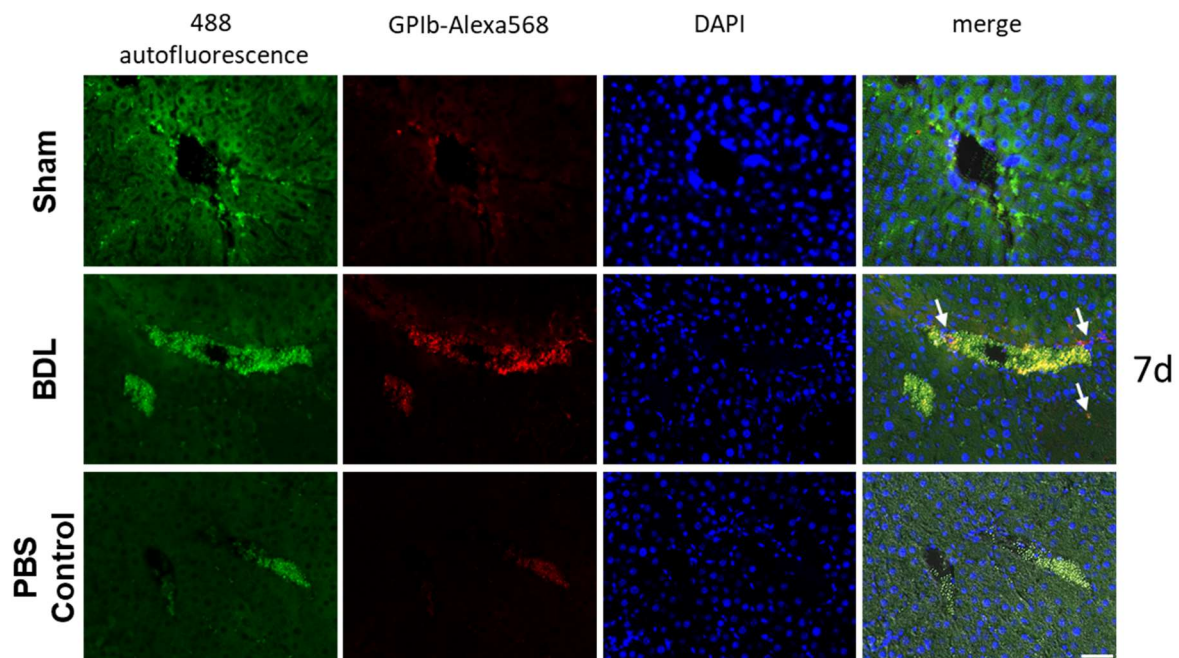


Figure 11. Platelet invasion into cholestatic liver tissue. Paraffin embedded sections of the liver [5 μ m] were stained with GPIb antibody to detect platelet accumulations in the liver. Additionally, fluorescence emission at 488 nm was detected to visualize autofluorescence of erythrocytes. DAPI was used as nucleus staining. After 7 days an enhanced number of platelet aggregates in the liver was detected in BDL mice that interact with other cells such as endothelial cells or white blood cells (indicated by arrows). Also, platelet positive staining is detected in the degraded liver tissue. (n = 5) Scale bar = 50 μ m

These results provide strong evidence that obstructive cholestasis led to major platelet activation defects and platelet consumption in the vessels of the diseased liver. Platelet activation was inhibited *in vivo* through plasma factors inducing inhibiting intrinsic and extrinsic

Results

platelet signaling pathways, leading to decreased platelet activation resulting in reduced thrombus formation *ex vivo* and altered hemostasis *in vivo*. Additionally, enhanced megakaryopoiesis in the spleen of BDL mice was observed following platelet accumulation in the liver and reduced platelet counts in the circulation.

4.2 High levels of bile acids account for platelet activation defects

A main characteristic of obstructive cholestasis is a bile stasis occurring in the blood and in the liver with high plasma concentrations of BAs. As described in Reich *et al* concentrations of up to 1.300 $\mu\text{mol/L}$ for the level of total BAs can be detected 7 days post BDL [181]. Accordingly, a high BA plasma concentration may also be responsible for platelet activation defects as observed in cholestatic mice.

4.2.1 Taurine-conjugated bile acids modulate platelet adhesion in mice

BAs are present in blood in different conjugation states. They can either be unconjugated, glycine conjugated, or taurine conjugated. In line with the conjugation state the affinity of the BAs regarding the different specific BA receptors vary. To investigate which BAs might influence platelet activation and hemostasis, a detailed murine BA composition analysis was performed.

4.2.1.1 Taurine-rich conjugation of bile acids in the plasma of mice

To analyze the effect of BAs on platelet activation and hemostasis, the content of different BAs in the total BA pool of C57BL6/J mice was examined with UPLC-MS/MS analysis of serum samples.

The analysis revealed that the total BA pool consisted of $41.6 \pm 6.33\%$ of taurine conjugated BAs, $55.18 \pm 11.93\%$ unconjugated BAs and only $3.32 \pm 0.52\%$ glycine-conjugated BAs (fig. 12, left). To further distinguish between the abundancy of the different taurine conjugated BAs, it was differentiated between the taurine conjugated BA specimens. Within the taurine conjugated BAs, 59.59% of all were either ω -, α - or β -muricholic acids (MC). These are only formed in mice and not humans [182]. All other BAs were in line with BAs found in the plasma of human beings. Under steady state conditions the taurocholic acid (TC) was the most abundant BA with 36.81% of all detected BA (fig. 12, right), whereas the most toxic BA tauroolithocholic acid (TLC) was not detectable.

Results

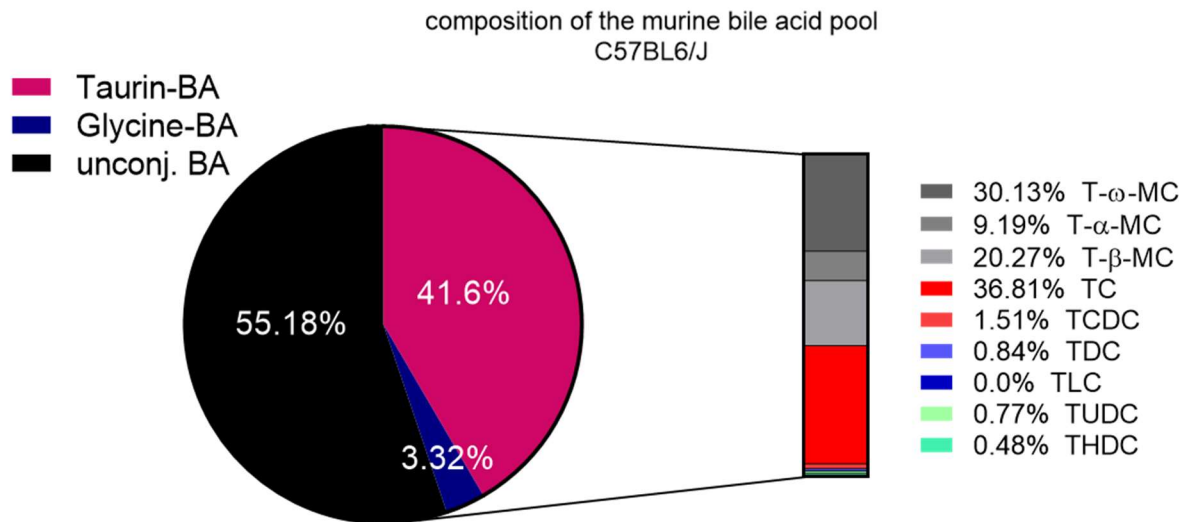


Figure 12. Bile acid pool analysis of serum samples from C57BL6/J mice. Serum samples from mice were analyzed by UPLC-MS/MS. Nearly 2/3 of the murine BA pool in the blood consists of unconjugated BAs. A detailed analysis of taurine-conjugated BAs shows the distribution of different BAs in %. T = taurine; MC = muricollic acid; TC = taurocholic acid; TCDC taurochenodeoxycholic acid; TDC taurodeoxycholic acid; TLC tauro-lithocholic acid; THDC tauro-hyodeoxycholic acid; TUDC tauro-ursodeoxycholic acid. (n = 6)

4.2.1.2 Bile acids account for dysregulated murine platelet activation and adhesion

To study the effect of BAs on platelet activation two different BAs were chosen. With cholestatic liver disease increasing concentrations of different BAs were present in mice, e.g., TCDC and TLC [181]. Prior activation with indicated agonists whole blood of mice was incubated with TCDC and TLC for 60 min. Since, TLC was solved in DMSO, a corresponding DMSO control (0.1%) was also prepared under the same conditions.

Platelet activation measured by P-selectin exposure as marker for degranulation revealed an unaltered activation state of platelets pretreated with BAs following CRP mediated GPVI activation (fig. 13A). Activation of GPCR with PAR4-peptide led to increased P-selectin exposure with PAR4 [70 μ M] and TCDC [50 μ M] ($p = 0.017$) and with PAR4 [200 μ M] and TLC [50 μ M] ($p = 0.021$). Interestingly, all other agonists did not facilitate platelet degranulation due to pre-incubation of BAs. Similar results were obtained when the activation of the $\alpha_{IIb}\beta_3$ integrin of platelets in the presence of BAs was determined (fig. 13B). TLC facilitated the platelet activation which was further induced with PAR4 [200 μ M] ($p = 0.003$), though the stimulation of platelets with all other tested agonists did not show major alterations.

Results

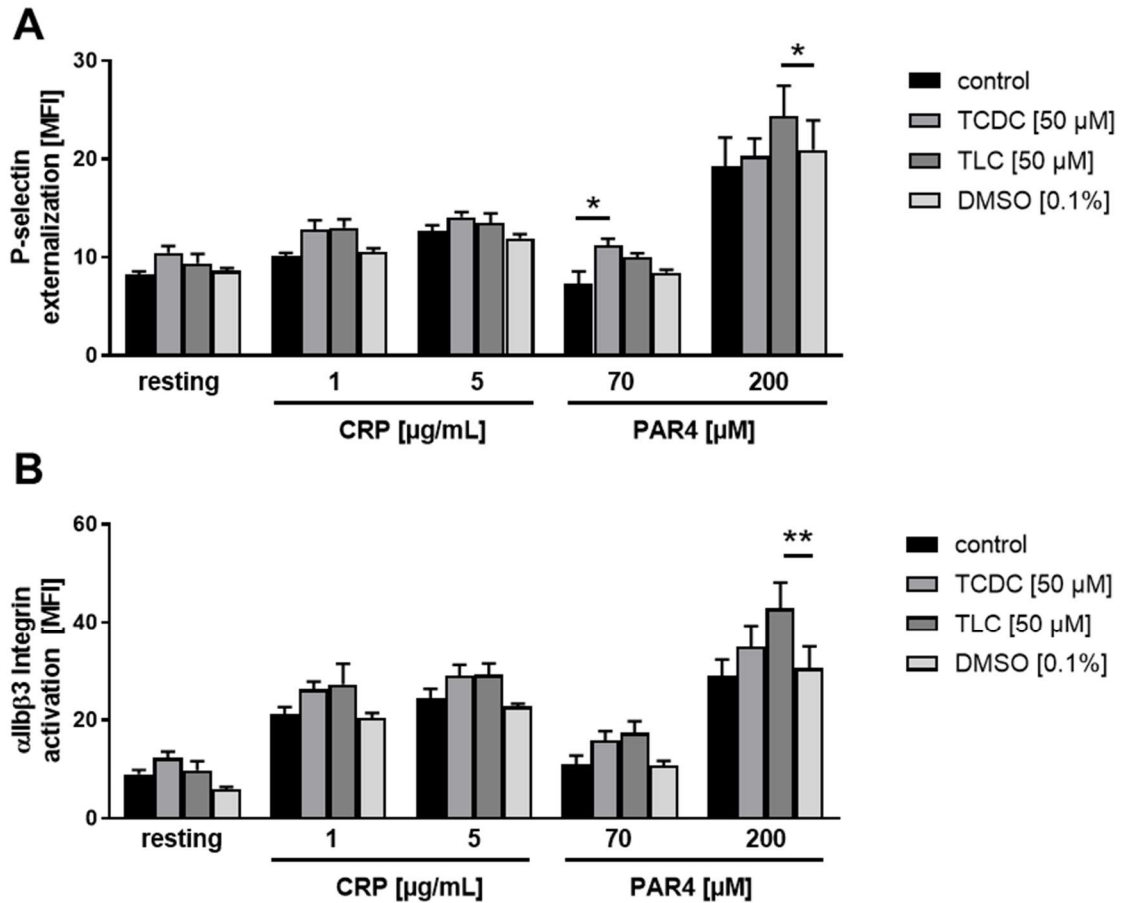


Figure 13. Bile acids have minor impact on murine platelet activation. Platelets drawn from C57Bl6/j mice were preincubated with indicated BAs and DMSO for 1 h at 37 °C. Subsequently, they were analyzed by flow cytometry regarding their specific side scatter (SSC) and forward scatter (FSC) profile. (A) P-selectin exposure was slightly enhanced following PAR-4 stimulation with pre-incubation of BAs ($n = 4$). (B) Integrin $\alpha\text{IIb}\beta\text{3}$ activation was only moderately increased ($n = 4$). * = $p < 0.05$, ** = $p < 0.01$; tested with unpaired students t -test. CRP = collagen-related peptide; MFI = mean fluorescence intensity; TCDC = tauro-deoxycholic acid; TLC = tauro-lithocholic acid

Even though BAs seemed to have a minor impact on platelet activation as measured via flow cytometry, the effect on platelet adhesion stayed unclear. Therefore, a matrix of collagen and fibrinogen was generated, allowing isolated platelets to adhere for 20 min after a preincubation with the indicated BAs.

On a fibrinogen matrix but not on a collagen matrix, a reduced adherence of platelets preincubated with TCDC or TLC was observed (fig. 14). Platelet adhesion to collagen was not altered by preincubation neither with TCDC ($p = 0.203$) nor with TLC compared to the respective control ($p = 0.119$; fig. 14 A+C). The adhesion of platelets on fibrinogen was significantly reduced with and without thrombin activation (fig. 14 B+D). Without activation (resting) platelet adhesion to fibrinogen was reduced ($p = 0.007$) following TCDC preincubation, while the activation of platelets with thrombin led to a reduction of platelet adhesion following preincubation with either TCDC ($p < 0.0001$) or TLC ($p = 0.0003$).

Results

Taken together, BAs are able to modulate murine platelet adhesion to fibrinogen but only have minor effects on platelet activation.

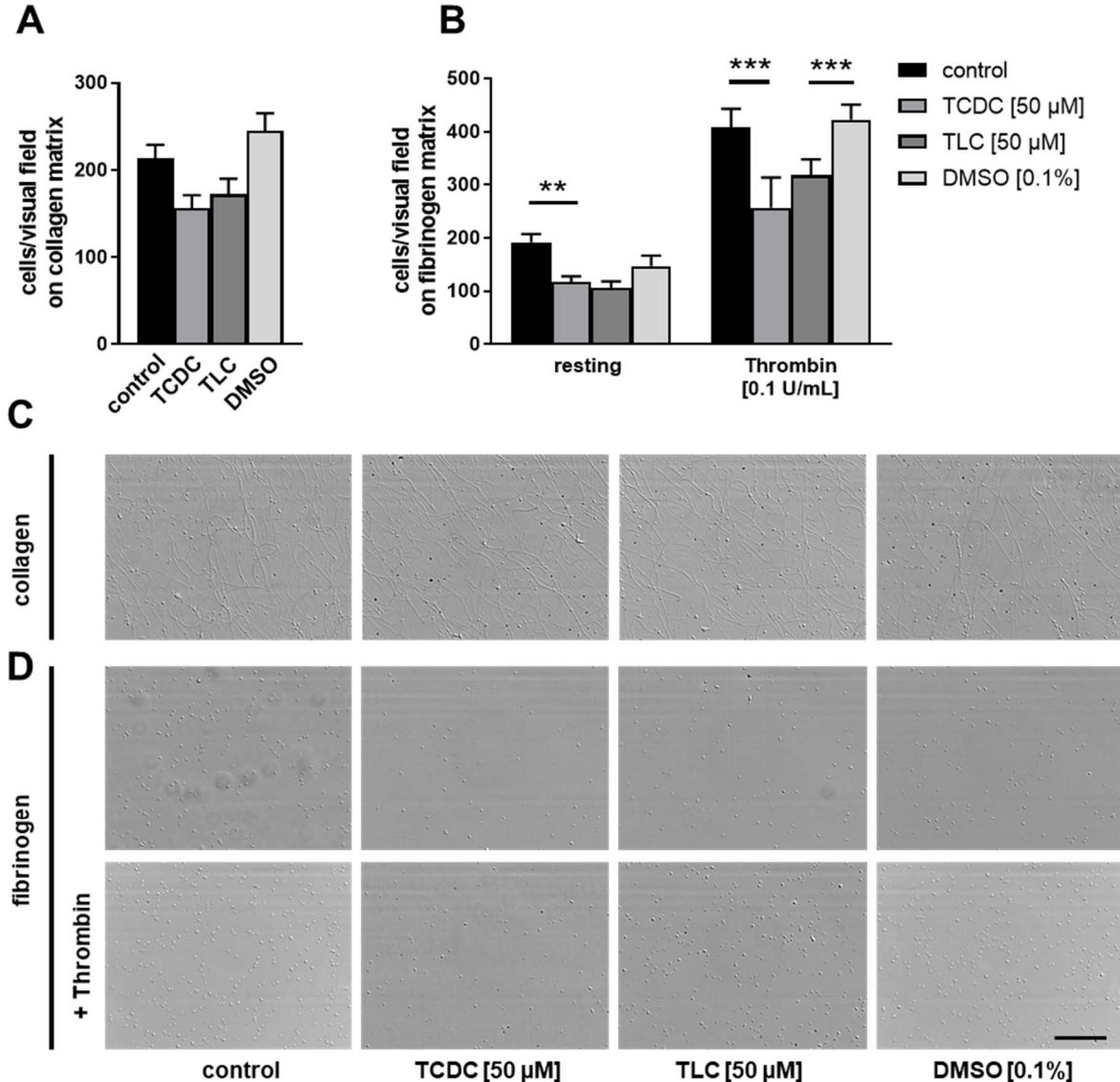


Figure 14. Bile acids influence static adhesion of platelets: Isolated murine platelets were preincubated with indicated BAs and DMSO for 1 h at 37 °C. Subsequently, they were allowed to adhere for 20 min on collagen [100 μg/ml] or fibrinogen [100 μg/ml] coated cover slips. (A) Adhesion on collagen matrix showed no significant differences of platelet adhesion ($n = 3$). (B) When platelets were activated with thrombin for 2 min before adhesion, reduced adhesion of platelets preincubated with BAs was detected compared to the respective control. ($n = 6$). (C) Representative images of adhesion experiments. Scale bar = 20 μm * = $p < 0.05$, ** = $p < 0.01$; tested with unpaired students t -test. TCDC = tauro-deoxycholic acid; TLC = tauro-lithocholic acid

4.2.2 Bile acids moderately alter integrin $\alpha IIb\beta 3$ activation of human platelets

Since BAs affect murine platelet activation and adhesion, we wanted to study the effect of different BAs on the activation of human platelets in a first translational approach. Since murine

Results

and human platelets have mostly homologous receptors and signaling pathways, the before tested taurine-conjugated BAs in murine platelets were used. Since TLC and TDC were solved in DMSO, a corresponding DMSO control was also prepared under the same conditions in every experiment.

4.2.2.1 Bile acids account for reduced integrin activation via GPVI receptor signaling

In a first approach, the effect of different BAs and the corresponding DMSO controls on isolated human platelets was tested. Flow cytometric analysis was used to measure platelet activation by the analysis of $\alpha_{IIb}\beta_3$ integrin activation and P-selectin exposure. Like murine platelets, isolated human platelets were preincubated for 1 h with the indicated BAs. Incubation with the hydrophilic BAs TC and TCDC led to a mild but significant decrease of $\alpha_{IIb}\beta_3$ integrin activation (TC: $p = 0.013$; TCDC: $p = 0.003$) following platelet activation with CRP that activated the major collagen receptor GPVI (fig. 15A). Compared to the hydrophobic BAs TDC and TLC, no activation defects were observed (fig. 15C), since DMSO, the respective control, already reduced CRP mediated $\alpha_{IIb}\beta_3$ integrin activation ($p = 0.038$). Regarding P-selectin externalization no differences between the different agonists or BAs were observed, indicating no regulation of platelet degranulation through BAs (fig. 15 B+D).

Regarding the clinical picture of obstructive cholestasis, it is known that high bile salt concentrations are present in the circulation for a longer time. To get a more detailed picture of the effects of long-lasting elevated plasma bile salt on platelet activation, platelets were coincubated with different BAs and DMSO over a time period of 6-24h. Human platelet-rich plasma was used, and the endogenous plasma BA concentration was increased by indicated amounts of BAs. Additionally, a glycine-conjugated BA for human platelet activation (GCDC) was tested. Since no effects of the GPCR mediated activation of $\alpha_{IIb}\beta_3$ integrin was detected, we only focused on the CRP mediated GPVI signaling pathway.

Results

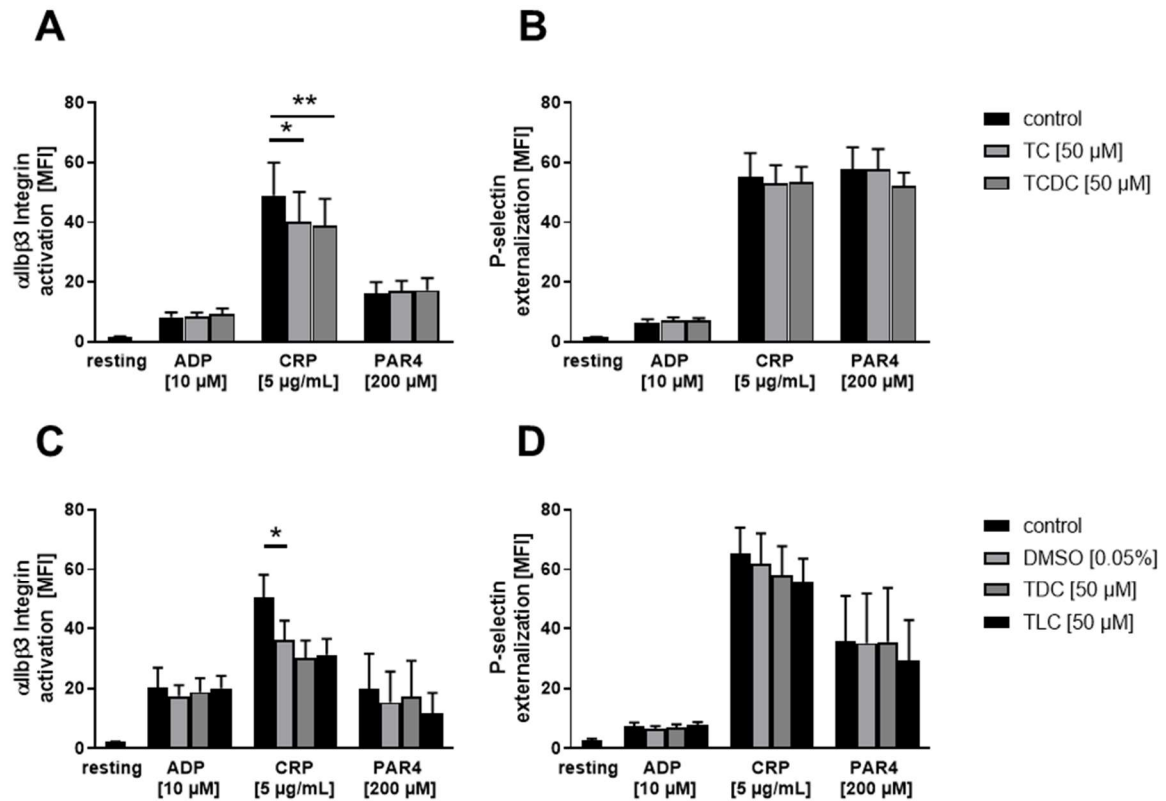


Figure 15. Bile acids have minor impact on short-term human platelet activation. Platelets drawn from healthy volunteers were preincubated with indicated BAs and DMSO for 1 h at 37°C. Subsequently, they were analyzed using a flow cytometer regarding their specific side scatter (SSC) and forward scatter (FSC) profile. (A) preincubation of platelets with hydrophilic BAs showed reduced Integrin $\alpha_{IIb}\beta_3$ activation following CRP stimulation, whereas no defects in degranulation were detected as shown by unaltered P-selectin externalization (B). (C) Integrin $\alpha_{IIb}\beta_3$ activation after preincubation with hydrophobic BAs showed no defects compared to the respective DMSO control. (D) No defects in degranulation were detected as measured by P-selectin externalization of platelets. ($n = 4$). * = $p < 0.05$, ** = $p < 0.01$; tested with unpaired students t -test. CRP = collagen-related peptide; MFI = mean fluorescence intensity; TC = tauro-cholic acid; TCDC = tauro-deoxycholic acid; TDC = taurodeoxycholic acid; TLC = tauro-lithocholic acid

The results point out that the activation of platelet $\alpha_{IIb}\beta_3$ integrin decreased from 6 h to 12 h incubation ($p = 0.0171$) and from 6 h to 24 h ($p < 0.0001$) even without the addition of BAs due to the susceptibility of platelets (fig. 16 A). The strongest inhibiting effect was detected after 6 h incubation time and CRP activation. The CRP activation was inhibited by TC ($p = 0.027$), TCDC ($p = 0.0389$) and GCDC ($p = 0.0030$; fig. 16A). Hydrophobic BAs only had a mild effect on integrin activation without reaching statistical significance after 24 h of coincubation and subsequent activation of GPVI signaling (fig. 16C). As measured before, coincubation even for longer time, had no effect on platelet degranulation as measured via P-selectin externalization despite using hydrophilic or hydrophobic BAs (fig. 16B+D).

Results

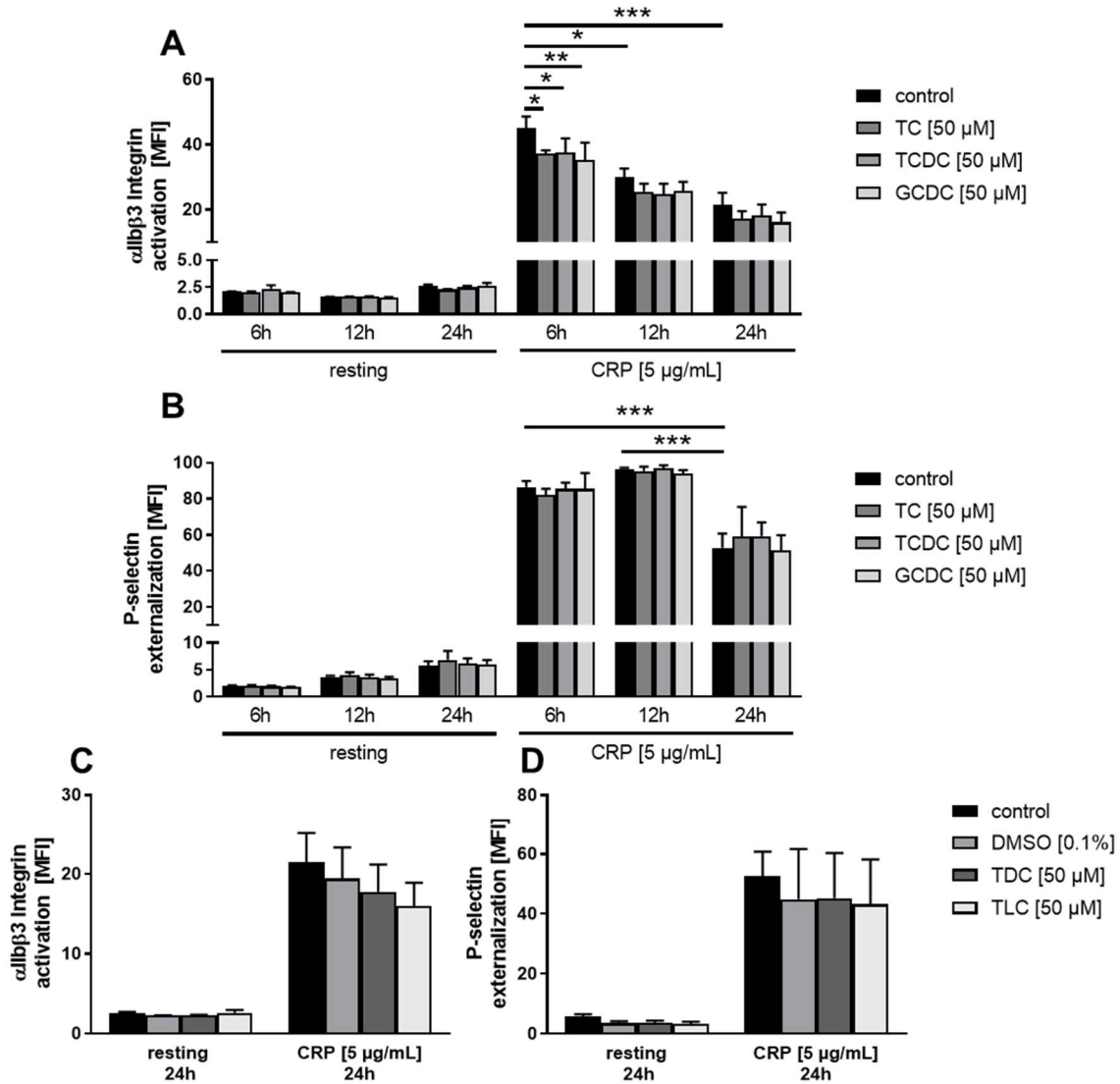


Figure 16. Effects of bile acids on long-term human platelet activation. Platelet-rich plasma (PRP) drawn from healthy volunteers was pre-incubation with indicated BAs and DMSO for 1 h at 37 °C. Subsequently, the samples were analyzed in the flow cytometer regarding their specific side scatter (SSC) and forward scatter (FSC) profile. (A) Integrin α IIb β 3 activation after pre-incubation with hydrophilic BAs showed activation with all tested hydrophilic BAs after 6 h. (B) No influence of BAs on P-Selectin externalization could be observed. Overall reduced time-dependent activation was observed due to platelet susceptibility. (C) Integrin α IIb β 3 activation after pre-incubation with hydrophobic BAs showed no defects compared to the respective DMSO controls. (D) No defects in degranulation measured via P-selectin externalization were observed. ($n = 4-7$). * = $p < 0.05$, ** = $p < 0.01$; tested with Two-Way ANOVA with Bonferroni's post hoc test. CRP = collagen-related peptide; MFI = mean fluorescence intensity; TC = tauro-cholic acid; TCDC = tauro-deoxycholic acid; TDC = taurodeoxycholic acid; TLC = tauro-lithocholic acid

4.2.2.2 Bile acids alter the adhesion of human platelets to fibrinogen

The analysis of murine platelets revealed no major activation defects but reduced platelet adhesion in the presence of BAs in a fibrinogen matrix. Experiments with human platelets showed reduced GPVI mediated integrin activation in flow cytometry 6 h after incubation with

Results

the hydrophilic BAs TC, TCDC and GCDC. Therefore, we analyzed the adhesion of human platelets under static conditions.

Adhesion of isolated human platelets with indicated BAs for 1 h revealed a down-regulation of platelet adhesion on a fibrinogen matrix. The presence of the hydrophilic BAs TC ($p = 0.0067$) and TCDC ($p = 0.010$) decreased adhesion. The DMSO dissolved BAs TDC ($p = 0.0117$) and TLC ($p = 0.0444$) also inhibited adhesion compared to the respective DMSO control (fig. 17). DMSO itself had no effects on platelet adhesion on fibrinogen.

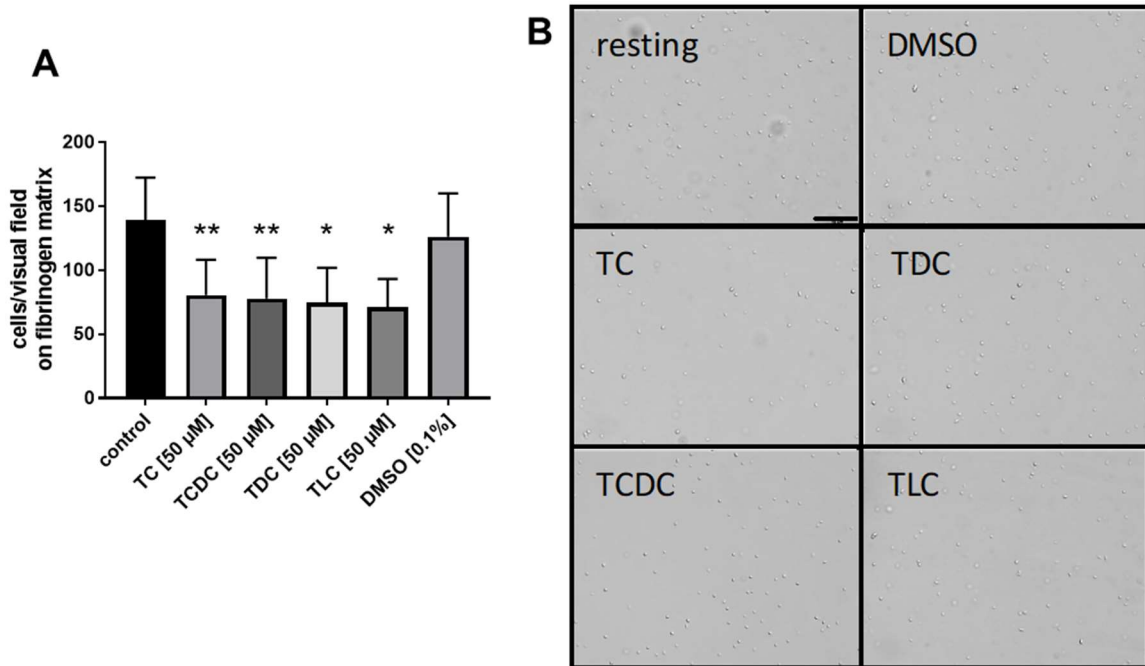


Figure 17. Bile acids influence static adhesion of human platelets to fibrinogen: Isolated human platelets from healthy volunteers were pre-incubated with indicated BAs and DMSO for 1 h at 37 °C. Subsequently, they were allowed to adhere to fibrinogen [100 μ g/mL] coated cover slips for 20 min. (A) Platelets show decreased adhesion in the presence of all indicated BAs compared to their respective control. ($n = 6$). (B) Representative images of adhesion experiments. Scale bar = 20 μ m * = $p < 0.05$, ** = $p < 0.01$; tested with One-Way ANOVA to respective control group. TC = tauro-cholic acid; TCDC = tauro-deoxycholic acid; TDC = taurodeoxycholic acid; TLC = tauro-lithocholic acid

Taken together these results provide evidence for a regulatory effect of BAs on the adhesion of platelets to fibrinogen. The adhesion of platelets to fibrinogen is mediated by $\alpha_{IIb}\beta_3$ integrin outside-in signaling while flow cytometric analysis focuses on the inside-out signaling to stimulate $\alpha_{IIb}\beta_3$ integrin activation. Thus, the main effect of platelet inhibition by BA is based on defective $\alpha_{IIb}\beta_3$ integrin outside in signaling leading to reduced platelet adhesion on fibrinogen. Therefore, these results highlight the regulatory effect of BAs on platelet adhesion that also might account for defective activation of platelets after BDL.

4.3 Partial hepatectomy impairs hemostasis and modulates platelet biogenesis

We analyzed platelet activation, hemostasis, and thrombocytopenia in another mouse model of liver disease that is characterized by acute cytokine signaling and loss of liver mass namely 2/3 PHx [93]. In a first approach, platelet activation, thrombosis, and hemostasis after PHx in C57Bl6 mice were studied. In a second step, thrombopoiesis in PHx mice was analyzed focusing on the regulation of thrombopoietin signaling in regenerative liver tissue, using WT mice as well as *IL-6R^{-/-}* mice, *Asgr2^{-/-}* mice and the fusion protein hIL-6. In a third approach, the liver regeneration in a genetic mouse model of thrombocytopenia was taken into consideration using the *Mpl^{-/-}* mouse strain.

4.3.1 PHx provokes reduced platelet activation resulting in impaired thrombus formation and hemostasis

4.3.1.1 Partial hepatectomy induces anemia and thrombocytopenia

PHx was performed to remove 2/3 of the liver in wildtype (WT) mice. As described in methods part 3.1 sham mice served as control group. Analysis of the total blood cell count revealed that platelet counts were significantly reduced by 16.4% 1 day after PHx (sham: $847.15 \pm 35.39 \times 10^3/\mu\text{L}$; PHx: $707.75 \pm 32.30 \times 10^3/\mu\text{L}$; $p = 0.0058$) and fully restored 7 days after PHx (fig. 18A). In line with recovering platelet counts, enhanced platelet size by 6% on day 1 (sham: 21.43 ± 0.26 ; PHx: 22.70 ± 0.20 ; $p = 0.0007$) and 10.4% on day 3 (sham: 21.23 ± 0.36 ; PHx: 23.43 ± 0.63 ; $p = 0.025$) was measured post PHx by flow cytometry using the geometric mean of GPIIb positive platelets in their FSC profile (fig. 18B). Despite thrombocytopenia, no major alterations in WBC counts were detected (fig. 18C). According to thrombocytopenia, RBC count was reduced 1 day after PHx by 9% (sham: $9.03 \pm 0.13 \times 10^6/\mu\text{L}$; PHx: $8.24 \pm 0.16 \times 10^6/\mu\text{L}$; $p = 0.0008$) and restored 7 days after PHx to normal counts (fig. 18D). Liver weight in relation to organ weight was calculated to measure the liver weight ratio. According to published data [93], the total liver mass was recovered after 14 days post PHx (fig. 18E).

Results

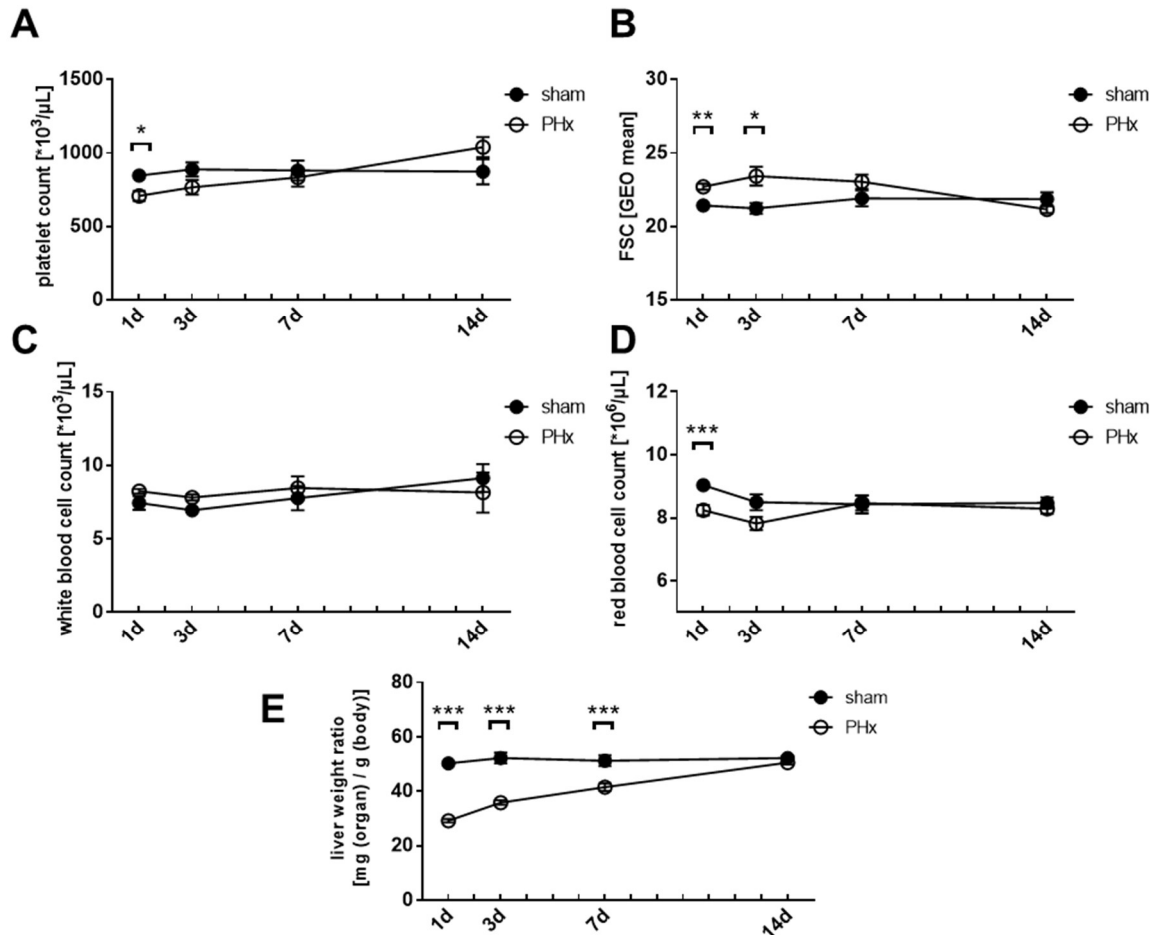


Figure 18. Mild thrombocytopenia and anemia early after partial hepatectomy. Whole blood from sham and PHx mice was taken and analyzed with a hematology analyzer (Sysmex KN-X21). (A) Platelet count analysis revealed mild thrombocytopenia 24 h after PHx (n= 1d: 22 sham, 30 PHx, 3d: 22 sham, 26 PHx; 7d: 16 sham, 20 PHx; 14d: 8 sham, 12 PHx). (B) Platelet size of PHx and sham mice measured via flow cytometry using the geometric mean of GPIb positive platelets. After PHx platelets display enlargement up to 3 days after operation (n= 1d: 10 sham, 14 PHx, 3d/7d/14d: 6 sham, 8 PHx). (C) White blood cell count is unaltered after PHx. (D) Red blood cell count of C57Bl6/J mice undergoing PHx indicates mild anemia for 1 day after PHx (n= 1d: 22 sham, 30 PHx, 3d: 22 sham, 26 PHx; 7d: 16 sham, 20 PHx; 14d: 8 sham, 12 PHx). (E) Calculated liver weight ratio shows full liver volume regeneration after 14 days (n= 5 sham, 8 PHx). * = $p < 0.05$, ** = $p < 0.01$, *** = $p < 0.001$ tested with unpaired students t-test.

4.3.1.2 Platelet activation defects are mainly established 24 h after partial hepatectomy

To investigate if a dysregulated platelet count was associated with platelet activation defects or alterations in platelet receptor abundance at the platelet surface, platelets from PHx operated mice and respective sham controls were analyzed by flow cytometry. Antibodies directed against the most abundant glycoproteins on the platelet surface revealed an unaltered glycoprotein exposure at the surface of platelets 1 day after PHx (fig. 19A). Analysis of platelet degranulation was evaluated via determination of P-selectin externalization upon platelet stimulation with indicated agonists. The results demonstrated that platelets from PHx mice displayed degranulation defects following stimulation with indicated agonists. In specific, the activation of the ITAM coupled GPVI receptor pathway showed degranulation defects using

Results

intermediate ($p = 0.0008$) and high ($p < 0.0001$) CRP concentrations, while GPCR activation induced degranulation defects at low thrombin ($p = 0.006$) or low ($p = 0.046$) and intermediate ($p = 0.028$) PAR-4 peptide concentrations. The second wave mediators U46 and ADP led also to reduced P-selectin exposure ($p = 0.013$; fig. 19B). Interestingly, the activation of integrin $\alpha_{IIb}\beta_3$ was only moderately decreased in response to intermediate ($p = 0.014$) and high ($p = 0.034$) CRP concentrations (fig. 19C), while the externalization of the β_3 subunit was significantly reduced in response to high doses of either CRP ($p < 0.0001$) or thrombin ($p = 0.010$) while no alterations were detected with ADP (fig. 19D).

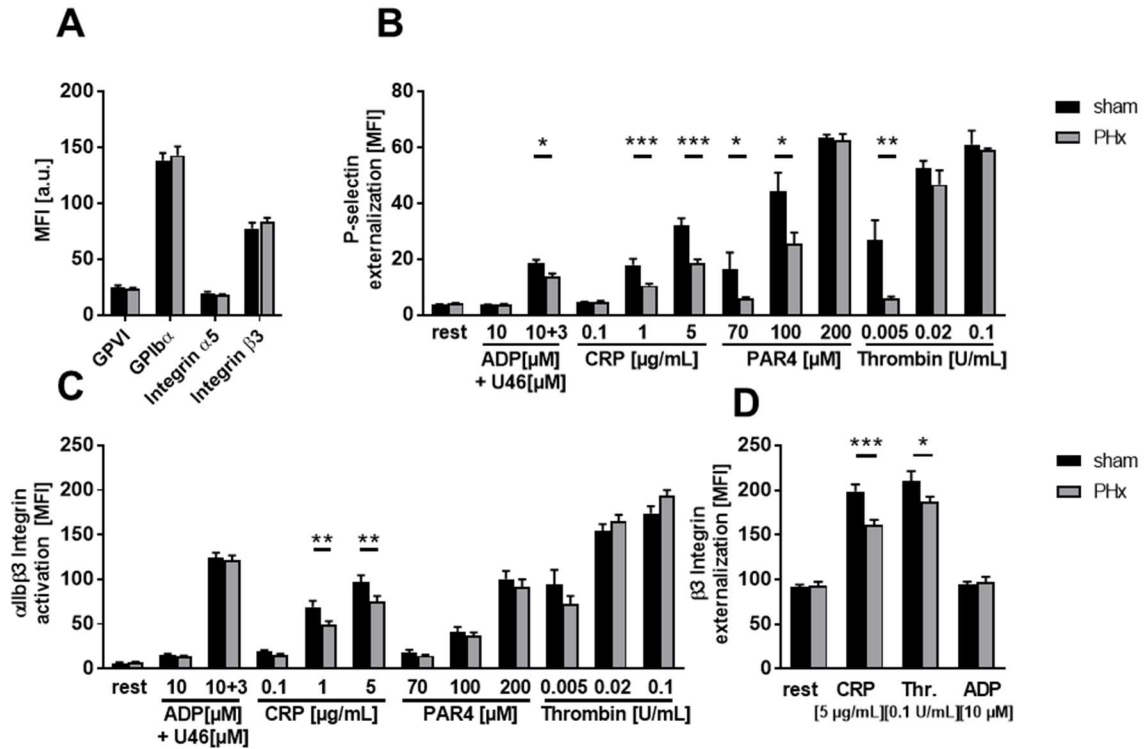


Figure 19. Platelet activation defects 1 day after PHx. At day one after PHx, platelets are analyzed in the flow cytometer regarding their specific side scatter (SSC) and forward scatter (FSC) profile. (A) Expression of indicated glycoproteins on the surface of platelets measured via mean fluorescence intensity (MFI) indicate no differences between sham and PHx mice ($n = 11$ sham + 18 PHx). (B) Externalization of P-selectin at the platelet surface in response to indicated agonists showed major degranulation defects ($n = 6$ sham, 9 PHx). (C) Defects in activation of $\alpha_{IIb}\beta_3$ integrin at the platelet surface was restricted to CRP stimulation. ($n = 6$ sham, 9 PHx). (D) Activation induced up-regulation of the β_3 integrin subunit at the platelet surface ($n = 6$ sham, 8 PHx). * = $p < 0.05$, ** = $p < 0.01$; tested with unpaired students *t*-test. CRP = collagen-related peptide.

4.3.1.3 Reduced thrombus formation results in dysregulated hemostasis one day after PHx

To investigate if platelet activation defects also provoked defects in thrombus formation under flow conditions, thrombus formation on collagen was analyzed in an *ex vivo* flow chamber. Hereby, thrombus formation was performed using two different arterial shear rates, $1000s^{-1}$, and $1700s^{-1}$, as thrombus formation under high arterial shear rates is GPIIb dependent. Perfusion of whole blood from PHx operated mice led to significantly reduced thrombus formation compared to sham controls (fig. 20A). At a shear rate of $1000s^{-1}$ a 16.9% reduced

Results

surface coverage was measured in PHx mice compared to WT (sham: $54.63 \pm 2.46\%$ PHx: $45.35 \pm 2.47\%$; $p = 0.027$), while the reduction was 35.7% (sham: $48.34 \pm 4.4\%$; PHx: $31.05 \pm 2.82\%$; $p = 0.0047$) using a high arterial shear rate of 1700s^{-1} (fig. 20B).

A reduced thrombus formation is often an indicator for dysregulated hemostasis or thrombosis. Thus, *in vivo* effects of platelet activation defects were investigated. As already described for BDL operated mice, the tail tip of the mice was cut to record the time until bleeding stopped. A prolonged tail bleeding time of PHx operated mice (315.9 ± 37.46 s) compared to sham controls ($174.8 \pm 25.6\text{s}$; $p = 0.0085$) was detected (fig. 20C). On the contrary, platelet activation defects and prolonged tail bleeding time resulted in no major alteration in arterial thrombosis. Fe₃Cl-induced injury of the carotid artery led to a comparable occlusion time of the vessel after 439 s \pm 57 in PHx mice and 409 s \pm 29 ($p = 0.47$) in sham controls (fig. 20D). Furthermore, no difference was examined regarding the appearance of the initial thrombus (sham: 202 ± 48 s; PHx: 156.4 ± 37 s; $p = 0.46$) (fig. 20E).

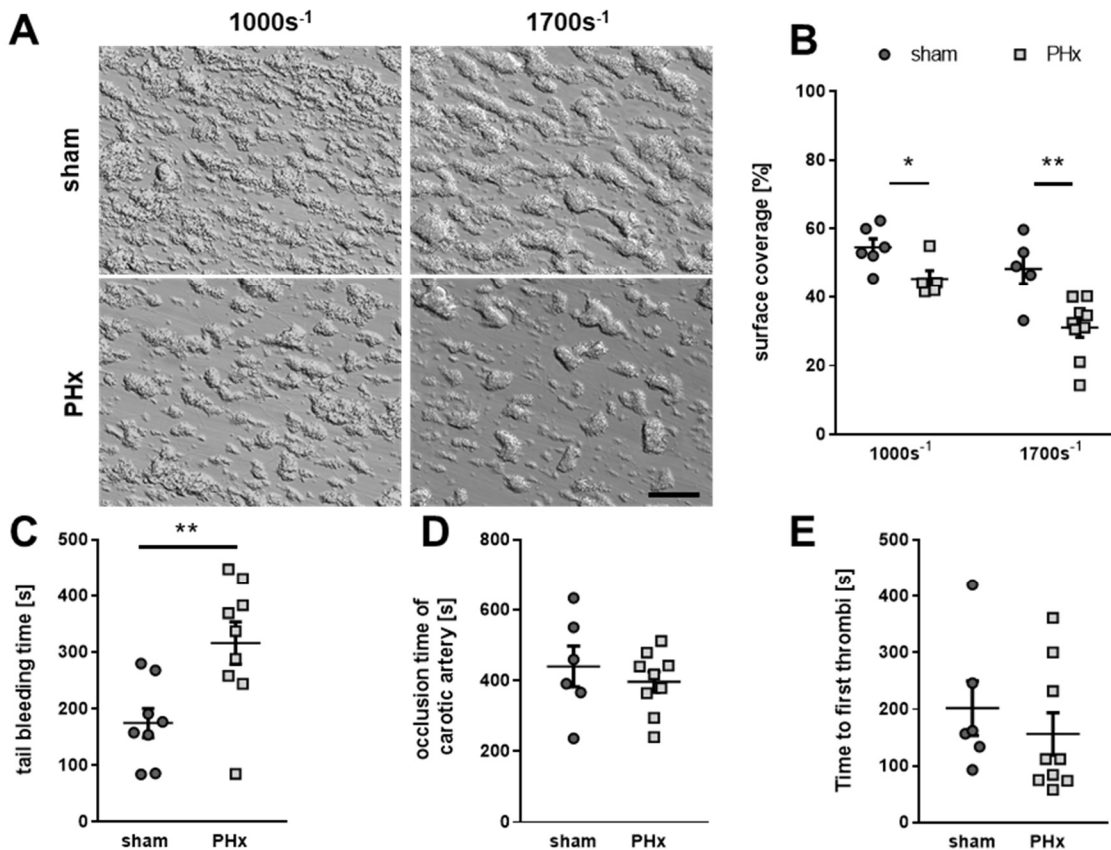


Figure 20. Partial hepatectomy causes defective thrombus formation and hemostasis 1 day after PHx. Sham and PHx mice were analyzed *ex vivo* and *in vivo*. (B) Murine whole blood laced with heparin was perfused over a collagen matrix [100 μg/ml] in the flow chamber system and revealed diminished thrombus formation with both tested shear rates (representative pictures as indicated; 1000s^{-1} $n = 6$ sham, 5 PHx; 1700s^{-1} $n = 5$ sham, 9 PHx). (A) Representative images of PHx mice and sham controls 1 day after PHx. Scale bar = 50 μm. (C) The tail tip of mice was dissected with a diameter of 1 mm and bleeding was recorded until it stopped. PHx mice compared to sham mice showed prolonged tail bleeding time ($n = 8-9$). (D) *In vivo* analysis of thrombosis of the carotid artery via Fe₃Cl induced injury of the vessel. Neither differences in the occlusion time of the artery nor development of the first thrombi were observed (E) (sham = 6; PHx = 9), ** = $p < 0.01$ tested with unpaired students *t*-test.

Results

4.3.1.4 Enhanced glycoprotein exposure but constant platelet activation defects 3 days after PHx

To investigate whether the measured activation defects 1 day after PHx are causally linked to thrombocytopenia, platelet activation was measured 3 days after PHx. At that time point platelet count was comparable to sham controls.

Analysis of GP exposure on the platelet surface revealed an increase of β_3 integrin ($p = 0.0050$), α_5 integrin ($p = 0.0053$) and GPIIb/IIIa ($p = 0.044$), while GPVI exposure was not altered 3 days after PHx (fig. 21A). Platelet degranulation defects measured via P-selectin externalization were still present 3 days after PHx. Compared to 1 day after PHx, the differences between sham and PHx mice diminished. GPVI dependent degranulation was still decreased with low ($p = 0.039$) and with moderate ($p = 0.0028$) CRP concentrations, while only moderate thrombin concentration still evoked reduction of platelet degranulation ($p = 0.013$; fig. 21B). Unexpectedly, GPVI dependent activation of $\alpha_{IIb}\beta_3$ integrin was still decreased on day 3 using moderate ($p = 0.0411$) and high ($p = 0.0036$) CRP concentrations, although active $\alpha_{IIb}\beta_3$ integrin was already upregulated ($p = 0.0091$) in resting platelets (fig. 21C). Still, externalization was unaltered upon stimulation with CRP or thrombin, while a mild stimulus like ADP still reflected enhanced β_3 upregulation on platelet surface (fig 21D).

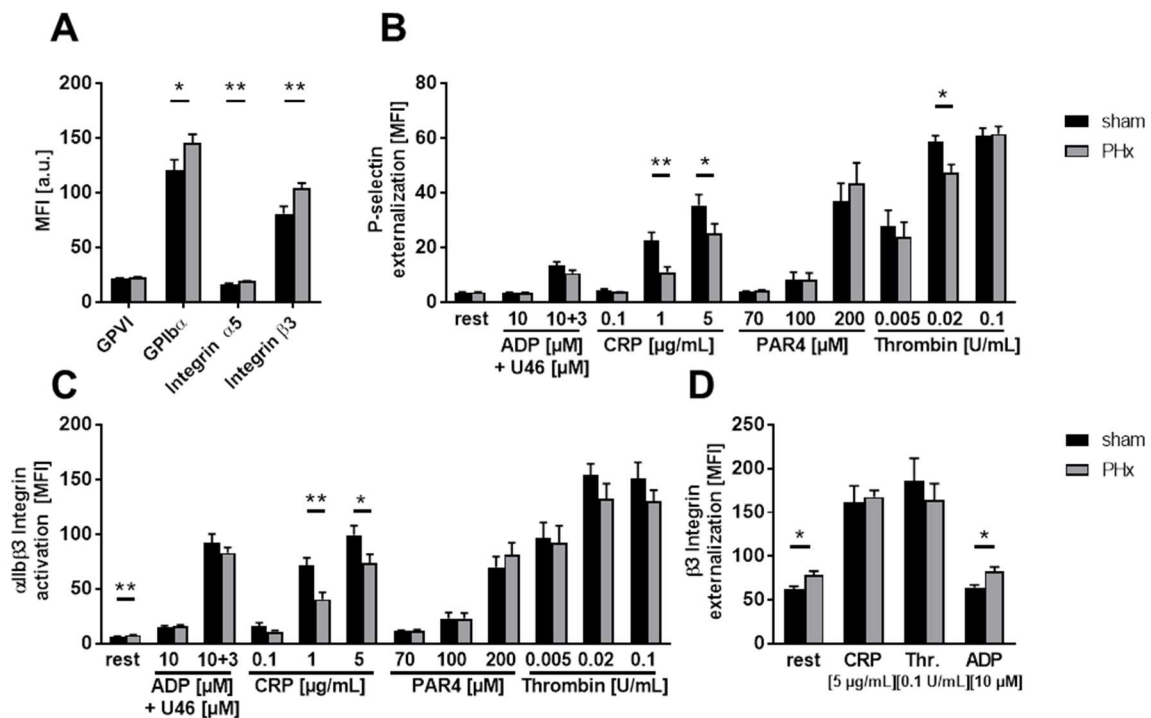


Figure 21. 3 days after PHx mild platelet activation defects were detected. 3 days after PHx Platelets were analyzed via flow cytometry regarding their specific side scatter (SSC) and forward scatter (FSC) profile. (A) Expression of indicated glycoproteins on the surface of platelets measured via mean fluorescence intensity (MFI) indicated enhanced glycoprotein expression of PHx mice ($n = 13$ sham + 18 PHx). (B) Externalization of P-selectin on the platelet surface with indicated agonists showed mild degranulation defects with CRP and thrombin ($n = 9$ sham, 12 PHx). (C) Activation of $\alpha_{IIb}\beta_3$ integrin at the platelet surface revealed pre-activated integrin on the surface of platelets, while CRP stimulation showed activation defects ($n = 9$ sham, 12 PHx). (D) Externalization of the β_3 integrin subunit upon platelet stimulation with indicated agonists ($n = 8$ sham, 9 PHx). * = $p < 0.05$, ** = $p < 0.01$; tested with students unpaired t-test. CRP = collagen-related peptide.

Results

4.3.1.5 Attenuated platelet defects result in defective thrombus formation and hemostasis 3 days after PHx

Next, it was of interest if the generation of three-dimensional thrombi was still decreased and if this affected the hemostasis 3 days after PHx. The already described moderate platelet activation defects translated into impaired thrombus formation by 18.7% (sham: $65.45 \pm 1.30\%$; PHx: $53.18 \pm 2.81\%$; $p = 0.0173$) using a shear rate of 1000 s^{-1} while no alterations were detected at a shear rate of 1700 s^{-1} (sham: $53.96 \pm 2\%$; PHx: $53.22 \pm 5.14\%$; fig. 22A+B). Moreover, bleeding time was still significantly prolonged 3 days after PHx compared to 1 day after PHx, even though three out of eight mice had already compensated for hemostatic defects (fig. 22C) Therefore, the bleeding time 3 days after PHx was prolonged with $526.1 \text{ s} \pm 131.5$ compared to sham controls (sham: $186.1 \pm 56.23 \text{ s}$, $p = 0.0256$).

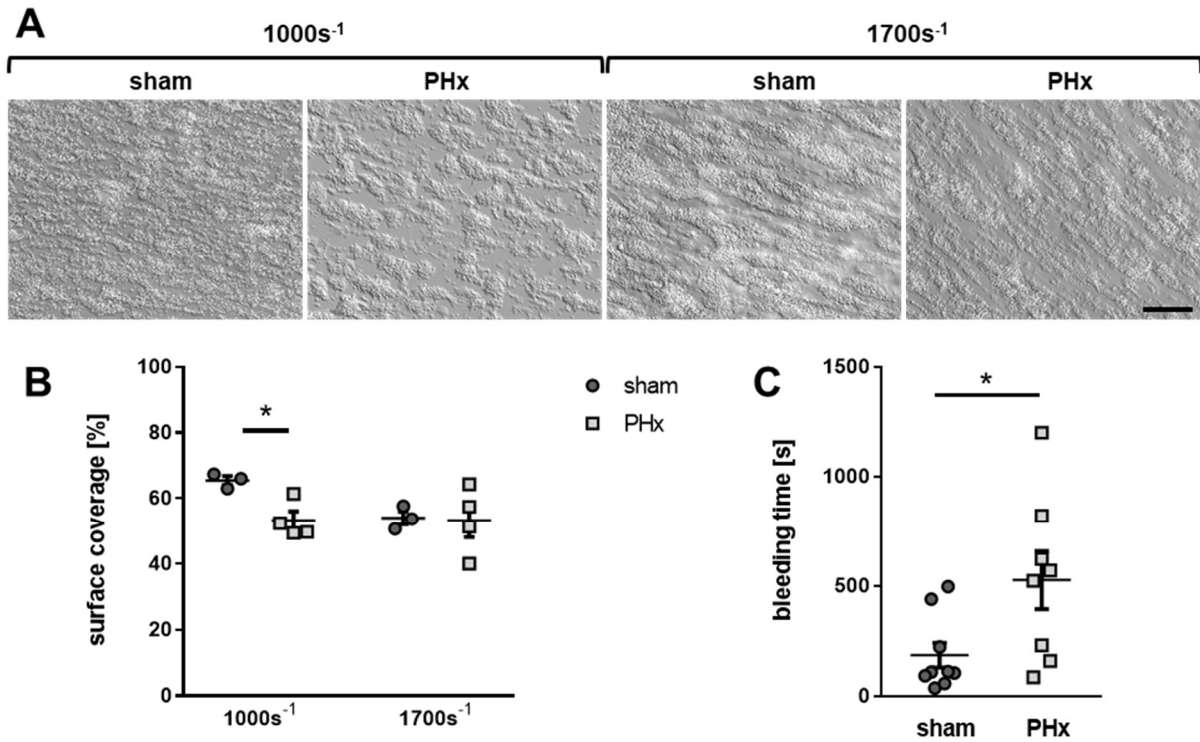


Figure 22. Partial hepatectomy causes defective thrombus formation and hemostasis 3 days after PHx. Sham and PHx mice were analyzed *ex vivo* and *in vivo*. (A) Murine whole blood anticoagulated with heparin was perfused over a collagen matrix [$100 \mu\text{g}/\text{ml}$] using a flow chamber system. Representative images of PHx mice and sham controls 3 days after PHx. (B) Generation of three-dimensional thrombi was diminished at a shear rate of 1000s^{-1} but unaltered at a shear rate of 1700s^{-1} ($n = 3$ sham, 4 PHx). Scale bar = $50 \mu\text{m}$ (C) The tail tip of mice was dissected with a diameter of 1 mm and bleeding was recorded until it stopped. PHx mice compared to sham mice showed prolonged tail bleeding time ($n = 8-9$ * = $p < 0.05$ tested with unpaired students *t*-test).

4.3.1.6 Unaltered platelet activation 7 and 14 days after PHx

The question rises if platelet activation defects persist, although platelet counts are completely recovered 7 days after PHx and the liver mass is fully restored through proliferation of hepatocytes 10-14 days after resection [93]. To exclude that liver resection might have a long-

Results

term influence on platelets, platelet activation and thrombus formation were examined at 7 and 14 days after PHx.

Flow cytometric analysis using platelets from mice 7 days after PHx showed no significant differences in their activation pattern, neither for the activation of $\alpha_{IIb}\beta_3$ integrin (fig. 23C), nor for degranulation measured via P-selectin with all tested agonists (fig. 23B). In addition, no alterations were detected when the GP exposure or the externalization of the β_3 integrin subunit was measured using different agonists such as CRP, PAR-4, thrombin, or ADP (fig. 23 A+D). Flow chamber experiments for indicated arterial shear rates showed no differences in the formation of three-dimensional thrombus formation (fig. 23 E+F) either.

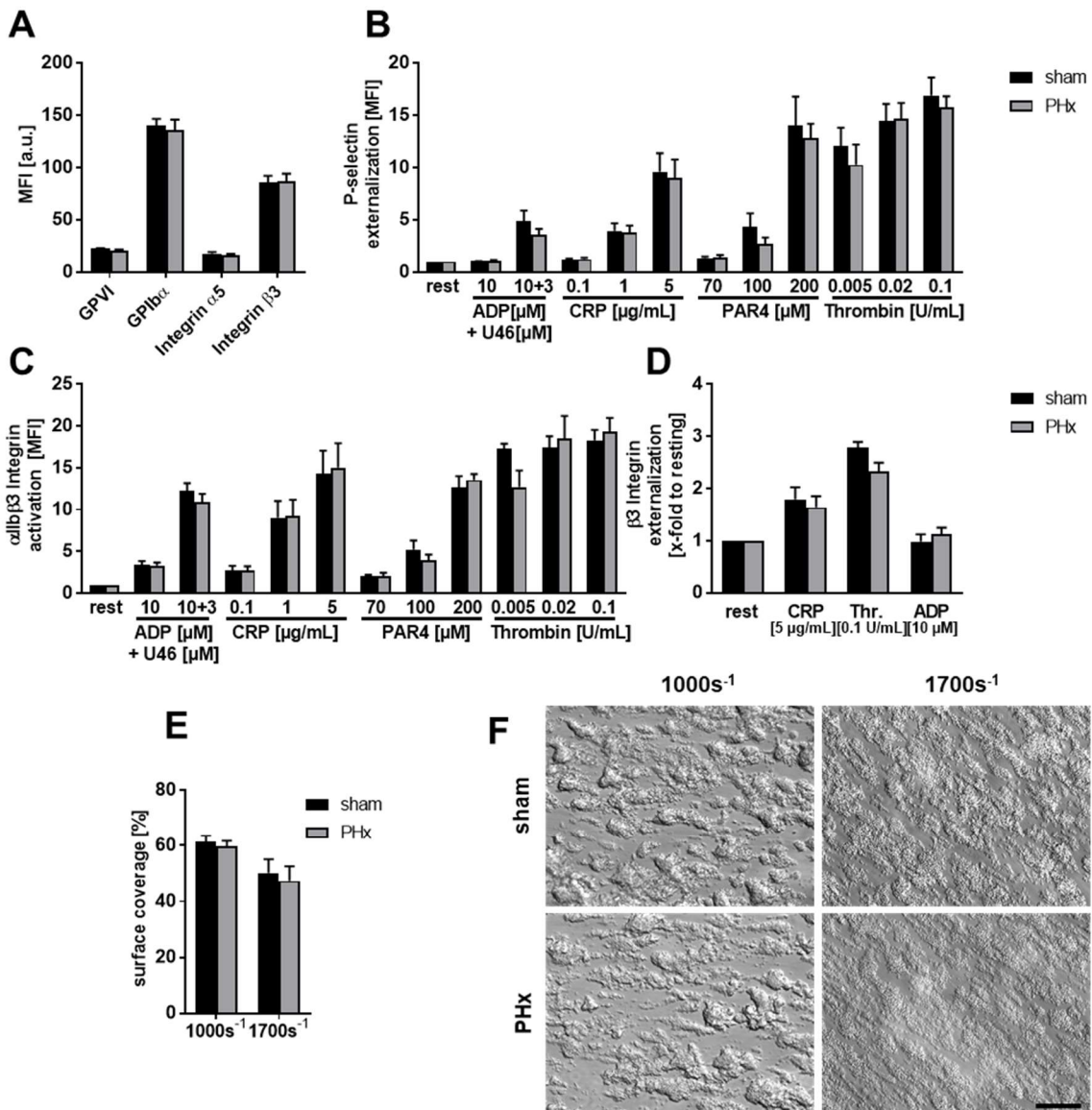


Figure 23. Unaltered platelet activation and thrombus formation 7 days after PHx. Platelets were analyzed in the flow cytometer regarding their specific side scatter (SSC) and forward scatter (FSC) profile. (A) Surface expression of indicated glycoproteins 7 days post PHx via MFI in flow cytometric analysis shows no difference (n = 9 sham, 11 PHx). (B) Platelet activation measured via externalization of P-selectin and (C) activation of $\alpha_{IIb}\beta_3$ integrin on the platelet surface 7 days after PHx (n = 6 sham, 9 PHx) revealed no difference of PHx mice. (D) Externalization upon platelet stimulation of the β_3 integrin subunit 7 days post PHx (n = 3 sham, 5 PHx). (E) Thrombus formation on a collagen matrix [100 μ g/ml] under arterial shear rates with (F) representative pictures (1000s⁻¹ and 1700s⁻¹ n = 3 sham, 5 PHx). Scale bar = 50 μ m; statistical significance was tested with unpaired students t-test. CRP = collagen-related peptide; Thr. = Thrombin

Results

Flow cytometric analysis from platelets 14 days after PHx showed no significant differences in their activation pattern with all tested agonists, neither for the activation of $\alpha_{IIb}\beta_3$ integrin, nor for the up-regulation of β_3 integrin on the platelet surface nor for degranulation as measured by P-selectin exposure (fig. 24 B-D). As expected, GP exposure of sham mice was comparable to PHx mice (fig. 24A). Flow chamber experiments for both tested arterial shear rates showed no differences in the formation of three-dimensional thrombi (fig. 24 E+F).

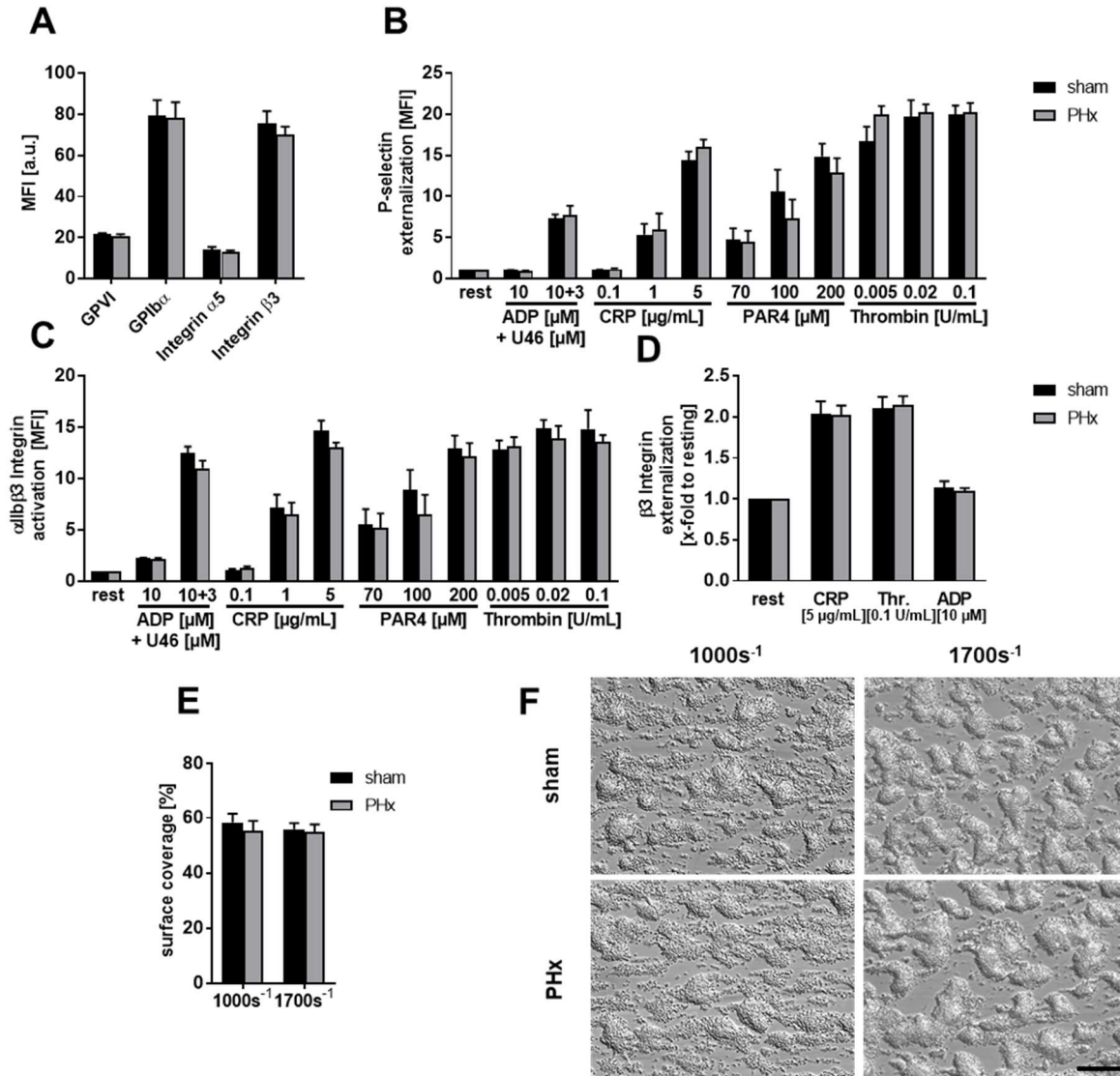


Figure 24. Unaltered platelet activation and thrombus formation 14 days after PHx. Platelets isolated from mice 14 days post PHx were analyzed via flow cytometry regarding their specific side scatter (SSC) and forward scatter (FSC) profile. (A) Expression of indicated glycoproteins measured via flow cytometric analysis showed no differences ($n = 10$ sham, 12 PHx). (B) Platelet activation measured via externalization of P-selectin and (C) activation of $\alpha_{IIb}\beta_3$ integrin on the platelet surface 14 days after PHx ($n = 6$ sham, 9 PHx) revealed no differences compared to controls. (D) Externalization of the β_3 integrin subunit after platelet stimulation 14 days post PHx ($n = 3$ sham, 4 PHx). (E) Thrombus formation on a collagen matrix [100 μ g/ml] under arterial shear rates with (F) representative pictures (1000s⁻¹ and 1700s⁻¹ $n = 5$). Scale bar = 50 μ m; statistical significance was tested with unpaired students *t*-test. CRP = collagen-related peptide; Thr. = Thrombin

Results

4.3.2 Platelet activation defects upon PHx are due to enhanced plasma levels of NO, PGI₂ and bile acids

In BDL operated mice platelet activation defects are mainly due to enhanced levels of NO and PGI₂. Furthermore, enhanced levels of NO and PGI₂ are already described in rats and humans after liver resection [179, 183]. As described above, platelet activation defects persist up to 3 days after PHx, resulting in reduced thrombus formation and prolonged tail bleeding time. Therefore, NO and PGI₂ plasma levels 1 and 3 days after PHx were measured. Since enhanced NO and PGI₂ plasma levels are known to modulate VASP phosphorylation, it was analyzed if an altered phosphorylation of the VASP was detectable in platelets of PHx and sham operated mice.

4.3.2.1 PHx induces elevated levels of PGI₂ and NO in the plasma for 1 day

PHx and sham operated mice were bled under isoflurane anesthesia and plasma was drawn by centrifugation. The plasma level of PGI₂ was measured via ELISA, while NO concentration was indirectly measured through the NO metabolites nitrite and nitrate.

A 1.94 - fold higher level of plasma PGI₂ was observed in PHx mice compared to sham controls 1d after surgery (sham: 343.58 ± 78.33 µg/mL; PHx: 665.3 ± 109.62 µg/mL; *p* = 0.040). This elevated PGI₂ concentration normalized 3 days after operation, while plasma PGI₂ levels in sham mice stayed comparable (fig. 25A). Similar results were obtained analyzing the NO metabolites nitrite and nitrate. The nitrite concentration in the plasma of sham mice was 35.13 ± 6.85 µmol/L compared to 129.9 ± 35.8 µmol/L in PHx treated mice 1 day after surgery (*p* = 0.0025). In PHx mice the concentration of nitrate was also elevated with a 6-fold higher level (PHx: 81.1 ± 10.85 µmol/L) compared to the respective sham controls (sham: 13 ± 4.77 µmol/L; *p* = 0.0389). No differences could be detected between PHx mice and sham controls neither in nitrite nor in nitrate concentrations 3 days after PHx (fig. 25B).

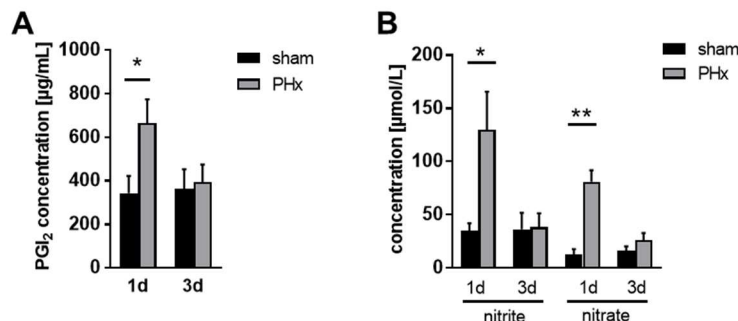


Figure 25. Enhanced levels of hemostatic inhibiting factors after partial hepatectomy. Plasma samples from PHx and sham mice were taken and analyzed via antibody specific assay and the griess reaction. (A) Prostacyclin I₂ (PGI₂) concentration in PHx mice is increased 1 day after PHx. (n= 1d: 6 sham, 6 PHx; 3d: 3 sham, 4 PHx) (B) Indirect measurement of NO via the metabolites nitrite and nitrate revealed enhanced NO accumulation in the blood of PHx mice 1 day after operation (n= 1d: 4 sham, 4 PHx; 3d: 3 sham, 6 PHx; * = *p* < 0.05, ** = *p* < 0.01 tested with students unpaired t-test.

Results

4.3.2.2 NO and PGI₂ induce enhanced VASP phosphorylation in platelets from PHx treated mice

Whether the enhanced plasma levels of PGI₂ and NO induce altered phosphorylation of VASP, platelets from PHx mice and sham controls were analyzed 1 and 3 days after surgery. VASP is a well-known inhibitor of platelet function that becomes activated through cGMP and cAMP [178]. Their increase either leads to a phosphorylation of VASP at Ser¹⁵⁷ and/or Ser²³⁹.

The stimulation of platelets with PGI₂ induces the formation of cAMP in platelets. Since phosphorylation at Ser¹⁵⁷ is mainly influenced by the cAMP signaling pathway, we stimulated platelet with PGI₂. PGI₂ induced enhanced VASP phosphorylation of platelets from PHx mice 1 day, but not 3 days after PHx (fig. 26A). Western blot analysis of platelets 1 day after surgery revealed enhanced VASP^{S157} phosphorylation after stimulation with PGI₂ ($p = 0.0468$) compared to sham controls (fig. 26B).

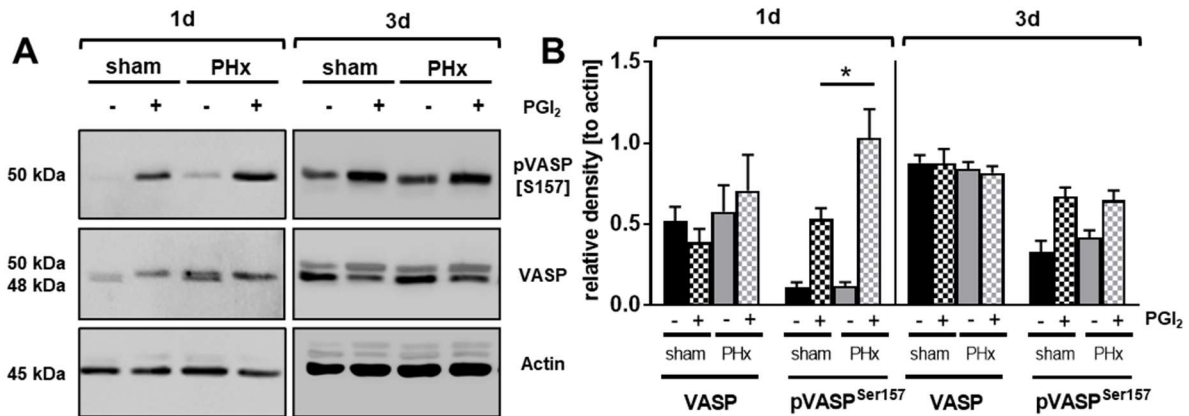


Figure 26. Phosphorylation of VASP at Ser157 in platelets one day after PHx. Isolated platelets from PHx and sham mice were incubated with PGI₂ [5 μM] for 5 min at 37°C and subsequently platelet lysates were generated. (A) Representative Western blot analysis of platelet lysates shows enhanced VASP phosphorylation at Ser157, but no difference in total VASP expression. (B) Densitometric analysis of Western blots 1 and 3 days after PHx. ($n = 4$ sham, 5 PHx). * = $p < 0.05$, tested with unpaired students *t*-test.

Similar results were obtained for platelets 1 day after PHx that were stimulated with the NO analogue sodium nitroprusside (SNP). NO directly interacts with cyclic guanylyl cyclase (cGC) in platelets, leading to VASP phosphorylation at Ser²³⁹. The VASP^{S239} phosphorylation in platelets stimulated with NO was also increased ($p = 0.012$) compared to sham controls (fig. 27A). The total protein expression of VASP was unaltered after PHx as detected via Western blot (fig. 27B). In summary, platelet activation defects result mainly from elevated NO and PGI₂ concentrations, which lead to increased activity of the endogenous platelet inhibitor VASP.

Results

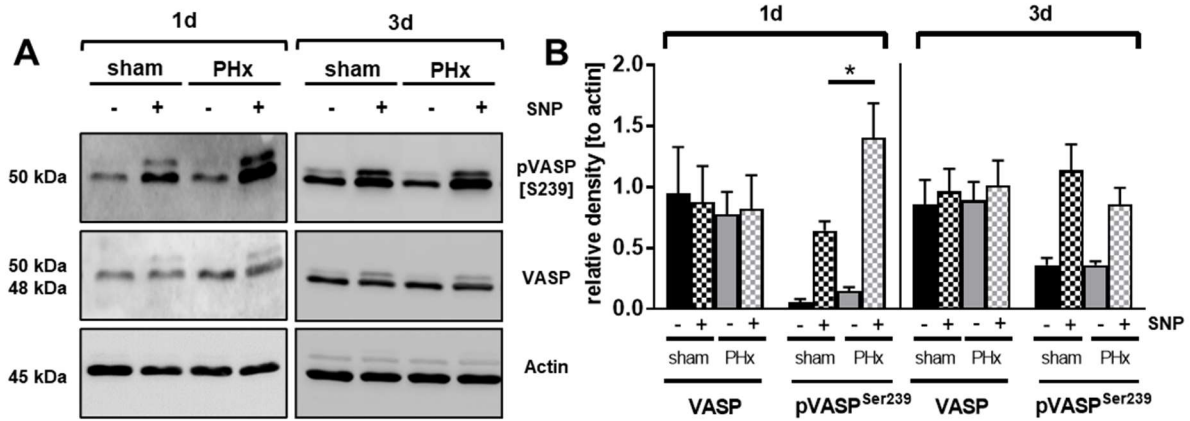


Figure 27. Phosphorylation of VASP at Ser236 in platelets one day after PHx. Isolated platelets from PHx and sham mice were incubated with SNP [1 μ M] for 2 min at 37 °C and subsequently platelet lysates were generated. (A) Representative Western blot analysis of platelet lysates shows enhanced vasodilator-stimulated phosphoprotein (VASP) phosphorylation at Ser239, but no difference in total VASP expression. (B) Densitometric analysis of the Western blots 1 and 3 days after PHx. (n= 5 sham, 4 PHx). * = $p < 0.05$, tested with unpaired students t-test.

4.3.2.3 Enhanced total bile acid concentration in plasma after PHx

In BDL mice, increased levels of BAs are present within the liver parenchyma and in the serum. The critical defects of platelet activation and hemostasis in BDL mice have already been demonstrated in section 4.1. Accordingly, *in vitro* analysis of platelet activation in mice and humans highlighted the inhibiting effect of BAs on platelet activation. Thus, we wanted to test if the plasma BA concentration is altered after PHx as well.

Analysis of different primary conjugations of BA after PHx revealed that the total amount of taurine conjugated BAs increased from $44.19 \pm 8.04\%$ to $69.55 \pm 22.45\%$ compared to sham controls (fig. 28A). Accordingly, unconjugated, and glycine-conjugated BA concentrations were decreased in PHx mice compared to sham 1 day after PHx. The total BA concentration in the serum of PHx treated mice increased to $749.94 \pm 396,34 \mu\text{mol/L}$ 1 day after surgery and was slightly enhanced until 3 days after surgery (fig. 28B).

The total BA concentration was increased 1 day after PHx (fig. 1B, $p = 0.0142$). The distinct analysis of the three conjugation possibilities of BAs revealed, that this increase in the total BA concentration was mainly mediated by unconjugated (fig. 28C; $p = 0.0264$) and taurine-conjugated (fig. 28D; $p = 0.0134$) bile salts, as a significant increase was measured compared to the control group. Glycine-conjugated bile salts showed no increase after 1 day compared to the control; at the same time, the measured concentration was one potential lower (fig. 28E). This highlights that mainly taurine- and unconjugated BAs influence platelet activation and thrombus formation after PHx in mice.

Results

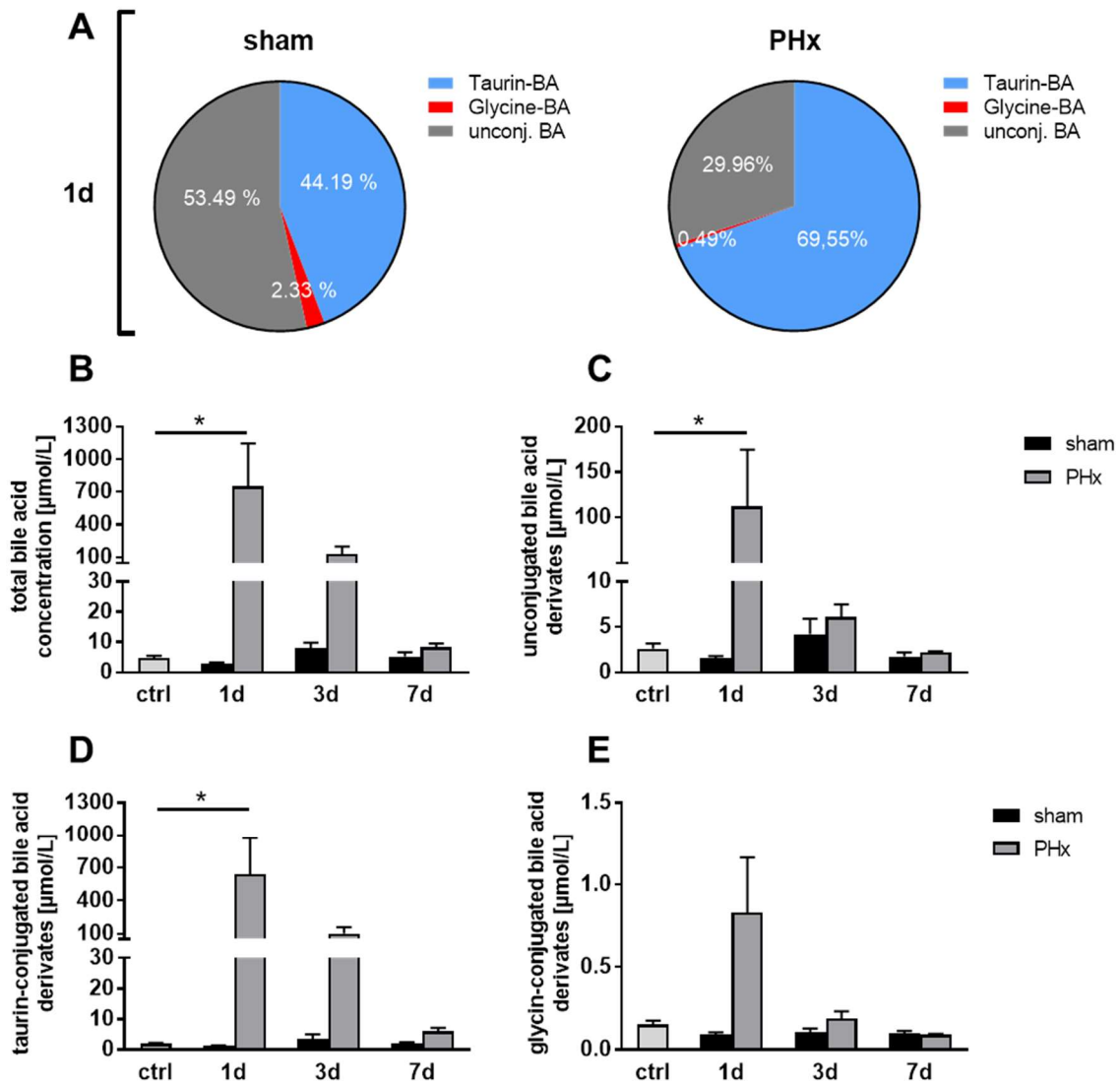


Figure 28. Enhanced taurine conjugation in mice undergoing PHx. From naïve C57Bl6/J mice (ctrl.) and 1, 3 and 7 days after PHx, serum samples were collected and analyzed by UPLC-MS/MS. (A) Percentage distribution of different conjugation states of the BAs show an increase in taurine conjugation in PHx mice. Time dependent analysis of BA composition shows an enhanced development of unconjugated BAs (A), total BAs (B) and taurine-conjugated BAs (C) in the serum 1 and 3 days after PHx. (E) No difference in the development of glycine-conjugated BAs. (n = 5 control mice (ctrl); 1d: 3 sham, 6 PHx; 3d: 3 sham, 4 PHx; 7d: 3 sham, 3 PHx).- * = $p < 0.05$, tested by Two-Way ANOVA with Bonferroni's post hoc test.

4.3.3 Efficiently restored thrombopoietin production is mediated via hepatic AMR and JAK2-STAT3 signaling

Platelet counts are regulated through TPO biosynthesis in hepatocytes [77]. Hepatic TPO production is mainly regulated through clearance of desialylated, senescent platelets that bind to the hepatic AMR in healthy mice. During the aging process platelets degrade their stored RNA, externalize more phosphatidylserine (PS) at the cell membrane and additionally lose their sialic acid moiety at GPs [184]. This binding of desialylated platelet to the AMR induces the activation of the JAK2/STAT3 signaling pathway resulting in enhanced TPO protein

Results

biosynthesis and accelerating TPO serum concentrations. The hepatic AMR binds to free terminal carbohydrate residues on GPs which are usually covered by sialic acid moieties [185]. Even though a reduced liver tissue was still present 3 days after PHx, platelet counts were efficiently restored at that time point. However, so far nothing is known about the regulation of TPO and platelet count after liver resection. Therefore, TPO production in the remaining liver tissue was analyzed in further detail.

4.3.3.1 Different mechanisms lead to enhanced platelet clearance after PHx

In a first approach, the exposure of PS of platelets from PHx and sham operated mice was measured. The exposure of PS at the surface of platelets is a marker for the pro-coagulant activity of platelets [186]. Besides, it is also a parameter to estimate the senescence of platelets, thus being actively involved in the platelet clearance by hepatocytes [184, 187]. Shortly after PHx when platelet counts were decreased and platelet activation was inhibited, differences in PS exposure were detected. A reduced PS exposure was measured on platelets stimulated with CRP 7 days after PHx ($p = 0.0170$), while no differences in PS exposure could be detected at any other time point (fig. 29A).

It is known that platelets could be cleared by the liver via glycan dependent mechanisms. Therefore, the sialic acid moiety of circulating platelets post PHx was investigated. The fraction of desialylated platelets was examined by platelet lectin binding of three different types of lectins: *Ricinus communis* agglutinin (RCA-1), *erythrina cristagalli* lectin (ECA) and *triticum vulgare* agglutinin (WGA – wheat germ agglutinin), all lectins that recognize terminal galactose residues. With all three lectins a reduced fraction of aged platelets could be measured in PHx compared to sham mice 1 day after operation (RCA-1: $p = 0.0467$; WGA: $p = 0.0008$; ECA: $p = 0.0946$). No difference in lectin binding could be observed between sham and PHx mice with all tested lectins 3 days after PHx. With recovering liver mass at day 7, the fraction of lectin positive platelets of PHx mice was higher in contrast to sham operated controls. With RCA-1 and WGA a significantly increased fraction could be found (RCA-1: $p = 0.0002$; WGA: $p = 0.0353$), while the ECA positive fraction was not increased (fig. 29C). Again, with fully recovered liver mass after 14 days the fraction of lectin positive platelets of PHx and sham operated mice was comparable. These results suggested accelerated desialylated platelet clearance 1 day after PHx and reduced lectin mediated platelet clearance because elevated lectin positive platelet fractions were detected 7 days after PHx. Whether these results were based on enhanced platelet turn-over, the RNA-content of platelets via Thiazole Orange staining in flow cytometric analysis was evaluated. Young, freshly generated platelets incorporate RNA until the RNA is degraded upon senescence [188]. Thiazole Orange staining

Results

revealed extended levels of RNA in platelets 7 days after PHx ($p = 0.0486$), while no differences could be measured at any other time point (fig 29.B).

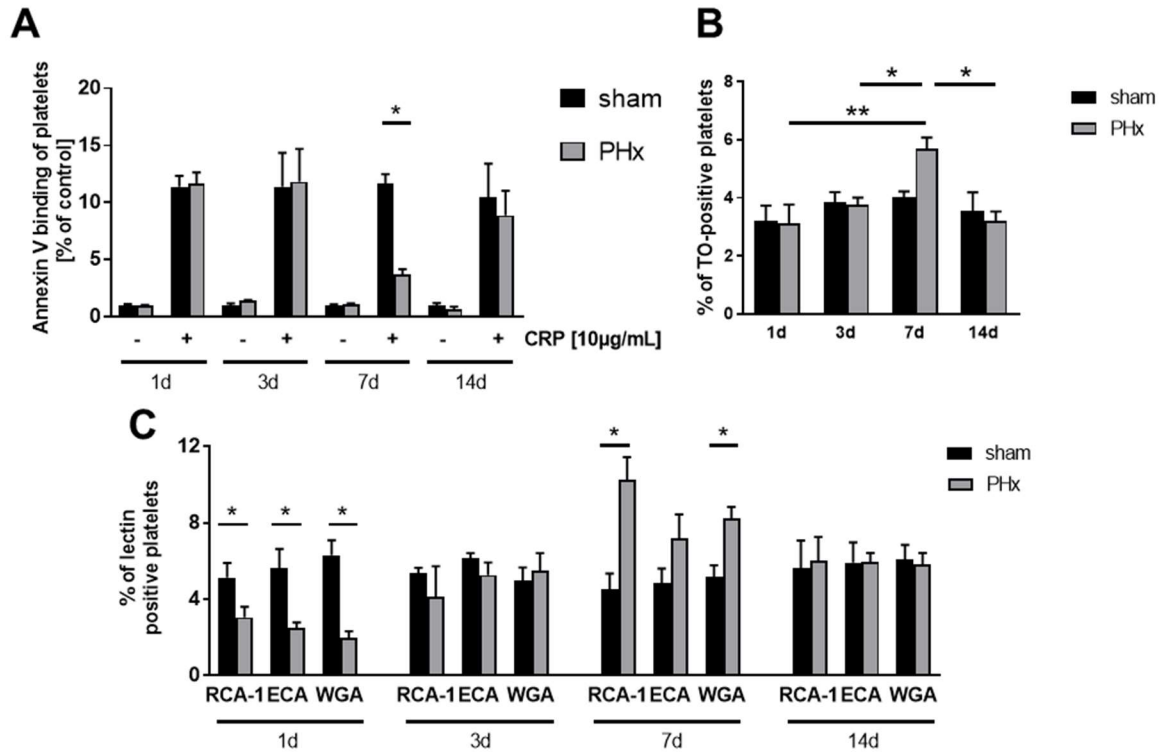


Figure 29. Analysis of platelet populations after PHx indicates tight platelet count regulation. Platelets from PHx and sham operated mice were analyzed using flow cytometry regarding their specific side scatter (SSC) and forward scatter (FSC) profile in combination with the platelet specific marker GPIb. (A) Annexin V-binding of GPIb positive platelets was normalized to the control group of each time point. Stimulation with CRP revealed diminished PS exposure on the surface of platelets 7 days after PHx ($n = 1+3d: 8 \text{ sham} + 9 \text{ PHx}; 7 + 14 \text{ d}: 4 \text{ sham}, 4 \text{ PHx}$). (B) Thiazole orange staining of RNA-rich, young GPIb positive platelets measured via flow cytometry shows upregulation of RNA content 7 days after PHx ($n = 8 \text{ sham} + \text{PHx for } 1\text{d} + 3\text{d}; 4 \text{ sham}, 5 \text{ PHx for } 7 + 14 \text{ d}$). (C) Analysis of platelets positive for binding of the RCA-1, ECA and WGA lectin at indicated time points exhibited a time dependent up- (1d) and down-regulation (7d) of the glycosylation state of platelet receptors ($n = 4 \text{ sham}, 5 \text{ PHx}$). * = $p < 0.05$, ** = $p < 0.01$; tested with ordinary Two-Way ANOVA with Bonferroni's post-hoc test. CRP = collagen-related peptide; RCA-1 = Ricinus communis agglutinin-1; ECA = erythrina cristagalli agglutinin; WGA = wheat germ (*Triticum vulgare*) agglutinin.

Additionally, it is known that increased shear stress induces desialylation of platelets in a vWF-GPIb α dependent manner [189]. Analysis of neuraminidase (Neu)-1 expression 1d after PHx revealed that platelets of PHx mice have a higher Neu-1 expression on their surface compared to their sham controls (fig. 30A). Binding of vWF to GPIb induced by the snake venom botrocetin (thus mimicking enhanced shear stress) led to increased Neu-1 expression in sham operated mice, while upregulation of Neu-1 was inhibited in PHx mice (fig. 30B). At the same time, no difference in the plasma activity of Neu-1 could be measured (fig. 30D). This effect of vWF-GPIb mediated increase of Neu-1 expression was confirmed by blocking vWF-binding to GPIb with an antibody that reacts with the N-terminal 45 kDa domain of mouse GPIb α (CD42b, XiaG5, Emfret analytics; fig. 30B). In addition, enhanced vWF-binding on platelets accompanied by enhanced levels of vWF in the plasma of PHx animals 1d after PHx was

Results

observed compared to sham controls (fig.30C+E). Considering a portal hypertension after PHx as described in literature [190], accompanied by reduced lectin binding compared to sham controls 1 day after PHx (fig. 30B), it is conceivable that shear stress induced vWF binding at least partially contributes to reduced lectin positive platelets.

These results suggest a reciprocal relationship between two clearance mechanisms at early and late time points after PHx: First, an enhanced clearance of desialylated platelets within the first day after PHx. Additionally, this effect of platelet desialylation is further increased in an autocrine manner due to defective platelet activation by enhanced shear stress. And second, an increased clearance of PS-positive platelets at late time points (Day 7). A notion that is supported by diminished PS exposure with enhanced RCA-1 binding of PHx platelets at day 7 and increasing numbers of RNA-rich, newly produced platelets 7 days after PHx.

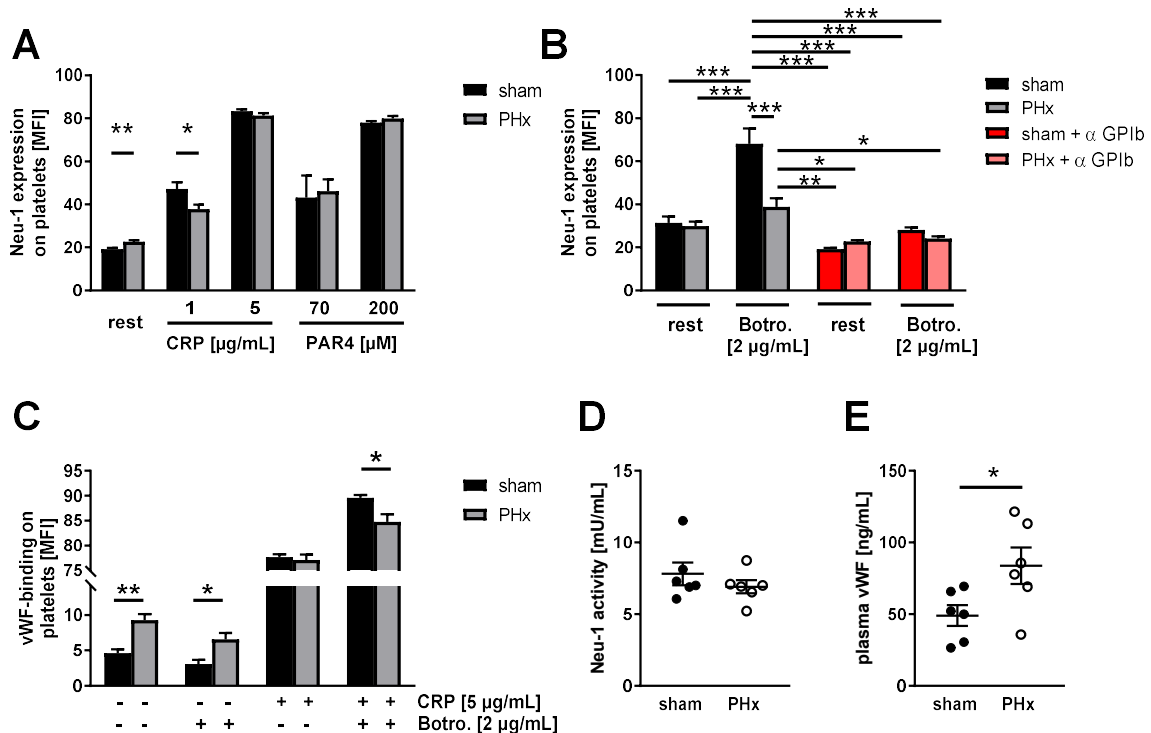


Figure 30 PHx results in enhanced plasma von Willebrand Factor (vWF) levels accompanied by enhanced vWF-platelet binding and neuraminidase-1 (Neu-1) expression on platelets 1d after PHx. Platelets from PHx and sham mice were analyzed in the flow cytometer regarding their specific side (SSC) and forward scatter (FSC) profile. (A) Expression of Neu-1 was investigated in unwashed whole blood on platelets positive for the platelet specific marker GPIb 1d after operation with indicated agonists (n=6). (B) Expression of Neu-1 on platelets stimulated with the snake venom Botrocetin (Botro.) and additional blockade of the N-terminal binding site of GPIb by antibody treatment (n=6). (C) Binding of von Willebrand Factor (vWF) after stimulation with Botro. and CRP in isolated platelets 1d after PHx. (D) Plasma activity of Neu-1 revealed no differences 24h after PHx compared to sham controls (n=6). (E) PHx leads to enhanced plasma levels of vWF compared to sham controls 1d after operation (n=6). Depicted are mean values + s.e.m.; * = $p < 0.05$, ** = $p < 0.01$, *** = $p < 0.001$ using unpaired students t-test and for (B) three-Way ANOVA with Bonferroni's post hoc test.

4.3.3.2 Platelets accumulate in the liver within the initial phase of liver regeneration

A decreased fraction of lectin positive platelets in whole blood of PHx mice accompanied by decreased platelet counts early after PHx assumed mechanisms for platelet consumption. To analyze whether platelets accumulate in the liver within the initial phase of liver regeneration, an immunofluorescence staining was performed that detects the platelet specific receptor GPIb. As shown in the immunofluorescent images, an extended number of GPIb positive platelets were observed 1 day after PHx in mice. Only a small number of GPIb positive platelets could be identified at all other times points after PHx (fig. 31). Sham operated mice displayed almost no GPIb positive staining. This provides evidence that PHx leads to platelet accumulation in the remnant liver tissue, strengthening the hypothesis of an interaction of platelet with non-parenchymal or parenchymal liver cells.

Results

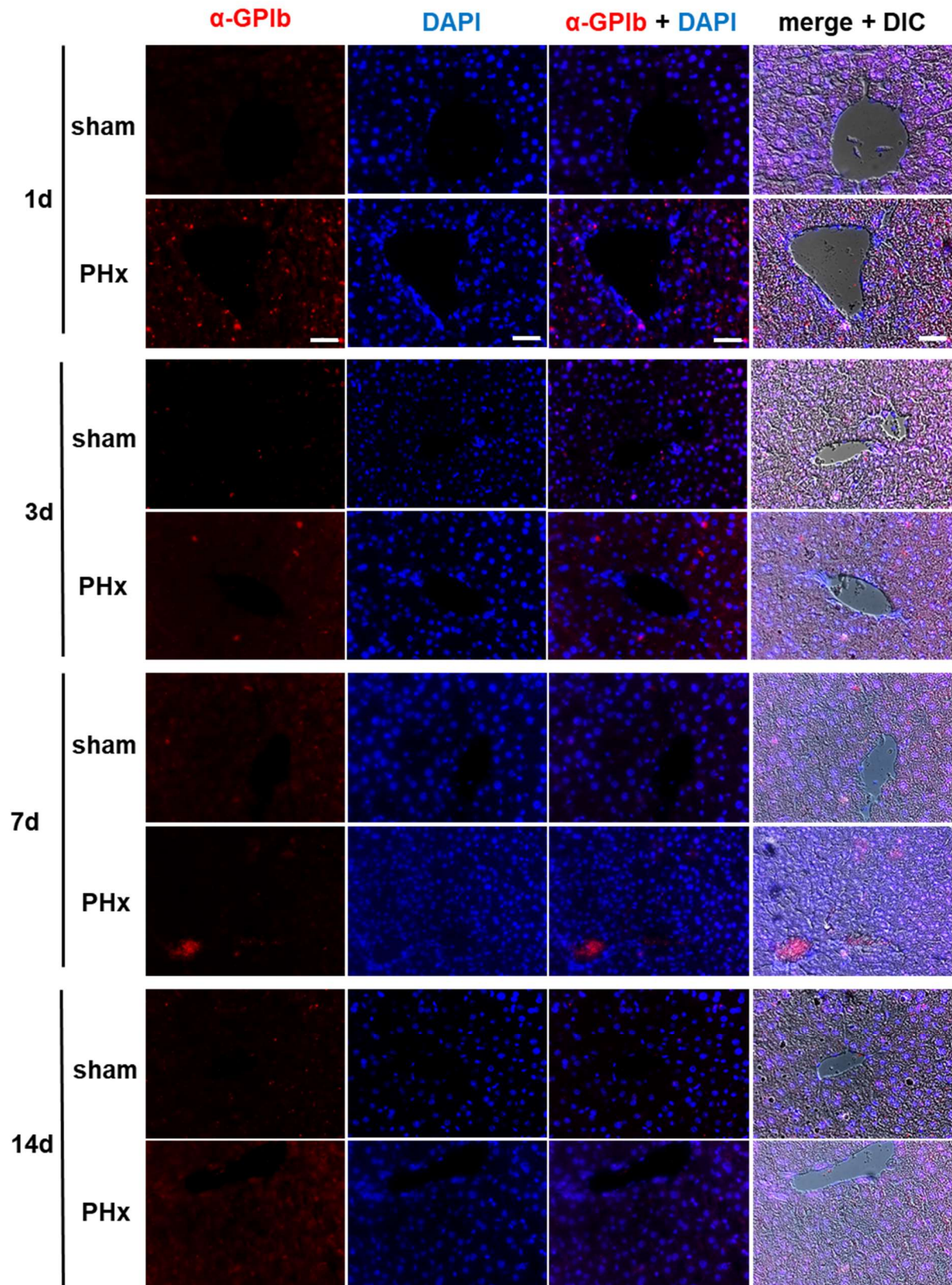


Figure 31. Platelet accumulation in the regenerative liver tissue after PHx. At indicated time points platelets were stained using paraffin embedded liver tissue sections [5 μ m]. Representative images show GPIb positive platelets in the liver. Platelets accumulate in liver tissue at day 1 and to a lesser extent at day 3 after PHx. Nucleus staining was performed with DAPI. Differential interference contrast (DIC) is shown to allow orientation in liver tissue (n =4). Scale bar = 50 μ m

Results

4.3.3.3 Regenerating liver tissue exhibits enhanced TPO production

Shortly after PHx, mild thrombocytopenia was observed along with a decreasing number of lectin-positive platelets. Platelet counts returned to normal but showed altered populations of lectin (increased) and annexin V-positive (decreased) platelets compared to sham controls 7 days after PHx. A negative reciprocal correlation between the fraction of young platelets, incorporating plasma TPO through their Mpl receptor and the TPO generation affecting megakaryopoiesis has been described [191]. Therefore, it was of interest to understand the molecular mechanisms underlying the regulation of TPO gene expression and secretion.

To investigate if the early restoration of platelet counts is mediated by the regulation of TPO production via AMR signaling the gene expression of both subunits of the AMR, *Asgr1* and *Asgr2* was analyzed. Since AMR and IL-6R share the same signaling pathway, the *Il-6r* gene expression was also analyzed. Gene expression analysis of the whole liver mass revealed that the expression of the *Asgr1* subunit was increased by 3.8 ± 0.99 -fold 6 h after PHx ($p = 0.0023$) compared to the native control. In the later regenerative phase, a second expression peak 3 days after PHx was detectable without reaching statistical significance ($p = 0.4797$; fig. 32A). On the other hand, the expression of the *Asgr2* subunit was only moderately increased 6 h after PHx without reaching statistical significance, while 3 days after PHx a 1.88 ± 0.38 -fold gene induction was measured compared to native controls ($p = 0.0003$; fig. 32B). Interestingly, the gene regulation of the acute phase cytokine receptor *Il-6r* was comparable to the AMR subunit expression. The gene expression enhanced 6 h after PHx by 5.94 ± 1.0 -fold ($p = 0.0004$), normalized at later time points and developed a second expression peak after 3 days by 3.0 ± 0.74 -fold ($p = 0.1876$; fig. 32C).

The expression of *Tpo* in liver lysates confirmed a biphasic regulation with elevated gene expression 6 h (2.98 ± 0.71 -fold; $p = 0.0023$) and 3 days (2.31 ± 0.2 -fold; $p = 0.0478$) after PHx (fig. 32D) that normalizes with regenerating liver and platelet counts 7 days after PHx. Since the *Tpo* gene expression in the liver was upregulated, the plasma content of TPO was analyzed using a murine TPO specific sandwich ELISA. As shown in fig. 32E an enhanced TPO plasma level of 88.36 ± 15.39 $\mu\text{g/mL}$ was detected 1 day after PHx compared to 47.65 ± 4.53 $\mu\text{g/mL}$ of the sham controls ($p = 0.0367$; fig. 32E). However, no differences were measured at all other time points. The second biphasic peak in TPO gene expression (day 3) was only indirectly reflected in the measured plasma level of TPO.

To set the TPO plasma level in relation to reduced liver mass after PHx, the ratio between both factors was calculated. The calculated ratio could prove an increased TPO production ($p = 0.0015$) in the remaining liver 3 days after PHx compared to sham controls. This ratio emphasized that the regenerative liver produced increased amounts of TPO to compensate for the decreased platelet count shortly after PHx (fig. 32F). At the same time, an increased

Results

amount of TPO must be produced from residual liver tissue, but only to counteract a repeated reduction of the TPO level in the plasma and the subsequent reduced platelet count.

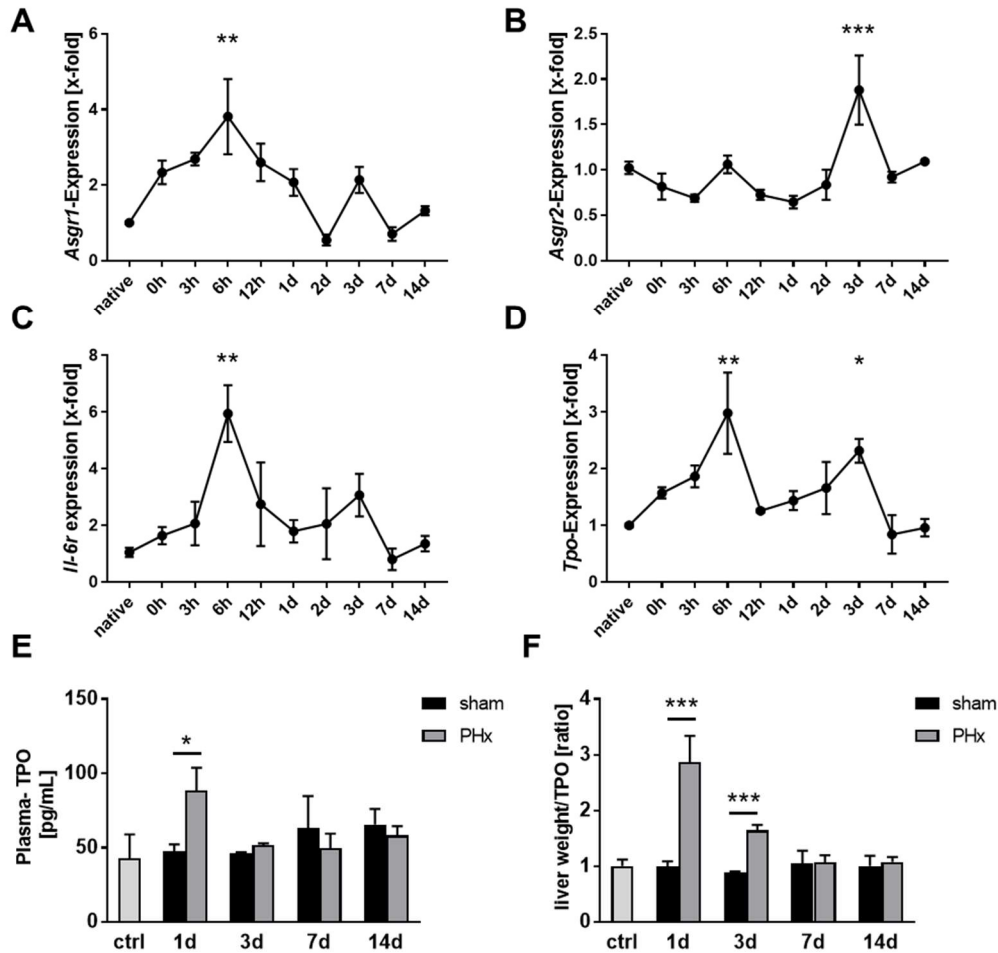


Figure 32. Enhanced TPO synthesis after PHx is associated with upregulated IL-6R and AMR. Gene expression in whole liver tissue of different target genes was analyzed using the $\Delta\Delta Ct$ method ($n = 3$ native mice; 0 h: 4 PHx mice; 3 h-14 d: 5-6 PHx mice). GAPDH was used as housekeeping gene. (A) Gene expression of the AMR subunit shows *Asgr1* upregulation 6 h after PHx. (B) Gene expression of the AMR subunit *Asgr2* shows upregulation 3 days after PHx. (C) IL-6R is upregulated 6 h after PHx. (D) *Tpo* expression is enhanced in a bi-phasic manner after 6 h and 3 d after PHx. (E) TPO plasma levels of controls (ctrl), sham and PHx mice were measured by ELISA and show elevated TPO levels 1 day after PHx. (F) Ratio between TPO plasma levels and liver weight ratio revealed elevated TPO synthesis of the remnant liver 3 days after PHx ($n =$ control 3; 1d = 6 sham, 7 PHx; 3/7/14d = 4 mice/group). * = $p < 0.05$, ** = $p < 0.01$, *** = $p < 0.001$; (A-D) tested with ordinary One-Way ANOVA with Dunnett's post-hoc test. (E-F) tested with ordinary Two-Way ANOVA with Bonferroni's post-hoc test.

4.3.3.4 Enhanced TPO expression and release is mediated by the JAK2/STAT3 pathway

To date, the regulation of hepatic TPO expression and release via the AMR/ JAK2/STAT3 signaling pathway was only investigated under steady state conditions [77, 148]. As enhanced gene expression of both receptors is in line with enhanced *Tpo* expression and plasma concentration, it was of interest to verify if the underlying signaling pathways under steady state conditions were also evident upon liver injury. Therefore, Western blots to analyze the

Results

phosphorylation of receptor kinase JAK2 and the transcription factor STAT3 in total liver lysates of native, sham and PHx operated mice at different time points were performed.

Both proteins exhibited a hyper-phosphorylation state 1 day after PHx compared to sham controls (fig. 33A). Densitometric analysis of Western blots revealed a higher phosphorylation of JAK2 upon PHx stimulus compared to controls ($p = 0.0142$; fig. 33B). Furthermore, an increase of STAT3 phosphorylation was detected 1 day after PHx ($p = 0.0003$; fig. 33C), but also a moderate increase 3 days after PHx without reaching statistical significance.

Taken together these results provided evidence that PHx stimulates TPO biosynthesis via an AMR/JAK2/STAT3 signaling pathway leading to enhanced TPO plasma levels.

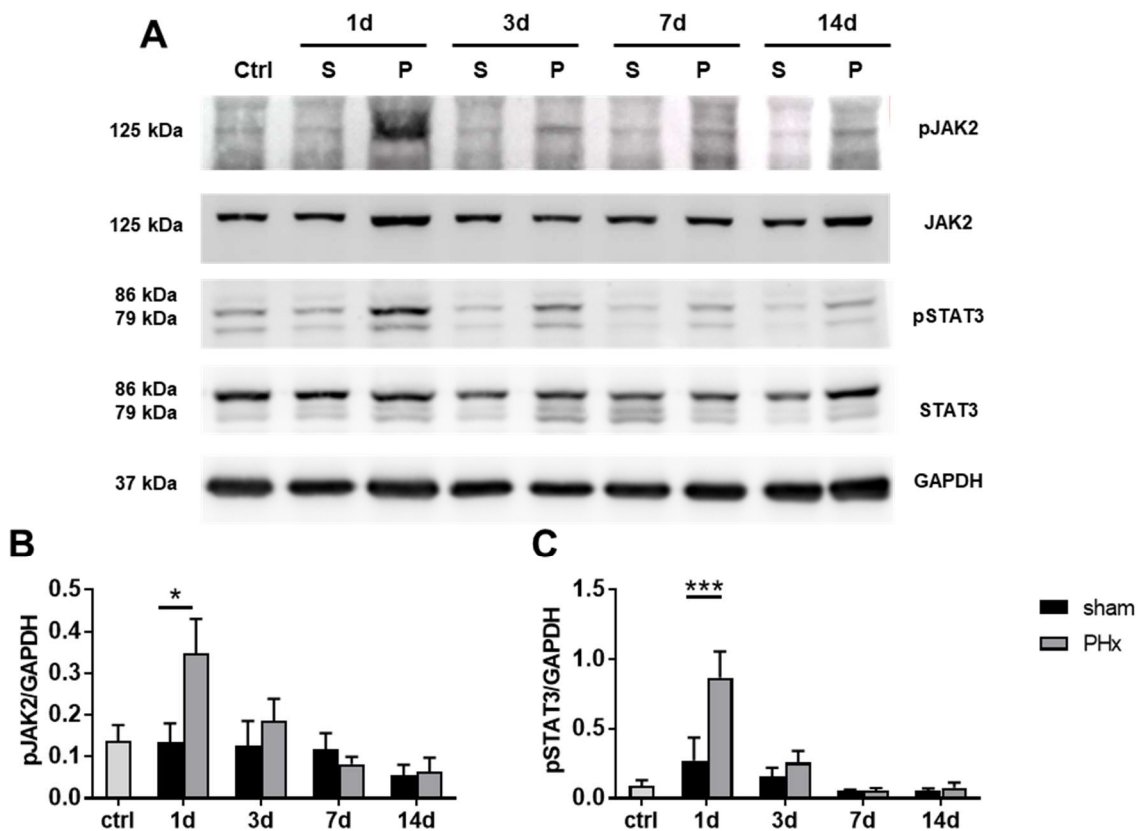


Figure 33. PHx induces JAK2/STAT3 signaling in WT mice early after PHx. Whole liver tissue of native control mice (ctrl.), sham and PHx operated C57Bl6/j mice was lysed and western blot analysis was performed. (A) Representative immunoblots of total liver cell lysates using anti-pJAK2 and anti-JAK2 antibodies and anti-pSTAT3 and anti-STAT3 monoclonal antibodies showing enhanced phosphorylation of both proteins one day after PHx. GAPDH was used as loading control. Densitometric analysis of pJAK2 (B) and pSTAT3 (C) in relation to the loading control GAPDH revealed statistically significant upregulation of protein phosphorylation upon liver injury. (n=4). * = $p < 0.05$, *** = $p < 0.001$; tested with ordinary Two-Way ANOVA with Bonferroni's post-hoc test.

4.3.4. PHx provokes mild splenomegaly with enhanced megakaryopoiesis and splenic platelet sequestration

After liver resection, a portal hypertension develops [192]. Megakaryopoiesis happens mainly in the BM but also to a smaller degree in splenic tissue of healthy mice [193]. Additionally, to the sequestration of platelets is mediated by the spleen as well [194]. Since enhanced TPO plasma levels were measured upon liver injury (fig. 31), megakaryopoiesis in spleen and BM was analyzed in further detail.

4.3.4.1 Augmented megakaryopoiesis in the spleen and bone marrow of PHx operated mice.

Moderate splenomegaly of PHx treated mice was observed as the spleen weight ratio was calculated. The spleen of PHx operated mice expanded from 1 to 7 days after PHx to a nearly doubled spleen mass (PHx day 1: 3.35 ± 0.14 g – PHx day 7: 6.22 ± 0.59 g, $p = 0.0031$). Splenomegaly decreased to a normal magnitude of the spleen with fully regenerated liver tissue after 14 days. (fig. 34A+B).

Additionally, HE-staining was performed to count the number of megakaryocytes in paraffin embedded tissue section of the femur BM and the spleen.

In line with splenomegaly, an enhanced number of megakaryocytes was observed in spleen tissue 3 ($p = 0.0019$) and 7 days ($p < 0.0001$) after PHx while megakaryopoiesis normalized 14 days after PHx (fig. 34C+D).

Results

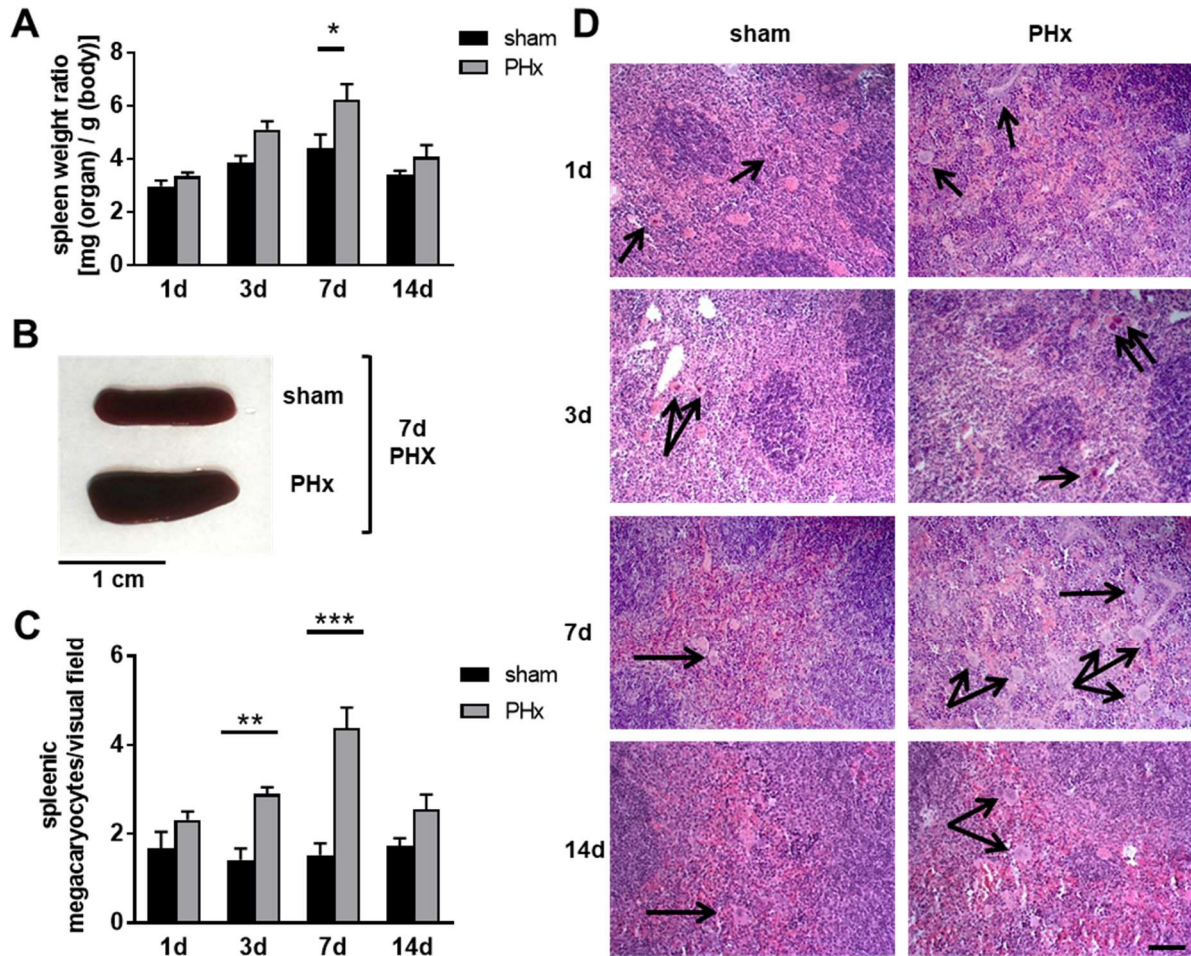


Figure 34. Mild splenomegaly and enhanced megakaryopoiesis in spleen following PHx. Murine splenic tissue from sham and PHx mice was analyzed at indicated time points. (A) Calculated spleen weight ratio revealed mild splenomegaly 7 days after PHx compared to respective sham controls. (n = 1d: 10 sham, 14 PHx; 3d: 9 sham, 9 PHx; 7d: 8 sham, 10 PHx, 14d: 5 sham, 5 PHx). (B) Representative images of the dissected spleen 7 days after PHx. (C) Megakaryocytes in the spleen tissue sections were counted and showed upregulation of MK's 3 and 7 days after PHx. (n = 5 sham, 5 PHx) (D) Representative images of the spleen tissue at indicated time points. Arrows indicate MK's in the spleen tissue. * = $p < 0.05$, ** = $p < 0.01$, *** = $p < 0.001$; tested with ordinary Two-Way ANOVA with Bonferroni's post-hoc test. Scale bar = 50 μm .

In addition to enhanced megakaryopoiesis in the spleen, an enhanced number of MKs was detected in BM using HE-staining of BM sections. After 3 ($p = 0.0011$) and 7 days ($p = 0.0112$) post PHx increased numbers of MKs were detected which normalized after 14 days compared to sham controls (fig. 35). Interestingly, megakaryopoiesis seemed to take place inversely in the spleen and the BM. While the MK number peaked after 3 days in the BM, the maximum number of MKs was reached at day 7 in the spleen.

Results

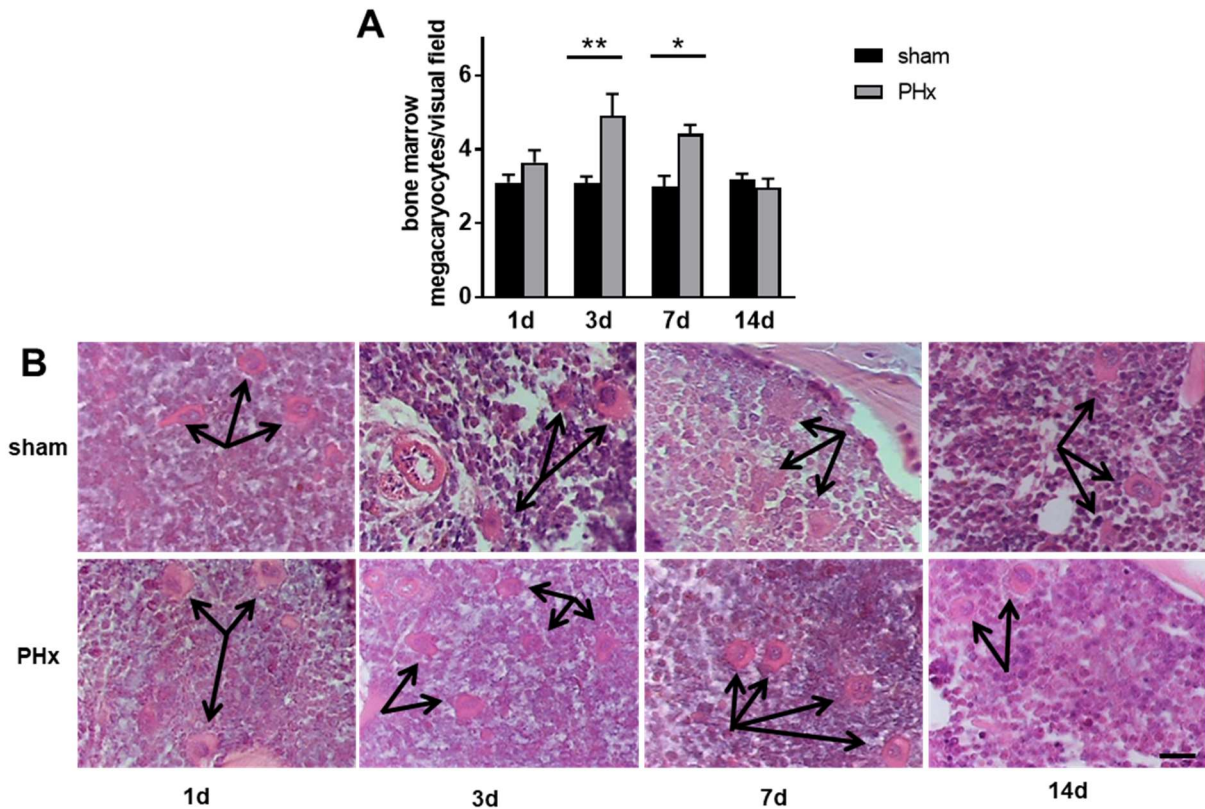


Figure 35. Enhanced megakaryopoiesis in the bone marrow after liver injury. Murine femur was dissected and the bone marrow (BM) of sham and PHx mice was obtained and analyzed for MKs at indicated time points. (A) Megakaryocytes in the BM tissue sections were counted and showed upregulation of MK's 3 and 7 days after PHx. ($n = 5$ sham, 5 PHx) (B) Representative images of the BM at indicated time points. Arrows indicate MK's in different regions of the BM. * = $p < 0.05$, ** = $p < 0.01$; tested with ordinary Two-Way ANOVA with Bonferroni's post-hoc test. Scale bar = 50 μm .

4.3.4.2 Enhanced sequestration of platelets into the spleen following liver injury

To analyze the sequestration of platelets into the spleen after PHx, GPIX specific monoclonal antibody staining in spleen tissue was performed. Accompanied by mild splenomegaly, sequestration of platelets was observed by an increased fraction of GPIX positive platelets in the spleen of mice 7 days post PHx compared to sham controls ($p = 0.0018$; fig. 36). Enhanced sequestration of GPIX positive platelets disappeared when the liver was fully regenerated 14 days after PHx. Thus, both – accelerated platelet sequestration and enhanced megakaryopoiesis in the spleen – might account for the increase in spleen size at later time points after PHx.

Taken together, the increase in megakaryocyte numbers in spleen and BM might be responsible for the increased number of newly produced platelets in the blood of PHx operated mice to compensate for thrombocytopenia.

Results

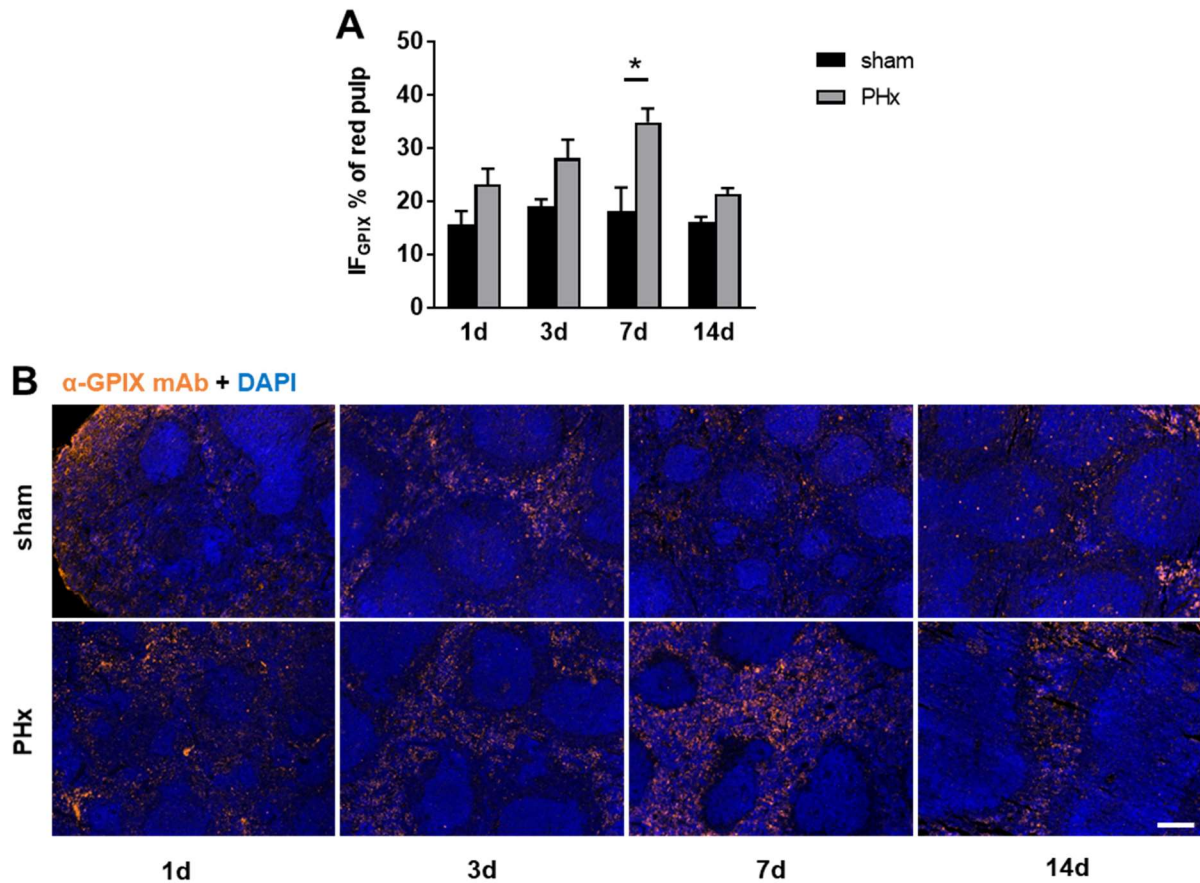


Figure 36. Enhanced platelet sequestration into the spleen following liver injury. Murine spleen tissue from sham and PHx mice was analyzed for platelet sequestration at indicated time points (A) A platelet specific marker (GPIX) was used to detect platelets combined with DAPI staining to distinguish between red and white pulp of the spleen. Total GPIX positive fluorescence area [$IF_{GPIX} / \mu m^2$] of the red pulp of the spleen sections was determined ($n = 4$) (B) Representative images of the spleen at indicated time points. * = $p < 0.05$; tested with ordinary Two-Way ANOVA with Bonferroni's post-hoc test. Scale bar = 50 μm .

4.4 IL-6R supports TPO expression and release to enhance megakaryopoiesis after liver injury and modulates platelet activation

Different reports in the past suggested that the IL-6R is involved in the regulation of TPO and platelet counts [87, 195]. Therefore, a mouse model with a constitutive IL-6R knock-out ($IL-6R^{-/-}$) was used to investigate if activation of the IL-6R after liver injury accompanies for the early restoration of platelet counts after PHx.

IL-6R plays a prominent role in liver regeneration after PHx [148]. IL-6R induces the generation of hepatocyte growth factor (HGF) which directly influences liver regeneration. Consequently, 80% of IL-6R deficient mice die within 48 h after liver ligation due to insufficient liver regeneration [148]. However, 20% of the mice have established a compensatory mechanism to survive and regain liver mass [148]. To further study the underlying mechanism if and how

Results

the IL-6R participates in the regulation of TPO and the restoration of platelet counts after PHx, *IL-6R^{-/-}* mice were analyzed for TPO regulation, JAK2/STAT3/5 signaling, megakaryopoiesis and platelet activation upon liver regeneration and inflammation.

4.4.1 Genetic deletion of IL-6R elicits a disturbed regulation of platelet counts and a hyperactive state of platelets

At first, it was of interest if platelet activation and total blood cell counts were affected by the genetic deletion of the IL-6R. Flow cytometric analysis of platelets was performed, and the total blood cell counts were measured.

4.4.1.1 Reduced liver regeneration and thrombocytosis in IL-6R knock-out mice

First, healthy *IL-6R^{-/-}* mice were analyzed because data are lacking about the impact of IL-6R in platelet activation. Interestingly, the deletion of the IL-6R affects the regulation of platelet counts. Already under steady state conditions, the loss of the IL-6R affects the number of platelets in the blood stream of these mice. An enhanced number of platelets (WT: $901.2 \pm 26.9 \times 10^3/\mu\text{L}$ vs. *IL-6R^{-/-}*: $1111.1 \pm 77.9 \times 10^3/\mu\text{L}$; $p = 0.03$) in the blood stream of *IL-6R^{-/-}* mice was observed compared to age-matched WT controls (fig. 37A).

As already described above, WT mice develop thrombocytopenia 1 day after PHx. In PHx treated *IL-6R^{-/-}* mice, platelet counts decreased as observed in WT mice. Thus, the thrombocytosis in native *IL-6R^{-/-}* mice turned into more severe thrombocytopenia after PHx compared to the respective WT mice (fig. 37A).

The loss of the IL-6R does not influence the RBC count (fig. 37B) or the WBC count (fig. 37C) neither in the native state nor after PHx compared to WT mice. However, a mild increase of WBCs after PHx in *IL-6R^{-/-}* mice was observed without reaching statistical significance. According to literature, a reduced liver regeneration within the first day after PHx was detected in *IL-6R^{-/-}* mice (fig. 37D). Interestingly, two out of seven mice had a remarkable better liver regeneration regarding calculated liver weight ratio. A calculated spearman correlation points to a positive correlation of the platelet count and the regenerated liver volume ($\rho = 0.7143 + p = 0.0881$; fig. 37E). These results provide first evidence for an IL-6R dependent regulatory pathway after PHx resulting in an enhanced liver regeneration and rising platelet counts in the blood.

Results

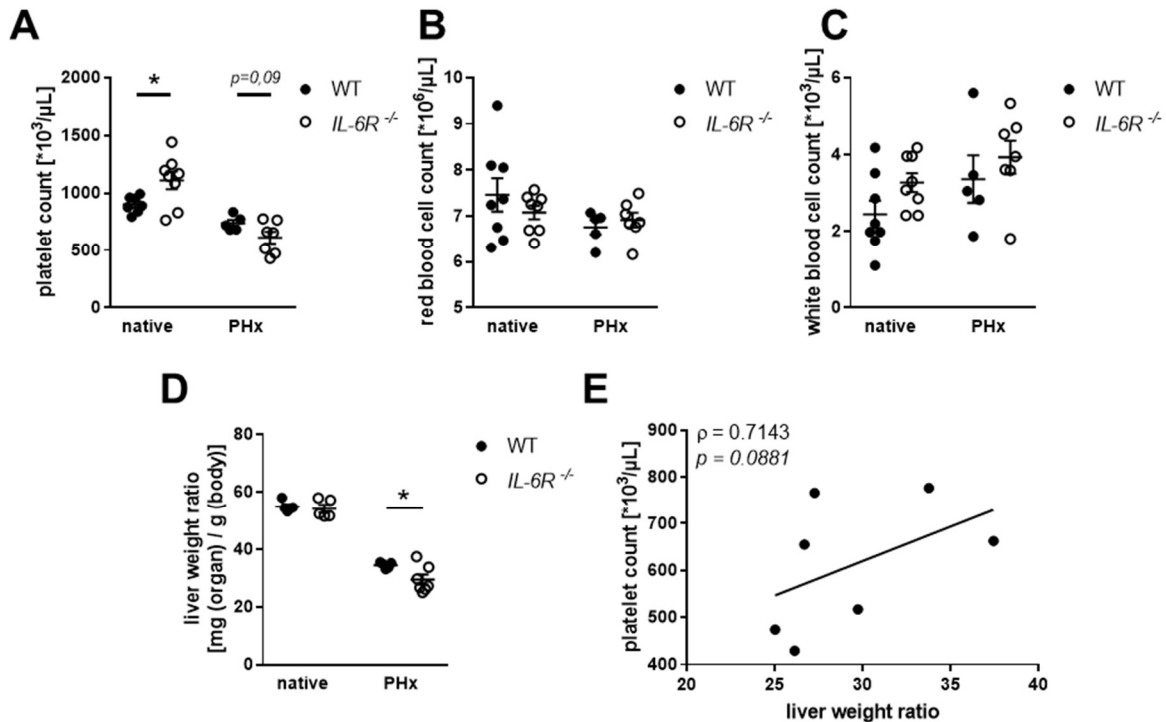


Figure 37. IL-6 receptor deficiency is accompanied by dysregulated platelet counts and impaired liver regeneration. Whole blood from WT and IL-6R^{-/-} mice was taken and analyzed using a hematology analyzer (Sysmex KN-X21). (A) Enhanced platelet counts in IL-6R^{-/-} mice under steady state (native) conditions but strongly decreased platelet counts after PHx compared to WT controls were detected. (B) Red blood cell counts of WT and IL-6R^{-/-} mice undergoing PHx indicated no differences between groups. (C) White blood cell counts are also unaltered between the tested groups ($n = \text{native: } 8 \text{ WT, } 8 \text{ IL-6R}^{-/-}$; $\text{PHx: } 5 \text{ WT, } 7 \text{ IL-6R}^{-/-}$). (D) Calculated liver weight ratio revealed reduced liver regeneration in IL-6R^{-/-} mice ($n = \text{native: } 5 \text{ WT, } 5 \text{ IL-6R}^{-/-}$). (E) Spearman correlation gives a first hint that the platelet count is positive correlated with liver regeneration in IL-6R^{-/-} mice ($\text{PHx: } 5 \text{ WT, } 7 \text{ IL-6R}^{-/-}$). * = $p < 0.05$, tested with unpaired students t-test.

4.4.1.2 Platelets from IL-6R^{-/-} mice exhibit enhanced degranulation and pre-activated $\alpha\text{IIb}\beta_3$ integrin

As the platelet counts in IL-6R^{-/-} mice were enhanced, the activation of these platelets was studied in further detail. Whole blood from WT and IL-6R^{-/-} mice was obtained and analyzed with respect to GP surface expression, platelet degranulation, and $\alpha\text{IIb}\beta_3$ integrin activation using flow cytometry.

No differences in GP expression of IL-6R^{-/-} platelets compared to WT platelets were observed (fig. 38A), whereas enhanced degranulation of α -granules as measured by P-selectin externalization was detected. Stimulation of the ITAM coupled GPVI receptor led to increased P-selectin externalization with low ($p = 0.029$), intermediate ($p = 0.0061$) and high doses ($p = 0.044$) of CRP. GPCR mediated signaling was affected as well, since activation of platelets with PAR4 peptide also led to enhanced P-selectin externalization with low ($p = 0.040$) and intermediate ($p = 0.0002$) concentrations of agonist compared to WT. Stimulation with the

Results

second wave mediators ADP ($p = 0.0001$) or ADP and U46619 ($p = 0.0002$) also led to enhanced platelet degranulation (fig. 38B).

Enhanced platelet activation of $IL-6R^{-/-}$ platelets was also reflected by elevated activation of integrin $\alpha_{IIb}\beta_3$. Stimulation with CRP at different concentrations led to enhanced $\alpha_{IIb}\beta_3$ integrin activation at the platelet surface (low – $p = 0.0265$; intermediate – $p < 0.00001$; high – $p = 0.0043$). Additionally, enhanced integrin activation was also detected with low ($p = 0.0193$) and intermediate ($p = 0.0001$) concentrations of PAR-4 peptide. Furthermore, activation of $\alpha_{IIb}\beta_3$ integrin was already detectable under resting conditions ($p = 0.0025$) using platelets from $IL-6R^{-/-}$ mice compared to WT controls (fig. 38C) suggesting that the loss of IL-6R leads to a pre-activated state of platelets under steady state conditions. This was further supported by the fact that there were no differences in the surface externalization of β_3 integrin of $IL-6R^{-/-}$ platelets detectable neither under resting nor under activated conditions (fig. 38D). This suggests that enhanced integrin activation is not a consequence of an enhanced copy number of the integrin at the platelet surface of $IL-6R^{-/-}$ platelets.

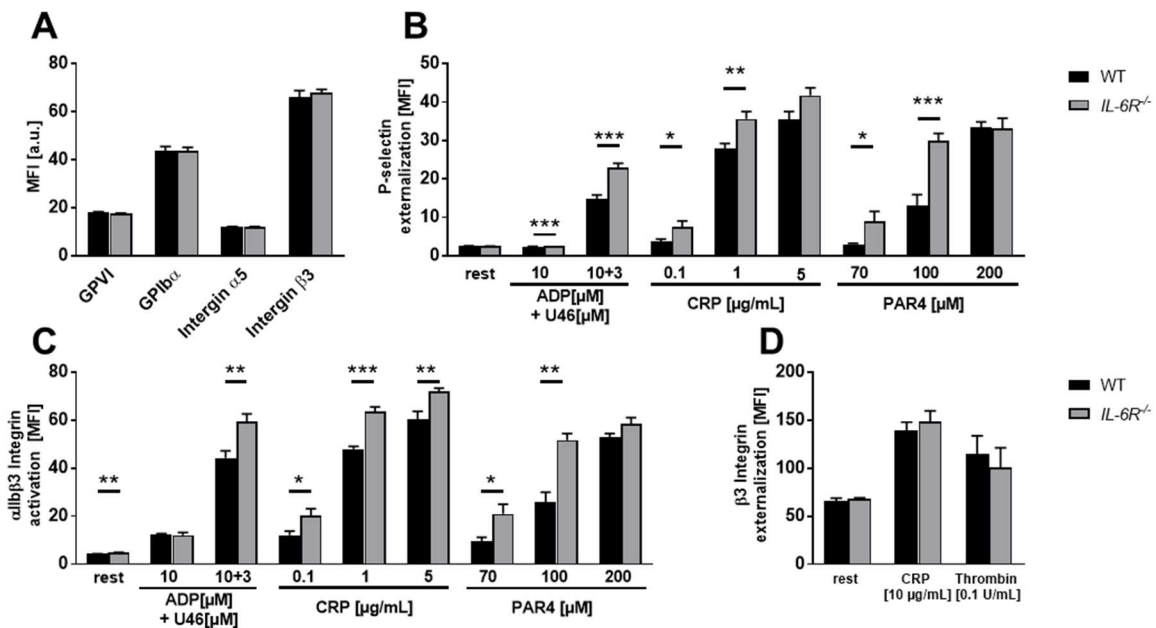


Figure 38. Platelets from $IL-6R^{-/-}$ exhibit enhanced platelet activation under resting and stimulated conditions. Platelets from native WT and $IL-6R^{-/-}$ mice were analyzed by flow cytometry regarding their specific side scatter (SSC) and forward scatter (FSC) profile. (A) Expression of indicated glycoproteins on the surface of platelets measured via mean fluorescence intensity (MFI) indicates no differences between groups. (B) Externalization of P-selectin on the platelet surface following stimulation with indicated agonists showed enhanced degranulation in response to GPCR and ITAM signaling. (C) Loss of $IL-6R$ leads to enhanced activation of $\alpha_{IIb}\beta_3$ integrin on the platelet surface with indicated agonists and under resting. (D) Externalization of β_3 integrin following platelet stimulation indicated no differences between groups ($n = 8$ WT, 8 $IL-6R^{-/-}$). * = $p < 0.05$, ** = $p < 0.01$, *** = $p < 0.001$; tested with students *t*-test. CRP = collagen-related peptide.

Results

4.4.1.3 GPVI mediated signaling pathways are predominantly affected in *IL-6R*^{-/-} platelets after liver resection

Mild thrombocytopenia appeared with platelet activation defects in WT mice 1 day after PHx. In *IL-6R*^{-/-} mice, thrombocytosis was observed under native conditions, but platelet counts drop to levels observed in WT mice after PHx. Therefore, it was of great interest if platelet activation was also affected by liver injury as observed in WT mice early after PHx.

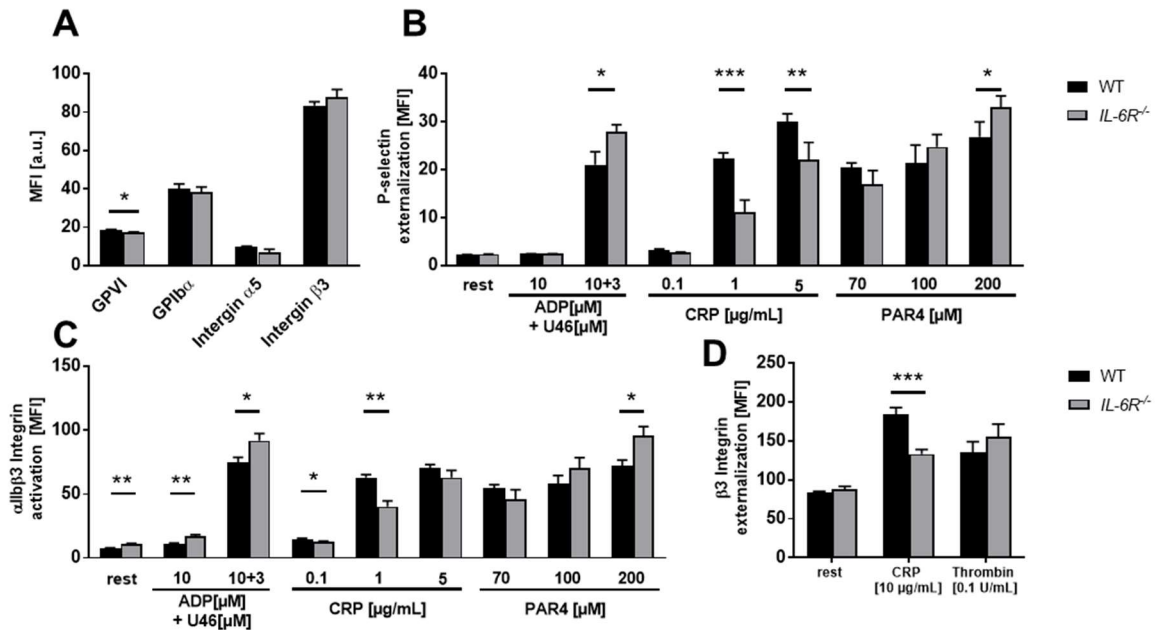


Figure 39. Loss of *IL-6R* leads to altered platelet activation after PHx. Platelets from WT and *IL-6R*^{-/-} mice were analyzed by flow cytometry regarding their specific side scatter (SSC) and forward scatter (FSC) profile one day after PHx. (A) Reduced GPVI exposure of *IL-6R* deficient platelets as measured by mean fluorescence intensity (MFI). (B-C) Externalization of P-selectin (B) and activation of $\alpha_{IIb}\beta_3$ integrin (C) on the surface of *IL-6R* deficient platelets showed enhanced platelet activation with G-protein-coupled Receptor (GPCR) stimulating agonists but reduced activation following CRP mediated GPVI signaling compared to WT controls. (D) Externalization of β_3 integrin upon platelet stimulation with indicated agonists. GPVI activation leads to reduced β_3 integrin exposure of *IL-6R* deficient compared to controls platelets ($n=5$ WT, 7 *IL-6R*^{-/-}). * = $p < 0.05$, ** = $p < 0.01$, *** = $p < 0.001$; tested with students unpaired t-test. CRP = collagen-related peptide; rest = resting.

Analysis of GP surface expression revealed that *IL-6R*^{-/-} platelets express 13.8% less GPVI on their surface 1 day after PHx (WT-MFI: 18.5 ± 0.26 vs. *IL-6R*^{-/-}-MFI: 17.1 ± 0.35 ; $p = 0.019$), while all other GPs were unaltered (fig. 39A). The externalization of P-selectin was still enhanced following GPCR activating agonists such as ADP + U46 ($p = 0.027$) and high PAR-4 peptide concentrations ($p = 0.0457$). However, degranulation with moderate ($p = 0.0004$) and high ($p = 0.0105$) concentrations of CRP led to decreased degranulation of *IL-6R*^{-/-} platelets compared to WT controls (fig. 39B). Analysis of $\alpha_{IIb}\beta_3$ integrin activation revealed a pre-activated state of *IL-6R*^{-/-} platelets compared to WT at resting conditions ($p = 0.0088$). GPCR activation results in enhanced integrin activation of *IL-6R*^{-/-} platelets by ADP ($p = 0.0107$), ADP combined with U46 ($p = 0.036$) and high PAR-4 peptide concentrations ($p = 0.022$) 1 day after PHx. Therefore, low ($p = 0.017$) and moderate ($p = 0.0033$) CRP concentrations led to a

Results

reduction in integrin activation (fig. 38C). Contrary to the results in native mice, the β_3 integrin surface externalization was reduced ($p = 0.0006$) upon high CRP stimulation (fig. 39D) that might account for reduced integrin activation in response to CRP.

4.4.1.4 Loss of IL-6R leads to the formation of dysregulated platelet populations under native conditions and after liver injury

Platelet counts as well as platelet activation of *IL-6R*^{-/-} mice were altered before and after PHx compared to WT controls. Moreover, the expression of IL-6R is upregulated after PHx suggesting that the receptor is involved in the regulation of TPO synthesis and thus in the regulation of megakaryopoiesis. Therefore, a detailed analysis of the different platelet populations was of strong interest to identify the role of the IL-6R in megakaryopoiesis and hemostasis. Hence, platelet size, RNA content, PS surface exposure as well as lectin binding of platelets from *IL-6R*^{-/-} mice were analyzed using flow cytometry.

The analysis of these parameters via thiazole orange staining of GPIb positive platelets demonstrated that the number of young platelets in the blood stream was increased in *IL-6R*^{-/-} mice before (size: $p = 0.0002$; RNA-content: $p = 0.405$) and after PHx (size: $p = 0.0003$; RNA-content: $p = 0.0182$) compared to WT controls (fig. 40A+C). Additionally, the data above indicated that PHx itself stimulates the production of new platelets because a significant difference in platelet size of native compared to PHx platelets was detected repeatedly ($p < 0.0001$; fig. 40A – compare fig. 18B). Interestingly, the population of lectin positive plates varies according to the lectin used for the measurement. Within ECA and WGA no differences between all tested groups could be detected. Therefore RCA-1 binding revealed a significantly enhanced fraction of lectin positive platelets in *IL-6R*^{-/-} mice after PHx compared to all other groups (native vs. PHx – *IL-6R*^{-/-}: $p = 0.0001$; WT vs. *IL-6R*^{-/-} – PHx: $p = 0.0021$; WT (native) vs. *IL-6R*^{-/-} – PHx: $p = 0.0423$; fig. 40B). Annexin V binding of platelets was measured as well to identify differences in the platelet fraction of old platelets as well as a marker for pro-coagulant activity of *IL-6R*^{-/-} platelets. In the native state, PS exposure of *IL-6R*^{-/-} platelets was enhanced upon CRP stimulation ($p = 0.0479$) compared to WT controls. However, no differences between both groups were detected after PHx (fig. 40D).

These results point to an important role of IL-6R in platelet count regulation, platelet activation and platelet aging under steady state conditions as well as after acute inflammation and liver resection.

Results

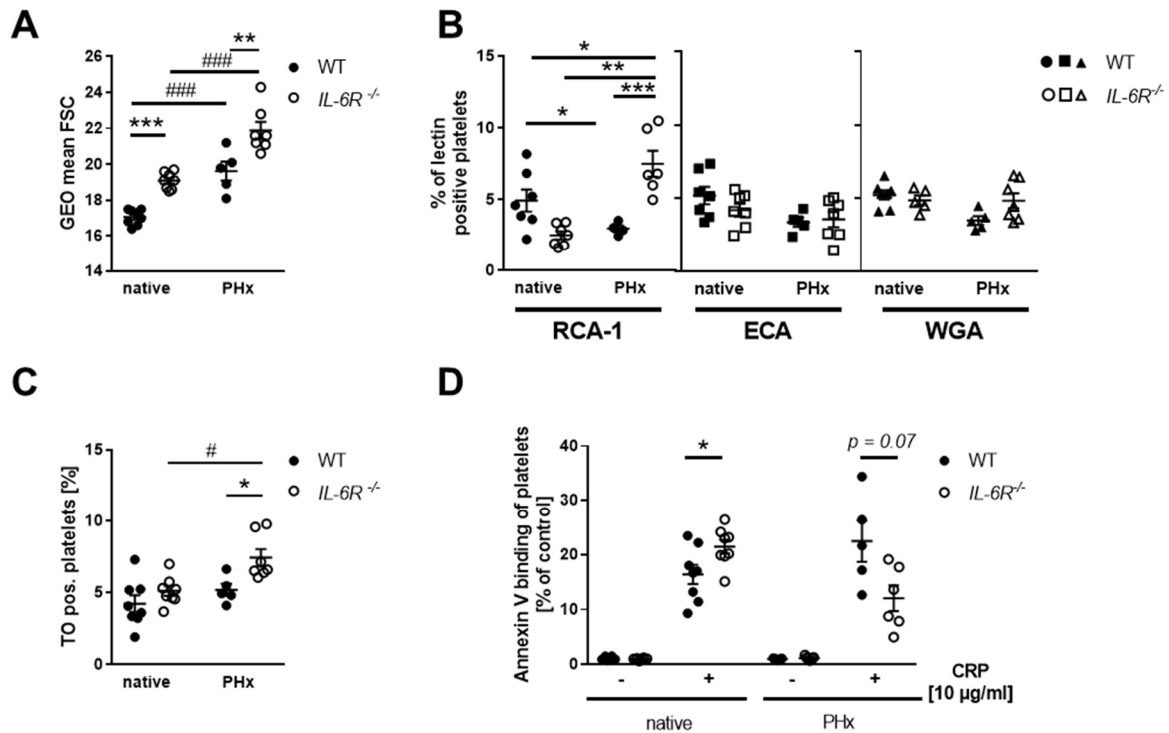


Figure 40. After PHx only GPVI mediated signaling is reduced in IL-6R^{-/-} derived platelets. Platelets from native WT and IL-6R^{-/-} mice were analyzed via the flow cytometry regarding their specific side scatter (SSC) and forward scatter (FSC) profile one day after PHx. (A) Expression of indicated glycoproteins on the surface of platelets measured via mean fluorescence intensity (MFI) indicate GPVI deficiency in IL-6R^{-/-} animals. (B) Externalization of P-selectin on the platelet surface with indicated agonists showed enhanced degranulation with G-protein-coupled Receptor (GPCR) stimulating agonists. However, CRP mediated GPVI signaling is reduced compared to WT. (C) Activation of $\alpha_{IIb}\beta_3$ integrin on the platelet surface with indicated agonists showed pre-active state of IL-6R^{-/-} animals and additional hyperreactivity due to all tested GPCR stimulating agonists. Again, only CRP stimulation results in activation defects (D) Externalization upon platelet stimulation of β_3 integrin subunit indicated a difference with CRP stimulation (n=5 WT, 7 IL-6R^{-/-}). * = $p < 0.05$, ** = $p < 0.01$, *** = $p < 0.001$; tested with unpaired students t-test. CRP = collagen-related peptide.

4.4.2 TPO expression and megakaryopoiesis are causally linked to IL-6R signaling under native conditions and after liver injury

The genetic loss of IL-6R led to enhanced platelet counts, enhanced platelet activation and dysregulated platelet fractions under native as well as under inflammatory conditions with reduced liver tissue. As platelet counts and platelet subpopulations are altered in IL-6R^{-/-} mice, the question arises if TPO biosynthesis and megakaryopoiesis are modulated by IL-6R. Therefore, TPO relevant signaling pathways and TPO serum content were analyzed in IL-6R^{-/-} mice before and after PHx.

Results

4.4.2.1 Elevated Ashwell Morell receptor expression in the total liver tissue of *IL-6R^{-/-}* mice

According to the experiments with WT mice described above, the expression of the AMR was examined in *IL-6R^{-/-}* mice. Liver lysates were analyzed for *Tpo* expression and the level of different AMR subunits compared to WT controls.

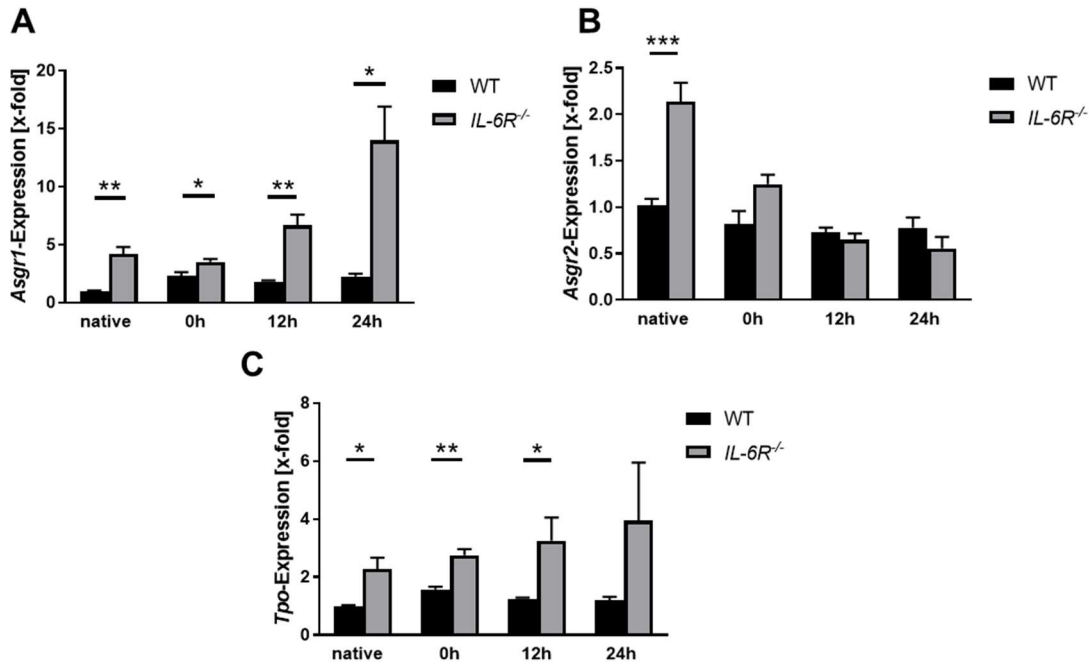


Figure 41. Enhanced TPO synthesis after PHx is associated with upregulated AMR in *IL-6R* deficient mice. Gene expression of different target genes in liver was analyzed using the $\Delta\Delta C_t$ method ($n = 4-5$ WT/time point + 5 *IL-6R^{-/-}*/time point). GAPDH was used as housekeeping gene. (A) Gene expression of the AMR subunit *Asgr1* showed upregulation at all tested time points in *IL-6R^{-/-}* compared to WT mice. (B) Gene expression of the AMR subunit *Asgr2* showed an upregulation in native mice, but not after PHx. (C) *Tpo* expression is enhanced in *IL-6R^{-/-}* mice before and after PHx. * = $p < 0.05$, ** = $p < 0.01$, *** = $p < 0.001$; (A-C) tested with ordinary One-Way ANOVA with Dunnett's post-hoc test.

As expected, both subunits of the AMR were upregulated in native *IL-6R^{-/-}* compared to WT mice. In specific, *Asgr1* was expressed 4.2 ± 0.58 - fold in *IL-6R^{-/-}* compared to WT mice (fig. 41A; $p = 0.008$), while the *Asgr2* subunit was expressed 2.1 ± 0.2 - fold in *IL-6R^{-/-}* mice compared to WT controls (fig. 41B; $p < 0.0001$). After PHx, enhanced expression of the *Asgr1* subunit was observed at all time points tested (0 h: 3.5 ± 0.2 - fold ($p = 0.040$); 12 h: 6.7 ± 0.9 - fold ($p = 0.007$); 24 h: 13.9 ± 2.9 - fold ($p = 0.0233$)) (fig. 41A). In contrast, no difference in the expression of the *Asgr2* subunit was detected between both groups after PHx (fig. 41B). The expression of *Tpo* under native conditions was enhanced likewise as shown by a 2.2 ± 0.3 - fold induction compared to WT controls ($p = 0.0462$). After PHx, a 2.7 ± 0.2 - fold induction (0h - $p = 0.0023$) as well as a 3.2 ± 0.7 - fold induction (12h - $p = 0.036$) in *Tpo* expression was measured in *IL-6R* deficient mice compared to controls. However, no significant difference between WT and *IL-6R^{-/-}* mice was detected 24 h after PHx, even though the total induction of *Tpo* was 3.9 ± 2.0 - fold compared to native WT controls (fig. 41C).

Results

4.4.2.2 Genetic deletion of *IL-6R* leads to delayed *TPO* regulation after PHx

As the expression pattern of the AMR and *Tpo* were regulated by the IL-6R, a detailed analysis of the signaling pathway downstream of the AMR was performed to elucidate how the IL-6R is involved in AMR-induced *Tpo* expression. Therefore, the phosphorylation of AMR target proteins such as JAK2 and STAT3/5 were analyzed by Western blot.

In the liver of *IL-6R*^{-/-} mice, JAK2 total protein expression as well as the phosphorylation of JAK2 were not altered compared to WT mice, neither under native nor under inflammatory conditions (1d post PHx; fig. 42B-C). In WT mice an increase of JAK2 phosphorylation 1d after PHx was detected as already described in part 4.3.3.4 (fig. 42C). A detailed analysis of the transcription factor STAT3, described as the main factor for TPO expression [77], revealed an upregulation of the total protein expression of STAT3 in WT mice compared to respective *IL-6R*^{-/-} mice 1d after PHx ($p = 0.038$). The analysis of STAT3 phosphorylation revealed significantly reduced pSTAT3 in native *IL-6R*^{-/-} compared to WT mice ($p = 0.015$). Despite decreased levels of total STAT3 protein expression, no differences in the phosphorylation of STAT3 1d after PHx were observed (fig. 42D+E). These results provide evidence that liver injury induces the phosphorylation of remaining STAT3 in the liver of WT and *IL-6R*^{-/-} mice.

Thus, phosphorylation of STAT3 might be responsible for elevated *Tpo* expression in IL-6R deficient mice 1d after PHx. However, in IL-6R deficient mice STAT3 might be not responsible for *Tpo* expression under native conditions because significantly reduced phosphorylation of STAT3 was detected. Therefore, the phosphorylation of STAT5, another important transcription factor of the STAT family, was examined in *IL-6R*^{-/-} mice (fig. 42F+G). Total protein expression of STAT5 under native as well as after PHx was indistinguishable between WT and *IL-6R*^{-/-} mice. Furthermore, no differences of STAT5 phosphorylation were observed between the different groups, neither under native conditions nor after PHx. Notably, three out of five tested native *IL-6R*^{-/-} mice showed enhanced STAT5 phosphorylation compared to their native WT control (Appendix fig. 3). However, the increase in STAT5 phosphorylation in three out of five *IL-6R*^{-/-} mice was not statistically significant. Accordingly, there seems to be a certain compensation for each mouse individually to compensate for significantly reduced STAT3 phosphorylation under native conditions.

Besides gene expression, total TPO protein content in liver tissue of *IL-6R*^{-/-} as well as the total serum content were analyzed. Western blot analysis revealed that TPO total protein concentration in the liver of *IL-6R*^{-/-} mice was elevated in both, native mice and 1d after PHx (fig. 42A).

Results

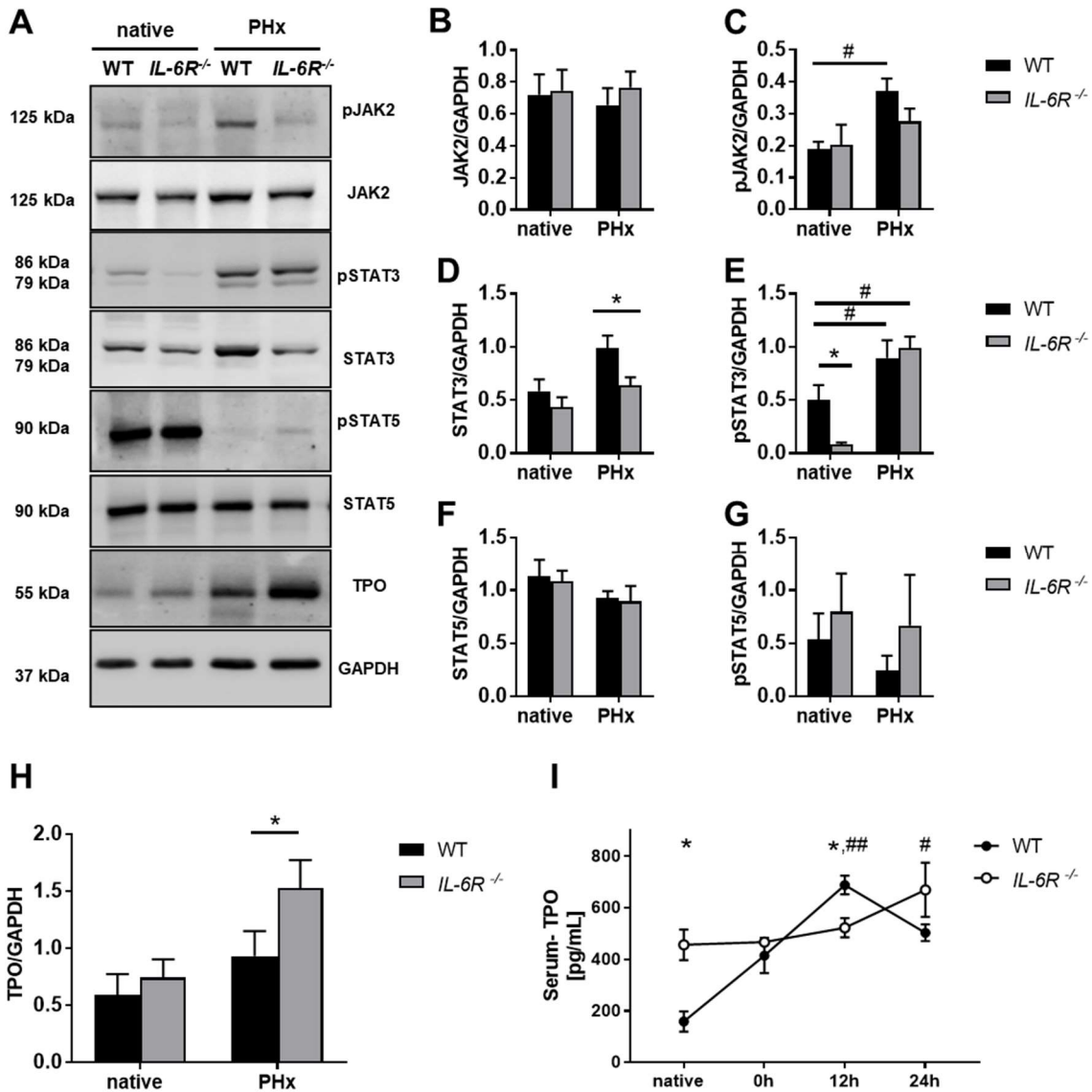


Figure 42. Dysregulated TPO protein expression and serum concentrations in native IL-6 deficient mice and after PHx. Whole liver lysates of native and PHx (1d) WT and IL-6R^{-/-} were analyzed via western blot. (A) Representative immunoblots of total liver cell lysates are shown, analyzed using anti-pJAK2 + anti-JAK2 antibodies, anti-pSTAT5 + STAT5 and anti-pSTAT3 + anti-STAT3 monoclonal antibodies. TPO polyclonal antibody was used, GAPDH served as loading control (n = 5 for each group). (B) Densitometric analysis of JAK2 and (C) pJAK2 revealed no significant differences between WT and IL-6R^{-/-} mice. (D) Densitometric analysis of STAT3 revealed reduced total STAT3 protein in IL-6R^{-/-} after PHx. (E) Analysis of STAT3 phosphorylation revealed a reduced abundance of pSTAT3 signal in native IL-6R^{-/-} mice. (F) Densitometric analysis of total STAT5 protein expression and (G) phosphorylation showed no differences between groups. (H) Densitometric analysis showed upregulated TPO expression in IL-6R^{-/-} mice after PHx but no differences in native mice. (I) Serum concentration of TPO were determined by ELISA and indicated an upregulation of TPO in native mice of both groups (Special characters indicate a difference to native WT mice (#) or differences between genotypes (*); #, * p < 0.05; ##, ** p < 0.01; ###, *** P < 0.001; tested with paired students t-test; (H-I) tested with ordinary Two-Way ANOVA with Sidak's post-hoc test.

However, the increase in native mice was observed only by trend, while the increased levels after PHx were statistically significant compared to WT mice (fig. 42H, $p = 0.040$). Serum analysis revealed a constantly enhanced WT TPO serum concentration of 456.4 ± 59.1 pg/mL in the blood of IL-6R^{-/-} mice, which is only moderately upregulated to 669.7 ± 105.3 pg/mL 1d after PHx without reaching statistical significance. In contrast, TPO serum concentration in WT

Results

mice, as already shown in fig. 32, was tightly regulated after PHx. Comparing both genotypes, a low concentration of 158.3 ± 39.1 pg/mL was detected in WT compared to 456.4 ± 59.1 pg/mL in native *IL-6R^{-/-}* mice ($p = 0.0069$). In the following course, serum concentration in WT mice reached its maximum with 688.4 ± 35.9 pg/mL 12h after PHx while *IL-6R^{-/-}* mice only displayed a significant reduced TPO concentration of 522.3 ± 37.8 pg/mL ($p = 0.0173$) at the same time point. However, TPO concentrations decreased in WT mice 1d after PHx, while the TPO serum levels of *IL-6R^{-/-}* mice steadily increased. TPO total protein and gene expression profiles as well as serum level analysis demonstrated that TPO was upregulated in *IL-6R^{-/-}* mice already under native conditions, exceeding WT expression levels on protein and RNA level after PHx (fig. 42I).

Thus, the sustained upregulated TPO gene and protein expression in *IL-6R^{-/-}* mice prohibited a fast and controlled TPO regulatory mechanism with altered phosphorylation of JAK2 and STAT3/5 despite enhanced AMR expression in native *IL-6R^{-/-}* mice and after PHx.

4.4.3 Extended splenic sequestration and megakaryopoiesis in spleen and bone marrow of *IL-6R^{-/-}* mice

In the absence of IL-6R, up-regulation of AMR subunits as well as increased TPO serum levels were detected compared to WT controls. This together with enhanced platelet counts in *IL-6R^{-/-}* mice suggested that megakaryopoiesis will be altered as well. In line with WT controls shown above, BM and splenic tissue were analyzed for the number of MKs. Since different platelet populations appeared in the blood of *IL-6R^{-/-}* mice (see fig. 40), splenic sequestration was examined as well.

4.4.3.1 Splenic sequestration is enhanced in *IL-6R^{-/-}* mice

For a better understanding of megakaryopoiesis in *IL-6R^{-/-}* mice, spleen weight ratio as well as splenic platelet sequestration was analyzed.

The analysis of the spleen weight ratio did not show differences between WT and *IL-6R^{-/-}* mice, neither in native mice, nor 1d after PHx (fig. 43A). The analysis of GPXI positive regions of the red pulp showed a significant enhanced number of platelets in the spleen suggesting enhanced splenic sequestration in native *IL-6R^{-/-}* mice (*WT - native*: $16.02 \pm 1.6\%$; *IL-6R^{-/-} - native*: $23.43 \pm 1.55\%$; $p = 0.0201$). In line with the analysis of PHx in WT mice and the respective sham controls above (fig. 36), an upregulation of GPXI fluorescence intensity was detected after PHx compared to native controls (*WT - native*: $16.02 \pm 1.6\%$; *WT - PHx*: $22.96 \pm 1.7\%$; $p = 0.0317$). In contrast, *IL-6R^{-/-}* mice showed also enhanced GPIX fluorescence intensity in spleen 1d after PHx (*WT - native*: $16.02 \pm 1.6\%$; *IL-6R^{-/-} - PHx*: $25.39 \pm 1.19\%$;

Results

$p = 0.0030$) compared to the native WT controls (fig. 43B+C). However, no differences between WT and *IL-6R*^{-/-} mice could be detected 1d after PHx because no further increase of platelet positive staining in the spleen was detected in *IL-6R*^{-/-} mice after liver injury.

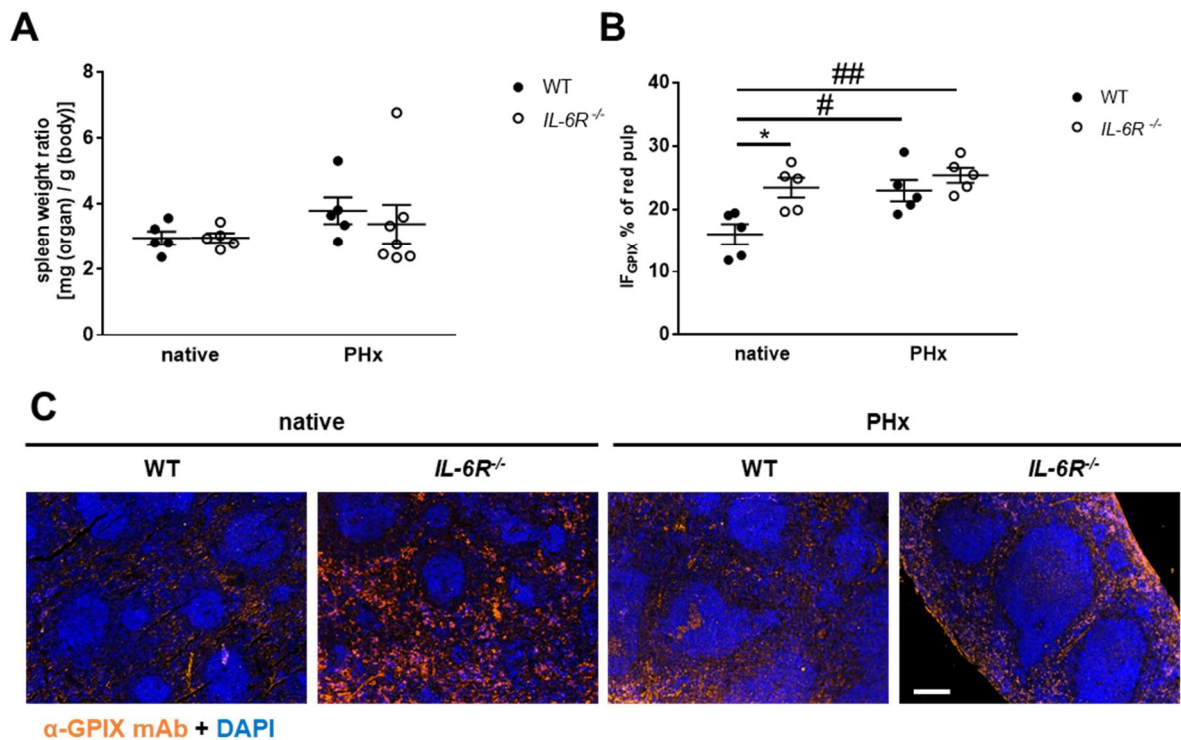


Figure 43. Enhanced platelet sequestration in the spleen of *IL-6R*^{-/-} mice. Murine splenic tissue from WT and *IL-6R*^{-/-} mice before and after PHX (24 h) were analyzed for platelet sequestration. (A) The calculated spleen weight ratio showed no splenomegaly in *IL-6R*^{-/-} mice. ($n =$ native: 5 WT, 5 *IL-6R*^{-/-}; PHx: 5 WT, 7 *IL-6R*^{-/-}). (B) A platelet specific marker (GPIX) was used together with DAPI to detect cell nuclei that allows distinguishing between red and white pulp of the spleen. Total GPIX positive fluorescence area [IF_{GPIX}/μm²] of the red pulp of the spleen sections was determined. *IL-6R*^{-/-} mice show more platelet sequestration into the spleen under native conditions. ($n = 5$) (C) Representative images of the spleen of both groups at indicated time points. * = $p < 0.05$; tested with ordinary Two-Way ANOVA with Bonferroni's post-hoc test. Scale bar = 50 μm.

4.4.3.2 Enhanced megakaryopoiesis in *IL-6R* deficient mice

To further analyze if the genetic loss of the *IL-6R* was causally linked to megakaryopoiesis, HE-staining of tissue sections of spleen and femur BM was performed to count the number of MKs in the hematopoietic tissue of mice.

Compared to WT, *IL-6R* deletion accounted for increasing numbers of MKs in spleen tissue either before or 1d after PHx (fig. 44A). Additionally, PHx provoked an upregulation of the total number of MK's compared to all other experimental groups (WT - PHx vs. *IL-6R*^{-/-} - PHx: $p < 0.0001$; WT - native vs. *IL-6R*^{-/-} - PHx: $p < 0.0001$; *IL-6R*^{-/-} - native vs. *IL-6R*^{-/-} - PHx: $p = 0.0286$). In BM tissue an enhanced number of MKs per visual field could be detected in native *IL-6R*^{-/-} mice compared to WT controls ($p = 0.0347$; fig. 44B). After PHx the total number of MK's was unaltered, while only a moderate increase in the WT mice appeared without reaching statistical significance. According to the previous data as neither splenic nor BM derived

Results

megakaryopoiesis was induced in WT mice 1d after PHx compared to sham controls (compare fig. 34 and 35).

Taken together, increased megakaryopoiesis was observed in the spleen of *IL-6R^{-/-}* mice before and after PHx. In the femoral BM, a slight upregulation of the MKs could be seen, although the effects were less pronounced.

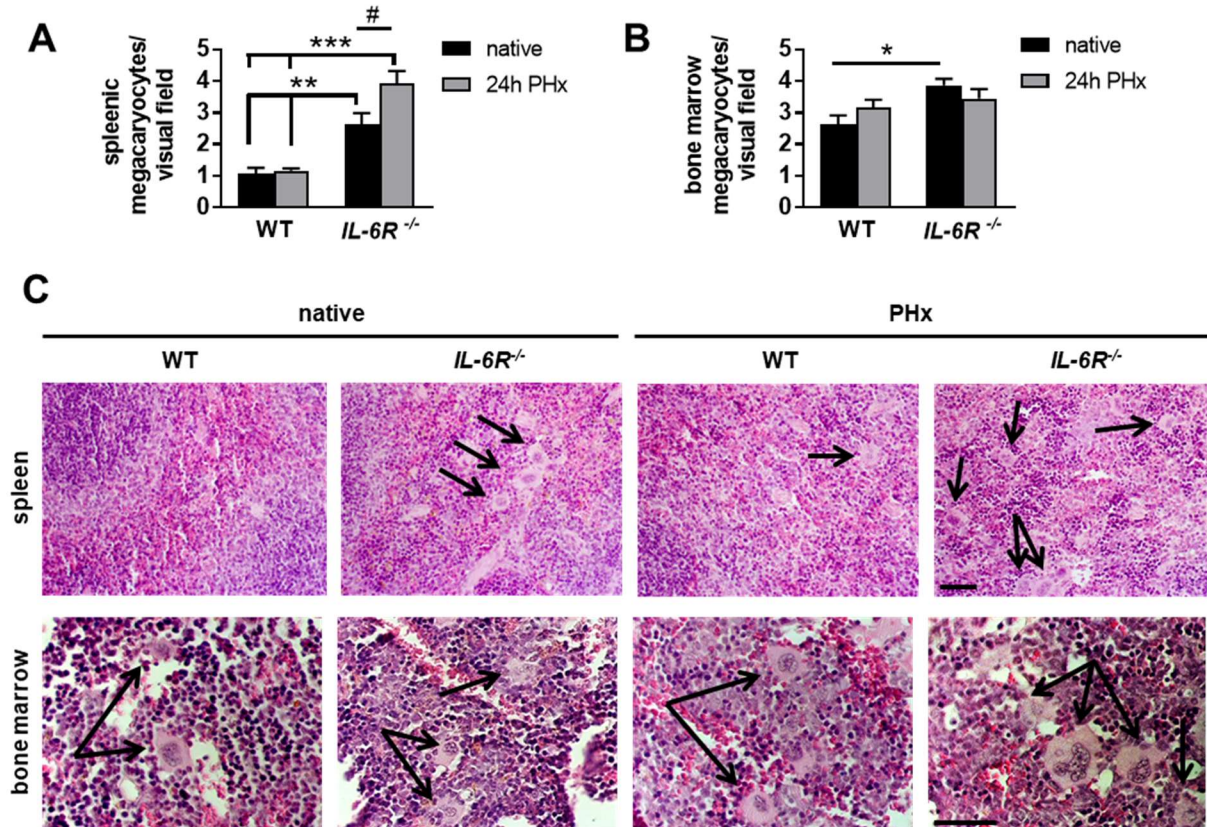


Figure 44. Enhanced megakaryopoiesis in the spleen of *IL-6R^{-/-}* mice before and 1 day after PHx. Spleen and femur from WT and *IL-6R^{-/-}* mice were dissected and analyzed for megakaryocytes before and after PHx (24h). The number of Megakaryocytes (MK) in the spleen (A) and bone marrow (B) of native mice and after PHx was evaluated ($n = 5$ ($n = 4$)) (C) Representative images of spleen and BM of WT and *IL-6R^{-/-}* mice. Arrows indicate MK's in different regions of the respective tissue. Special characters indicate for differences between time points (#) or groups (WT and *IL-6R^{-/-}*; *); #, * $p < 0.05$; ##, ** $p < 0.01$; ###, *** $p < 0.001$; tested with ordinary Two-Way ANOVA with Bonferroni's post-hoc test.

4.4.4 Genetic loss of *Asgr2* leads to upregulation of *IL-6R* gene expression.

As shown above, the *IL-6R* had a major impact on platelet count restoration and regulation in native mice as well as after liver injury and resection. To date, the AMR is described as a major regulator of TPO expression and platelet count regulation while nothing is known about the impact of the *IL-6R* in these processes [77]. Interestingly, the hepatic AMR is composed of two subunits, namely *Asgr1* and *Asgr2* [78]. As the genetic deletion of the *IL-6R* leads to a compensatory upregulation of the AMR, the question arises if the genetic loss of the *Asgr2* subunit, inducing functional loss of the AMR, also accounted for a compensatory upregulation of the *IL-6R*.

Results

Therefore, gene expression analysis of whole liver tissue of *Asgr2*^{-/-} mice was performed, revealing significantly increased *Il-6r* expression by up to 1.75 ± 0.08 -fold ($p = 0.0131$) normalized to WT gene induction. Additionally, *Tpo* expression was elevated to 4.54 ± 1.16 -fold compared to WT mice ($p = 0.041$). Interestingly, even though functional AMR were described to contain ASGR1 and ASGR2 subunits, the expression of the *Asgr1* subunit was elevated by 3.81 ± 0.93 -fold ($p = 0.039$) in the liver of *Asgr2*^{-/-} mice (fig. 45A). Next, protein expression and transcription factor activation were investigated to analyze whether the deletion of an AMR subunit leads to changes in TPO protein expression. Western blot analysis of whole liver tissue lysates demonstrated enhanced TPO protein synthesis in *Asgr2*^{-/-} mice ($p = 0.035$) (fig. 45B+E). Interestingly, no differences in total protein expression as well as in the phosphorylation of either STAT3 or STAT5 could be examined in native *Asgr2*^{-/-} compared to WT mice (fig. 45B-D).

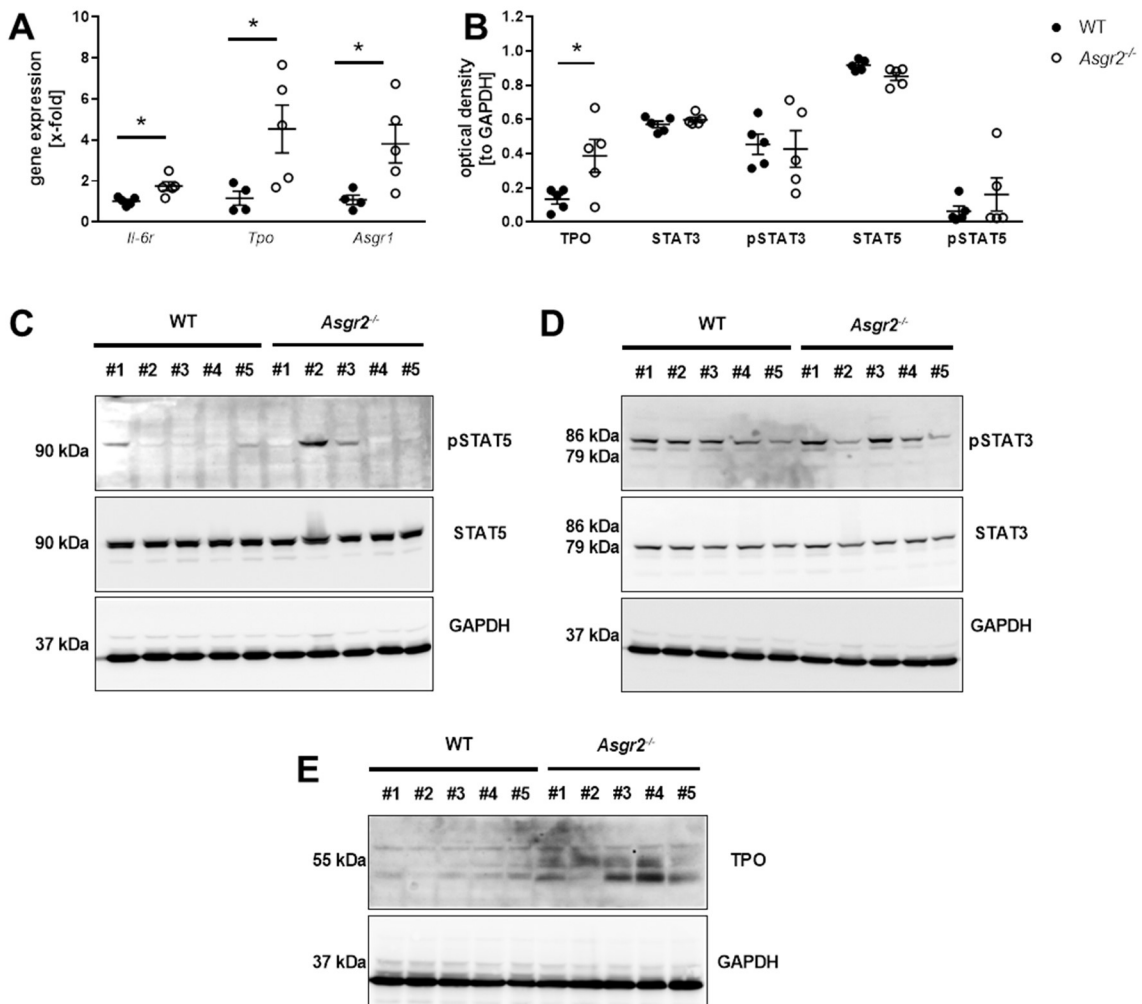


Figure 45. *Asgr2*^{-/-} mice display higher TPO synthesis. The liver of WT and *Asgr2*^{-/-} mice was analyzed for gene expression and phosphorylation of different transcription factors. (A) Gene expression of different target genes was analyzed using the $\Delta\Delta C_t$ method ($n = 5$). GAPDH was used as housekeeping gene. (B) Densitometric analysis revealed enhanced TPO expression in the liver of *Asgr2*^{-/-} mice. (C) Representative immunoblots of total liver cell lysates using (C) TPO polyclonal antibody, (D) anti-pSTAT5 + STAT5 and (E) anti-pSTAT3 + anti-STAT3 monoclonal antibodies. GAPDH served as loading control ($n = 5$). * = $p < 0.05$; tested with ordinary Two-Way ANOVA with Bonferroni's post-hoc test.

Results

4.5 IL-6 trans-signaling induces thrombopoiesis after PHx

It is known that IL-6 induces liver regeneration after 2/3 hepatectomy [149], but administration of IL-6 in concentrations exceeding the endogenous levels resulted in a delay of cell cycle progression and subsequent reduced liver regeneration [196, 197]. Recent studies revealed that IL-6 trans-signaling controls liver regeneration [148] and as previously shown data suggest, IL-6R is also involved in thrombopoiesis. Therefore, a focus was set on the effect of IL-6 trans-signaling on thrombopoiesis in ongoing analysis, as the recombinant fusion protein hIL-6 was used. The fusion protein hIL-6 consists of the sIL-6R and IL-6 that combined mimics IL-6 trans-signaling [198]. hIL6 has a 10 times higher bioactivity than IL-6 alone and has a longer bioavailability *in vivo* [199]. In the study of Behnke *et al* it was already shown, that administration of hIL-6 results in improved liver regeneration by Ki67 and phospho-H3-staining in liver tissue after PHx [173]. We administered 20 μg of hIL6 24h pre-operation, while a control group only received the same volume PBS.

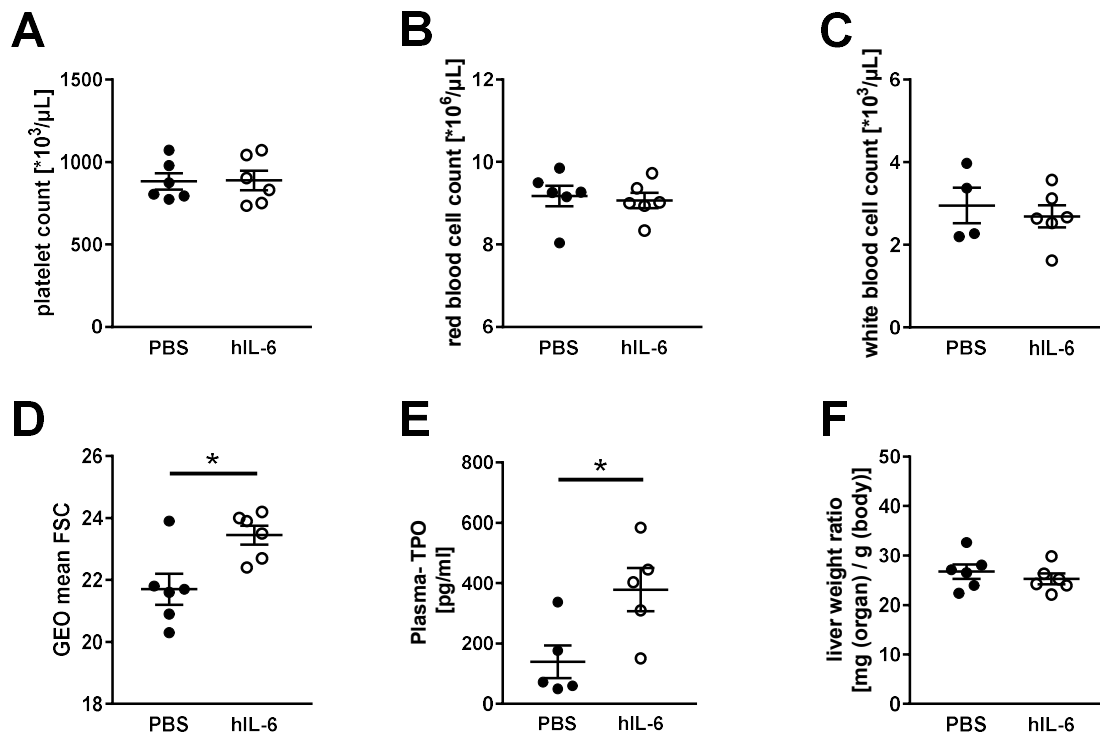


Figure 46 Pre-operative administration of hyper-IL-6 (hIL-6) leads to enhanced TPO plasma concentrations. (A) Platelet counts, (B) red blood cell counts and (C) white blood cell counts of C57Bl6 mice after hyper-IL-6 [20 μg] administration. Mice undergoing PBS administration served as controls ($n = 6$). (D) Platelet size was measured via flow cytometry using the geometric mean of the FSC signal of GPIb positive platelets 1d after PHx treated with or without hyper-IL-6 ($n = 6$). (E) Plasma concentration of TPO in PBS controls and hyper-IL-6 mice 1d after PHx ($n = 6$). (F) Calculated liver weight ratio of PHx mice after administration of hyper-IL6 or PBS ($n = 6$). Depicted are mean values + s.e.m.; * indicates statistical difference between experimental groups; * = $p < 0.05$ tested with unpaired students t-test.

Results

While no difference in platelet, RBC or WBC count could be observed after hIL6 treatment (fig. 46A-C), enhanced platelet size was measured in hIL-6 treated mice compared to controls 1d after PHx (PBS: 21.7 ± 0.49 ; hIL-6: 23.45 ± 0.3 ; $p = 0.0133$; fig. 46D). Additionally, hIL-6 application induced enhanced TPO plasma levels of 378.3 ± 72.05 pg/mL compared to the PBS controls with 138.8 ± 54.57 pg/mL 1 day after PHx ($p = 0.0293$; fig. 46E). At the same time, no difference in the liver weight ratio could be observed 1d after PHx in hIL-6 treated mice compared to PBS controls (fig. 46F).

4.5.1 Administration of hyper-IL-6 induces decreased platelet activation 1d after PHx.

While genetic deletion of the IL-6R resulted in higher activation of platelets, it stayed unclear, whether IL-6 trans- or classic signaling was the prominent signaling pathway behind enhanced platelet activation. To further analyze the effect of IL-6 trans-signaling on platelet activation, platelet activation and receptor expression was analyzed.

Analysis of glycoprotein expression revealed no difference of GPVI, Integrin α_5 or β_3 expression. Unexpectedly, a 23.6% reduced GPIIb α expression on the platelet surface 1d post PHx was measured after hIL-6 treatment (PBS - MFI: 71.53 ± 4.42 ; hIL-6 MFI: 54.67 ± 3.76 ; $p = 0.0157$). Platelet degranulation measured via P-selectin exposure showed activation defects with intermediate ($p = 0.029$) and high ($p = 0.044$) concentrations of CRP, while intermediate concentrations of PAR4-peptide resulted in almost no platelet degranulation ($p = 0.006$) in hIL-6 mice compared to PBS controls 1d post PHx. Similar results were obtained, after the analysis of $\alpha_{IIb}\beta_3$ integrin activation. GPVI mediated integrin activation also showed activation defects with intermediate ($p = 0.0386$) and high ($p = 0.022$) concentration of CRP, while GPCR mediated activation defects were detectable with intermediate levels of PAR-4 peptide ($p = 0.006$) as well as combination of the second wave mediators ADP and U46 ($p = 0.034$).

Taken together these results demonstrate, that specific activation of IL-6 trans signaling after PHx led to reduced platelet activation compared to control mice, accompanied by decreased GPIIb α surface expression of platelets.

Results

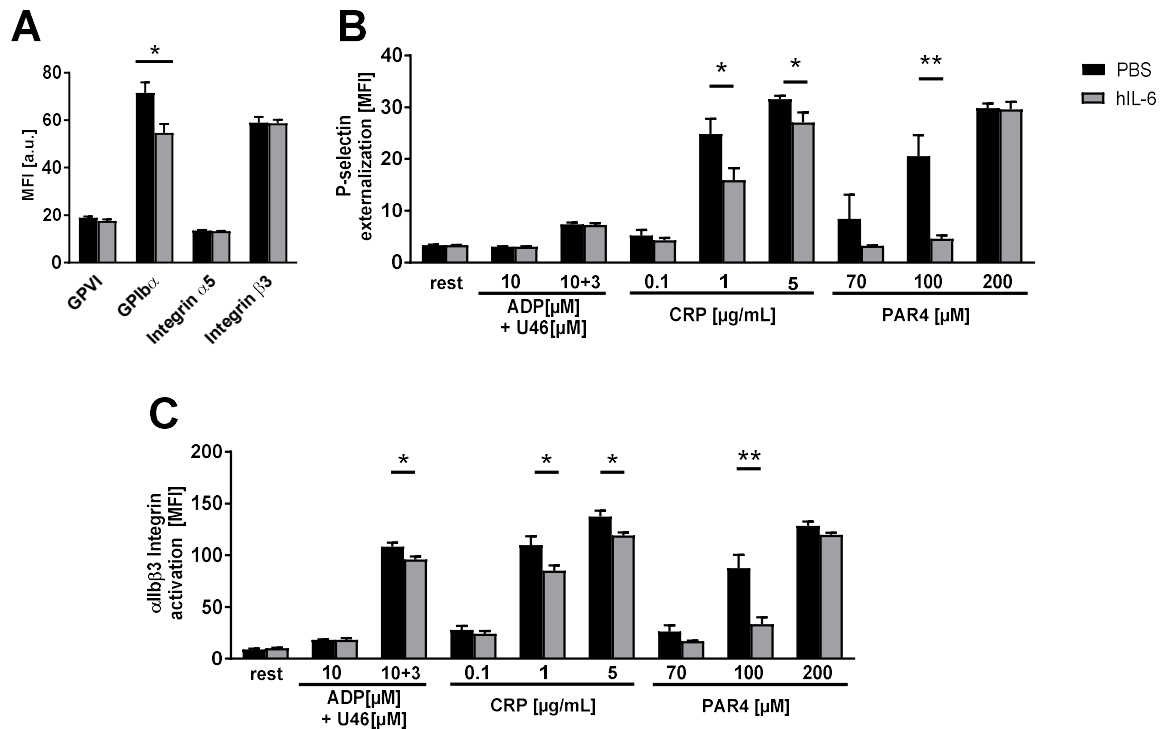


Figure 47 Administration of hIL-6 results in decreased GPIIb/IIIa expression and reduced platelet activation 1d after PHx. hIL-6 was administered 24h before PHx operation [20 μg], while PBS administration served as control group. Platelets were analyzed by flow cytometry regarding their specific side scatter (SSC) and forward scatter (FSC) profile 1 day after PHx. (A) Expression of indicated glycoproteins on the surface of platelets measured via mean fluorescence intensity (MFI) indicate GPIIb/IIIa deficiency in hIL-6 mice 1d after PHx. (B) Externalization of P-selectin on the platelet surface with indicated agonists showed reduced degranulation in GPIIb/IIIa and GPCR mediated platelet signaling cascades (C) Activation of αIIbβ3 integrin on the platelet surface with indicated agonists showed reduced platelet activation after hIL-6 administration 1d after PHx (n = 6). * = p < 0.05, ** = p < 0.01, tested with students unpaired t-test. CRP = collagen-related peptide.

4.5.2 Hyper-IL-6 induces splenic megakaryopoiesis after liver resection

Since an elevated amount of circulating TPO was found in the plasma of hIL-6 treated mice accompanied by increased platelet size 1d after PHx, megakaryopoiesis might be also affected by hIL-6 administration. For further analysis HE-staining of femoral BM and splenic tissue sections was performed.

Even though no difference in the spleen weight ratio appeared after PHx in hIL-6 treated mice compared to PBS control mice (fig. 48A), an elevated number of MKs was found in splenic tissue of hIL-6 treated mice (fig. 48B). In comparison, no difference in the number of MKs in the femoral BM could be measured (fig. 48C).

Results

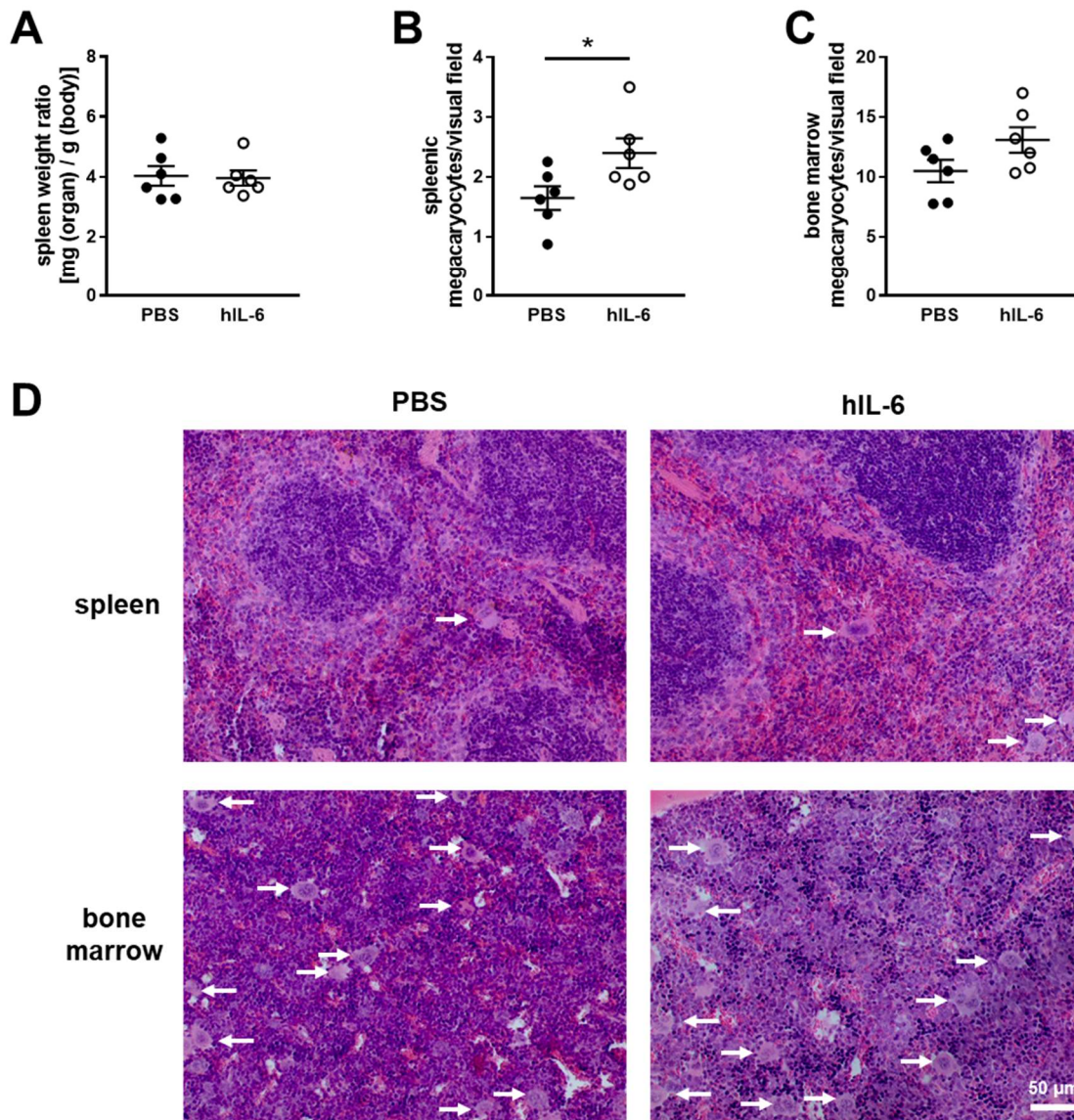


Figure 48 Pre-operative administration of hyper-IL-6 results in enhanced splenic megakaryopoiesis 1d after PHx. (A) Calculated spleen weight ratio of PHx mice after administration of hyper-IL6 [20 μg] or PBS (n = 6). (B) Number of megakaryocytes in paraffin embedded spleen tissue (n = 6) and (C) BM of the femur (n = 6). (D) Representative images from spleen and BM tissue stained with HE. Depicted are mean values + s.e.m.; * indicates statistical difference between experimental groups; * = $p < 0.05$ tested with unpaired students t-test

Overall, these results indicate that the specific induction of IL-6 trans-signaling led to enhanced induction of thrombopoiesis after PHx compared to WT – PHx mice, as TPO plasma levels increased with subsequent enhanced splenic megakaryopoiesis. However, no difference in platelet count could be observed, even though an enhanced platelet size was measured. Besides, inhibiting effects of IL-6 trans-signaling on platelet activation could be observed.

4.6 Thrombocytopenia leads to delayed liver regeneration

The mouse model of PHx is used to study the regenerative capacity of the liver. Different reports in the past suggested that platelets are involved in liver regeneration, but the underlying mechanisms are poorly understood. Platelet derived serotonin stimulates hepatocyte growth factor (HGF) biosynthesis [200] to support liver regeneration. Another platelet derived factor that is known to stimulate tissue regeneration is SDF-1 α [201]. SDF-1 α builds up a gradient resulting in the invasion of stem cells from the BM into the regenerative tissue. As platelets are a major source of SDF-1 α in blood, a genetic model of thrombocytopenia and the effects of reduced SDF-1 α abundance on liver regeneration were investigated.

4.6.1 Chronic thrombocytopenia results in reduced liver regeneration

As a genetic model of thrombocytopenia, mice lacking the thrombopoietin receptor, also known as myeloproliferative leukemia protein (*Mpl*^{-/-} mice), were used. Genetic deletion of the Mpl receptor results in a 90% reduced platelet count [202], as the megakaryocytic growth hormone thrombopoietin is unable to induce megakaryopoiesis. As the Mpl receptor is only expressed on HSCs, MKs and platelets, a constitutive knock-out is megakaryocyte and platelet specific.

4.6.1.1 Genetic deletion of Mpl receptor results in reduced total blood cell count after PHx

To confirm thrombocytopenia in *Mpl*^{-/-} mice, the total blood cell counts in native mice, 1 and 7 days after PHx were determined. As expected, native *Mpl*^{-/-} mice showed a significantly reduced platelet count of $99.1 \pm 13.1 \times 10^3$ platelets/ μ L blood compared to WT controls with $841.8 \pm 63.86 \times 10^3$ platelets/ μ L (*Mpl*^{-/-} = 11.7% of WT; $p < 0.0001$; fig. 45A). Early after PHx (1d) mild thrombocytopenia was observed in WT mice (compare fig. 18A), while in *Mpl*^{-/-} mice, platelet counts dropped to $52.55 \pm 22.93 \times 10^3/\mu$ L (*Mpl*^{-/-} sham) and $56.67 \pm 25.06 \times 10^3/\mu$ L (*Mpl*^{-/-} PHx) compared to native mice. After 7 days, decreased platelet counts in *Mpl*^{-/-} sham and PHx mice was compensated and normalized to native conditions (fig. 49A).

RBC counts were not regulated upon genetic deletion of the Mpl receptor under native conditions. In contrast to WT mice (9% reduction of RBC counts, compare fig. 18B), a severe anemia was observed in *Mpl*^{-/-} mice 24 h after PHx (RBC count 1d after PHx – WT: $8,24 \pm 0,16 \times 10^6/\mu$ L vs. *Mpl*^{-/-}: $6.21 \pm 0.34 \times 10^6/\mu$ L; $p = 0.0011$). While WT mice showed no differences in RBC counts 7 days after PHx, a reduction was still detectable in *Mpl*^{-/-} PHx mice compared to their respective sham controls without reaching statistical significance ($p = 0.2$; fig. 49B)

Results

Unexpectedly, a difference of 26.7% in the total white blood cell count was examined in native *Mpl*^{-/-} mice compared to WT controls (*WT native*: $7.59 \pm 0.85 \times 10^3/\mu\text{L}$; *Mpl*^{-/-} native: $5.56 \pm 0.43 \times 10^3/\mu\text{L}$; $p = 0.0341$). This difference in WBC count increased after PHx. In *Mpl*^{-/-} mice the WBC count dropped in sham and PHx mice 1 day after operation. WBC counts recovered in sham animals to basal levels 7 days after operation. In contrast, prolonged low WBC counts were observed in *Mpl*^{-/-} mice 7 days after PHx. However, no statistically significant difference between sham and PHx treated *Mpl*^{-/-} mice were detected at any time point (fig. 49C).

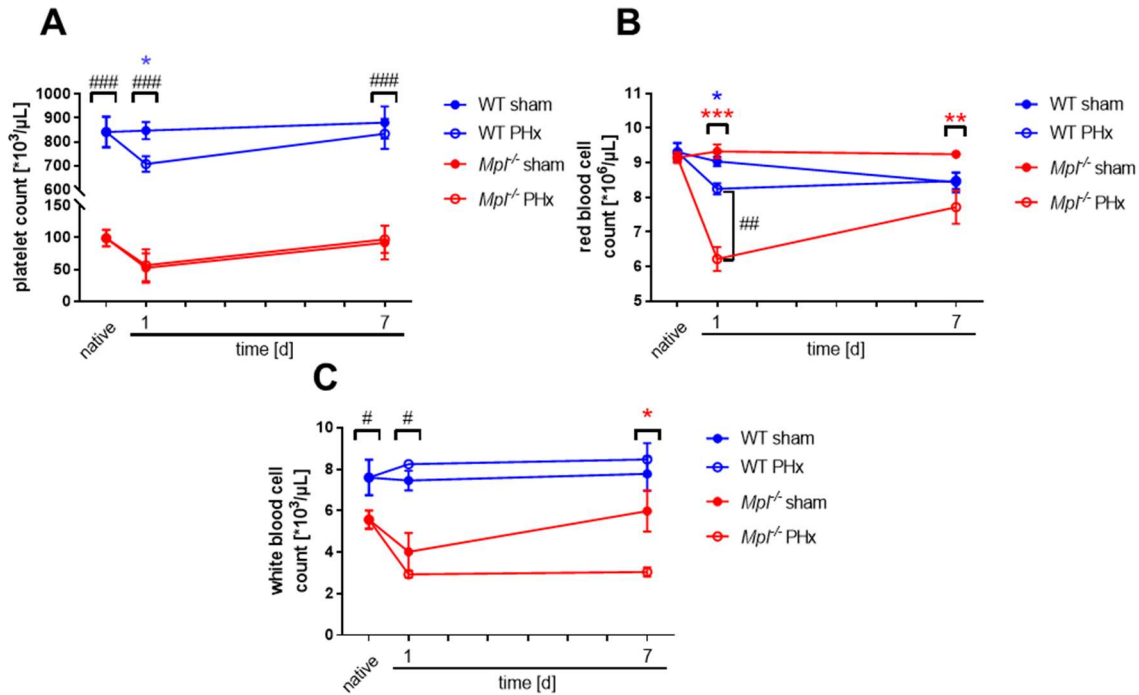


Figure 49. *Mpl*^{-/-} mice display thrombocytopenia, leukocytopenia and anemia after PHx. Whole blood from WT and *Mpl*^{-/-} mice before and after PHx (indicated time points) was taken and analyzed with a hematology analyzer (Sysmex KN-X21). (A) The analysis of platelet counts revealed thrombocytopenia (11.7% of WT) in native mice and after PHx. (B) Severe anemia in *Mpl*^{-/-} mice 1d after PHx compared to all other groups. (C) Prolonged leukocytopenia (73.2% of WT) in *Mpl*^{-/-} mice after PHx. ($n = 8-30$ WT; $3-8$ *Mpl*^{-/-}). Colorized asterisks indicate the statistical difference in between one genotype, while rhombus indicates the differences between both genotypes. *, # = $p < 0.05$, **, ### = $p < 0.01$, ***, ### = $p < 0.001$; tested by ordinary Two-Way ANOVA with Bonferroni's post-hoc test.

4.6.1.2 Reduced IL-6 plasma levels in thrombocytopenic mice account for reduced liver regeneration

Different studies provide evidence that platelets are key players in liver regeneration [194]. To analyze the effects of thrombocytopenia on liver regeneration, the liver weight ratio was calculated between WT (sham + PHx) and *Mpl*^{-/-} (sham + PHx) mice. The difference in liver weight ratio between WT and *Mpl*^{-/-} mice demonstrated a 19.3% reduction (WT-PHx: 29.21 ± 0.65 vs. *Mpl*^{-/-} PHx: 23.57 ± 0.77 ; $p = 0.0457$) in liver volume 1d after PHx. This delay in liver volume could still be determined 7 days after liver resection (PHx - WT vs. PHx - *Mpl*^{-/-}: $p = 0.030$). Respective *Mpl*^{-/-} sham controls displayed liver weight ratios comparable to WT

Results

sham controls (fig. 50A). Additionally, the spleen weight ratio of WT and *Mpl*^{-/-} mice was determined but no difference was measured between WT - PHx and *Mpl*^{-/-} - PHx animals even though a more severe thrombocytopenia developed in *Mpl*^{-/-} mice. Nevertheless, WT and *Mpl*^{-/-} mice developed a mild splenomegaly compared to their respective sham controls 7 days after PHx (WT-sham: 4.42 ± 0.5 g vs. PHx: 6.22 ± 0.59 g; *p* = 0.0136; *Mpl*^{-/-}- sham: 4.47 ± 0.57 g vs. PHx: 7.81 ± 2.33 g; *p* = 0.0136; fig. 50B).

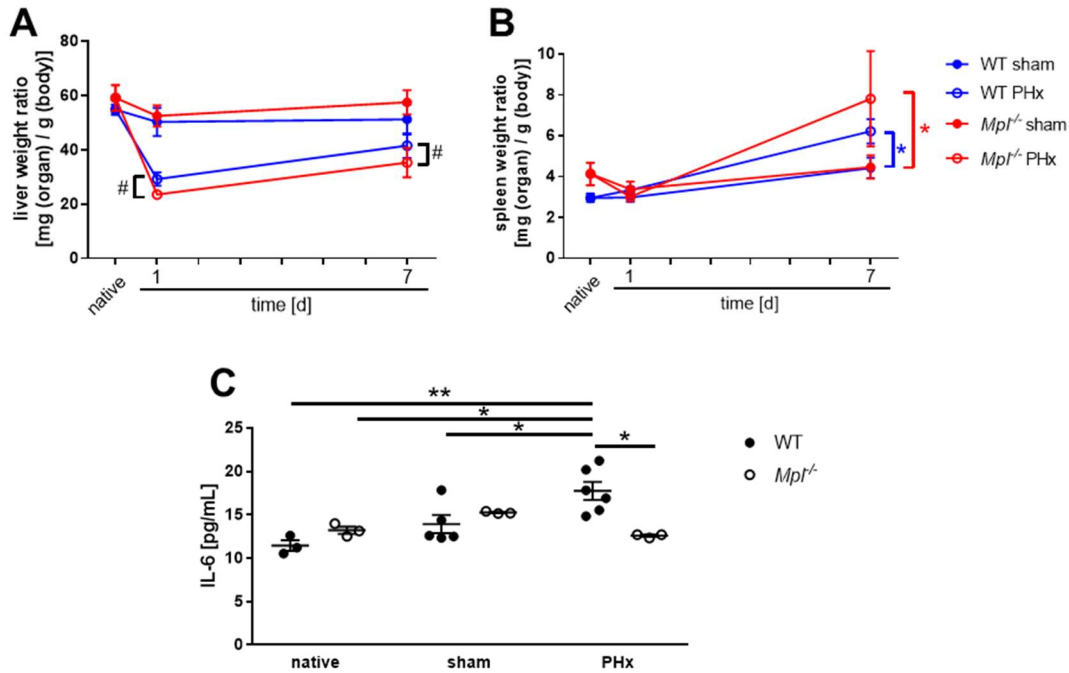


Figure 50. *Mpl*^{-/-} mice develop splenomegaly and show reduced liver regeneration and IL-6 plasma levels (A) Calculated liver weight ratio revealed delayed liver mass regeneration between WT and *Mpl*^{-/-} mice after PHx. (B) Analysis of the Spleen weight ratio showed formation of splenomegaly 7 days after PHx in *Mpl*^{-/-} mice compared to respective WT controls. (C) IL-6 plasma levels were measured via ELISA. (*n* = 3-6). For A and B: Colorized asterisks indicate the statistical difference in between one genotype, while rhombus indicates the differences between both genotypes. For C: asterisk indicates the difference between indicated groups. *, # = *p* < 0.05, **, ## = *p* < 0.01 tested by ordinary Two-Way ANOVA with Bonferroni's post-hoc test.

As previously demonstrated, the acute phase cytokine IL-6 is a major hepato-protective player by activating the IL-6R. Therefore, it was of interest if reduced liver regeneration in *Mpl*^{-/-} mice is linked to the IL-6 signaling pathway, as TPO is the natural ligand of the Mpl receptor. As expected, IL-6 plasma levels were increased in WT mice 1d after PHx in contrast to their respective native (*p* = 0.0023) and sham (*p* = 0.0478) controls (fig. 50C). In contrast, reduced IL-6 levels were detected in the plasma of *Mpl*^{-/-} mice compared to WT mice 1d after PHx (*p* = 0.0148). These results provide first evidence that thrombocytopenia leads to reduced IL-6 plasma levels and affects liver regeneration after PHx. Thus, both the direct platelet effects and platelet-induced effects on IL-6 plasma levels might account for delayed liver regeneration.

Results

4.6.2 Thrombocytopenia results in reduced plasma SDF-1 α concentration after partial hepatectomy

In literature, it is controversially discussed whether liver regeneration is only mediated through the proliferation of parenchymal liver cells or if, BM derived stem cells are invading into the diseased liver to support regeneration. The stem cell derived factor-1 α (SDF-1 α), acts as chemoattractant that builds up a gradient towards the regenerative tissue and attracts stem cells from the BM to the site of injury. To elucidate the impact of platelet derived SDF-1 α , the SDF-1 α plasma concentration of WT mice and *Mpl*^{-/-} mice was investigated.

The analysis of WT mice revealed an enhanced SDF-1 α plasma concentration of 398.18 ± 42.84 pg/mL in the primary phase of liver regeneration 1d after PHx compared to sham controls with 246.81 ± 28.04 pg/mL ($p = 0.0111$; fig. 51A). With regard to progressive tissue regeneration, the concentration of SDF-1 α decreased to normal plasma levels of 247.86 ± 27.24 pg/mL 3 days after PHx (compared to 1d PHx; $p = 0.0219$). Upon thrombocytopenia, a reduced SDF-1 α plasma level of 205.64 ± 11.22 pg/mL could be detected in *Mpl*^{-/-} mice compared to WT mice 1d after PHx ($p = 0.0111$). Thus, platelets are responsible for the up-regulation of SDF-1 α in the plasma of mice early after PHx, while no differences between WT and *Mpl*^{-/-} were observed in native or sham mice (fig. 51B). Therefore, platelet derived SDF-1 α might be a supporting factor for liver regeneration after PHx.

Taken together, reduced liver regeneration in thrombocytopenic mice is accompanied by the loss of an SDF-1 α gradient early after PHx and reduced IL-6 plasma levels that all might account for platelet mediated effects on liver regeneration.

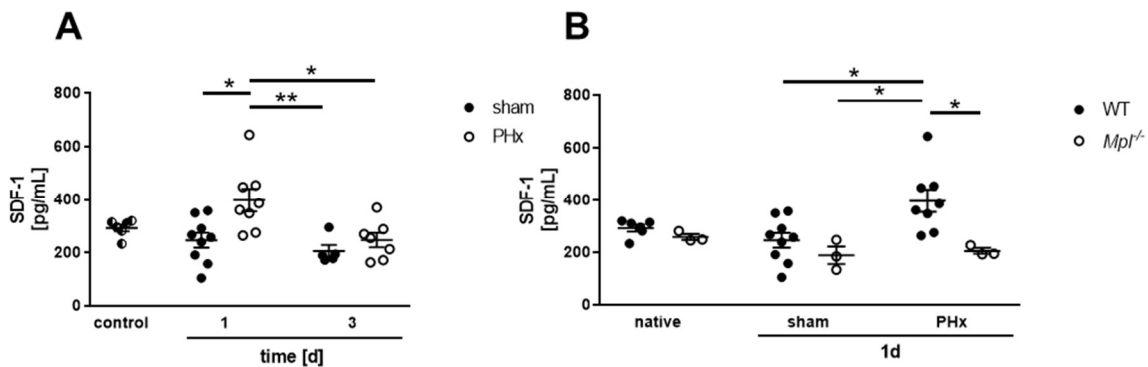


Figure 51. *Mpl*^{-/-} mice display reduced SDF-1 plasma levels early after PHx. SDF-1 plasma levels were measured by ELISA at indicated time points after PHx. (A) within the first 24 h the SDF-1 plasma levels rise compared to sham controls and normalize 3 days after PHx. ($n = 6-9$). (B) SDF-1 levels in the *Mpl*^{-/-} mice are not regulated after PHx. ($n = 3-9$); * = $p < 0.05$, ** = $p < 0.01$ tested ordinary Two-Way ANOVA with Bonferroni's post-hoc test.

5. Discussion

The results of this study reveal that different liver injury models – the cholestatic liver disease and liver resection – modulate primary hemostasis involving platelet activation defects resulting in mild thrombocytopenia and enhanced bleeding risk *in vivo*. According to the present observations, multiple effects influence platelet activation through increased production of inhibitory plasma factors by the vascular endothelium. These factors include for instance NO and PGI₂, which both induce a strong phosphorylation of platelet VASP. Additionally, high plasma levels of BAs, typically parameters of liver disease, affect platelet activation of murine and human platelets propagating further inhibition of primary hemostasis. The enhanced platelet consumption due to invading platelets in the inflammatory liver tissue is thereby encountered by enhanced megakaryopoiesis in the spleen and BM of mice in both models.

Besides, the results of the present study provide strong evidence for a compensatory upregulation of TPO signaling in the liver following inflammatory liver disease with reduced liver volume. TPO synthesis is mediated through an AMR/IL-6R-JAK2-STAT3 signaling pathway to synergistically control TPO hemostasis necessary to compensate the enhanced platelet turnover after liver injury. The genetic deletion of the IL-6R or the c-Mpl receptor highlight the prominent role of both receptors in maintaining physiological platelet counts after liver resection. Furthermore, mice lacking these receptors show diminished or even no liver regeneration after PHx emphasizing the importance of platelets in liver regeneration.

5.1 Bile duct ligation impairs platelet function and propagates bleeding risk *in vivo*

In this study, total blood cell counts and platelet function 7 days after BDL were analyzed. These results were already published in 2017 including the analysis of platelet activation 3 and 21 days after BDL [203]. To this date, little evidence for mechanisms behind platelet activation and primary hemostatic defects were given in cholestatic liver disease [162, 163]. At all examined time points defects in platelet function could be measured which resulted in altered hemostasis in the first 7 days after BDL. Thrombocytopenia is one aspect often accompanied by defective primary hemostasis. Moderately decreased platelet counts are already described for patients suffering from liver injury [163]. Possible reasons might be altered levels of TPO, an enhanced platelet turn-over or increased splenic platelet sequestration [204-206]. After BDL, moderate thrombocytopenia could only be observed within the first 3 days (see table 9). Platelet counts reached physiological levels 7 days after BDL, even though platelet activation

Discussion

defects persisted until day 21 which suggests that platelet activation defects are responsible for impaired primary hemostasis within the first 7 days after BDL. Enhanced megakaryopoiesis in the spleen of BDL mice at day 7 (fig. 6) counteracts thrombocytopenia at early time points after BDL that might be due to enhanced sequestration of platelets in the spleen. Additionally, increased platelet consumption might be reasonable as platelet aggregates accumulate in the sinusoidal space of the diseased liver (fig. 11). A study from Laschke *et al* provided evidence, that after BDL a massive accumulation of platelets in the liver sinusoids occurs that was prevented due to platelet depletion with an α -GPIb antibody [165].

5.1.1 Different mechanisms account for decreased platelet activation

Different studies showed that the vascular integrity upon cholestasis is altered, as enhanced NO production in endothelial cells through eNOS, as well as enhanced plasma levels of prostaglandin were measured in cholestatic patients and after experimental BDL in rodents [179, 183]. NO and PGI₂ induce platelet inhibition through activation of cAMP and cGMP in platelets resulting in enhanced VASP phosphorylation, subsequently inhibiting platelet function by reduced $\alpha_{IIb}\beta_3$ integrin signaling, and defective calcium mobilization and cytoskeletal reorganization [178]. The present study firstly correlates enhanced levels of NO and PGI₂ with platelet activation defects in the murine model of obstructive cholestasis. Although only a moderate increase in PGI₂ could be measured 7 days after BDL, significantly enhanced levels of the NO metabolites nitrite and nitrate are present in BDL mice 7 days after operation (fig. 8). These enhanced plasma levels could be causally linked to impaired platelet activation 7 days after PHx [203]. VASP phosphorylation at Ser¹⁵⁷ and Ser²³⁶ were enhanced in platelets from BDL mice 7 days after induction of cholestasis [203]. Additionally, enhanced levels of t-PA and PAP-complexes were measured in mice after BDL (fig. 8). This strongly suggests that increased circulating t-PA which induces plasmin activity and enhanced PAP-complexes that indirectly reflect plasmin activity [207], might be responsible for increased plasmin plasma concentration in BDL mice. Two different mechanisms act synergistically in cholestatic liver injury that accounts for enhanced plasma t-PA levels: 1st A diseased liver has a reduced hepatic clearance and 2nd biosynthesis of t-PA is enhanced in mice after BDL [208, 209]. In agreement with the murine model of BDL, enhanced levels of t-PA are also described for patients suffering from liver diseases such as primary biliary cholangitis (PBC) or other liver diseases [210, 211]. To this date, the clinical aspects of t-PA upregulation are not investigated, but in mice, several studies demonstrated a crucial role of t-PA upregulation in cholestatic liver injury. Either inhibition of t-PA or genetic deletion of the physiological inhibitor plasminogen activator inhibitor-1 (PAI1) led to severe liver damage [212-214]. Thus, here observed upregulation of t-PA might be a protective mechanism after BDL.

Discussion

It is known that high levels of plasmin lead to platelet receptor shedding such as GPIb and $\alpha_{IIb}\beta_3$ integrin resulting in reduced platelet activation [180, 215]. As stated in Gowert *et al*, platelet receptor shedding of GPs and integrins in BDL mice, provoked by enhanced levels of circulating plasmin, are in part responsible for reduced platelet activation measured 7 days after BDL [203]. In addition, enhanced VASP phosphorylation 7 days after BDL contributes to intrinsic platelet inhibition.

5.1.2 BDL provokes reduced platelet activation *in vitro*

The aforementioned mechanisms in cholestatic liver disease provoke reduced platelet $\alpha_{IIb}\beta_3$ integrin activation and reduced degranulation measured via P-selectin externalization and serotonin release. Interestingly, GPVI induced platelet signaling was almost diminished following CRP stimulation, while GPCR stimulation via thrombin or ADP still showed reduced platelet responses (fig. 9). Even though these *in vitro* analyses showed crucial activation defects, platelet function after liver disease is still controversially discussed in literature. Differences in diverse liver diseases appear to influence platelet activation and platelet-vessel wall interaction. *In vitro* platelet activation studies using platelets from patients with PBC provided evidence for a hyperactive state of platelets as increased CD42b and enhanced extracellular neoepitopes termed ligand-induced binding sites (LIBS – active integrin $\alpha_{IIb}\beta_3$ binding sites) could be measured via flow cytometry [162, 216]. However, Ingeberg and colleagues studied aggregation and ATP release of platelets from PBC patients revealing reduced platelet activation upon cholangitis [217]. In addition, enhanced plasma levels of soluble GPVI and soluble P-selectin in patients with liver disease were measured [218-220]. Both factors are soluble fragments of GPVI (sGPVI) or P-selectin (sP-selectin) that are shed from the platelet surface in a metalloproteinase-dependent manner which indicates prior platelet activation [218, 219]. This implies an enhanced activation of platelets at an early stage of liver failure, resulting in reduced platelet activation with progression of liver disease.

Moreover, not only results from clinical studies vary in their conclusion on platelet activation after cholestatic liver disease. Studies on platelet activation after BDL – mainly performed in rats – also differ with regard to Ca^{2+} mobilization. Atucha *et al* published different data regarding Ca^{2+} mobilization in rats after BDL. In the latest study regarding platelet activation, thrombin stimulation led to enhanced Ca^{2+} influx in platelets [221]. In contrast, earlier studies provided evidence for defective Ca^{2+} entry and mobilization after BLD in rats [222, 223]. Calcium mediated signaling is one main aspect in platelet activation as it controls integrin activation, degranulation, and cytoskeletal reorganization [224]. Orai1, a calcium channel located at the cell membrane of platelets, is upregulated upon platelet stimulation to modulate calcium influx [225]. Additionally, a calcium activated chloride-channel Ano6, is known to

Discussion

modulate the cytosolic calcium activity [226]. Since almost no platelet activation after GPVI stimulation was obtained with platelets of BDL mice, a detailed analysis of GPVI dependent calcium signaling would be interesting. In the study of Atucha *et al*, only thrombin-mediated effects were analyzed although calcium signaling is mediated by GPVI as well.

However, platelet activation defects in mice affect thrombus formation on a collagen matrix *ex vivo*, resulting in prolonged tail bleeding time 7 days after BDL *in vivo* (fig. 10). In agreement with the presented data above, prolonged tail bleeding times in rats undergoing BDL was also examined earlier [227]. An additional explanation was stated by Witters *et al*, suggesting that ADP-degrading enzymes are responsible for platelet activation defects after BDL in rats leading to reduced platelet aggregation [228]. In contrast to the here presented observations (fig. 9), intrinsic platelet activation was unaltered in BDL rats. This might be due to different flow cytometric analysis of platelets since platelets in washed whole blood were examined in this study while Witters and colleagues used platelets in unwashed platelet rich plasma [228].

5.1.3 Potential effects of bilirubin on platelet activation in BDL mice

Another elevated plasma factor in mice after cholestatic liver injury is bilirubin. Plasma levels of bilirubin were 63 times higher in BDL mice compared to sham controls (see table 9). As it was already shown that bilirubin triggers erythrocyte death resulting in anemia 21 days after BDL in mice, it is tempting to speculate that high levels of bilirubin are responsible for the decrease in erythrocyte numbers 7 days after BDL (figure 7) [229]. This should be assessed rather critically, as the RBC counts on day 1 and day 7 of the BDL sham controls vary too much compared to the RBC counts of the PHx surgery series sham controls (comparison of sham mice in PHx (fig. 18)). Since the sham operation for PHx and BDL is performed using the same procedure, there should be no differences in the total blood cell counts. Nevertheless, patients suffering from Gilbert's syndrome (GS) are protected against cardiovascular diseases [230]. A clinical symptom of GS is hyperbilirubinemia and therefore bilirubin is discussed as an antithrombotic agent. This assumption is strengthened by a study from Kundur *et al* who recently detected reduced platelet activation upon ADP stimulation in GS patients [231]. Additionally, bilirubin inhibits platelet activation and increases the antioxidant status that may also play a role in cholestatic liver disease [230, 232]. These findings suggest that bilirubin might influence platelet activation upon BDL in mice as well. However, further studies are needed to further elucidate the role of bilirubin in platelet activation and hemostasis.

Overall, the findings in the presented study reveal that mild thrombocytopenia develops after BDL in mice. However, thrombocytopenia is accompanied by severe platelet activation defects that are not only due to thrombocytopenia but also to elevated plasma factors known to inhibit platelet activation. Platelet activation defects are provoked by a dual system of intrinsic and

Discussion

extrinsic platelet inhibition. Enhanced plasma levels of PGI₂ and NO mediate intrinsic platelet inhibition through the phosphorylation of VASP. Extrinsic platelet inhibition is caused by enhanced levels of t-PA and plasmin that facilitate platelet receptor shedding that all led to reduced thrombus formation 7 days after BDL. Furthermore, enhanced platelet accumulation in the diseased liver is observed due to hepatic platelet consumption after BDL. Taken together, cholestatic liver disease promotes platelet activation defects leading to diminished thrombus formation *ex vivo* and severe hemostatic defects *in vivo*.

5.2 Bile acids as a modulator of platelet activity

A factor that is steadily increased upon cholestatic liver disease is the total BA concentration in the blood. To this date, clear evidence of the influence of BAs on platelet activation is missing. Aggregation studies of platelets drawn from bile duct ligated rats and patients suffering from cirrhosis indicate that BAs affect platelet activation [233, 234]. However, in the study of Gowert *et al*, slightly reduced $\alpha_{IIb}\beta_3$ integrin activation and P-selectin exposure after GPVI stimulation could be observed while an upregulation of P-selectin with high thrombin concentration was observed in cholic acid fed mice [203]. Hence, no decreased thrombus formation under flow could be observed in these mice. This discrepancy might be due to a reduced total BA concentration in cholic acid fed mice (329 $\mu\text{mol/L}$) compared to mice 7 days after BDL (Sham 5.7 $\mu\text{mol/L}$ vs. BDL 1.252 $\mu\text{mol/L}$ after 7 days) [181]. Moreover, in a study from 2017, it was shown that BAs do not contribute to altered calcium hemostasis of platelets from rats with biliary cirrhosis, even though stimulation with the unconjugated BAs CA and DCA modulated calcium influx and store release of rat platelets [235].

The analysis of serum BA composition of WT mice revealed that taurine conjugation (fig. 12) of BAs is predominant in mice, speculating a higher importance of those BAs in the modulation of platelet activation. In 2016, it was published that the soluble BA receptor FXR is expressed in platelets and modulates platelet activation through upregulation of cGMP and subsequent phosphorylation of VASP^{S239} resulting in diminished $\alpha_{IIb}\beta_3$ integrin signaling and thrombus formation under flow [236]. Therefore, it is tempting to speculate that also other BA receptors are expressed in platelets that may alter primary hemostasis upon high BA plasma levels. The authors only used a synthetic active agonist to stimulate the FXR and only moderate defects with the unconjugated BA CDCA [300 μM] were observed in aggregometry studies[237]. It is possible that after BDL another receptor, such as the TGR5, might play a role in BA induced modulation of platelet activation because the TGR5 exhibits a higher affinity for taurine-conjugated BAs [238]. Moreover, integrin outside-in signaling defect was observed in human (fig. 17) and murine (fig. 14) platelet adhesion on a fibrinogen matrix after pre-incubation with taurine-conjugated BAs. Additionally, a reduced $\alpha_{IIb}\beta_3$ integrin activation after GPVI stimulation

Discussion

1 (fig. 15) and 6 h (fig. 16) after pre-incubation of platelets with BAs was observed in flow cytometric studies. A reduced integrin outside-in signaling was also shown by Moraes *et al* resulting in reduced filopodia and lamellipodia formation which is congruent with the reduced adhesion presented in this study [236].

Interestingly, it was shown that incubation of platelets with BAs also leads to platelet swelling [239], which was observed after FXR stimulation [237]. Different pathophysiological conditions involved in glucose metabolism are also characterized by enhanced BA serum levels like hyperlipidemia, obesity or type 2 diabetes mellitus in humans [240-242]. In the clinical picture of these diseases, enhanced BA concentrations accompanied by platelet swelling were observed. Indeed, the mean platelet volume is also a clinical tool to discriminate the severity of PBC patients [243, 244]. Thus, it would be of utmost interest to study the influence of BDL, cholic acid feeding of mice and BA treatment of platelets on the mean platelet volume and the associated signaling of platelets.

Overall, reduced integrin signaling is observed 7 days after BDL. Furthermore, reduced adhesion of platelets on fibrinogen that were pre-incubated with different BAs was observed suggesting BA induced integrin inside-out and outside-in defects. However, enhanced P-selectin exposure of platelets pre-treated with BAs following thrombin stimulation was also observed. These findings of P-selectin exposure and integrin activation were confirmed in cholic acid fed mice by Gowert *et al* [203]. These contradictory results suggest a dual role of BAs on the regulation of platelet signaling that leads to the enhanced generation of coated platelets. Further studies of the FXR receptor revealed an induction of coated platelets as P-selectin and PS-exposure are enhanced due to specific FXR stimulation. Coated platelets are defined by the retention of proteins in α -granules, enhanced PS-exposure and an abnormal $\alpha_{IIb}\beta_3$ integrin affinity to fibrinogen exceeding the affinity for the $\alpha_{IIb}\beta_3$ integrin specific monoclonal antibody PAC-1 [50, 245]. Additionally, closure of $\alpha_{IIb}\beta_3$ integrin is described in coated platelets resulting in significantly reduced platelet activation by various stimuli [246, 247]. In literature, it is speculated that after an initial activation peak, a calpain-mediated inactivation of the $\alpha_{IIb}\beta_3$ integrin takes place [248]. Based on these findings, the authors speculate that FXR stimulation leads to the generation of pro-coagulant active platelets while the part of aggregatory platelets is reduced [246]. This BA mediated shift in platelet population suggested an inhibitory effect on platelet activation due to reduced $\alpha_{IIb}\beta_3$ integrin activation, although this is only a modulation of platelet function within thrombus formation.

Taken together, the notion of BA induced formation of coated platelets would also fit to observed effects of impaired $\alpha_{IIb}\beta_3$ integrin signaling and enhanced P-selectin exposure after BA treatment of platelets in the present study. Additionally, different results obtained from platelets of experimental cirrhosis in rodents or cirrhotic patients could be explained if BAs might be also responsible for decreased aggregation due to diminished $\alpha_{IIb}\beta_3$ integrin signaling

Discussion

but preserve an enhanced pro-coagulant surface. However, it will be of great importance to further elucidate the specific signaling cascades following BA mediated modulation of platelet activation. In several studies the concentrations of BA receptor agonists (synthetic active or natural) vary from μM to mM range, even though BAs are able to induce platelet membrane degradation [239]. Therefore, results obtained with a concentration in the mM range seem to be overpowered, as e.g., the binding affinities for BAs to their respective receptor FXR or TGR5 are in μM range, as used in this thesis [181, 249]. Moreover, the results differ from the used BA receptor agonist and concentrations, speculating that different BA receptors are involved in platelet signaling.

5.3 Diminished platelet activation and bleeding risk in mice with partial hepatectomy

As already shown for cholestatic liver injury, liver resection is accompanied by thrombocytopenia as well. Several studies describe a reduced platelet count in patients after liver resection predicting a poor patient outcome. In the murine model of PHx, thrombocytopenia is detected and characterized by enhanced platelet size within the first day after liver resection, accompanied by a mild anemia (fig.18). However, the enhanced platelet size persists until day 3, while blood cell counts normalize. In further progression, reduced blood cell counts are fully restored and platelet swelling disappears with progressive liver regeneration. At the same time, decreased platelet degranulation due to reduced P-selectin exposure and reduced externalization and activation of $\alpha_{\text{IIb}}\beta_3$ integrin are observed. This *in vitro* platelet activation defects persist 3 days after PHx, speculating that hemostatic defects are due to low platelet counts and defective platelet activation.

5.3.1 Enhanced VASP phosphorylation in platelets upon liver resection

In accordance with cholestatic liver injury, enhanced plasma levels of PGI_2 and the NO metabolites nitrite and nitrate were measured 1 day after PHx. These plasma factors induce the phosphorylation of VASP at Ser¹⁵⁷ and Ser²³⁶ as shown by Western blot analysis (fig. 26 + fig.27). To this point, evidence for the upregulation and hepatoprotective effects of plasma NO and prostacyclin after PHx in rodents were given [250-252]. Yet, this is the first report to causally link these enhanced levels of NO and PGI_2 to reduced platelet activation. *Per se* platelets show no enhanced VASP phosphorylation, but an additional stimulus with the NO analogue SNP or PGI_2 led to a significant increase in VASP phosphorylation. This suggests that platelets from PHx mice react more sensitively to inhibitory stimuli. In 2000, a study in pigs revealed that plasma levels of PGE and PGI_2 as measured in blood drawn from the hepatic

Discussion

vein, were enhanced directly after PHx, while blood taken from the periphery showed a significantly decreased level of prostaglandins [253]. Interestingly, it was already shown, that enhanced production of NO via eNOS takes place in the remnant liver tissue, while no differences could be observed in other tissues after PHx [253]. Detailed analysis of prostaglandin plasma levels and eNOS activity revealed that NO production peaks already 1 h after hepatectomy while prostaglandin peaks after 3 h [253-255]. Both factors thereby show a biphasic and higher peak 6-10 h after PHx. NO is only produced locally in the remnant liver as NO has modulating properties regarding the orchestration of hepatocyte cell cycle after PHx [256]. Therefore, it is tempting to speculate that platelet activation defects are the most prominent immediately after their passage through the liver. The platelet activation defects measured in this work were measured in peripheral blood. Accordingly, it would be useful to draw blood from the hepatic vein to further investigate this aspect. Beside NO and PGI₂, t-PA and plasmin plasma levels were elevated after cholestatic liver injury. Since no platelet receptor shedding could be detected after PHx, no evidence for enhanced plasmin activity affecting platelet activation was given. However, it is known that t-PA and urokinase-plasminogen activator (u-PA) levels increase dramatically after PHx to activate single chain hepatocyte growth factor (HGF) stored in the ECM of liver tissue [257]. This might also induce plasmin conversion, which is an indicator for hypercoagulability. An additional factor which influences secondary hemostasis and platelet activity is tissue factor. It was shown that hepatocytes produce enhanced tissue factor after PHx, which induces conversion of prothrombin to thrombin [258]. Thrombin is a strong platelet agonist that also indicates enhanced coagulation.

Overall, it might be possible that primary hemostasis is locally inhibited in the liver to regulate platelet activation in the remnant liver. This notion is supported by the analysis of VASP phosphorylation of peripherally obtained platelets, as it shows differences only after stimulation with the platelet antagonists NO and PGI₂ (fig.24+26).

5.3.2 Role of bile acids on platelet activation after PHx

After cholestatic liver injury, a bile stasis occurs that modulates platelet activation as already described under 5.1. Analysis of the serum BA composition highlighted a significantly enhanced concentration of total BAs at day 1 and 3 (without reaching statistical significance) after PHx compared to sham mice (fig. 28). Different studies already highlighted the importance of BAs in the regulation of liver regeneration after PHx through the two BA receptors FXR and TGR5 [259]. Whereas an enhanced level of bile salts was found already after 1 hour in the remnant liver tissue, the serum BA concentration peaks 24 h after PHx [260, 261]. This increased bile salt content allows the activation of FXR and TGR5 in the liver [259]. The here

Discussion

presented results strongly suggest that platelets are influenced by the rising BA concentration early after PHx. As the BA concentration is elevated up to 3 days after PHx, decreased activation of $\alpha_{IIb}\beta_3$ integrin signaling might be explained by elevated BA concentrations because plasma levels of NO and PGI₂ were already reduced at that time point (fig. 25). As already described above, platelet swelling due to the activation of the BA receptor FXR was observed by Unsworth and colleagues [237] (see section 5.2). An enhanced platelet size was measured up to 3 days after PHx, whereas an enhanced number of Thiazole Orange (TO)-positive platelets was found only 7 days after PHx (fig. 29). Platelet size and RNA-content are usually a tool to discriminate between young and old platelets [262-264]. To distinguish whether platelet size is related to platelet age, it is also important to consider the fact that platelet size might be influenced by stimulation with BAs. As BA lead to platelet swelling under native conditions [237], it would be also conceivable that FXR activation affects platelet size after PHx. Therefore, size differentiation after liver resection probably can no longer be used to distinguish between young and old platelets.

This would again explain that despite the increase in platelet size, no change in the number of newly formed, young platelets can be measured with the TO staining shortly after PHx. Nonetheless, BAs modulate platelet activation leading to reduced platelet activation, while no differences in Annexin V binding could be observed 1 day after PHx. Therefore, a supporting effect of BA on coagulation after PHx remains speculative and should be analyzed in near future.

5.3.3 Platelet activation defects after partial hepatectomy lead to bleeding risk *in vivo*

Mice show platelet activation defects 1 and 3 days after PHx. Notably, GPVI mediated signaling was impaired at both time points with respect to both activation markers tested – P-selectin exposure and $\alpha_{IIb}\beta_3$ integrin activation. However, enhanced expression of β_3 integrin was measured 3 days after PHx. Additionally, enhanced active $\alpha_{IIb}\beta_3$ integrin was measured at the surface of resting platelets 3 days after PHx despite agonist mediated activation defects. It is possible that an upregulation of the active $\alpha_{IIb}\beta_3$ integrin is mediated due to an increased number of newly formed platelets. Newly formed platelets display a greater response to stimulation with agonists and display enhanced receptor expression [262]. This notion is further supported by the fact that 3 days after PHx the mild thrombocytopenia is negotiated, and enhanced expression of various platelet receptors except for GPVI is measured at the platelet surface (fig. 21). The defects 1 day after PHx resulted in reduced thrombus formation under flow and a prolonged tail bleeding time, while no defects in the occlusion of the carotid artery after vessel injury were observed (fig. 20). Patients suffering from liver resection show a bleeding tendency and altered coagulation, considering that a reduced hepatic clearance takes

Discussion

place due to the reduced remnant liver mass. Additionally, thrombotic events like pulmonary embolism or portal vein thrombosis are described [265-267], that are further supported by a dysfunction of the vWF regulating metalloprotease ADAMTS13 [268]. One example of the described effects is that also an enhanced concentration of circulating vWF factor could be measured 1 day after PHx accompanied by enhanced vWF binding to platelets, even though no difference after agonist stimulation was obtained (fig. 30).

Taken together, this implies a variety of different hemostatic factors that are either up or down regulated in a compensatory manner following liver resection. If this compensation system is deregulated, a prothrombotic or bleeding phenotype may occur. Interestingly 3 days after PHx, prolonged tail bleeding time was observed. Yet, two different populations seem to develop. One half of the mice show longer bleeding defects than 1 day after PHx, while the other half shows no bleeding tendency at all. Moreover, 3 days after liver resection, the activation defects measured in platelets are converted into reduced thrombus formation at an arterial shear rate of 1000s^{-1} [269], while GPIb-V-XI dependent platelet adhesion [270] and thrombus formation at 1700s^{-1} is unaffected (fig. 23). This highlights that particularly GPVI signaling of platelets is affected after liver injury as similar defects of CRP mediated GPVI signaling were observed in platelets from cholestatic mice. One potential driver of thrombo-inflammation described in literature is the collagen receptor GPVI [271]. A study from Bender *et al* showed, that GPVI deficient mice establish deep vein thrombosis subsequently leading to enhanced lung embolism [272]. As hepatic vein thrombosis and lung embolism are also associated with liver resection [265-267], one could speculate an influence of GPVI signaling after liver resection. These results from literature, compared to the severe GPVI mediated activation defects upon liver inflammation that are presented in this study, highlight an enhanced role of thrombo-inflammation events after liver injury. GPVI-mediated thrombo-inflammation events occur due to interaction of platelets and immune cells. In this manner, integrin signaling has only a subservient role [271]. However, to further elucidate the role of thrombo-inflammation in liver diseases, detailed analysis is required.

5.3.4 Platelet activation correlates with phases of liver regeneration

Overall, this study provides evidence that a reduced hemostasis is mediated by plasmatic inhibition of platelets 1d after PHx. At the same time an increased appearance of platelet aggregates is detected as an enhanced number of GPIb positive platelets were measured in the regenerating liver (fig. 30).

Several studies indicate that platelets tend to be highly activated directly by ECM proteins after PHx. Fibrin(ogen)-mediated integrin signaling plays a critical role in hepatic regeneration after PHx in mice [273]. Platelets accumulate due to elevated fibrinogen deposition in the

Discussion

regenerating liver emphasizing that platelets are directly activated and localized in the regenerating liver shortly after liver resection [274]. Additionally, Kirschbaum *et al* showed that vWF mediated platelet accumulation in the remnant liver propagates liver regeneration within the first two hours after hepatectomy [275]. Interestingly, enhanced binding of vWF on isolated platelets of PHx mice was measured 1d after PHx accompanied by enhanced levels of plasma vWF (fig. 30). However, a reduced hemostasis was still predominant 1d after PHx. Thus, platelet inhibition through plasma factors exceeds vWF mediated adhesion effects of platelets 1 d after PHx resulting in reduced hemostasis. Besides fibrinogen and vWF, podoplanin is also important for liver regeneration. The physiological ligand for podoplanin, the C-type lectin receptor-2 (CLEC-2) on the platelet surface was also observed to be hepatoprotective. Kono *et al.* observed an upregulation of podoplanin in the regenerating liver tissue 6h after PHx and a reduced number of platelet aggregates in the remnant liver in CLEC-2-deficient mice accompanied by reduced liver regeneration [276]. Besides platelets adhesion, other cell types known to be important for liver regeneration might be recruited to the regenerative liver by a remodeled ECM. For instance, liver regeneration is dependent on interaction of the ECM and $\alpha_M\beta_2$ integrin on leucocytes as implied by studies with acetaminophen overdose which is accompanied by leucopenia leading to reduced liver regeneration after PHx [277, 278]. It is convincing that the ECM of the remnant liver promotes interaction of platelets and leucocytes since evidence in other liver repair models were already given [279].

The liver regeneration is divided in three merging stages: the priming phase (first 6 h), the proliferative phase (6-72 h after PHx) and the termination phase (72 h after PHx until a fully regenerated liver mass) [280]. Within the priming phase ECM remodeling in the remnant liver takes place, accompanied by the activation of TNF- α and IL-6 signaling resulting in upregulation of growth factors [280]. Besides the already described effects of the ECM after PHx on platelet activation, other aspects support increased platelet activation according to literature. For instance, platelet derived serotonin and sphingosine-1 phosphate (S1P), released by α - and dense granules after platelet activation promote liver regeneration [200, 281]. Kirschbaum *et al*, also proved that enhanced PS exposure of platelets activates hepatocytes to 'phagocyte' platelets, initiating a horizontal mRNA transfer resulting in hepatocyte proliferation *in vitro* and *in vivo* [187]. In the study of Kirschbaum *et al*, this effect was shown only 1 h after PHx, whereas later time points were not investigated. In this thesis, no difference in PS exposure could be measured 1d after PHx (fig. 29). The positive effects of platelets on liver regeneration described in the literature have all been shown in the priming phase of liver regeneration. With the entrance of the proliferative phase, several platelet inhibitors such as NO, PGI₂ and BAs increase in the plasma of PHx mice (see 5.3.1+5.3.2). This indicates that platelet activation is necessary for the priming of liver regeneration within

Discussion

the first hours after PHx. This fact is further strengthened as induced thrombocytosis is hepatoprotective in the otherwise lethal model of 90% hepatectomy [282]. This enhanced platelet activation further supports the hypothesis of enhanced platelet consumption after PHx. Thus, enhanced platelet consumption eventually accounts for thrombocytopenia measured 1d after PHx (fig. 18). Afterwards in the proliferative phase of liver cells, platelet activation is reduced as clearly shown in this thesis resulting in reduced hemostasis. With the transition to the termination phase, platelet activation normalizes, resulting in an unaltered hemostasis. To summarize the discussed aspects, platelet activation and hemostasis correlate with the phases of liver regeneration. However, to further investigate this hypothesis platelet activation assays within in the priming phase of liver regeneration (1 and 3 hours) are needed.

5.4 The crucial role of IL-6R and AMR in TPO regulation and platelet biogenesis

Mild thrombocytopenia was detected in mice after PHx. Within the progression of various liver diseases, thrombocytopenia is often a clinical factor predicting a poor prognosis for patients [283]. Multiple reasons account for thrombocytopenia in liver disease. A reduced amount of TPO in cirrhotic patients might lead to reduced platelet counts, but also enhanced platelet consumption in the diseased liver was observed. Another important factor is hypersplenism, accompanied by enhanced platelet sequestration into the spleen that induces thrombocytopenia [194]. In all these examples, TPO synthesis, megakaryopoiesis and platelet turnover appear to be affected. Notably, a time dependent shift in the platelet populations (annexinV -, lectin, TO-positive platelets) was measured after liver resection. Reduced amount of Annexin V positive platelets was observed with a simultaneously increased fraction of reticulated (RNA-positive) platelets 7 days after PHx (fig. 29). The enhanced number of reticulated platelets indicates enhanced platelet turnover, since only platelets younger than 24 h are positive for TO staining [188]. Furthermore, the simultaneously reduced Annexin V positive platelets 7 days after PHx indicate improved senescent platelet clearance due to macrophage scavenger receptors rather than PS exposure due to platelet activation defects. Platelets have different pathways to induce the exposure of PS. One pathway is induced by platelet stimulation that leads to rapid PS exposure for a pro-coagulant active surface, while another one is induced via apoptotic signaling pathways through mitochondria [284, 285]. In the second mentioned pathway the PS exposure takes hours. As no elevated *in vitro* platelet activation was measured 7 days after PHx, increased platelet apoptosis must be considered, since reduced PS exposure was measured 7 days after PHx (fig. 23). In contrary, lectin binding of platelets revealed a reduced fraction of lectin positive platelets 1 day after PHx, but an enhanced amount of lectin positive platelets 7 days after PHx. Interestingly, studies showed

Discussion

enhanced neuraminidase activity 18 h (for membrane-bound neuraminidase) and 24 h (for soluble neuraminidase) after PHx in the rat liver [286]. Interestingly, different results were obtained in this study, after the examination of the Neu-1 plasma activity in mice (fig 30). However, only plasma activity and not membrane bound activity of Neu-1 was measured. It might be possible that this increase in neuraminidase activity described in literature for membrane-bound Neu-1 mediates the dissociation of the sialic acid moiety on platelet GPs to stimulate platelet consumption through binding of platelets to hepatocytes via the hepatic lectin receptor, the AMR. Additionally, platelets are a source for glycosyltransferases themselves that induce glycan remodeling after platelet activation [185]. Indeed, an enhanced expression of Neu-1 was measured on the surface of platelets after stimulation with various agonists and also by simulating enhanced shear stress (fig. 30).

Even though liver resection resulted in an enhanced platelet expression of Neu-1, experiments with botrocetin also revealed Neu-1 externalization defects after PHx. As an enhanced shear stress is associated with liver regeneration as portal hypertension develops [190], lectin binding is influenced in an autocrine manner by platelet degranulation. Thus, reduced platelet activation early after PHx might also result in reduced neuraminidase exposure. This would in turn account for the reduced number of desialylated platelets in the circulation of PHx mice suggesting that shear stress induced vWF binding at least partially contributes to reduced lectin positive platelets that were detected after PHx.

However, an enhanced number of platelets was observed 1d after PHx in the remnant liver tissue (fig. 31). The effect of glycan dependent platelet receptor binding might also account for consumption of lectin positive platelets from the blood due to a “adhesion” mechanism. Thus, reducing the number of lectin-positive platelets in the blood, even though platelet degranulation and subsequent Neu-1 externalization is inhibited due to NO and PGI₂ 1d after PHx. The enhanced fraction of lectin and TO positive platelets 7 days after PHx might be caused by enhanced platelet turnover. Firstly, platelet clearance of PS-positive platelet increases the numerical amount of lectin positive platelet in the blood. Secondly, an enhanced platelet turnover facilitates enhanced senescence of platelets, leading to increased amounts of lectin binding sites and enhanced PS-exposure [184]. An excessive platelet turn-over is also accompanied by increased platelet sequestration into the spleen, as Stritt *et al.* proved in *Twf2a*^{-/-} mice with enhanced platelet turn-over [287]. In addition to moderate splenomegaly, increased platelet sequestration was observed, accompanied by changes in lectin-, annexin V- and TO-positive platelet populations 7 days after PHx (fig. 36).

The hypothesis of enhanced platelet turn-over after liver resection is supported by the upregulation of TPO biosynthesis and the signaling cascade regulating TPO generation, as TPO is primarily generated in liver tissue [288]. On the one hand upregulation of the AMR subunits *Asgr1* and *Asgr2* in a biphasic manner appears after PHx. On the other hand, *Il-6r*

Discussion

transcription is enhanced 6 h after PHx (fig. 32). It was firstly shown in 2015, that TPO is regulated via hepatic AMR stimulation leading to an activation of the JAK2/STAT3 signaling cascade in hepatocytes. Glycoprotein receptors like GPIb are desialylated on the platelet surface [289]. Thus, desialylated glycoproteins on platelets bind at the surface of hepatocytes to the AMR, activating a signaling cascade via phosphorylation of JAK2 and subsequent activation of the transcription factor STAT3. This in turn induces gene expression of *Tpo* [77]. However, this effect only observed in healthy mice might be even accelerated after an inflammatory stimulus like the liver resection.

Several studies showed that IL-6 also influences TPO plasma levels, as IL-6 perfusion into mice or administration of IL-6 to cancer patients lead to enhanced platelet counts [87, 195]. Which cells of the liver account for enhanced TPO regeneration remained unclear. As mentioned above, Grazosky *et al* postulated, that desialylated platelets directly bind to the hepatocytic membrane inducing TPO generation through the AMR [77]. Deppermann *et al* recently postulated that desialylated platelet clearance is mediated through KCs in the liver [290]. The macrophage galactose lectin receptor (MGL) and the ASGR1 subunit form a functional receptor that mediates platelet clearance. In this study, direct interaction of platelets and hepatocytes are doubted, as platelets were too big in size to get in direct cell contact with hepatocytes through the *fenestrae* of LSECs. Nonetheless, the debate about size of *fenestrae* needs to be elucidated more extensively than in the study of Deppermann *et al*. They discussed only one size of *fenestrae* of LSECs, but is it known, that depending on the area of the liver lobule *fenestrae* size and number is varying [291]. Additionally, larger and even more *fenestrae* form after PHx due to portal hypertension induced shear stress on the endothelium[292]. Braet *et al* also showed that microvilli from parenchymal cells protrude through the *fenestrae*. The measured platelet size in this study again correlates to *fenestrae* size (see EM images in Braet *et al* [292]). Thus, it might be possible, that at least after liver dissection, a direct cell-cell contact of platelets and hepatocytes is enabled.

So far, platelet clearance in the liver and TPO generation was examined only under steady state conditions while nothing is known about the mechanism responsible for TPO generation upon inflammation or liver resection. After PHx, inflammatory stimuli like IL-6 and TGF- β 1 mediated signaling are predominant [146]. Based on the results here, it remains unclear which cells mediate platelet clearance through AMR in the liver, even though hepatocytes and KCs might act synergistically after PHx. Gene expression analysis revealed a first peak of *Il-6r* and *Asgr1* expression 6 h after PHx, which might suggest a KC mediated platelet consumption. The second, biphasic peak is measured 3 days after PHx that is accompanied by an upregulation of both subunits of the AMR, which might account for a mainly hepatocytic driven platelet clearance. The biphasic expression of *Tpo* 6 h and 3 days after PHx, might be

Discussion

explained by different signaling events that occur between different cells upon the progression of liver regeneration.

However, after liver resection TPO biosynthesis is enhanced up to 3 days after PHx as TPO generation and plasma concentration rise (fig. 32). According to literature, enhanced levels of plasma TPO also occur after minor liver resection [293]. The present study provides strong evidence that the remnant liver produces enhanced amounts of TPO due to synergistic interaction of desialylated platelets that stimulate the AMR, and IL-6 mediated IL-6R stimulation that both induce JAK2 and STAT3 signaling (fig. 33). Enhanced phosphorylation of STAT3 is measured only 24 h after PHx in WT mice that does not account for enhanced TPO generation after 3 days. Different studies observed a peak of STAT3 phosphorylation and IL-6 plasma levels after 6 h and 48 h after operation [273, 294]. Interestingly, platelets may influence both pathways to induce STAT3 activation. Recently, the first *in vivo* evidence was given that platelets directly interact with LSECs to stimulate IL-6 secretion, which in turn induces HGF secretion [295]. Additionally, studies from Marta *et al* provide evidence that platelets release the soluble form of the IL-6R upon activation [85]. Thus, immediately after liver resection, it might be possible that sIL-6R is released by platelets to induce trans-signaling on hepatocytes to support IL-6R induced TPO generation [296]. Trans-signaling was found to be the crucial signaling pathway that controls liver regeneration [148]. The upregulation of TPO in plasma of PHx mice resulted in enhanced megakaryopoiesis in the BM of these mice. Besides, as mentioned above, moderate splenomegaly was examined 7 days after liver resection because of TPO mediated megakaryopoiesis in the spleen of PHx mice (fig. 34). Altogether, an enhanced platelet turn-over was detected after liver resection in mice accompanied by an upregulation of IL-6R and AMR dependent signaling pathways inducing JAK2-STAT3 phosphorylation. This leads to enhanced TPO generation to stimulate megakaryopoiesis in the spleen and in BM. Taken together, this is the first report how the acute phase cytokine receptor IL-6R is directly involved in the modulation of platelet counts to overcome thrombocytopenia upon inflammation in liver disease. These identified processes are summarized in fig. 52.

5.5 IL-6R deficiency induces enhanced platelet turn over and platelet hyper reactivity

5.5.1 IL-6R is involved in platelet turn over and platelet activation

To further elucidate the importance of IL-6R signaling after liver dissection, IL-6R deficient mice were examined. Interestingly, *IL-6R*^{-/-} mice had an increased platelet count under steady state conditions but showed severe thrombocytopenia 1 day after PHx accompanied by a reduced liver regeneration compared to WT (fig. 37A). In fact, liver regeneration seems to be positively correlated with the platelet count in *IL-6R*^{-/-} mice (fig. 37E). IL-6R signaling directly stimulates HGF synthesis, thus it is obvious that HGF and TPO correlate with the amount of reticulated platelets after liver cirrhosis considering the crucial role of IL-6R in TPO biosynthesis [297]. Mice with enhanced platelet turn-over show characteristics like enhanced platelet size, platelet sequestration in the spleen and hyper reactivity of platelets [287]. In a steady state system, *IL-6R*^{-/-} platelets also show enhanced activation with all tested agonist with regard to $\alpha_{IIb}\beta_3$ integrin activation and P-selectin exposure while GP expression and externalization is unaltered (fig. 38). The hyper reactive state of *IL-6R*^{-/-} platelets persists except for GPVI stimulation 1 day after PHx. Activation of the GPVI signaling pathway also led to reduced platelet activation (fig. 39). This again highlights the crucial involvement of GPVI signaling in the regulation of platelet activation after liver damage. To further elucidate the role of GPVI signaling, profound studies in GPVI deficient mice undergoing PHx accompanied by platelet function assays are necessary. Regarding platelet activation, it is known that platelets express the GP130 receptor on their membrane [296] and store sIL-6R in their granules that is released upon activation [85]. Thus, a potential autocrine effect of IL-6 trans-signaling on platelet activation is conceivable. In comparison, platelets release a high number of agonists upon initial activation to further modulate platelet activation such as ADP or TxA₂ [23]. For further analysis of IL-6R dependent platelet activation, administration of hIL-6 is of interest. After administration of hIL-6 a reduced activation of platelets was observed with different agonists regarding $\alpha_{IIb}\beta_3$ integrin activation and degranulation 1d after PHx compared to control mice (fig. 47). To date, only one *in vivo* model was used to causally link IL-6 signaling to thrombotic events – the experimental model of chronic cholangitis. In 2013 it was shown that enhanced platelet aggregation and thrombocytosis is caused by enhanced levels of IL-6 [298]. The authors proclaim an activating effect of IL-6 on platelets as inhibition of IL-6 via administration of a monoclonal antibody resulted in protection against IL-6 induced thrombosis of arterioles of the *musculus cremaster* [298]. Regarding the IL-6 mediated effects in chronic cholangitis, it must be considered that IL-6 promotes the generation of tissue factor [299], that directly

Discussion

enhances thrombin induced clot formation. Thus, inhibiting effects of IL-6 treatment on thrombosis models are not relevant enough to conclude a stimulatory effect of IL-6 on platelet activation. However, Marino *et al* showed that platelet degranulation as well as aggregation are unaffected by IL-6 trans-signaling by itself, nor on thrombin-induced platelet aggregation [296]. Additionally, Senchenkova *et al* confirms these observations, as platelet activation is unaltered after thrombin stimulation of isolated human platelets combined with IL-6 [300]. Contrary to that, stimulation of GPVI receptor with the snake venom convulxin and IL-6 resulted in enhanced P-selectin externalization and $\alpha_{IIb}\beta_3$ integrin activation. In conclusion, the effect of IL-6 signaling on platelet activation, especially after an inflammatory stimulus like liver resection remains unclear. On the one hand the presented data of *IL-6R^{-/-}* after PHx clearly demonstrate a connection between GPVI and IL-6 signaling; on the other hand, no conclusion on the effect of IL-6 trans-signaling in mice without an inflammatory stimulus like PHx can be gathered. Therefore, platelet activation must be analyzed in mice that only received a single administration of hIL-6. In addition, the effect of hIL-6 on platelet activation *in vitro* is of further interest. Additional activation studies in *sIL-6R^{-/-}*, IL-6 antibody treated mice or mice with a platelet specific constitutive activated GP130 receptor would gain further insight into IL-6 mediated platelet activation.

After liver resection, platelet populations regarding RNA-content, PS exposure and glycosylation state varied at different time points after PHx. As 80% of *IL-6R^{-/-}* mice die 48h after liver resection, mice were examined only until 1d after PHx [148]. Nonetheless, genetic deletion of IL-6R leads to differences in platelet membrane composition and receptor glycosylation before and after PHx. Alteration in platelet size and platelet RNA-content suggest enhanced platelet production in *IL-6R^{-/-}* mice, before and after PHx compared to WT controls. Annexin V binding reveals enhanced PS exposure in native *IL-6R^{-/-}* mice compared to WT controls. After PHx, the fraction of PS-positive platelets is reduced. This might be due to different reasons for altered platelet PS-exposure before and after PHx in *IL-6R^{-/-}* mice. In a steady state system, *IL-6R^{-/-}* platelets show increased activation responses. This led one to speculate that enhanced activation through increased Ca^{2+} mobilization triggered PS-exposure; while long term induced PS exposure through apoptotic pathways can be ignored. In contrast, after PHx, it is conceivable that platelets from *IL-6R^{-/-}* mice have a higher PS-exposure mediated platelet clearance resulting in a reduced fraction of PS-positive platelets. However, it is difficult to distinguish between these two signaling pathways. This would require a more detailed study of platelet apoptosis.

Additionally, gene expression of both AMR subunits is elevated in native *IL-6R^{-/-}* mice (fig. 41) [8]. Depending on the lectin used, differences in the lectin binding assays were obtained in *IL-6R^{-/-}* platelets 1 day after PHx (fig. 40). It was already shown that different lectins are able

Discussion

to induce different signaling cascades in platelets resulting in the formation of oxidative stress [301]. Accordingly, there may be differences in the binding of the used lectins to the desialylated glycoproteins on *IL-6R^{-/-}* platelets. In consequence, no conclusion can be drawn from the three different lectin bindings measured on the surface of *IL-6R^{-/-}* platelets after PHx. It is only obvious that healthy *IL-6R^{-/-}* platelets display the same lectin binding as WT mice 1 day after PHx. This would further strengthen the hypothesis of an enhanced platelet-turn over in *IL-6R^{-/-}* mice. The differences in platelet clearance in *IL-6R^{-/-}* mice are supported by different AMR subunit expressions after PHx. *Asgr1* and *Asgr2* transcription are upregulated in native *IL-6R^{-/-}* mice, while only *Asgr1* is upregulated immediately after liver resection (time point PHx 0h; fig. 41). This might reinforce different platelet clearance mechanisms mediated through KCs (MGL/*Asgr1*) or directly by hepatocytes (*Asgr1/Asgr2*) depending on a steady state or an inflammatory situation.

5.5.2. AMR and IL-6R act synergistically to control platelet counts.

However, *IL-6R^{-/-}* mice show exaggerated *Tpo* transcription before and after liver resection, emphasizing the important modulating role of IL-6R in TPO generation. Interestingly, in mice with genetic deletion of the GP130 subunit, platelet counts are reduced by 30% compared to WT controls [302]. This highlights the importance of GP130 mediated signaling cascades which includes the IL-6R signaling. Furthermore, enhanced TPO biogenesis was detected on RNA and protein level that was accompanied by enhanced splenic sequestration of platelets before and after liver resection. Based on these results, enhanced platelet turn-over of *IL-6R^{-/-}* mice is assumed. Enhanced platelet turn-over leads to increased TPO consumption in the plasma due to newly formed c-Mpl rich platelets [191]. As enhanced numbers of newly produced platelets were also measured via TO-staining in *IL-6R^{-/-}* mice before and after PHx, it is convincing to argue that TPO plasma levels might be influenced by elevated platelet turn-over in healthy *IL-6R^{-/-}* mice. However, upon IL-6R deficiency this aspect might not be conceivable, as the relationship between TPO plasma levels and platelet counts are not always conserved in a pathophysiological state [303-305].

As already described above, JAK2/STAT3 signaling induces TPO expression in WT mice after PHx. Under steady state conditions, JAK2-STAT3 signaling does not account for enhanced TPO generation in *IL-6R^{-/-}* mice, but STAT5 might be a promising candidate (fig. 42; see Appendix fig. 3). After PHx, JAK2 phosphorylation is still not observed, while STAT3 phosphorylation occurs. Thus, the question arises how STAT3 phosphorylation emerges without JAK2 phosphorylation. It is known that the different members of the JAK family kinases (JAK1, JAK2, JAK3 and TYK 2) act synergistically depending on the receptor stimulus [306]. Thus, other JAK family kinase members could compensate the down regulated JAK2 signaling

Discussion

in *IL-6R^{-/-}* mice. Beside moderate STAT5 phosphorylation, no STAT3 phosphorylation was found in healthy *IL-6R^{-/-}* mice. Since 7 different STAT family members are expressed in mammals, other STAT family members might be phosphorylated to compensate reduced STAT3 activation or they might even co-localize with other transcription factors (e.g. c-Jun) under steady state conditions [307, 308]. As a future perspective, additional phosphorylation assays for different JAK and STAT protein family members have to be performed to shed light on the signaling mechanics leading to *Tpo* gene expression. Additionally, promoter sequence analysis of the *Tpo* gene (CHIP-seq) might also identify transcription factors other than STAT family members leading to *Tpo* transcription.

To elucidate if *il-6r* expression or the downstream STAT-TPO signaling is influenced by AMR deletion, mice lacking the *Asgr2* subunit (no functional AMR on hepatocytes) were examined. As expected, gene expression analysis showed upregulation of the *Il-6r* and *Asgr1* in steady state conditions of *Asgr2^{-/-}* mice (fig. 45). This supports the assumption that hepatic IL-6R and AMR synergistically control *Tpo* gene expression. Moreover, the different AMR subunits *Asgr1* and *Asgr2* might compensate for each other. Contrary to the published data of Grozovsky *et al*, *Tpo* expression and generation in liver tissue of *Asgr2^{-/-}* is elevated [77]. The upregulation of *Asgr1* thereby further supports the notion of a KC mediated compensation for the loss of *Asgr2* on hepatocytes. Again, upregulation of neither STAT3 nor STAT5 signaling was detected in *Asgr2^{-/-}* mice, supporting the relevance of further investigations on different STAT family members and their impact on IL-6R/AMR induced TPO signaling.

5.5.3 The role of IL-6R in platelet sequestration

A common feature regarding enhanced platelet sequestration is splenomegaly [204]. Even though *IL-6R^{-/-}* mice show enhanced TPO plasma levels leading to increasing numbers of MKs in the BM and in the spleen, no splenomegaly could be observed (fig. 43). However, enhanced platelet sequestration in *IL-6R^{-/-}* mice is observed already in healthy mice and 1d after PHx. Macrophage-1 antigen (MAC-1, Cd11b/18 or integrin $\alpha_M\beta_2$) is expressed on macrophages and is able to bind through the GPIIb-IX complex to platelets [309]. A study from Hoffmeister *et al* showed that platelet clearance is mediated through MAC-1 recognition on macrophages [310]. As IL-6 signaling is involved in the expression of MAC-1 on macrophages it is feasible that IL-6R deficient mice lack MAC-1, resulting in reduced platelet destruction [147, 311]. However, this might be still accompanied by splenic platelet sequestration, as it depends on the one hand on splenic blood flow and the other hand on the intrasplenic platelet transit time [312]. Thereby intrasplenic platelet transit time seems to be independent of spleen size.

In summary, genetic deletion of IL-6R reveals a critical role of IL-6R in TPO biosynthesis and platelet biogenesis. IL-6R deficiency induces an enhanced platelet turn-over and elevated

Discussion

platelet activation upon agonist stimulation. The simultaneous analysis of the *Il-6r* expression in *Asgr2^{-/-}* also highlights the exceptional role of the IL-6R in the regulation of *Tpo* expression, not only after an inflammatory stimulus after liver injury but already under steady state. Thus, the study identified a potential crosstalk of two different TPO regulating receptor pathways, as the AMR and IL-6R are upregulated in compensatory manner after genetic deletion of one another to regulate platelet counts.

5.5.4 Trans-signaling through hyper-IL-6 induces thrombopoiesis

IL-6 signaling can be discriminated in two distinct activation pathways. Membrane-bound IL-6R, mainly expressed on hepatocytes and immune cells as KCs, forms a receptor complex with GP130 after ligand binding of IL-6. This signaling pathway is stated as classic IL-6 signaling [313]. The other pathway, the IL-6-trans-signaling pathway is activated through GP130 and a complex formed out of soluble IL-6R (sIL-6R) and IL-6. The primary formed complex can induce a signaling on every cell that expresses GP130 on its membrane [313, 314]. In this study the fusion protein hIL-6 was administered before PHx to further distinguish between both mentioned pathways and their influence on platelet biogenesis. As shown in fig. 46 and fig. 48 administration of hIL-6 led to an increase in megakaryopoiesis and circulating TPO 1 day after PHx. Even though no enhanced regenerated liver mass was detected after the single administration of hIL-6, Behnke *et al* already showed that hIL-6 administration *in vivo* resulted in enhanced hepatocyte proliferation [173]. This is the first evidence that IL-6 trans-signaling is the important signaling pathway responsible for an increase in thrombopoiesis. For a better differentiation of the potential role of IL-6 trans-signaling after PHx, it would be of interest to study the effect of a single administration of hIL-6 without a further liver resection. Furthermore, to diminish the possible effects of classical IL-6 signaling, it would be of great interest to perform the administration of hIL-6 in *IL-6R^{-/-}* mice.

5.6 Thrombocytopenic mice display reduced liver regeneration

Platelets are an important regulator of liver regeneration after liver dissection. To this date, multiple pathways are described how platelets influence liver regeneration through direct or cooperative effects with hepatocytes, LSECs or KCs [315]. Lesurtel *et al* already showed the impact of thrombocytopenia on liver regeneration via platelet depletion [200]. According to literature, the genetic deletion of the TPO receptor c-mpl also causes thrombocytopenia [202]. Here, the platelet count was reduced by 90% in *Mpl^{-/-}* mice compared to WT mice (fig. 49). Interestingly, also leucopenia was detected in *Mpl^{-/-}* mice contrary to already published data [202]. However, delayed liver regeneration was observed in *Mpl^{-/-}* mice as revealed by the calculation of the liver weight ratio (fig. 50A). After liver resection KCs are important for IL-6

Discussion

and TNF- α supply since depletion of KCs leads to reduced liver regeneration [316, 317]. As leucopenia and severe anemia develop in *Mpl*^{-/-} mice after liver resection, the question arises how this affects liver regeneration besides thrombocytopenia. As described in detail above, IL-6 is an important factor for liver regeneration. *Mpl*^{-/-} mice show significant reduced IL-6 plasma levels after PHx (fig. 50C). Liver resection promotes the interaction of platelets with KCs, resulting in IL-6 and TNF- α release [316, 317]. The reduced level of circulating IL-6 in *Mpl*^{-/-} mice compared to WT controls confirms that platelets can induce IL-6 release. However, no conclusion can be drawn regarding the cell type that is stimulated by platelets to produce IL-6 due to leucopenia in *Mpl*^{-/-} mice.

Of great interest for liver regeneration is the amount of circulating SDF-1 α after PHx. SDF-1 α receptor deletion (CXC-motif chemokine receptor 7(CXCR7)) leads to decreased liver regeneration [318]. It is known that liver regeneration is mediated through liver hyperplasia. However, CXCR 7 is expressed on oval cells, indicating a proliferating effect on these cells in the regenerative liver [319]. This is conceivable since enhanced levels of circulating SDF-1 α were observed 1 day after PHx in WT mice (fig. 51). Even though LSECs are a source for hepatic SDF-1 α production before and after PHx [320], platelets are a major source of SDF-1 α as well [321]. Even though studies implied, that LSECs produce major amounts of SDF-1 α in the circulation after PHx, thrombocytopenia leads to diminished SDF-1 α plasma levels, comparable to native control mice suggesting that platelets are a major source of SDF-1 after PHx (fig. 51). At least 24 h after PHx, the origin of the circulating SDF-1 α is platelet derived as the SDF-1 α plasma concentration of *Mpl*^{-/-} mice 24 h after PHx is comparable to native mice. To further distinguish between LSECs and platelet derived SDF-1 α after PHx earlier time points would need more examination in a thrombocytopenic model. Beside hepatocytes, other liver cells like cholangiocytes and LSECs need to proliferate after PHx. Therefore, BM derived sinusoidal progenitor cells (SPCs) are considered to support the proliferation of LSECs [322, 323]. As published by Harp *et al*, BM derived SPC proliferation increases by two-fold, while mobilization of SPCs from the BM into the circulation increases two- to four-fold after PHx. Likewise, the authors declare a total amount of 25% of BM derived LSECs in the regenerating liver tissue 3 days after PHx [323]. As SDF-1 α acts as chemoattractant for CD34⁺ progenitor cells (e.g. BM derived SPCs), it might be possible that platelet derived SDF-1 α builds up a chemokine gradient that is lost due to thrombocytopenia, resulting in reduced liver regeneration [201, 324]. Altogether, the genetic model of thrombocytopenia supports the pivotal role of platelets in liver regeneration. Additionally, platelet derived SDF-1 α was identified as a major circulating compound of SDF-1 α in the plasma of PHx mice, potentially mediating BM derived SPC mobilization. However, further studies need to be established to characterize the impact of platelets in BM derived recruitment of stem cells and the impact of platelets in liver regeneration via the recruitment of CD34⁺ progenitor cells.

5.7 Conclusion

Overall, using two different murine models of liver injury, the results clearly demonstrate, that platelet activation and thrombus formation is reduced, leading to hemostatic defects after liver injury. After liver injury a variety of signaling cascades are stimulated such as platelet inhibition through NO, PGI₂ or BAs probably to regulate platelet activation. Additionally, BA mediated effects on platelet activation could be firstly linked to *in vivo* liver injury models, predicting a modulating role of BAs in primary hemostasis and liver disease. These effects are responsible for decreased platelet activation *in vivo* resulting in altered hemostasis.

GPVI signaling could be identified as one major regulator of platelet activation following liver injury that might also be involved in the inflammatory response after PHx, or BDL. GPVI deficiency results in reduced thrombotic events without accelerating bleeding events [325]. A drug that prevents platelet adhesion via blocking of GPVI binding to collagen (Revacept) already succeeded in clinical phase study II [326]. Thus, GPVI might be a suitable target to control platelet mediated inflammation after liver injury. However further studies on the impact of GPVI signaling is needed to elucidate the role of platelet GPVI in thrombo-inflammation after liver injury.

Until now, the regulation of the AMR/STAT/TPO signaling cascade was only investigated in healthy mice. In this study, it was shown that an inflammatory stimulus like liver resection results in an upregulation of hepatic AMR expression subsequently leading to an increase in TPO expression. Furthermore, this study describes for the first time that IL-6R also acts as regulating receptor for megakaryopoiesis and emphasizes its role after inflammatory liver injury in a genetic knock-out model. Thus, emphasizing that the pro-inflammatory cytokine IL-6 plays a crucial role in platelet count regulation. In this context, it was demonstrated that IL-6 trans-signaling might be the key regulator of thrombopoiesis regarding IL-6 signaling by administration of the sIL-6R/IL-6 fusion protein hyper-IL-6. However, the interplay between AMR and IL-6R needs to be further elucidated, but these data clearly highlight a compensatory role of both receptors.

For a further understanding of IL-6R mediated hematopoiesis, future studies need to address the difference between classical IL-6 and trans-signaling in more detail as well as the potential role of the GP130 super-family receptor.

6. References

1. Jurk, K. and B.E. Kehrel, [*Pathophysiology and biochemistry of platelets*]. Internist (Berl), 2010. **51**(9): p. 1086, 1088-92, 1094.
2. Kehrel, B.E., [*Blood platelets: biochemistry and physiology*]. Hamostaseologie, 2003. **23**(4): p. 149-58.
3. George, J.N., *Platelets*. Lancet, 2000. **355**(9214): p. 1531-9.
4. Schmitt, A., et al., *Of mice and men: comparison of the ultrastructure of megakaryocytes and platelets*. Exp Hematol, 2001. **29**(11): p. 1295-302.
5. Lefrancais, E., et al., *The lung is a site of platelet biogenesis and a reservoir for haematopoietic progenitors*. Nature, 2017. **544**(7648): p. 105-109.
6. Selvadurai, M.V. and J.R. Hamilton, *Structure and function of the open canalicular system - the platelet's specialized internal membrane network*. Platelets, 2018. **29**(4): p. 319-325.
7. Angenieux, C., et al., *Time-Dependent Decay of mRNA and Ribosomal RNA during Platelet Aging and Its Correlation with Translation Activity*. PLoS One, 2016. **11**(1): p. e0148064.
8. Quach, M.E., W. Chen, and R. Li, *Mechanisms of platelet clearance and translation to improve platelet storage*. Blood, 2018. **131**(14): p. 1512-1521.
9. Allard, B., et al., *The ectonucleotidases CD39 and CD73: Novel checkpoint inhibitor targets*. Immunol Rev, 2017. **276**(1): p. 121-144.
10. Kaczmarek, E., et al., *Identification and characterization of CD39/vascular ATP diphosphohydrolase*. J Biol Chem, 1996. **271**(51): p. 33116-22.
11. Martin, F.A., R.P. Murphy, and P.M. Cummins, *Thrombomodulin and the vascular endothelium: insights into functional, regulatory, and therapeutic aspects*. Am J Physiol Heart Circ Physiol, 2013. **304**(12): p. H1585-97.
12. Wu, K.K. and J.Y. Liou, *Cellular and molecular biology of prostacyclin synthase*. Biochem Biophys Res Commun, 2005. **338**(1): p. 45-52.
13. Foudi, N., et al., *Prostaglandin E2 receptor subtypes in human blood and vascular cells*. Eur J Pharmacol, 2012. **695**(1-3): p. 1-6.
14. Radziwon-Balicka, A., et al., *Differential eNOS-signalling by platelet subpopulations regulates adhesion and aggregation*. Cardiovasc Res, 2017. **113**(14): p. 1719-1731.
15. Suslova, T.E., et al., *Platelet hemostasis in patients with metabolic syndrome and type 2 diabetes mellitus: cGMP- and NO-dependent mechanisms in the insulin-mediated platelet aggregation*. Front Physiol, 2014. **5**: p. 501.
16. Massberg, S., et al., *Enhanced in vivo platelet adhesion in vasodilator-stimulated phosphoprotein (VASP)-deficient mice*. Blood, 2004. **103**(1): p. 136-42.
17. Jurk, K. and B.E. Kehrel, *Platelets: physiology and biochemistry*. Semin Thromb Hemost, 2005. **31**(4): p. 381-92.
18. Itoh T., K.C.Y., Takase H.M., Miyajima A.Watson, S. P., et al., *GPVI and integrin alphaIIb beta3 signaling in platelets*. J Thromb Haemost, 2005. **3**(8): p. 1752-62.
19. Ruggeri, Z.M. and G.L. Mendolicchio, *Adhesion mechanisms in platelet function*. Circ Res, 2007. **100**(12): p. 1673-85.
20. Shattil, S.J., M.H. Ginsberg, and J.S. Brugge, *Adhesive signaling in platelets*. Curr Opin Cell Biol, 1994. **6**(5): p. 695-704.
21. Fox, J.E., et al., *On the role of the platelet membrane skeleton in mediating signal transduction. Association of GP IIb-IIIa, pp60c-src, pp62c-yes, and the p21ras GTPase-activating protein with the membrane skeleton*. J Biol Chem, 1993. **268**(34): p. 25973-84.

Appendix

22. Jackson, S.P., *Arterial thrombosis--insidious, unpredictable and deadly*. Nat Med, 2011. **17**(11): p. 1423-36.
23. Varga-Szabo, D., I. Pleines, and B. Nieswandt, *Cell adhesion mechanisms in platelets*. Arterioscler Thromb Vasc Biol, 2008. **28**(3): p. 403-12.
24. Kloczewiak, M., et al., *Platelet receptor recognition site on human fibrinogen. Synthesis and structure-function relationship of peptides corresponding to the carboxy-terminal segment of the gamma chain*. Biochemistry, 1984. **23**(8): p. 1767-74.
25. Bledzka, K., S.S. Smyth, and E.F. Plow, *Integrin alphaIIb beta3: from discovery to efficacious therapeutic target*. Circ Res, 2013. **112**(8): p. 1189-200.
26. Ni, N., et al., *Avidity modulation activates adhesion under flow and requires cooperativity among adhesion receptors*. Biophys J, 2003. **85**(6): p. 4122-33.
27. Kashiwagi, H., et al., *Affinity modulation of platelet integrin alphaIIb beta3 by beta3-endonexin, a selective binding partner of the beta3 integrin cytoplasmic tail*. J Cell Biol, 1997. **137**(6): p. 1433-43.
28. Fox, J.E., *Transmembrane signaling across the platelet integrin glycoprotein IIb-IIIa*. Ann N Y Acad Sci, 1994. **714**: p. 75-87.
29. Nieswandt, B., D. Varga-Szabo, and M. Elvers, *Integrins in platelet activation*. J Thromb Haemost, 2009. **7 Suppl 1**: p. 206-9.
30. Law, D.A., et al., *Integrin cytoplasmic tyrosine motif is required for outside-in alphaIIb beta3 signalling and platelet function*. Nature, 1999. **401**(6755): p. 808-11.
31. Salsmann, A., et al., *A new functional role of the fibrinogen RGD motif as the molecular switch that selectively triggers integrin alphaIIb beta3-dependent RhoA activation during cell spreading*. J Biol Chem, 2005. **280**(39): p. 33610-9.
32. Hechler, B. and C. Gachet, *Purinergic Receptors in Thrombosis and Inflammation*. Arterioscler Thromb Vasc Biol, 2015. **35**(11): p. 2307-15.
33. Fabre, J.E., et al., *Decreased platelet aggregation, increased bleeding time and resistance to thromboembolism in P2Y1-deficient mice*. Nat Med, 1999. **5**(10): p. 1199-202.
34. Maayani, S., et al., *Agonist concentration-dependent differential responsivity of a human platelet purinergic receptor: pharmacological and kinetic studies of aggregation, deaggregation and shape change responses mediated by the purinergic P2Y1 receptor in vitro*. Platelets, 2003. **14**(7-8): p. 445-62.
35. Andre, P., et al., *P2Y12 regulates platelet adhesion/activation, thrombus growth, and thrombus stability in injured arteries*. J Clin Invest, 2003. **112**(3): p. 398-406.
36. Hirata, M., et al., *Cloning and expression of cDNA for a human thromboxane A2 receptor*. Nature, 1991. **349**(6310): p. 617-20.
37. Raychowdhury, M.K., et al., *Alternative splicing produces a divergent cytoplasmic tail in the human endothelial thromboxane A2 receptor*. J Biol Chem, 1994. **269**(30): p. 19256-61.
38. Jones, R.L., N.H. Wilson, and R.A. Armstrong, *Characterization of thromboxane receptors in human platelets*. Adv Exp Med Biol, 1985. **192**: p. 67-81.
39. Ekambaram, P., et al., *The thromboxane synthase and receptor signaling pathway in cancer: an emerging paradigm in cancer progression and metastasis*. Cancer Metastasis Rev, 2011. **30**(3-4): p. 397-408.
40. David-Ferreira, J.F., *The blood platelet: electron microscopic studies*. Int Rev Cytol, 1964. **17**: p. 99-148.
41. Bearer, E.L., J.M. Prakash, and Z. Li, *Actin dynamics in platelets*. Int Rev Cytol, 2002. **217**: p. 137-82.
42. Bender, M., et al., *ADF/n-cofilin-dependent actin turnover determines platelet formation and sizing*. Blood, 2010. **116**(10): p. 1767-75.

Appendix

43. Pleines, I., et al., *Megakaryocyte-specific RhoA deficiency causes macrothrombocytopenia and defective platelet activation in hemostasis and thrombosis*. Blood, 2012. **119**(4): p. 1054-63.
44. Riddel, J.P., Jr., et al., *Theories of blood coagulation*. J Pediatr Oncol Nurs, 2007. **24**(3): p. 123-31.
45. Kahn, M.L., et al., *A dual thrombin receptor system for platelet activation*. Nature, 1998. **394**(6694): p. 690-4.
46. Offermanns, S., *Activation of platelet function through G protein-coupled receptors*. Circ Res, 2006. **99**(12): p. 1293-304.
47. Shapiro, M.J., et al., *Protease-activated receptors 1 and 4 are shut off with distinct kinetics after activation by thrombin*. J Biol Chem, 2000. **275**(33): p. 25216-21.
48. Gale, A.J., *Continuing education course #2: current understanding of hemostasis*. Toxicol Pathol, 2011. **39**(1): p. 273-80.
49. Dachary-Prigent, J., et al., *Annexin V as a probe of aminophospholipid exposure and platelet membrane vesiculation: a flow cytometry study showing a role for free sulfhydryl groups*. Blood, 1993. **81**(10): p. 2554-65.
50. Dale, G.L., et al., *Stimulated platelets use serotonin to enhance their retention of procoagulant proteins on the cell surface*. Nature, 2002. **415**(6868): p. 175-9.
51. Schreuder, M., P.H. Reitsma, and M.H.A. Bos, *Blood coagulation factor Va's key interactive residues and regions for prothrombinase assembly and prothrombin binding*. J Thromb Haemost, 2019. **17**(8): p. 1229-1239.
52. Kruihof, E.K. and S. Dunoyer-Geindre, *Human tissue-type plasminogen activator*. Thromb Haemost, 2014. **112**(2): p. 243-54.
53. Collen, D. and B. Wiman, *Fast-acting plasmin inhibitor in human plasma*. Blood, 1978. **51**(4): p. 563-9.
54. Long, M.W., *Megakaryocyte differentiation events*. Semin Hematol, 1998. **35**(3): p. 192-9.
55. Machlus, K.R., J.N. Thon, and J.E. Italiano, Jr., *Interpreting the developmental dance of the megakaryocyte: a review of the cellular and molecular processes mediating platelet formation*. Br J Haematol, 2014. **165**(2): p. 227-36.
56. Davis, R.E., et al., *Localization of megakaryocytes in normal mice and following administration of platelet antiserum, 5-fluorouracil, or radiostrontium: evidence for the site of platelet production*. Exp Hematol, 1997. **25**(7): p. 638-48.
57. Avanzi, M.P. and W.B. Mitchell, *Ex vivo production of platelets from stem cells*. Br J Haematol, 2014. **165**(2): p. 237-47.
58. Bunting, S., et al., *Normal platelets and megakaryocytes are produced in vivo in the absence of thrombopoietin*. Blood, 1997. **90**(9): p. 3423-9.
59. Bruns, I., et al., *Megakaryocytes regulate hematopoietic stem cell quiescence through CXCL4 secretion*. Nat Med, 2014. **20**(11): p. 1315-20.
60. Avecilla, S.T., et al., *Chemokine-mediated interaction of hematopoietic progenitors with the bone marrow vascular niche is required for thrombopoiesis*. Nat Med, 2004. **10**(1): p. 64-71.
61. Niswander, L.M., et al., *SDF-1 dynamically mediates megakaryocyte niche occupancy and thrombopoiesis at steady state and following radiation injury*. Blood, 2014. **124**(2): p. 277-86.
62. Psaila, B., D. Lyden, and I. Roberts, *Megakaryocytes, malignancy and bone marrow vascular niches*. J Thromb Haemost, 2012. **10**(2): p. 177-88.
63. Tomer, A., L.A. Harker, and S.A. Burstein, *Purification of human megakaryocytes by fluorescence-activated cell sorting*. Blood, 1987. **70**(6): p. 1735-42.

Appendix

64. Tomer, A., *Human marrow megakaryocyte differentiation: multiparameter correlative analysis identifies von Willebrand factor as a sensitive and distinctive marker for early (2N and 4N) megakaryocytes*. Blood, 2004. **104**(9): p. 2722-7.
65. Behnke, O. and A. Forer, *From megakaryocytes to platelets: platelet morphogenesis takes place in the bloodstream*. Eur J Haematol Suppl, 1998. **61**: p. 3-23.
66. Thon, J.N., et al., *Cytoskeletal mechanics of proplatelet maturation and platelet release*. J Cell Biol, 2010. **191**(4): p. 861-74.
67. Alhasan, A.A., et al., *Circular RNA enrichment in platelets is a signature of transcriptome degradation*. Blood, 2016. **127**(9): p. e1-e11.
68. Schubert, S., A.S. Weyrich, and J.W. Rowley, *A tour through the transcriptional landscape of platelets*. Blood, 2014. **124**(4): p. 493-502.
69. Rowley, J.W., et al., *Dicer1-mediated miRNA processing shapes the mRNA profile and function of murine platelets*. Blood, 2016. **127**(14): p. 1743-51.
70. Bartley, T.D., et al., *Identification and cloning of a megakaryocyte growth and development factor that is a ligand for the cytokine receptor Mpl*. Cell, 1994. **77**(7): p. 1117-24.
71. Gurney, A.L., et al., *Genomic structure, chromosomal localization, and conserved alternative splice forms of thrombopoietin*. Blood, 1995. **85**(4): p. 981-8.
72. de Sauvage, F.J., et al., *Stimulation of megakaryocytopoiesis and thrombopoiesis by the c-Mpl ligand*. Nature, 1994. **369**(6481): p. 533-8.
73. Kaushansky, K., et al., *Thrombopoietin, the Mpl ligand, is essential for full megakaryocyte development*. Proc Natl Acad Sci U S A, 1995. **92**(8): p. 3234-8.
74. Fielder, P.J., et al., *Regulation of thrombopoietin levels by c-mpl-mediated binding to platelets*. Blood, 1996. **87**(6): p. 2154-61.
75. McCarty, J.M., et al., *Murine thrombopoietin mRNA levels are modulated by platelet count*. Blood, 1995. **86**(10): p. 3668-75.
76. McIntosh, B. and K. Kaushansky, *Transcriptional regulation of bone marrow thrombopoietin by platelet proteins*. Exp Hematol, 2008. **36**(7): p. 799-806.
77. Grozovsky, R., et al., *The Ashwell-Morell receptor regulates hepatic thrombopoietin production via JAK2-STAT3 signaling*. Nat Med, 2015. **21**(1): p. 47-54.
78. Grewal, P.K., *The Ashwell-Morell receptor*. Methods Enzymol, 2010. **479**: p. 223-41.
79. Hudgin, R.L., et al., *The isolation and properties of a rabbit liver binding protein specific for asialoglycoproteins*. J Biol Chem, 1974. **249**(17): p. 5536-43.
80. Grozovsky, R., et al., *Regulating billions of blood platelets: glycans and beyond*. Blood, 2015. **126**(16): p. 1877-84.
81. Wolber, E.M. and W. Jelkmann, *Interleukin-6 increases thrombopoietin production in human hepatoma cells HepG2 and Hep3B*. J Interferon Cytokine Res, 2000. **20**(5): p. 499-506.
82. Gabay, C. and I. Kushner, *Acute-phase proteins and other systemic responses to inflammation*. N Engl J Med, 1999. **340**(6): p. 448-54.
83. Soderquist, B., et al., *Secretion of IL-6, IL-8 and G-CSF by human endothelial cells in vitro in response to Staphylococcus aureus and staphylococcal exotoxins*. APMIS, 1998. **106**(12): p. 1157-64.
84. Schmidt-Arras, D. and S. Rose-John, *IL-6 pathway in the liver: From physiopathology to therapy*. J Hepatol, 2016. **64**(6): p. 1403-15.
85. Marta, R.F., et al., *Normal platelets possess the soluble form of IL-6 receptor*. Cytokine, 2005. **29**(1): p. 13-7.
86. Aparicio-Siegmund, S., et al., *Trans-signaling of interleukin-6 (IL-6) is mediated by the soluble IL-6 receptor, but not by soluble CD5*. Biochem Biophys Res Commun, 2017. **484**(4): p. 808-812.

Appendix

87. Kaser, A., et al., *Interleukin-6 stimulates thrombopoiesis through thrombopoietin: role in inflammatory thrombocytosis*. *Blood*, 2001. **98**(9): p. 2720-5.
88. D'Hondt, V., et al., *Thrombopoietic effects and toxicity of interleukin-6 in patients with ovarian cancer before and after chemotherapy: a multicentric placebo-controlled, randomized phase Ib study*. *Blood*, 1995. **85**(9): p. 2347-53.
89. Lazarus, H.M., et al., *Phase I multicenter trial of interleukin 6 therapy after autologous bone marrow transplantation in advanced breast cancer*. *Bone Marrow Transplant*, 1995. **15**(6): p. 935-42.
90. van Gameren, M.M., et al., *Effects of recombinant human interleukin-6 in cancer patients: a phase I-II study*. *Blood*, 1994. **84**(5): p. 1434-41.
91. Gordon, M.S., et al., *A phase I trial of recombinant human interleukin-6 in patients with myelodysplastic syndromes and thrombocytopenia*. *Blood*, 1995. **85**(11): p. 3066-76.
92. Narazaki, M., et al., *Activation of JAK2 kinase mediated by the interleukin 6 signal transducer gp130*. *Proc Natl Acad Sci U S A*, 1994. **91**(6): p. 2285-9.
93. Michalopoulos, G.K. and M.C. DeFrances, *Liver regeneration*. *Science*, 1997. **276**(5309): p. 60-6.
94. Schiebler, T.H., W. Schmidt, and K. Zilles, *Anatomie: Zytologie, Histologie, Entwicklungsgeschichte, makroskopische und mikroskopische Anatomie des Menschen*. 2013: Springer-Verlag.
95. Wolf, D.C., *Evaluation of the Size, Shape, and Consistency of the Liver*, in *Clinical Methods: The History, Physical, and Laboratory Examinations*, rd, et al., Editors. 1990: Boston.
96. Krinke, G., *Normative histology of organs in The laboratory mouse (eds Hedrich, HJ & Bullock, G.) 146*. 2004, Elsevier Academic Press.
97. Sanger, C., et al., *Intrahepatic Vascular Anatomy in Rats and Mice--Variations and Surgical Implications*. *PLoS One*, 2015. **10**(11): p. e0141798.
98. *Bile Duct Cancer (Cholangiocarcinoma) Treatment (PDQ(R)): Health Professional Version*, in *PDQ Cancer Information Summaries*. 2002: Bethesda (MD).
99. Selden, C., M. Khalil, and H.J. Hodgson, *What keeps hepatocytes on the straight and narrow? Maintaining differentiated function in the liver*. *Gut*, 1999. **44**(4): p. 443-6.
100. Parviz, F., et al., *Hepatocyte nuclear factor 4alpha controls the development of a hepatic epithelium and liver morphogenesis*. *Nat Genet*, 2003. **34**(3): p. 292-6.
101. McCuskey, R.S., *The hepatic microvascular system in health and its response to toxicants*. *Anat Rec (Hoboken)*, 2008. **291**(6): p. 661-71.
102. Bilzer, M., F. Roggel, and A.L. Gerbes, *Role of Kupffer cells in host defense and liver disease*. *Liver Int*, 2006. **26**(10): p. 1175-86.
103. Basit, H., M.L. Tan, and D.R. Webster, *Histology, Kupffer Cell*, in *StatPearls*. 2020: Treasure Island (FL).
104. Flisiak, R., *Role of Ito cells in the liver function*. *Pol J Pathol*, 1997. **48**(3): p. 139-45.
105. Itoh, T., et al., *Liver Stem Cells*, in *Regenerative Medicine-from Protocol to Patient*. 2016, Springer. p. 209-240.
106. Redinger, R.N. and D.M. Small, *Bile composition, bile salt metabolism and gallstones*. *Arch Intern Med*, 1972. **130**(4): p. 618-30.
107. Hofmann, A.F., *The enterohepatic circulation of bile acids in mammals: form and functions*. *Front Biosci (Landmark Ed)*, 2009. **14**: p. 2584-98.
108. Kullak-Ublick, G.A., et al., *Stable expression and functional characterization of a Na⁺-taurocholate cotransporting green fluorescent protein in human hepatoblastoma HepG2 cells*. *Cytotechnology*, 2000. **34**(1-2): p. 1-9.
109. Meier, P.J. and B. Stieger, *Bile salt transporters*. *Annu Rev Physiol*, 2002. **64**: p. 635-61.

Appendix

110. Gerloff, T., et al., *The sister of P-glycoprotein represents the canalicular bile salt export pump of mammalian liver*. J Biol Chem, 1998. **273**(16): p. 10046-50.
111. Kipp, H. and I.M. Arias, *Trafficking of canalicular ABC transporters in hepatocytes*. Annu Rev Physiol, 2002. **64**: p. 595-608.
112. Meier, P.J., *Molecular mechanisms of hepatic bile salt transport from sinusoidal blood into bile*. Am J Physiol, 1995. **269**(6 Pt 1): p. G801-12.
113. Nathanson, M.H. and J.L. Boyer, *Mechanisms and regulation of bile secretion*. Hepatology, 1991. **14**(3): p. 551-66.
114. Anwer, M.S. and D. Hegner, *Effect of organic anions on bile acid uptake by isolated rat hepatocytes*. Hoppe Seylers Z Physiol Chem, 1978. **359**(8): p. 1027-30.
115. Anwer, M.S. and B. Stieger, *Sodium-dependent bile salt transporters of the SLC10A transporter family: more than solute transporters*. Pflugers Arch, 2014. **466**(1): p. 77-89.
116. Hagenbuch, B. and P.J. Meier, *Sinusoidal (basolateral) bile salt uptake systems of hepatocytes*. Semin Liver Dis, 1996. **16**(2): p. 129-36.
117. Hirohashi, T., H. Suzuki, and Y. Sugiyama, *Characterization of the transport properties of cloned rat multidrug resistance-associated protein 3 (MRP3)*. J Biol Chem, 1999. **274**(21): p. 15181-5.
118. Francavilla, A., et al., *Regulation of liver size and regeneration: importance in liver transplantation*. Transplant Proc, 1988. **20**(1 Suppl 1): p. 494-7.
119. Alison, M.R., S. Islam, and S. Lim, *Stem cells in liver regeneration, fibrosis and cancer: the good, the bad and the ugly*. J Pathol, 2009. **217**(2): p. 282-98.
120. Riehle, K.J., et al., *New concepts in liver regeneration*. J Gastroenterol Hepatol, 2011. **26 Suppl 1**: p. 203-12.
121. Lowes, K.N., et al., *Oval cell numbers in human chronic liver diseases are directly related to disease severity*. Am J Pathol, 1999. **154**(2): p. 537-41.
122. Roskams, T., A. Katoonizadeh, and M. Komuta, *Hepatic progenitor cells: an update*. Clin Liver Dis, 2010. **14**(4): p. 705-18.
123. Alison, M.R., M.H. Golding, and C.E. Sarraf, *Pluripotential liver stem cells: facultative stem cells located in the biliary tree*. Cell Prolif, 1996. **29**(7): p. 373-402.
124. Fausto, N. and J.S. Campbell, *The role of hepatocytes and oval cells in liver regeneration and repopulation*. Mech Dev, 2003. **120**(1): p. 117-30.
125. Roskams, T.A., L. Libbrecht, and V.J. Desmet, *Progenitor cells in diseased human liver*. Semin Liver Dis, 2003. **23**(4): p. 385-96.
126. Fausto, N., *Involvement of the innate immune system in liver regeneration and injury*. J Hepatol, 2006. **45**(3): p. 347-9.
127. Chen, H.L., et al., *Jaundice revisited: recent advances in the diagnosis and treatment of inherited cholestatic liver diseases*. J Biomed Sci, 2018. **25**(1): p. 75.
128. Trauner, M., et al., *Endotoxin impairs biliary glutathione and HCO₃⁻ excretion and blocks the choleric effect of nitric oxide in rat liver*. Hepatology, 1997. **25**(5): p. 1184-91.
129. Trauner, M., et al., *Endotoxin downregulates rat hepatic ntcp gene expression via decreased activity of critical transcription factors*. J Clin Invest, 1998. **101**(10): p. 2092-100.
130. Woreta, T.A. and S.A. Alqahtani, *Evaluation of abnormal liver tests*. Med Clin North Am, 2014. **98**(1): p. 1-16.
131. Keitel, V., et al., *Expression and localization of hepatobiliary transport proteins in progressive familial intrahepatic cholestasis*. Hepatology, 2005. **41**(5): p. 1160-72.
132. Haglund, U.H., et al., *Right hemihepatectomy*. J Gastrointest Surg, 2008. **12**(7): p. 1283-7.

Appendix

133. Hasegawa, E., et al., *Efficacy and anticarcinogenic activity of interferon for hepatitis C virus-related compensated cirrhosis in patients with genotype 1b low viral load or genotype 2*. Hepatol Res, 2007. **37**(10): p. 793-800.
134. Garcea, G. and G.J. Maddern, *Liver failure after major hepatic resection*. J Hepatobiliary Pancreat Surg, 2009. **16**(2): p. 145-55.
135. Fausto, N., *Liver regeneration: from laboratory to clinic*. Liver Transpl, 2001. **7**(10): p. 835-44.
136. Rahman, T.M. and H.J. Hodgson, *Animal models of acute hepatic failure*. Int J Exp Pathol, 2000. **81**(2): p. 145-57.
137. Bolesta, S. and S.L. Haber, *Hepatotoxicity associated with chronic acetaminophen administration in patients without risk factors*. Ann Pharmacother, 2002. **36**(2): p. 331-3.
138. Cataldegirmen, G., et al., *RAGE limits regeneration after massive liver injury by coordinated suppression of TNF-alpha and NF-kappaB*. J Exp Med, 2005. **201**(3): p. 473-84.
139. Higgins, G. and R. Anderson, *Restoration of the liver of white rats following surgical partial hepatectomy*. Arch Cardiol, 1931. **12**: p. 18.
140. Furchtgott, L.A., C.C. Chow, and V. Periwal, *A model of liver regeneration*. Biophys J, 2009. **96**(10): p. 3926-35.
141. Skullman, S., I. Ihse, and J. Larsson, *Influence of malnutrition on regeneration and composition of the liver in rats*. Acta Chir Scand, 1990. **156**(10): p. 717-22.
142. Fausto, N., *Liver regeneration*. J Hepatol, 2000. **32**(1 Suppl): p. 19-31.
143. Kountouras, J., P. Boura, and N.J. Lygidakis, *Liver regeneration after hepatectomy*. Hepatogastroenterology, 2001. **48**(38): p. 556-62.
144. Overturf, K., et al., *Serial transplantation reveals the stem-cell-like regenerative potential of adult mouse hepatocytes*. Am J Pathol, 1997. **151**(5): p. 1273-80.
145. Bucher, N.L., *Regeneration of Mammalian Liver*. Int Rev Cytol, 1963. **15**: p. 245-300.
146. Michalopoulos, G.K., *Liver regeneration*. J Cell Physiol, 2007. **213**(2): p. 286-300.
147. Kopf, M., et al., *Impaired immune and acute-phase responses in interleukin-6-deficient mice*. Nature, 1994. **368**(6469): p. 339-42.
148. Fazel Modares, N., et al., *IL-6 Trans-signaling Controls Liver Regeneration After Partial Hepatectomy*. Hepatology, 2019. **70**(6): p. 2075-2091.
149. Cressman, D.E., et al., *Liver failure and defective hepatocyte regeneration in interleukin-6-deficient mice*. Science, 1996. **274**(5291): p. 1379-83.
150. Gewiese-Rabsch, J., et al., *Role of IL-6 trans-signaling in CCl(4)induced liver damage*. Biochim Biophys Acta, 2010. **1802**(11): p. 1054-61.
151. Gawaz, M. and S. Vogel, *Platelets in tissue repair: control of apoptosis and interactions with regenerative cells*. Blood, 2013. **122**(15): p. 2550-4.
152. Blanchard, R.A., et al., *Acquired vitamin K-dependent carboxylation deficiency in liver disease*. N Engl J Med, 1981. **305**(5): p. 242-8.
153. Fair, D.S. and R.A. Marlar, *Biosynthesis and secretion of factor VII, protein C, protein S, and the Protein C inhibitor from a human hepatoma cell line*. Blood, 1986. **67**(1): p. 64-70.
154. Schipper, H.G. and J.W. ten Cate, *Antithrombin III transfusion in patients with hepatic cirrhosis*. Br J Haematol, 1982. **52**(1): p. 25-33.
155. Kelly, D.A. and J.A. Summerfield, *Hemostasis in liver disease*. Semin Liver Dis, 1987. **7**(3): p. 182-91.
156. Rapaport, S.I., *Coagulation problems in liver disease*. Blood Coagul Fibrinolysis, 2000. **11 Suppl 1**: p. S69-74.
157. Wion, K.L., et al., *Distribution of factor VIII mRNA and antigen in human liver and other tissues*. Nature, 1985. **317**(6039): p. 726-9.

Appendix

158. Hollestelle, M.J., et al., *Tissue distribution of factor VIII gene expression in vivo--a closer look*. Thromb Haemost, 2001. **86**(3): p. 855-61.
159. Mammen, E.F., *Coagulation abnormalities in liver disease*. Hematol Oncol Clin North Am, 1992. **6**(6): p. 1247-57.
160. Tripodi, A., et al., *Hypercoagulability in cirrhosis: causes and consequences*. J Thromb Haemost, 2011. **9**(9): p. 1713-23.
161. Caldwell, S.H., et al., *Coagulation disorders and hemostasis in liver disease: pathophysiology and critical assessment of current management*. Hepatology, 2006. **44**(4): p. 1039-46.
162. Lisman, T., F.W. Leebeek, and P.G. de Groot, *Haemostatic abnormalities in patients with liver disease*. J Hepatol, 2002. **37**(2): p. 280-7.
163. Lisman, T. and R.J. Porte, *Activation and regulation of hemostasis in acute liver failure and acute pancreatitis*. Semin Thromb Hemost, 2010. **36**(4): p. 437-43.
164. Takahashi, H., et al., *Thrombin and plasmin generation in patients with liver disease*. Am J Hematol, 1989. **32**(1): p. 30-5.
165. Laschke, M.W., et al., *Platelet-dependent accumulation of leukocytes in sinusoids mediates hepatocellular damage in bile duct ligation-induced cholestasis*. Br J Pharmacol, 2008. **153**(1): p. 148-56.
166. Sitia, G., et al., *Antiplatelet therapy prevents hepatocellular carcinoma and improves survival in a mouse model of chronic hepatitis B*. Proc Natl Acad Sci U S A, 2012. **109**(32): p. E2165-72.
167. Lesurtel, M., et al., *Platelet-derived serotonin mediates liver regeneration*. Science, 2006. **312**(5770): p. 104-7.
168. Matsuo, R., et al., *Platelets Strongly Induce Hepatocyte Proliferation with IGF-1 and HGF In Vitro*. J Surg Res, 2008. **145**(2): p. 279-86.
169. Takahashi, K., et al., *Human platelets inhibit liver fibrosis in severe combined immunodeficiency mice*. World J Gastroenterol, 2013. **19**(32): p. 5250-60.
170. Wang, L., et al., *Platelets' increase is associated with improvement of liver fibrosis in entecavir-treated chronic hepatitis B patients with significant liver fibrosis*. Hepatol Int, 2018. **12**(3): p. 237-243.
171. Lang, P.A., et al., *Aggravation of viral hepatitis by platelet-derived serotonin*. Nat Med, 2008. **14**(7): p. 756-61.
172. Greene, A.K. and M. Puder, *Partial hepatectomy in the mouse: technique and perioperative management*. J Invest Surg, 2003. **16**(2): p. 99-102.
173. Behnke, K., et al., *B Cell-Mediated Maintenance of Cluster of Differentiation 169-Positive Cells Is Critical for Liver Regeneration*. Hepatology, 2018. **68**(6): p. 2348-2361.
174. Fotinos, A., et al., *Loss of oligophrenin1 leads to uncontrolled Rho activation and increased thrombus formation in mice*. J Thromb Haemost, 2015. **13**(4): p. 619-30.
175. Wu, Q., et al., *An elevated percentage of reticulated platelet is associated with increased mortality in septic shock patients*. Medicine (Baltimore), 2015. **94**(19): p. e814.
176. Bradford, M.M., *A rapid and sensitive method for the quantitation of microgram quantities of protein utilizing the principle of protein-dye binding*. Anal Biochem, 1976. **72**: p. 248-54.
177. Mariotti, V., et al., *Animal models of biliary injury and altered bile acid metabolism*. Biochim Biophys Acta Mol Basis Dis, 2018. **1864**(4 Pt B): p. 1254-1261.
178. Aktas, B., et al., *Dipyridamole enhances NO/cGMP-mediated vasodilator-stimulated phosphoprotein phosphorylation and signaling in human platelets: in vitro and in vivo/ex vivo studies*. Stroke, 2003. **34**(3): p. 764-9.

Appendix

179. Lopez-Sanchez, L.M., et al., *Inhibition of nitric oxide synthesis during induced cholestasis ameliorates hepatocellular injury by facilitating S-nitrosothiol homeostasis*. Lab Invest, 2010. **90**(1): p. 116-27.
180. Michelson, A.D. and M.R. Barnard, *Plasmin-induced redistribution of platelet glycoprotein Ib*. Blood, 1990. **76**(10): p. 2005-10.
181. Reich, M., et al., *TGR5 is essential for bile acid-dependent cholangiocyte proliferation in vivo and in vitro*. Gut, 2016. **65**(3): p. 487-501.
182. Li, J. and P.A. Dawson, *Animal models to study bile acid metabolism*. Biochim Biophys Acta Mol Basis Dis, 2019. **1865**(5): p. 895-911.
183. O'Brien, A.J., et al., *Immunosuppression in acutely decompensated cirrhosis is mediated by prostaglandin E2*. Nat Med, 2014. **20**(5): p. 518-23.
184. van der Meijden, P.E.J. and J.W.M. Heemskerk, *Platelet biology and functions: new concepts and clinical perspectives*. Nat Rev Cardiol, 2019. **16**(3): p. 166-179.
185. Lee-Sundlov, M.M., et al., *Circulating blood and platelets supply glycosyltransferases that enable extrinsic extracellular glycosylation*. Glycobiology, 2017. **27**(2): p. 188-198.
186. Schoenwaelder, S.M., et al., *Two distinct pathways regulate platelet phosphatidylserine exposure and procoagulant function*. Blood, 2009. **114**(3): p. 663-666.
187. Kirschbaum, M., et al., *Horizontal RNA transfer mediates platelet-induced hepatocyte proliferation*. Blood, 2015. **126**(6): p. 798-806.
188. Weiss, D. and E. Townsend, *Evaluation of reticulated platelets in dogs*. Comparative Haematology International, 1998. **8**(3): p. 166-170.
189. Riswari, S.F., et al., *Desialylation of platelets induced by Von Willebrand Factor is a novel mechanism of platelet clearance in dengue*. PLoS Pathog, 2019. **15**(3): p. e1007500.
190. Sato, Y., et al., *Acute portal hypertension reflecting shear stress as a trigger of liver regeneration following partial hepatectomy*. Surg Today, 1997. **27**(6): p. 518-26.
191. Kuter, D.J. and R.D. Rosenberg, *The reciprocal relationship of thrombopoietin (c-Mpl ligand) to changes in the platelet mass during busulfan-induced thrombocytopenia in the rabbit*. Blood, 1995. **85**(10): p. 2720-30.
192. Doignon, I., et al., *Immediate neuroendocrine signaling after partial hepatectomy through acute portal hyperpressure and cholestasis*. J Hepatol, 2011. **54**(3): p. 481-8.
193. Slayton, W.B., et al., *The spleen is a major site of megakaryopoiesis following transplantation of murine hematopoietic stem cells*. Blood, 2002. **100**(12): p. 3975-82.
194. Lisman, T. and J.P. Luyendyk, *Platelets as Modulators of Liver Diseases*. Semin Thromb Hemost, 2018. **44**(2): p. 114-125.
195. Laterveer, L., et al., *Continuous infusion of interleukin-6 in sublethally irradiated mice accelerates platelet reconstitution and the recovery of myeloid but not of megakaryocytic progenitor cells in bone marrow*. Exp Hematol, 1993. **21**(13): p. 1621-7.
196. Bellido, T., et al., *Transcriptional activation of the p21(WAF1,CIP1,SDI1) gene by interleukin-6 type cytokines. A prerequisite for their pro-differentiating and anti-apoptotic effects on human osteoblastic cells*. J Biol Chem, 1998. **273**(33): p. 21137-44.
197. Wustefeld, T., et al., *Hyperstimulation with interleukin 6 inhibits cell cycle progression after hepatectomy in mice*. Hepatology, 2000. **32**(3): p. 514-22.
198. Fischer, M., et al., *I. A bioactive designer cytokine for human hematopoietic progenitor cell expansion*. Nat Biotechnol, 1997. **15**(2): p. 142-5.
199. Peters, M., et al., *In vivo and in vitro activities of the gp130-stimulating designer cytokine Hyper-IL-6*. J Immunol, 1998. **161**(7): p. 3575-81.
200. Lesurtel, M. and P.A. Clavien, *Platelet-derived serotonin: translational implications for liver regeneration*. Hepatology, 2014. **60**(1): p. 30-3.

Appendix

201. Aiuti, A., et al., *The chemokine SDF-1 is a chemoattractant for human CD34+ hematopoietic progenitor cells and provides a new mechanism to explain the mobilization of CD34+ progenitors to peripheral blood.* J Exp Med, 1997. **185**(1): p. 111-20.
202. Murone, M., D.A. Carpenter, and F.J. de Sauvage, *Hematopoietic deficiencies in c-mpl and TPO knockout mice.* Stem Cells, 1998. **16**(1): p. 1-6.
203. Gowert, N.S., et al., *Defective Platelet Activation and Bleeding Complications upon Cholestasis in Mice.* Cell Physiol Biochem, 2017. **41**(6): p. 2133-2149.
204. Aster, R.H., *Pooling of platelets in the spleen: role in the pathogenesis of "hypersplenic" thrombocytopenia.* J Clin Invest, 1966. **45**(5): p. 645-57.
205. Goulis, J., et al., *Thrombopoietin concentrations are low in patients with cirrhosis and thrombocytopenia and are restored after orthotopic liver transplantation.* Gut, 1999. **44**(5): p. 754-8.
206. Stein, S.F. and L.A. Harker, *Kinetic and functional studies of platelets, fibrinogen, and plasminogen in patients with hepatic cirrhosis.* J Lab Clin Med, 1982. **99**(2): p. 217-30.
207. Kane, K.K., *Fibrinolysis--a review.* Ann Clin Lab Sci, 1984. **14**(6): p. 443-9.
208. Nagaoka, M.R., M. Kouyoumdjian, and D.R. Borges, *Hepatic clearance of tissue-type plasminogen activator and plasma kallikrein in experimental liver fibrosis.* Liver Int, 2003. **23**(6): p. 476-83.
209. Wang, H., et al., *Transcriptional profiling after bile duct ligation identifies PAI-1 as a contributor to cholestatic injury in mice.* Hepatology, 2005. **42**(5): p. 1099-108.
210. Segal, H., et al., *Coagulation and fibrinolysis in primary biliary cirrhosis compared with other liver disease and during orthotopic liver transplantation.* Hepatology, 1997. **25**(3): p. 683-8.
211. Leiper, K., et al., *Tissue plasminogen activator, plasminogen activator inhibitors, and activator-inhibitor complex in liver disease.* J Clin Pathol, 1994. **47**(3): p. 214-7.
212. Wang, H., Y. Zhang, and R.O. Heuckeroth, *Tissue-type plasminogen activator deficiency exacerbates cholestatic liver injury in mice.* Hepatology, 2007. **45**(6): p. 1527-37.
213. Bergheim, I., et al., *Critical role of plasminogen activator inhibitor-1 in cholestatic liver injury and fibrosis.* J Pharmacol Exp Ther, 2006. **316**(2): p. 592-600.
214. Wang, H., Y. Zhang, and R.O. Heuckeroth, *PAI-1 deficiency reduces liver fibrosis after bile duct ligation in mice through activation of tPA.* FEBS Lett, 2007. **581**(16): p. 3098-104.
215. Pasche, B., et al., *Structural changes in platelet glycoprotein IIb/IIIa by plasmin: determinants and functional consequences.* Blood, 1994. **83**(2): p. 404-14.
216. Pihusch, R., et al., *Platelet function rather than plasmatic coagulation explains hypercoagulable state in cholestatic liver disease.* J Hepatol, 2002. **37**(5): p. 548-55.
217. Ingeberg, S., et al., *Platelet aggregation and release of ATP in patients with hepatic cirrhosis.* Scand J Gastroenterol, 1985. **20**(3): p. 285-8.
218. Egan, K., et al., *Increased soluble GPVI levels in cirrhosis: evidence for early in vivo platelet activation.* J Thromb Thrombolysis, 2017. **43**(1): p. 54-59.
219. Semenov, A.V., et al., *Production of soluble P-selectin by platelets and endothelial cells.* Biochemistry (Mosc), 1999. **64**(11): p. 1326-35.
220. Vardareli, E., et al., *Soluble P selectin levels in chronic liver disease: relationship to disease severity.* Hepatogastroenterology, 2007. **54**(74): p. 466-9.
221. Atucha, N.M., et al., *Altered calcium signalling in platelets from bile-duct-ligated rats.* Clin Sci (Lond), 2007. **112**(3): p. 167-74.
222. Atucha, N., et al., *Altered calcium regulation in freshly isolated aortic smooth muscle cells from bile duct-ligated rats: role of nitric oxide.* Cell Calcium, 2003. **33**(2): p. 129-35.

Appendix

223. Atucha, N.M., et al., *Reduced capacitative calcium entry in the mesenteric vascular bed of bile duct-ligated rats*. Eur J Pharmacol, 2005. **525**(1-3): p. 117-22.
224. Lang, F., et al., *Regulation of STIM1/Orai1-dependent Ca²⁺ signalling in platelets*. Thromb Haemost, 2013. **110**(5): p. 925-30.
225. Liu, G., et al., *Rapid Upregulation of Orai1 Abundance in the Plasma Membrane of Platelets Following Activation with Thrombin and Collagen Related Peptide*. Cell Physiol Biochem, 2015. **37**(5): p. 1759-66.
226. Liu, G., et al., *Involvement of Ca²⁺ Activated Cl⁻ Channel Ano6 in Platelet Activation and Apoptosis*. Cell Physiol Biochem, 2015. **37**(5): p. 1934-44.
227. Albornoz, L., et al., *Prolonged bleeding time in experimental cirrhosis: role of nitric oxide*. J Hepatol, 1999. **30**(3): p. 456-60.
228. Witters, P., et al., *ADP-degrading enzymes inhibit platelet activation in bile duct-ligated rats*. J Thromb Haemost, 2010. **8**(2): p. 360-8.
229. Lang, E., et al., *Conjugated bilirubin triggers anemia by inducing erythrocyte death*. Hepatology, 2015. **61**(1): p. 275-84.
230. Kundur, A.R., I. Singh, and A.C. Bulmer, *Bilirubin, platelet activation and heart disease: a missing link to cardiovascular protection in Gilbert's syndrome?* Atherosclerosis, 2015. **239**(1): p. 73-84.
231. Kundur, A.R., et al., *Mildly elevated unconjugated bilirubin is associated with reduced platelet activation-related thrombogenesis and inflammation in Gilbert's syndrome*. Platelets, 2017. **28**(8): p. 779-785.
232. Kundur, A.R., A.C. Bulmer, and I. Singh, *Unconjugated bilirubin inhibits collagen induced platelet activation*. Platelets, 2014. **25**(1): p. 45-50.
233. Pereira, J., et al., *In vivo effect of bile salts on platelet aggregation in rats*. Thromb Res, 1995. **80**(4): p. 357-62.
234. Annie-Jeyachristy, S., A. Geetha, and R. Surendran, *Changes in the level of cytosolic calcium, nitric oxide and nitric oxide synthase activity during platelet aggregation: an in vitro study in platelets from normal subjects and those with cirrhosis*. J Biosci, 2008. **33**(1): p. 45-53.
235. Romecin, P., et al., *Bile Acids Do Not Contribute to the Altered Calcium Homeostasis of Platelets from Rats with Biliary Cirrhosis*. Front Physiol, 2017. **8**: p. 384.
236. Moraes, L.A., et al., *Farnesoid X Receptor and Its Ligands Inhibit the Function of Platelets*. Arterioscler Thromb Vasc Biol, 2016. **36**(12): p. 2324-2333.
237. Unsworth, A.J., et al., *Farnesoid X Receptor and Liver X Receptor Ligands Initiate Formation of Coated Platelets*. Arterioscler Thromb Vasc Biol, 2017. **37**(8): p. 1482-1493.
238. Maruyama, T., et al., *Identification of membrane-type receptor for bile acids (M-BAR)*. Biochem Biophys Res Commun, 2002. **298**(5): p. 714-9.
239. Shiao, Y.J., et al., *The mode of action of primary bile salts on human platelets*. Biochim Biophys Acta, 1993. **1146**(2): p. 282-93.
240. Varol, E., et al., *Mean platelet volume is elevated in patients with low high-density lipoprotein cholesterol*. Angiology, 2014. **65**(8): p. 733-6.
241. Coban, E., et al., *The mean platelet volume in patients with obesity*. Int J Clin Pract, 2005. **59**(8): p. 981-2.
242. Kodiatte, T.A., et al., *Mean platelet volume in Type 2 diabetes mellitus*. J Lab Physicians, 2012. **4**(1): p. 5-9.
243. Tahtaci, M., et al., *Increased mean platelet volume is related to histologic severity of primary biliary cirrhosis*. Eur J Gastroenterol Hepatol, 2015. **27**(12): p. 1382-5.
244. Tanoglu, A., Y.S. Sakin, and E. Karagoz, *Mean platelet volume may predict histological severity of primary biliary cirrhosis, but drugs and comorbidities are major concerns*. Eur J Gastroenterol Hepatol, 2016. **28**(1): p. 116.

Appendix

245. Dale, G.L., *Coated-platelets: an emerging component of the procoagulant response*. J Thromb Haemost, 2005. **3**(10): p. 2185-92.
246. Mattheij, N.J., et al., *Dual mechanism of integrin alphaIIb beta3 closure in procoagulant platelets*. J Biol Chem, 2013. **288**(19): p. 13325-36.
247. Jackson, S.P. and S.M. Schoenwaelder, *Procoagulant platelets: are they necrotic?* Blood, 2010. **116**(12): p. 2011-8.
248. Mattheij, N.J., et al., *Coated platelets function in platelet-dependent fibrin formation via integrin alphaIIb beta3 and transglutaminase factor XIII*. Haematologica, 2016. **101**(4): p. 427-36.
249. Makishima, M., et al., *Identification of a nuclear receptor for bile acids*. Science, 1999. **284**(5418): p. 1362-5.
250. Schoen Smith, J.M. and W.W. Lauth, *Nitric oxide and prostaglandins potentiate the liver regeneration cascade*. Can J Gastroenterol, 2006. **20**(5): p. 329-34.
251. Yoshida, D., et al., *Roles of vascular endothelial growth factor and endothelial nitric oxide synthase during revascularization and regeneration after partial hepatectomy in a rat model*. Surg Today, 2011. **41**(12): p. 1622-9.
252. Yu, Y., M. Tamai, and Y.I. Tagawa, *Nitric oxide is critical for avoiding hepatic lipid overloading via IL-6 induction during liver regeneration after partial hepatectomy in mice*. Exp Anim, 2017. **66**(4): p. 293-302.
253. Lai, O.F., et al., *Changes in prostaglandin and nitric oxide levels in the hyperdynamic circulation following liver resection*. J Gastroenterol Hepatol, 2000. **15**(8): p. 895-901.
254. Obolenskaya, M., et al., *Epr evidence of nitric oxide production by the regenerating rat liver*. Biochem Biophys Res Commun, 1994. **202**(1): p. 571-6.
255. Tsujii, H., et al., *Prostaglandin E2 and rat liver regeneration*. Gastroenterology, 1993. **105**(2): p. 495-9.
256. Carnovale, C.E. and M.T. Ronco, *Role of nitric oxide in liver regeneration*. Ann Hepatol, 2012. **11**(5): p. 636-47.
257. Mars, W.M., R. Zarnegar, and G.K. Michalopoulos, *Activation of hepatocyte growth factor by the plasminogen activators uPA and tPA*. Am J Pathol, 1993. **143**(3): p. 949-58.
258. Sullivan, B.P., et al., *Hepatocyte tissue factor activates the coagulation cascade in mice*. Blood, 2013. **121**(10): p. 1868-74.
259. van de Laarschot, L.F., et al., *The role of bile salts in liver regeneration*. Hepatol Int, 2016. **10**(5): p. 733-40.
260. Huang, J. and D.A. Rudnick, *Elucidating the metabolic regulation of liver regeneration*. Am J Pathol, 2014. **184**(2): p. 309-21.
261. Huang, W., et al., *Nuclear receptor-dependent bile acid signaling is required for normal liver regeneration*. Science, 2006. **312**(5771): p. 233-6.
262. Jones, C.I., *Platelet function and ageing*. Mamm Genome, 2016. **27**(7-8): p. 358-66.
263. Verdoia, M., et al., *Impact of renal function on mean platelet volume and its relationship with coronary artery disease: A single-centre cohort study*. Thromb Res, 2016. **141**: p. 139-44.
264. Yang, J., et al., *mTORC1 promotes aging-related venous thrombosis in mice via elevation of platelet volume and activation*. Blood, 2016. **128**(5): p. 615-24.
265. Melloul, E., et al., *Pulmonary embolism after elective liver resection: a prospective analysis of risk factors*. J Hepatol, 2012. **57**(6): p. 1268-75.
266. Yoshiya, S., et al., *Portal vein thrombosis after hepatectomy*. World J Surg, 2014. **38**(6): p. 1491-7.
267. Buc, E., et al., *Hepatic veins as a site of clot formation following liver resection*. World J Gastroenterol, 2011. **17**(3): p. 403-6.

Appendix

268. Groeneveld, D.J., et al., *Balance between von Willebrand factor and ADAMTS13 following major partial hepatectomy*. Br J Surg, 2016. **103**(6): p. 735-743.
269. Pugh, N., et al., *Synergism between platelet collagen receptors defined using receptor-specific collagen-mimetic peptide substrata in flowing blood*. Blood, 2010. **115**(24): p. 5069-79.
270. Jackson, S.P., W.S. Nesbitt, and E. Westein, *Dynamics of platelet thrombus formation*. J Thromb Haemost, 2009. **7 Suppl 1**: p. 17-20.
271. Rayes, J., S.P. Watson, and B. Nieswandt, *Functional significance of the platelet immune receptors GPVI and CLEC-2*. J Clin Invest, 2019. **129**(1): p. 12-23.
272. Bender, M., et al., *Combined in vivo depletion of glycoprotein VI and C-type lectin-like receptor 2 severely compromises hemostasis and abrogates arterial thrombosis in mice*. Arterioscler Thromb Vasc Biol, 2013. **33**(5): p. 926-34.
273. Beier, J.I., et al., *Fibrin-mediated integrin signaling plays a critical role in hepatic regeneration after partial hepatectomy in mice*. Ann Hepatol, 2016. **15**(5): p. 762-72.
274. Groeneveld, D., et al., *Intrahepatic fibrin(ogen) deposition drives liver regeneration after partial hepatectomy in mice and humans*. Blood, 2019. **133**(11): p. 1245-1256.
275. Kirschbaum, M., et al., *Transient von Willebrand factor-mediated platelet influx stimulates liver regeneration after partial hepatectomy in mice*. Liver Int, 2017. **37**(11): p. 1731-1737.
276. Kono, H., et al., *The platelet-activating receptor C-type lectin receptor-2 plays an essential role in liver regeneration after partial hepatectomy in mice*. J Thromb Haemost, 2017. **15**(5): p. 998-1008.
277. Kopec, A.K., et al., *Fibrin(ogen) drives repair after acetaminophen-induced liver injury via leukocyte alphaMbeta2 integrin-dependent upregulation of Mmp12*. J Hepatol, 2017. **66**(4): p. 787-797.
278. Selzner, N., et al., *ICAM-1 triggers liver regeneration through leukocyte recruitment and Kupffer cell-dependent release of TNF-alpha/IL-6 in mice*. Gastroenterology, 2003. **124**(3): p. 692-700.
279. Slaba, I., et al., *Imaging the dynamic platelet-neutrophil response in sterile liver injury and repair in mice*. Hepatology, 2015. **62**(5): p. 1593-605.
280. Abu Rmilah, A., et al., *Understanding the marvels behind liver regeneration*. Wiley Interdisciplinary Reviews: Developmental Biology, 2019. **8**(3): p. e340.
281. Kawasaki, T., et al., *Activation of human liver sinusoidal endothelial cell by human platelets induces hepatocyte proliferation*. J Hepatol, 2010. **53**(4): p. 648-54.
282. Myronovych, A., et al., *Role of platelets on liver regeneration after 90% hepatectomy in mice*. Journal of hepatology, 2008. **49**(3): p. 363-372.
283. Qamar, A.A., et al., *Incidence, prevalence, and clinical significance of abnormal hematologic indices in compensated cirrhosis*. Clin Gastroenterol Hepatol, 2009. **7**(6): p. 689-95.
284. Reddy, E.C. and M.L. Rand, *Procoagulant Phosphatidylserine-Exposing Platelets in vitro and in vivo*. Front Cardiovasc Med, 2020. **7**: p. 15.
285. Schoenwaelder, S.M., et al., *Two distinct pathways regulate platelet phosphatidylserine exposure and procoagulant function*. Blood, 2009. **114**(3): p. 663-6.
286. Valiakina, T.I., et al., *[Soluble and membrane-bound neuraminidase in regenerating rat liver]*. Biokhimiia, 1975. **40**(4): p. 733-8.
287. Stritt, S., et al., *Profilin 1-mediated cytoskeletal rearrangements regulate integrin function in mouse platelets*. Blood Adv, 2018. **2**(9): p. 1040-1045.
288. Qian, S., et al., *Primary role of the liver in thrombopoietin production shown by tissue-specific knockout*. Blood, 1998. **92**(6): p. 2189-91.
289. Wang, Y., et al., *Desialylation of O-glycans on glycoprotein Iba drives receptor signaling and platelet clearance*. Haematologica, 2020.

Appendix

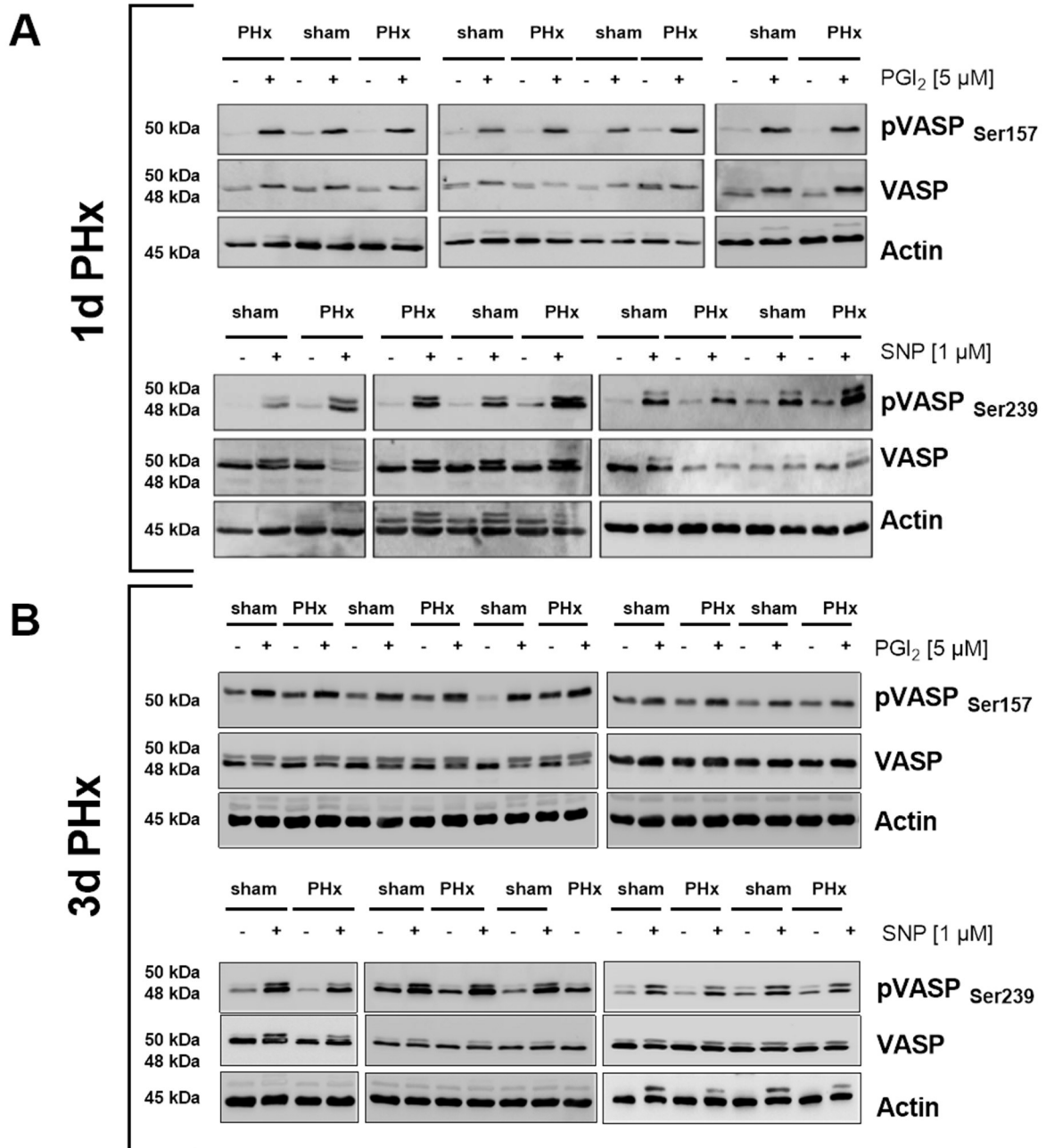
290. Deppermann, C., et al., *Macrophage galactose lectin is critical for Kupffer cells to clear aged platelets*. J Exp Med, 2020. **217**(4).
291. Ni, Y., et al., *Pathological process of liver sinusoidal endothelial cells in liver diseases*. World J Gastroenterol, 2017. **23**(43): p. 7666-7677.
292. Braet, F., et al., *Liver sinusoidal endothelial cell modulation upon resection and shear stress in vitro*. Comp Hepatol, 2004. **3**(1): p. 7.
293. Haegele, S., et al., *Deficiency in thrombopoietin induction after liver surgery is associated with postoperative liver dysfunction*. PLoS One, 2015. **10**(1): p. e0116985.
294. Sorg, U.R., et al., *Cooperative role of lymphotoxin beta receptor and tumor necrosis factor receptor p55 in murine liver regeneration*. J Hepatol, 2016. **64**(5): p. 1108-1117.
295. Meyer, J., et al., *Platelet Interactions with Liver Sinusoidal Endothelial Cells and Hepatic Stellate Cells Lead to Hepatocyte Proliferation*. Cells, 2020. **9**(5).
296. Marino, M., et al., *Novel path to IL-6 trans-signaling through thrombin-induced soluble IL-6 receptor release by platelets*. J Biol Regul Homeost Agents, 2013. **27**(3): p. 841-52.
297. Panasiuk, A., et al., *Reticulated platelets as a marker of megakaryopoiesis in liver cirrhosis; relation to thrombopoietin and hepatocyte growth factor serum concentration*. Hepatogastroenterology, 2004. **51**(58): p. 1124-8.
298. Senchenkova, E.Y., et al., *Interleukin-6 mediates the platelet abnormalities and thrombogenesis associated with experimental colitis*. Am J Pathol, 2013. **183**(1): p. 173-81.
299. Neumann, F.-J., et al., *Effect of human recombinant interleukin-6 and interleukin-8 on monocyte procoagulant activity*. Arteriosclerosis, thrombosis, and vascular biology, 1997. **17**(12): p. 3399-3405.
300. Senchenkova, E.Y., et al., *Novel Role of T Cells and IL-6 (Interleukin-6) in Angiotensin II-Induced Microvascular Dysfunction*. Hypertension, 2019. **73**(4): p. 829-838.
301. Signorello, M.G., S. Ravera, and G. Leoncini, *Lectin-induced oxidative stress in human platelets*. Redox Biol, 2020. **32**: p. 101456.
302. Betz, U.A., et al., *Postnatally induced inactivation of gp130 in mice results in neurological, cardiac, hematopoietic, immunological, hepatic, and pulmonary defects*. J Exp Med, 1998. **188**(10): p. 1955-65.
303. Griesshammer, M., et al., *High levels of thrombopoietin in sera of patients with essential thrombocythemia: cause or consequence of abnormal platelet production?* Ann Hematol, 1998. **77**(5): p. 211-5.
304. Uppenkamp, M., et al., *Thrombopoietin serum concentration in patients with reactive and myeloproliferative thrombocytosis*. Ann Hematol, 1998. **77**(5): p. 217-23.
305. Ng, A.P., et al., *Mpl expression on megakaryocytes and platelets is dispensable for thrombopoiesis but essential to prevent myeloproliferation*. Proc Natl Acad Sci U S A, 2014. **111**(16): p. 5884-9.
306. Lin, C.M., F.A. Cooles, and J.D. Isaacs, *Basic Mechanisms of JAK Inhibition*. Mediterr J Rheumatol, 2020. **31**(Suppl 1): p. 100-104.
307. Wang, Y. and D.E. Levy, *Comparative evolutionary genomics of the STAT family of transcription factors*. JAKSTAT, 2012. **1**(1): p. 23-33.
308. Villarino, A.V., Y. Kanno, and J.J. O'Shea, *Mechanisms and consequences of Jak-STAT signaling in the immune system*. Nat Immunol, 2017. **18**(4): p. 374-384.
309. Simon, D.I., et al., *Platelet glycoprotein ibalalpha is a counterreceptor for the leukocyte integrin Mac-1 (CD11b/CD18)*. J Exp Med, 2000. **192**(2): p. 193-204.
310. Hoffmeister, K.M., et al., *Glycosylation restores survival of chilled blood platelets*. Science, 2003. **301**(5639): p. 1531-4.
311. Wong, P.K., et al., *The role of the interleukin-6 family of cytokines in inflammatory arthritis and bone turnover*. Arthritis Rheum, 2003. **48**(5): p. 1177-89.

Appendix

312. Wadenvik, H. and J. Kutti, *The spleen and pooling of blood cells*. Eur J Haematol, 1988. **41**(1): p. 1-5.
313. Schmidt-Arras, D. and S. Rose-John, *IL-6 pathway in the liver: From physiopathology to therapy*. Journal of hepatology, 2016. **64**(6): p. 1403-1415.
314. Rose-John, S. and P.C. Heinrich, *Soluble receptors for cytokines and growth factors: generation and biological function*. Biochemical Journal, 1994. **300**(2): p. 281-290.
315. Takahashi, K., et al., *Platelet and liver regeneration after liver surgery*. Surg Today, 2019.
316. Robinson, M.W., C. Harmon, and C. O'Farrelly, *Liver immunology and its role in inflammation and homeostasis*. Cell Mol Immunol, 2016. **13**(3): p. 267-76.
317. Meijer, C., et al., *Kupffer cell depletion by CI2MDP-liposomes alters hepatic cytokine expression and delays liver regeneration after partial hepatectomy*. Liver, 2000. **20**(1): p. 66-77.
318. Shido, K., et al., *Platelets prime hematopoietic and vascular niche to drive angiocrine-mediated liver regeneration*. Signal Transduct Target Ther, 2017. **2**.
319. Hatch, H.M., et al., *SDF-1alpha/CXCR4: a mechanism for hepatic oval cell activation and bone marrow stem cell recruitment to the injured liver of rats*. Cloning Stem Cells, 2002. **4**(4): p. 339-51.
320. DeLeve, L.D., X. Wang, and L. Wang, *VEGF-sdf1 recruitment of CXCR7+ bone marrow progenitors of liver sinusoidal endothelial cells promotes rat liver regeneration*. Am J Physiol Gastrointest Liver Physiol, 2016. **310**(9): p. G739-46.
321. Chatterjee, M. and M. Gawaz, *Platelet-derived CXCL12 (SDF-1alpha): basic mechanisms and clinical implications*. J Thromb Haemost, 2013. **11**(11): p. 1954-67.
322. Harb, R., et al., *Bone marrow progenitor cells repair rat hepatic sinusoidal endothelial cells after liver injury*. Gastroenterology, 2009. **137**(2): p. 704-12.
323. Wang, L., et al., *Liver sinusoidal endothelial cell progenitor cells promote liver regeneration in rats*. J Clin Invest, 2012. **122**(4): p. 1567-73.
324. Ohmori, S., et al., *High expression of CD34-positive sinusoidal endothelial cells is a risk factor for hepatocellular carcinoma in patients with HCV-associated chronic liver diseases*. Hum Pathol, 2001. **32**(12): p. 1363-70.
325. Andrews, R.K., J.F. Arthur, and E.E. Gardiner, *Targeting GPVI as a novel antithrombotic strategy*. Journal of blood medicine, 2014. **5**: p. 59.
326. Schüpke, S., et al., *Revacept, a Novel Inhibitor of Platelet Adhesion, in Patients Undergoing Elective PCI-Design and Rationale of the Randomized ISAR-PLASTER Trial*. Thromb Haemost, 2019. **119**(9): p. 1539-1545.

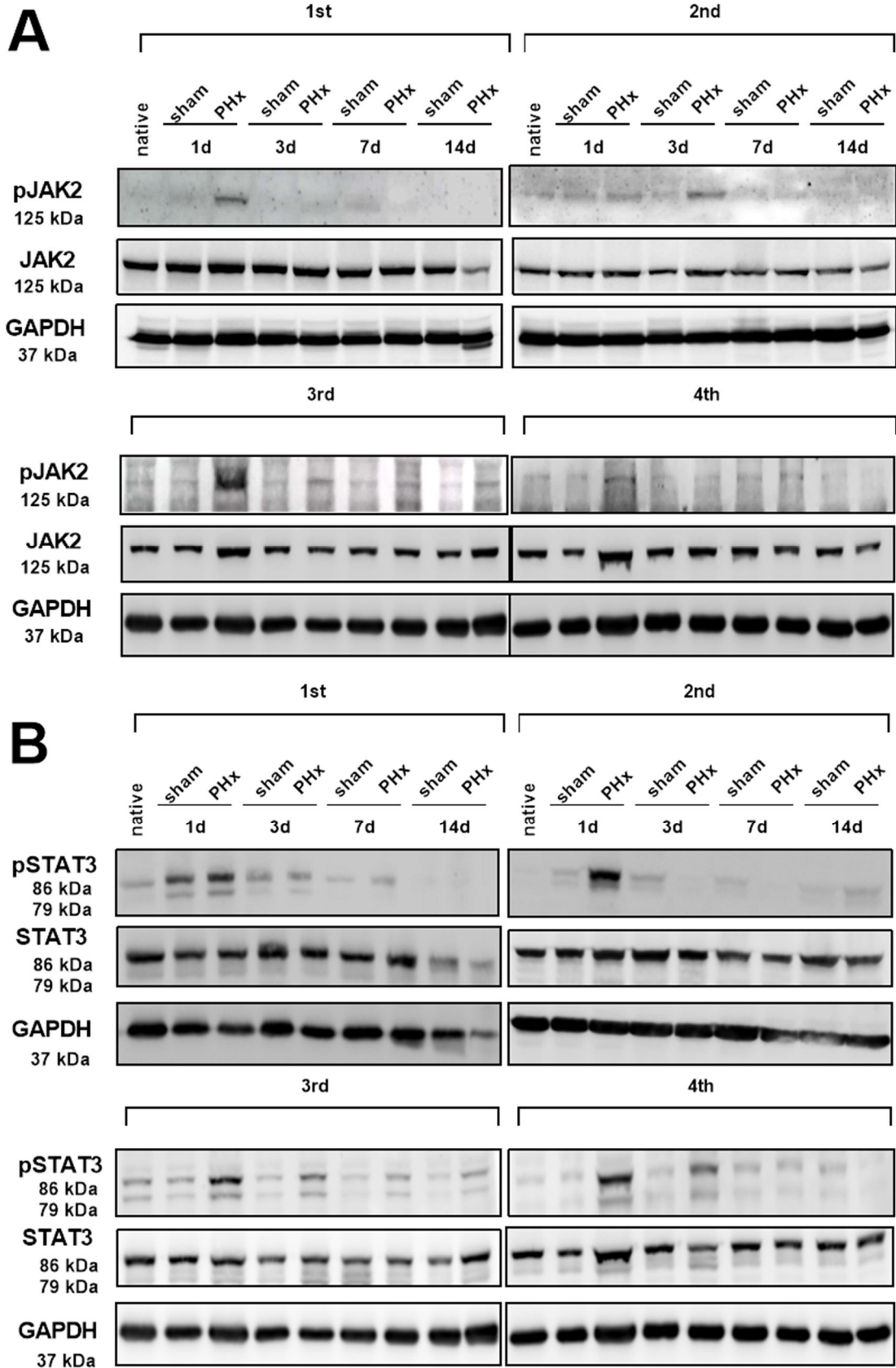
7. Appendix

7.1 Unshown data



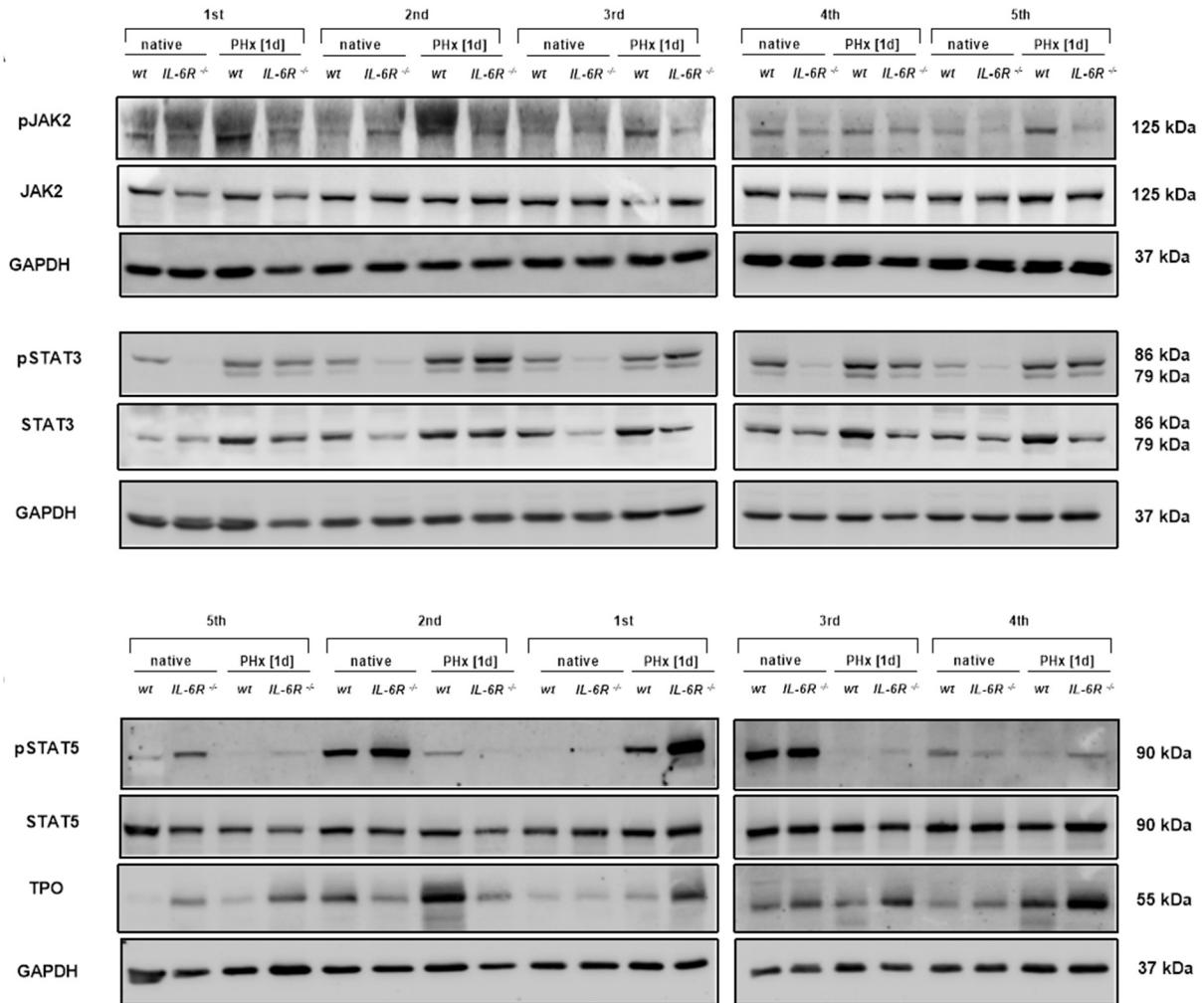
Appendix figure 1 Phosphorylation of VASP at in platelets one and three days after PHx. Isolated platelets from PHx and sham mice were incubated with PGI₂ [5 μM] for 5 min or with SNP [1 μM] for 2 min at 37°C and subsequently platelet lysates were generated. (A) Western blot analysis of platelet lysates shows enhanced vasodilator-stimulated phosphoprotein (VASP) phosphorylation at Ser157 and Ser329 1 day after PHx, but no difference in total VASP expression. (B) Western blot analysis of platelet lysates shows neither enhanced VASP phosphorylation at Ser157 or Ser 239 nor altered VASP expression 3 days after PHx.

Appendix



Appendix figure II PHx induces JAK2/STAT3 signaling in WT mice within the first day. Whole liver lysates of native control mice (ctrl.), sham and PHx operated C57Bl6/j mice was lysed and western blot analysis was performed. immunoblots of total liver cell lysates using (A) anti-pJAK2 and anti-JAK2 antibodies and (B) anti-pSTAT3 and anti-STAT3 monoclonal antibodies showing enhanced phosphorylation of both proteins one day after PHx. GAPDH was used as loading control (n=4).

Appendix



Appendix figure III PHx induces JAK2/STAT3 signaling in WT mice within the first day. Whole liver lysates of native and PHx (1d) WT and IL-6R^{-/-} were analyzed via western blot. (A) Representative immunoblots of total liver cell lysates using anti-pJAK2 + anti-JAK2 antibodies, anti-pSTAT5 + STAT5 and anti-pSTAT3 + anti-STAT3 monoclonal antibodies. TPO polyclonal antibody was used with GAPDH as loading control (n= 5 for each group)

7.2 Danksagung

An erster Stelle möchte ich mich bei Frau Margitta Elvers bedanken für die Möglichkeit in ihrem Institut meine Promotion anzufertigen und die Möglichkeit teilweise schon eigenverantwortlich Wissenschaft zu durchdenken und auch umzusetzen.

Des Weiteren möchte ich mich bei Herrn Jürgen Scheller bedanken, für die Übernahme des Gutachtens meiner Promotion und die wissenschaftliche Kooperation mit seiner AG, welche zur erfolgreichen Umsetzung meines Promotionsthemas beigetragen hat.

In Zuge dessen möchte ich auch der Experimentellen Hepatologie danken. Neben dem gebotenen Fachwissen und den operativen Fähigkeiten, die mir beigebracht wurden, war ich über jede Gelegenheit froh, eine „angewandte Leberforschung“ umzusetzen.

Natürlich bin ich auch den jetzigen (und inzwischen ehemaligen) Mitgliedern unserer AG dankbar. Auch wenn es manchmal schwierig war, konnten wir im Endeffekt immer alle zusammen lachen. Ich bin vor allem Lisa, Laura und Kim dankbar, dass ihr meine unermüdlichen Wuttiraden und meine gestresste Art ertragen habt und ich immer wieder mit den gleichen Dingen zu euch kommen konnte. Besonderen Dank möchte ich an Martina aussprechen! Ohne dich hätte ich nur sehr schwer im Labor überlebt und du hast mir so manches Mal aus der Patsche geholfen, wenn ich mich mal wieder überplant habe.

Insgesamt bin ich dankbar dafür, dass ich meine Promotion in einem so guten Arbeitsumfeld anfertigen durfte.

Ich möchte mich auch bei all meinen Freunden bedanken, die sich so manches mal mein Leid anhören mussten – egal wie groß es war. Besonders bedanken muss ich mich auch bei den tapferen Menschen, die sich der Korrektur meiner Arbeit gewidmet haben: Michelle, Martha, Katja, Lizzi und vor allem Alex!

An dieser Stelle möchte ich meinen Freund Nico besonders erwähnen. Ich bin dankbar dafür, dass er mir ein Umfeld in Düsseldorf gegeben hat, in dem ich mich zu Hause fühle.

Besonders hervorheben möchte ich meine Familie. Ich bin meinen Eltern dankbar, dass Sie mir ermöglicht haben zu studieren und mich immer in Allem unterstützt haben. All meinen Geschwistern, dass Sie meine forsche Art aushalten, sich um mich Sorgen und ich weiß, dass ich mit jeder Angelegenheit zu ihnen kommen könnte. Ich bin vor Allem dankbar, dass ich immer die Person sein durfte, die ich bin und mich nie verstellen musste, um Normen zu entsprechen.

7.3 List of publications

- (1) Gowert NS, Klier M, Reich M, **Reuswig F**, Donner L, Keitel V, Häussinger D, Elvers M.
Defective Platelet Activation and Bleeding Complications upon Cholestasis in Mice.
Cell Physiol Biochem. 2017;41(6):2133-2149. doi: 10.1159/000475566. Epub 2017
Apr 20.

- (2) Urbahn MA*, Kaup SC*, **Reuswig F***, Krüger I, Spelleken M, Jurk K, Klier M, Lang PA,
Elvers M.
Phospholipase D1 regulation of TNF-alpha protects against responses to LPS.
Sci Rep. 2018 Jul 3;8(1):10006. doi: 10.1038/s41598-018-28331-y.

- (3) Chatterjee M, Ehrenberg A, Toska LM, Metz LM, Klier M, Krueger I, **Reuswig F**, Elvers
M.
Molecular Drivers of Platelet Activation: Unraveling Novel Targets for Anti-Thrombotic
and Anti-Thrombo-Inflammatory Therapy.
Int J Mol Sci. 2020 Oct 24;21(21):7906. doi: 10.3390/ijms21217906.

- (4) **Reuswig F**, Fazel Modares N, Brechtenkamp M, Wienands L, Krüger I, Behnke K, Lee-
Sundlov MM, Herebian D, Scheller J, Hoffmeister KM, Häussinger D, Elvers M.
Efficiently Restored Thrombopoietin Production by Ashwell-Morell Receptor and IL-6R
Induced Janus Kinase 2/Signal Transducer and Activator of Transcription Signaling
Early After Partial Hepatectomy.
Hepatology. 2020 Dec 28. doi: 10.1002/hep.31698. Epub ahead of print.

* The authors contributed equally to this work

7.4 International Conferences

1. Poster presentation: *Platelet defects upon surgical liver disease models in mice*
XXVI th Congress of the International Society on Thrombosis and Haemostasis (ISTH) 2017. Berlin, Germany.
2. Poster presentation: *Platelet defects upon surgical liver disease models in mice*
Member of the organizing committee – *Team: Fundraising*
1st PhD Symposium deLIVER – Technology in Hepatology 2017. Düsseldorf, Germany
3. Poster presentation: *Platelet defects upon surgical liver disease models in mice*
34th Annual meeting of the German association for the study of the liver (GASL) 2018. Hamburg, Germany
4. Poster presentations: *The role of NMDA receptors in platelet specific hemostasis & Moderate decreased platelet counts but high platelet activation defects alter hemostasis and arterial thrombosis after partial hepatectomy in mice*
XXVII th Congress of the International Society on Thrombosis and Haemostasis (ISTH) 2019. Melbourne, Australia
5. Oral presentation: *Moderate platelet defects but efficiently restored Thrombopoietin production early after partial hepatectomy via JAK2-STAT3 signaling in mice*
Poster presentation: *The role of NMDA receptors in platelet specific hemostasis*
64th Annual Meeting of the Society of Thrombosis and Haemostasis Research (GTH) 2020. Bremen, Germany
6. Oral presentation: *Moderate platelet defects but efficiently restored Thrombopoietin production early after partial hepatectomy via JAK2-STAT3 signaling in mice*
XXVIII th Congress of the International Society on Thrombosis and Haemostasis (ISTH) 2020. Virtual Congress

7.5 Affidavit

I affirm in lieu of oath that the dissertation was written by me independently and without unauthorized outside help, in accordance with the "Quality principles of good scientific practice at the Heinrich-Heine-University Düsseldorf". Furthermore, I confirm that this thesis has not yet been submitted as part of another examination process neither in identical nor in similar.

Düsseldorf, December 2020 _____

7.6 Eidesstattliche Erklärung

Ich versichere an Eides Statt, dass die Dissertation von mir selbständig und ohne unzulässige fremde Hilfe unter Beachtung der „Grundsätze zur Sicherung guter wissenschaftlicher Praxis an der Heinrich-Heine-Universität Düsseldorf“ erstellt worden ist. Ich erkläre außerdem, dass die Dissertation weder in gleicher noch in ähnlicher Form bereits in einem anderen Prüfungsverfahren vorgelegen hat.

Düsseldorf, Dezember 2020 _____